Generation and characterization of genetically modified donor pigs for islet xenotransplantation

von Sarah Grimus

Inaugural-Dissertation zur Erlangung der Doktorwürde
der Tierärztlichen Fakultät
der Ludwig-Maximilians-Universität München

Generation and characterization of genetically modified donor pigs for islet xenotransplantation

von Sarah Grimus

aus Unterschneidheim

München 2024

Aus dem Veterinärwissenschaftlichen Department der Tierärztlichen Fakultät
der Ludwig-Maximilians-Universität München

Lehrstuhl für Molekulare Tierzucht und Biotechnologie

Arbeit angefertigt unter der Leitung von: Prof. Dr. Elisabeth G. Kemter

Mitbetreuung durch: Univ.-Prof. Dr. Eckhard Wolf

Gedruckt mit Genehmigung der Tierärztlichen Fakultät

der Ludwig-Maximilians-Universität München

Dekan:	Univ.-Prof. Dr. Reinhard K. Straubinger, Ph.D.
Berichterstatter:	Prof. Dr. Elisabeth G. Kemter
Korreferent:	Univ.-Prof. Dr. Laurent Frantz

Tag der Promotion: 06. Juli 2024

Für meine Familie

TABLE OF CONTENTS

INDEX OF ABBREVIATIONS

A2UCOE	autonomously replicating sequence with universal chromatin opening element
AAVS1	adeno-associated virus integration site 1
ACE	anterior chamber of the eye
ACTB	beta-actin
ADCC	antibody-dependent cellular cytotoxicity
AHXR	acute humoral xenograft rejection
AIs	allogeneic islets
APCs	antigen-presenting cells
APIs	adult porcine islets
B4GALNT2	β-1,4-N-acetyl-galactosaminyl transferase 2
B4GALNT2L	B4GALNT2-like
BAC	bacterial artificial chromosome
BCR	B cell receptor
BSA	bovine serum albumin
CAG	chicken β-actin
CaM	calmodulin
Cas	CRISPR-associated proteins
CCL2	C-C motif chemokine ligand 2
CEP112	centrosomal protein 112
CGM	continuous glucose sensors
CIITA-DN	human dominant-negative mutant class II transactivator
CiMM	center for innovative medial models
CMAH	cytidine monophosphate-N-acetylneuraminic acid hydroxylase
COL1A1	collagen type I alpha 1 chain
CPRPs	complement pathway regulatory proteins
CRISPR	clustered regularly interspaced short palindromic repeats
CTLA4-Ig	cytotoxic T-lymphocyte antigen 4-immunoglobulin
CXCL10	C-X-C motif chemokine ligand 10
CXR	cellular xenograft rejection
DAF	decay-accelerating activator
DAMPs	damage-associated molecular patterns
DM	diabetes mellitus
DNA	deoxyribonucleic acid
DPF	designated-pathogen-free

DXR	delayed xenograft rejection
ECL	enhanced chemiluminescence
eGFP	enhanced green fluorescent protein
EPCR	endothelial protein C receptor
EPIs	embryonic islets
Epo	electroporation
ET	embryo transfer
FACS	fluorescence activated cell sorting
FcRs	Fc receptors
FI	fluorescence imaging
for	forward
FPIs	foetal porcine islets
FVIIa	coagulation factor VIIa
GAPDH	glyceraldehyde-3-phosphate dehydrogenase
gDNA	genomic deoxyribonucleic acid
GFP	green fluorescent protein
GGTA1	α-1,3- galactosyltransferase
gm	genetic modifications
gRNA	guide-ribonucleic acid
GSIS	a glucose-stimulated insulin secretion
HA	homology arm
HAR	hyperacute rejection
HBSS	Hanks buffered salt solution
hC1-INH	human complement-regulatory protein C1 inhibitor
hCD31	human cluster of differentiation 31
hCD39	human ectonucleoside triphosphate diphosphohydrolase-1
hCD46	human membrane cofactor protein
hCD47	human cluster of differentiation 47
hCD55	human decay-accelerating factor
hCD59	human membrane inhibitor of reactive lysis
hCD73	human ecto-5′-nucleotidase
hCIITA-DN	human dominant-negative mutant class II transactivator
hCTLA4-Ig	human cytotoxic T-lymphocyte associated protein 4
HDR	homology directed repair
hEPCR	human endothelial protein C receptor
hESC	human embryonic stem cells
het	heterozygous

hHO-1	human heme oxygenase 1
hHT	human 1,2- fucosyltransferase
HIAR	heat-induced antigen retrieval
HLA	human leukocyte antigen
HO-1	heme oxygenase-1
hPD-L1	human programmed cell death ligand 1
hPSC	pluripotent stem cells
hTM	human thrombomodulin
i.p.	intraperitoneal
IAP	integrin-associated protein
IBMIR	instant blood-mediated inflammatory reaction
IFN-γ	interferon-gamma
IgG	immunoglobulin G
IHC	immunohistochemistry
IL-1β	Interleukin 1 beta
IL8	interleukin 8
INS	insulin
IP-10	inducible protein 10
IPGTT	intraperitoneal glucose tolerance test
iRFP	infrared fluorescent protein
KO	knockout
LEA29Y	lymphocyte-associated antigen 29Y
LMW-DS	Low molecular weight dextran sulfate
MAC	membrane attack complex
MCP	membrane cofactor protein
MCP1	macrophage chemotactic protein 1
MFI	mean fluorescence intensity
MHC	major histocompatibility complex
MSOT	multispectral optoacoustic tomography
n.a.	not analyzed
Nabs	natural antibodies
NETs	neutrophil extracellular traps
Neu5Gc	N-glycolylneuraminic acid
NF-κB	nuclear factor kappa B
NHEJ	non-homologous end joining
NHPs	non-human primates
NK cells	natural killer cells

NPIs	neonatal islets
NSG	NOD-scid Il2rγnull
PCR	polymerase chain reaction
pCTLA4-Ig	porcine CTLA4-Ig transgene
PCV2	porcine circovirus type 2
PD-1	programmed cell death protein 1
Pdx1	pancreatic and duodenal homeobox 1
PECAM1	platelet EC adhesion molecule 1
PFA	paraformaldehyde
pH11	porcine Hipp11
PICs	proinflammatory cytokines
PIs	porcine islets
PKCs	porcine kidney cells
RE	restriction enzyme
rev	reverse
RNP	ribonucleoprotein
ROS	reactive oxygen species
RT	room temperature
SCC	single cell clone
SCNT	somatic cell nuclear transfer
sCR1	soluble complement receptor 1
SC-β-cells	stem cell-derived β-cells
SDS-page	Sodium dodecyl sulphate-polyacrylamide gel electrophoresis
shTNFRI-Fc	soluble human TNFRI-Fc
SIRPα	signal regulatory protein alpha
SLA	swine leukocyte antigen
sTNFR	soluble TNF-α receptor
T1DM	type 1 diabetes mellitus
T2DM	type 2 diabetes mellitus
TAT	thrombin-antithrombin
TBM	thrombomodulin
TCRs	T cell receptors
TF	tissue factor
TFPI	tissue factor pathway inhibitor
tg	transgene
TLA	targeted locus amplification
TLRs	Toll-like receptors

TNFAIP3	tumor necrosis factor α–induced protein 3
TNF-α	tumor necrosis factor-alpha
TRAIL	tumor necrosis factor-related apoptosis-inducing ligand
WA	Withaferin A
WB	western blot
WT	wild-type
XTx	xenotransplantation
α-Gal	galactose-α-1,3-galactose
β2M	beta 2-microglobulin

I. INTRODUCTION

Type 1 diabetes (T1DM) is one of the most common metabolic and endocrinological diseases in children and adolescents worldwide, due to autoimmune destruction of the insulin-producing pancreatic β-cells (DOVI et al., 2022) and the incidence is expected to continuously rise (GREGORY et al., 2022). Treatment for T1DM requires lifelong administration of exogenous insulin to delay the onset of long-term complications. Although insulin therapy is the predominant standard of care, it cannot fully replicate the natural pattern of insulin secretion by the pancreas (WALKER et al., 2021; BORNSTEIN et al., 2022), increasing the risk of severe hypoglycemia leading to hypoglycemic coma, especially for patients with brittle diabetes (LIN et al., 2020). For these patients, β-cell replacement therapy is a superior therapeutic option (WALKER et al., 2021). Allotransplantation of either whole pancreas or isolated pancreatic islets is a potential treatment option for T1DM. However, the current supply of organ donors falls short of meeting clinical demand. Porcine islet xenotransplantation is a promising alternative to overcome the shortage of organ donors (EISENSON et al., 2022). For successful application of islet xenotransplantation, the graft will require depletion of genes as well as integration of robustly expressed xenoprotective transgenes (KEMTER et al., 2020). Advancements in genetic engineering offer new opportunities to overcome graft rejection and to improve their engraftment and insulin secretion capacity (KEMTER et al., 2018). By advancing our understanding of xenogeneic islet graft physiology and refining techniques for donor pig genome modification, this research will help to pave the way for enhanced efficacy and safety in the application of porcine islet xenotransplantation as a viable therapeutic strategy for individuals with Type 1 diabetes.

To address current hurdles in islet xenotransplantation, this study focused on generating, characterizing, and optimizing genetically multi-modified islet donor pigs with a robust and predictable transgene expression pattern, while also ensuring that no segregation of genetic modifications occurs during breeding. A further objective of this study was the generation and characterization of a new reporter pig model for monitoring intracellular calcium dynamics that will provide comprehensive insights into the functionality and maturity of β-cells pre- and post-transplantation.

II. REVIEW OF THE LITERATURE

1. Islet transplantation to cure diabetes mellitus

Diabetes mellitus (DM) is one of the most prevalent medical conditions that demand an improved medical treatment. More than 500 million people are diabetic globally and the number is projected to reach 695 million by the year 2045 (CAYABYAB et al., 2021; BORNSTEIN et al., 2022). Along with disrupted pancreatic endocrine function, diabetes can lead to severe complications like nephropathy, cardiovascular diseases, retinopathy, and neuropathy (SHAH et al., 2020; TAN et al., 2020; CAYABYAB et al., 2021; KRENTZ et al., 2021; SAMSU, 2021). Two vastly agreed pathophysiologies of diabetes include pancreatic β-cell destruction in the case of T1DM, and insulin resistance and insulin secretory defects in the case of type 2 DM (T2DM) (SAKRAN et al., 2022). The patients with T1DM are 5-10% of the total diabetic population (BORNSTEIN et al., 2022) and the incidence is expected to rise rapidly (GREGORY et al., 2022). Currently, insulin therapy is the life-saving treatment for T1DM but it does not emulate some of the important functional aspects of pancreatic β-cells, in particular, the physiological kinetics of insulin release in response to glucose, the first-pass hepatic insulin extraction (WALKER et al., 2021; BORNSTEIN et al., 2022), and the intercellular crosstalk between β- and α-cells within the pancreatic islets that is critical for metabolic regulation (WALKER et al., 2021). The development of rapidly acting insulin analogues, novel insulin pump systems, and continuous glucose sensors (CGM) in the interstitial fluid (semi-closed-loop artificial pancreas) which control insulin by highly sophisticated algorithms have significantly improved clinical diabetes care. Although these novel devices increased time in target glucose ranges, high-quality observational data are lacking (FUCHS & HOVORKA, 2021). There are still many challenges for patients with T1DM to achieve treatment goals and prevent complications (COCHA et al., 2021; DERMAWAN & KENICHI PURBAYANTO, 2022; TEMPLER, 2022). With the current hybrid closed-loop systems, the users are still required to control the continuity of the subcutaneous catheters, validate CGM blood glucose data in case of potential sensor inaccuracy problems, calculate the carbohydrate intake, and provide information to the device for planned physical activities. Psychological aspects, including dislike of having the closed-loop system permanently connected to the body or disturbance of daily life by frequent alarm messages, also remain a barrier (FUCHS & HOVORKA, 2021). A fully closed-loop system, which can overcome the requirement for user input, or fully implanted devices are far away from reality (TEMPLER, 2022). Importantly, 25% of T1DM patients exhibit hypoglycaemia unawareness, and insulin therapy can result in severe

hypoglycaemia leading to hypoglycaemic coma (LIN et al., 2020). For those patients, β-cell replacement therapy is a superior therapeutic option (WALKER et al., 2021). According to recent data, up to 5 million diabetic patients globally would need β-cell replacement therapy (KRENTZ et al., 2021). Allotransplantation of whole pancreas or isolated pancreatic islets is a potential treatment option for T1DM. Despite improved outcomes over the years, whole pancreas transplantation is not widely performed as it is a highly invasive procedure (KOCHAR & JAIN, 2021) and needs lifelong maintenance of immunosuppression (NELSON et al., 2022). Allogeneic islet transplantation into the portal vein, according to the Edmonton protocol, is the most common clinical approach for β-cell replacement therapy (BORNSTEIN et al., 2022). The majority of islets are lost during/after transplantation into the portal vein, and often more than one pancreas is needed to obtain sufficient islet mass for one recipient (KOCHAR & JAIN, 2021). The insufficient availability of human pancreata or islets due to a limited number of suitable human donors is also a major obstacle in allotransplantation **(Figure 1)**.

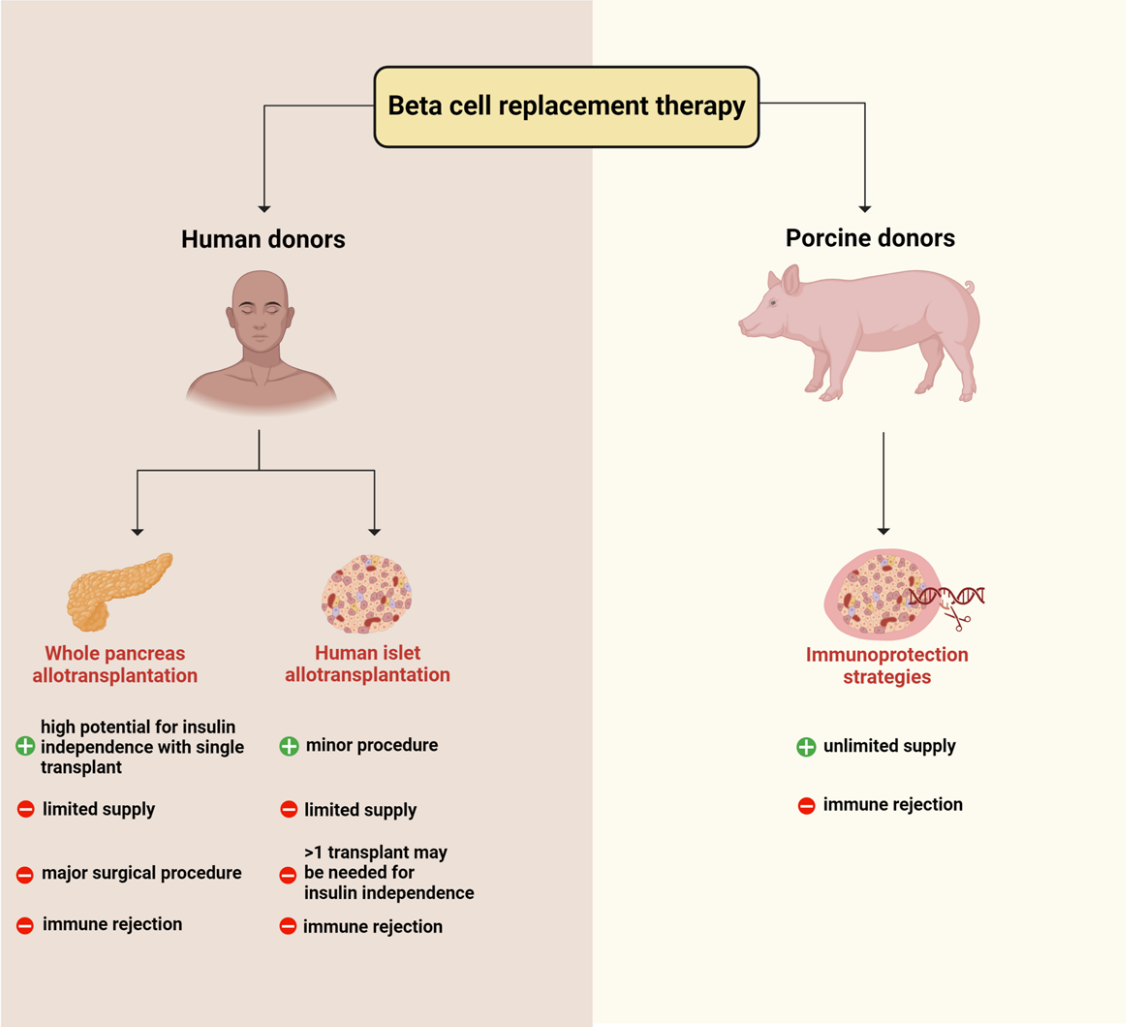

Figure 1: Possible action lines for β-cell replacement therapy.

Whole human pancreas or pancreatic islet allotransplantation are potential biological treatment options for T1DM. However, the main hurdles are the insufficient availability of human pancreata or islets and allograft rejection control by immunosuppressive drugs. Porcine donors can be an alternative islet source for transplantation into humans. Immune rejection of the xenogeneic islets is the main barrier in pig-to-human xenotransplantation. Immunoprotection approaches include genetic modifications of the donor. Created with BioRender.com.

Insulin-producing β-cells derived from human embryonic stem cells (hESC) or other human pluripotent stem cells (hPSC) can provide an unlimited supply for β-cell replacement therapy and are an attractive alternative to islet allotransplantation (reviewed in BARTOLOMÉ, 2022; HOGREBE et al., 2023; SHILLEH & RUSS, 2023). However, stem cell-derived β-cells (SC-β-cells) can be functionally immature and their glucose-stimulated insulin-secreting ability is lower compared to endogenous islets (SHAHJALAL et al., 2018; BARTOLOMÉ, 2022). Although significant progress has been made in gaining *in vitro* functional maturity of

SC-β-cells (VELAZCO-CRUZ et al., 2020), upon engraftment, a substantial mass of SC-β-cells can be lost potentially due to transdifferentiation and dedifferentiation into other cell types, or cell death (SHAHJALAL et al., 2018). Porcine pancreatic islets are another potential source of insulin-producing cells (COWAN, 2022). As porcine insulin differs from human insulin only in one amino acid (alanine instead of threonine at the carboxy terminus of the B chain) and is active in humans, porcine islet xenotransplantation is a reasonable option for β-cell replacement therapy (COWAN, 2022). Porcine islets (PIs) of different developmental stages, i.e., embryonic (EPIs), foetal (FPIs), neonatal (NPIs), and adult (APIs), have been tested for xenotransplantation (MOU et al., 2022). Considerable long survival times have been achieved in preclinical trials (up to >603 days) by transplanting wild-type (WT) porcine islets into immunosuppressed non-human primates (NHPs) **(Table 1)**. Although encouraging, the results of these studies were highly variable and many of the immunosuppressive regimens used are not clinically applicable.

Table 1: Use of WT porcine xenoislets in NHPs

Islets	Recipient NHPs	Immunosuppression regimen	Survival	References
NPI	Rhesus monkey	ATG + CVF + rapamycin + anti-TNF + anti-CD154 (+Treg)	>603 days	(SHIN et al., 2015)
NPI	Rhesus monkey	CTLA4-Ig + rapamycin + basiliximab + anti-CD154	>260 days	(CARDONA et al., 2006)
NPI	Rhesus monkey	CTLA4-Ig + rapamycin + anti-IL-2R + anti-CD40	>203 days	(THOMPSON et al., 2011b)
API	Cynomolgus monkey	Rapamycin + FTY720 + basiliximab + anti-CD154	>187 days	(HERING et al., 2006)
NPI	Rhesus monkey	anti-IL-2R + anti-CD154 + belatacept + rapamycin	>187 days	(RUSSELL et al., 2007)
NPI	Rhesus monkey	MMF + CTLA4-Ig + LFA-3-Ig + anti-IL-2R + anti-LFA-1	114 days	(THOMPSON et al., 2012)

NPI – Neonatal porcine islets; API – Adult porcine islets

2. Immunological barriers in islet xenotransplantation

The major hurdle in using porcine islets for β-cell replacement therapy in humans is the rejection of xenogeneic islets by the recipient's immune system. Components of both the innate and adaptive immune systems are activated by the xenogeneic cells or molecules, leading to xenograft rejection (KANAK et al., 2014). One key factor is the inter-species incompatibility of immune regulatory molecules. In general, xenograft rejection can be categorized as: (i) hyperacute rejection (HAR) that occurs within 24 hours post-transplantation; (ii) delayed

xenograft rejection (DXR) that occurs within days to weeks post-transplantation; and (iii) chronic rejection that occurs months to years after xenotransplantation. DXR may be caused by acute humoral xenograft rejection (AHXR), cellular xenograft rejection (CXR), and coagulation dysregulation (ZHOU et al., 2022). HAR and AHXR are primarily due to the interaction of naturally occurring antibodies in humans and NHPs with porcine xenoantigens (ZHOU et al., 2022). CXR involves both innate immune cells (macrophages, NK cells, and neutrophils) and adaptive immune cells (B cells and T cells). If the islets are infused into the portal vein (according to the most widely used clinical procedure for islet allotransplantation), they come in direct contact with the recipient's blood, which may trigger an instant blood-mediated inflammatory reaction (IBMIR) with kinetics similar to HAR (ZEYLAND et al., 2015; KANAK et al., 2019). IBMIR is responsible for the majority of peri-transplant islet loss (KALE & ROGERS, 2023). At other transplantation sites, such as intraperitoneal or under the kidney capsule, a local inflammatory response is initiated by proinflammatory cytokines and "danger" signals released by the islets upon ischemic damage (WANG et al., 2021). IBMIR and local inflammation involve the recruitment of innate and adaptive immune cells, which can cause further damage and subsequent xenograft rejection (EISENBARTH, 2019). Different strategies are used to evade the host's immune reaction against the xenograft, such as genetic engineering of the donor pigs.

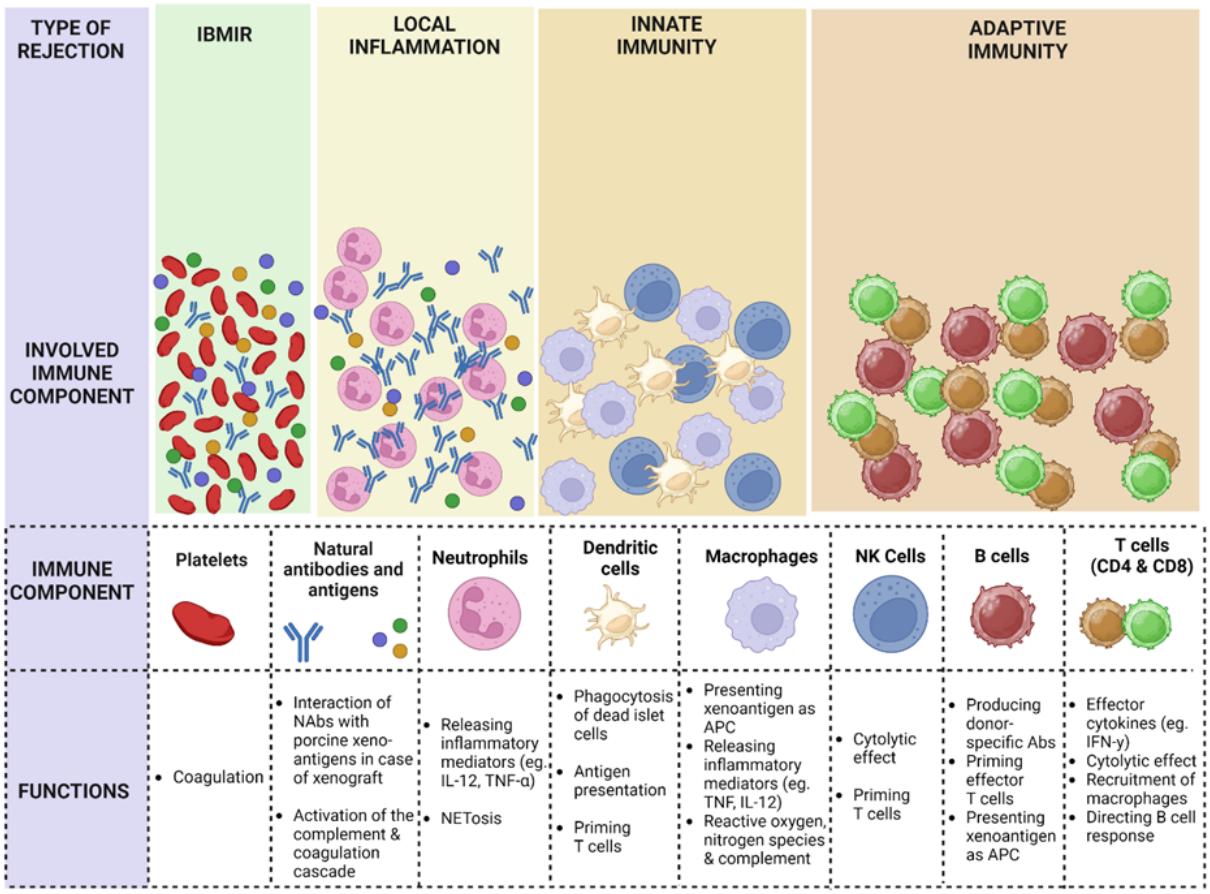

Figure 2: Sequence of host immune responses to islet grafts and the components of the immune system involved at each step.

The immune responses include IBMIR, local inflammation, innate immune response, and adaptive immune response (modified from WANG et al., 2021). Created with BioRender.com.

3. Pharmacological inhibition of the instant blood-mediated inflammatory reaction (IBMIR)

More than 50% of the islets infused into the portal circulation are lost during the peri-transplant period due to IBMIR (RAJESWAR et al., 2020; HU et al., 2022) an innate immune response observed in autologous, allogeneic, as well as xenogeneic islet transplantation directed to the islets which are initially free-floating in small liver veins. IBMIR involves the activation of complement and coagulation pathways, the activation and aggregation of platelets, the release of chemokines and proinflammatory cytokines, and the infiltration of innate immune cells such as dendritic cells, neutrophils, and monocytes **(Figure 2)** (KANAK et al., 2014; RAJESWAR et al., 2020). Free human or porcine islets exhibit elevated expression of tissue factor (TF), interleukin 8 (IL8), and macrophage chemotactic protein 1 (MCP1) (KANAK et al., 2019). The coagulation reaction is triggered by TF, and the peak thrombin-antithrombin (TAT) complex

can be detected on islets as early as 15 minutes after 6 autologous islet infusion. MCP1 and IL8 mediate the recruitment of innate immune cells within 3 hours after the islets interact with the recipient's blood (KANAK et al., 2019; VON ZUR-MUHLEN et al., 2019). Additionally, thrombin can also enhance immune cell recruitment into the transplanted islets (ESTRADA et al., 2015). The activated immune cells release cytokines and chemokines which further amplify the immune response against the xenograft (ESTRADA et al., 2015). Interleukin 1 beta (IL-1β) and tumor necrosis factor-alpha (TNF-α) damage the islets through nuclear factor kappa B (NF-κB)-mediated apoptosis (KANAK et al., 2019). Additional proinflammatory cytokines and damage-associated molecular patterns (DAMPs) released by the damaged islets can further increase the local inflammation and the recruitment and activation of immune cells (WANG et al., 2021). Dendritic cells phagocytose dead or damaged islet cells and present alloantigens or xenoantigens on their surface, resulting in the priming of $CD8^+$ and $CD4^+$ T cells (EISENBARTH, 2019). Various strategies have been tested to reduce the peri-transplant islet loss due to IBMIR. TF on the islet cells is the main trigger of IBMIR and blocking TF by specific monoclonal antibodies or using active site-inactivated coagulation factor VIIa (FVIIa) abrogated IBMIR *in vitro* (MOBERG et al., 2002). Site-inactivated FVIIa binds to TF but does not initiate coagulation, hence indirectly blocking the TF. Johansson et al. (JOHANSSON et al., 2005) showed that Ro69, a selective FVIIa inhibitor, alleviates IBMIR in a dose-dependent manner, and blocks the generation of FVIIa-TT as well as TAT complex formation on isolated islets *in vitro*. Similarly, the antioxidant nicotinamide inhibited TF and MCP1 in isolated human pancreatic islets *in vitro* (MOBERG et al., 2003). Another effective approach to alleviate IBMIR is blocking the inflammatory mediators. For instance, the blockade of IL-1β alone by anakinra or double blockade of IL-1β and TNF-α by anakinra and etanercept during the peri-transplant period improved the outcomes of preclinical islet transplantation studies (MCCALL et al., 2012; NAZIRUDDIN et al., 2018). Similarly, blocking NF-κB by Withaferin A (WA) improved syngeneic islet survival and transplant outcomes in a mouse model (SORELLE et al., 2013). WA also reduced the level of pro-inflammatory cytokines and infiltration of immune cells into islets in an *in vitro* model of IBMIR (KANAK et al., 2014). Another important molecule in IBMIR is interferon-gamma (IFN-γ) inducible protein 10 (IP-10 alias C-X-C motif chemokine ligand 10, CXCL10) which has been shown to elevate in the serum of islet recipients in clinical trials. Using islets from *Cxcl10* KO mice or blocking IP-10 using monoclonal antibodies significantly improved syngeneic islet graft survival *in vivo* (YOSHIMATSU et al., 2017). Exogenous administration of activated protein C, an anticoagulant enzyme, exhibited anti-inflammatory and anti-apoptotic effects and protected

transplanted islets in diabetic mice (CONTRERAS et al., 2004), but its efficiency in clinical studies remains undetermined. Recently, Yao et al. (2021) demonstrated that cibinetide, a non-hematopoietic erythropoietin analogue, protected human islets and alleviated IBMIR both *in vitro* and post-transplantation in mice. Similarly, α-1 antitrypsin, a serine protease inhibitor, inhibited IBMIR and improved the engraftment of human islets following intraportal transplantation in mice (WANG et al., 2017). Low molecular weight dextran sulphate (LMW-DS) has been shown to alleviate IBMIR and increase islet engraftment and survival in a dose-dependent fashion (GOTO et al., 2004; VON ZUR-MUHLEN et al., 2019), and a high dose of LMW-DS eliminated leukocyte infiltration and increased pig islet survival in diabetic mice (GOTO et al., 2004). IBMIR can also be alleviated by combined administration of high doses of heparin and soluble complement receptor 1 (sCR1), a recombinant complement inhibitor (TAKAKI & SHIMODA, 2020). Many of the above-described strategies have yet to be tested in clinical studies, and using heparin is the current standard practice to prevent IBMIR in clinical islet transplantation. IBMIR can be more severe in xenogeneic compared to allogeneic and autologous islet transplantation (KANAK et al., 2014). In addition to the presence of TF, IL8, and MCP1, porcine islets express the oligosaccharides galactose-α-1,3-galactose (α-Gal), N-glycolylneuraminic acid (Neu5Gc) and Sda, commonly known as xenoantigens (COWAN, 2022; FENG et al., 2022). Therefore, porcine islets encounter a very strong host immune response in humans and NHPs (BOTTINO & TRUCCO, 2015; RAJESWAR et al., 2020). Genetically modifying donor pigs to address the molecular incompatibilities is a potent approach to improve the survival and efficacy of islet xenografts.

4. Genetic Modification of Islet Source Pigs

For pig-to-NHP or pig-to-human islet xenotransplantation, various genetic modifications have been suggested to overcome IBMIR and subsequent rejection mechanisms.

4.1. Eliminating the porcine xenoantigens

Natural antibodies (NAbs) in humans and NHPs are a major obstacle in islet engraftment and a major trigger for IBMIR against the porcine islets. The three most studied oligosaccharide xenoantigens present on porcine cells, but absent in humans and partially also in NHPs, are α-Gal, Neu5Gc, and Sda (COWAN, 2022; FENG et al., 2022). The enzymes involved in the synthesis of α-Gal, Neu5Gc, and Sda are α-1,3- galactosyltransferase (GGTA1), cytidine monophosphate-N-acetylneuraminic acid hydroxylase (CMAH), and β-1,4-N-acetyl-galactosaminyl transferase 2 (B4GALNT2)/B4GALNT2-like (B4GALNT2L), respectively

(BYRNE et al., 2015). Humans have pre-formed NAbs against the three major xenoantigens, NHPs have only preformed antibodies against α-Gal and Sda, which makes the immune response against porcine xenografts more severe compared to allografts (KEMTER et al., 2020; COWAN, 2022). NAbs are classified as innate immune components produced in response to some ligands in the normal human flora (GALILI, 2013; HUAI et al., 2016). Anti-α-Gal NAbs are among the most abundant immunoglobulins in human blood and constitute 1-4% of the circulating immunoglobulins. In contrast, the levels of anti-Neu5Gc and anti-Sda are variable in humans and hence their relevance to xenotransplantation is less defined compared to anti-α-Gal antibodies (COWAN, 2022; SYKES & SACHS, 2022). Soon after the islets encounter the host blood, the interaction between xenoantigens and NAbs rapidly activates the complement system (YAN et al., 2022). Complement activation leads to the formation of the C5b- 9 complex, as well as the production of chemoattractants, C3a and C5a, causing infiltration of macrophages and neutrophils (YAN et al., 2022). The result of complement activation is the formation of the membrane attack complex (MAC) which is deposited in the cellular lipid bilayer and leads to graft rejection due to cell lysis and death (TJERNBERG et al., 2008; YAN et al., 2022). Eliminating the porcine xenoantigens by knocking out the genes involved in their synthesis can improve xenoislets' engraftment and survival in NHP preclinical trials **(Table 2)**. α-Gal has a strong presence on NPIs but only a weak expression on APIs (RAYAT et al., 2003). Intraportal transplantation of NPIs in immunosuppressed diabetic rhesus monkeys revealed that *GGTA1*-KO NPIs had an elongated survival time of up to 249 days compared to WT NPIs (up to 137 days) (THOMPSON et al., 2011a). Moreover, the primary nonfunction rate for *GGTA1*-KO NPIs was reduced to 20% compared to 80% for WT NPIs (THOMPSON et al., 2011a). Martin et al. (2015) reported that both WT and *GGTA1*-KO NPIs transplanted into separate liver lobes of the same nondiabetic rhesus monkey (dual-islet transplant model) triggered a surprisingly similar host immune reaction at 1 and 2 hours post-transplantation. Additionally, there was an extensive deposition of platelets, antibodies, and complement and infiltration of macrophages and neutrophils (MARTIN et al., 2015). Samy et al. (2018) compared the host immune response against WT and *GGTA1*-KO xenogeneic NPIs to that against allogeneic islets (AIs) in the dual-islet model in the rhesus monkey. The host immune response against the xenogeneic WT NPIs was more robust compared to that against allogeneic islets. Moreover, despite better post-transplantation engraftment, *GGTA1*-KO NPIs also showed increased antibody deposition and immune cell infiltration compared to AIs (SAMY et al., 2018). These studies demonstrated that IBMIR is more intense in xenogeneic compared to allogeneic settings. Moreover, although it improved

the engraftment of NPIs, the desired graft survival duration was not achieved with only the *GGTA1*-KO, suggesting that eliminating more xenoantigens might be required. Neu5Gc is found on neonatal, juvenile as well as adult porcine islets (LEE et al., 2016; TECTOR et al., 2020). Due to the presence of a functional *CMAH* gene in NHPs (SPRINGER et al., 2014), the studies investigating Neu5Gc elimination are mostly limited to *in vitro* models. The reports about the ability of Neu5Gc to generate an immune response in humans are contradictory. The *in vitro* comparison of islets from genetically modified (gm) pigs that differed only in *CMAH*-KO (*GGTA1*-KO/*CMAH*-KO/hCD46-tg vs. *GGTA1*-KO/hCD46-tg) revealed that the absence of Neu5Gc on islet cells did not change the antibody binding (LEE et al., 2016). When transplanted into humans for early clinical trials, WT NPIs generated a dominant anti-α-Gal response as well as an anti- Neu5Gc response at least in some of the recipients (GROTH et al., 1994; BLIXT et al., 2009). Very little information is available on the expression of Sda in porcine islets and the effect of Sda elimination on the immunogenicity of the xenoislets (BYRNE et al., 2018). However, an *in vitro* study has shown that the human-anti-pig antibody binding is significantly reduced by α-Gal deletion (*GGTA1*-KO), and this reduction is further amplified by Neu5Gc deletion (*CMAH*-KO) and Sda deletion (*B4GALNT2*-KO) (MARTENS et al., 2017). Moreover, NHPs have some additional NAbs that can recognize a currently unidentified xenoantigen on the porcine cells (the fourth antigen) (ESTRADA et al., 2015). Hence, based on the studies from the currently identified xenoantigens, the knockout of 3 genes responsible for porcine xenoantigens production (3KO) is a desired genetic modification for successful xenotransplantation into humans (LADOWSKI et al., 2019).

4.2. Inhibition of complement activation

The exposure of the xenograft to NAbs triggers the activation of the complement system via both classical as well as alternative pathways (KEMTER et al., 2018; YAN et al., 2022). Complement activation is partly regulated by the complement pathway regulatory proteins (CPRPs) including membrane cofactor protein (MCP/CD46), decay-accelerating activator (DAF/CD55), and membrane inhibitor of reactive lysis (CD59) (LU et al., 2022). Once activated, the complement pathways merge at C3 which is then converted into C3a and C3b (ZHOU et al., 2019). CD55 accelerates the decay of the C3 convertase and the C5 convertase, and CD46 is involved in the inactivation of both C3b and C4b. Whereas, CD59 prevents the polymerization of C9 and its insertion into the membrane attack complex (MAC) (GELLER & YAN, 2019). As porcine CPRPs are not effective in the human complement pathway, the transgenic expression of human CPRPs in gm donor pigs is required to inhibit host complement activation and support xenograft survival after pig-to-human xenotransplantation

(MIYAGAWA et al., 2022). To evaluate the expediency of hCD46 in intraportal islet xenotransplantation, APIs from WT, hCD46-tg, or *GGTA1*-KO pigs were transplanted into immunosuppressed diabetic monkeys, and the release of porcine C-peptide was used as an indicator of early xenograft injury (VAN DER WINDT et al., 2009). Although the degree of IBMIR was not reduced by hCD46-tg expression, hCD46-tg APIs facilitated a longer survival time and longer insulin independence duration of 87–396 days compared to 5–36 days in the case of WT APIs. In contrast, *GGTA1*-KO APIs showed a similar performance as WT APIs, consistent with the fact that APIs have anyway low α-Gal levels. Hence, hCD46-tg expression or *GGTA1*- KO alone was not sufficient to attenuate IBMIR, but hCD46-tg expression increased the APIs' survival time (VAN DER WINDT et al., 2009). Hawthorne et al. (HAWTHORNE et al., 2014) reported that gm NPIs (*GGTA1*-KO/hCD55-tg/hCD59-tg/human 1,2-fucosyltransferase (hHT)-tg) showed minimal signs of IBMIR and an absence of thrombosis compared to WT NPIs which were lost within hours after transplant due to immense IBMIR. A similar conclusion was drawn in another study that compared *GGTA1*-KO/hCD46-tg APIs with WT or hCD46-tg APIs (BOTTINO et al., 2014). In both studies, the genetic modifications prevented IBMIR, however, the long-term survival of the islets was not achieved due to a cellular immune response (BOTTINO et al., 2014; HAWTHORNE et al., 2014). Moreover, the *in vitro* incubation of *GGTA1*-KO/hCD46-tg NPIs with whole human blood reduced complement activation but accelerated coagulation compared to WT NPIs (NAGARAJU et al., 2015). Recently, two different preclinical trials were conducted in the dual-islet transplantation model of the rhesus monkey to compare *GGTA1*-KO/hCD46-tg with *GGTA1*-KO NPIs (SAMY et al., 2019; SONG et al., 2021). No significant difference was found in the deposition of platelets and antibodies, complement activation, and neutrophil infiltration at 1 h post-transplantation. At 24 h post-transplantation, however, platelet deposition and neutrophil infiltration were significantly lower in *GGTA1*-KO/hCD46-tg NPIs and there was no difference in the antibody deposition and complement activation (SAMY et al., 2019). A possible explanation of antibody deposition and complement activation in these studies is the presence of other xenoantigens. This further reaffirms the idea of knocking out additional xenoantigens and expressing human CPRPs to counteract IBMIR. Moreover, the presence of platelet aggregation and coagulation activation highlights the requirement of intercepting the coagulation pathway as well.

4.3. Prevention of coagulation dysregulation

In the preclinical trial of NPIs xenotransplantation into the rhesus monkeys, hCD46-tg expression in the NPIs had no or a moderate effect on the coagulation pathway (NAGARAJU et al., 2015; SONG et al., 2021), indicating the need for additional genetic modification to alleviate coagulation activation. In normal physiological conditions, thrombomodulin (TBM) binds thrombin and changes its substrate specificity from coagulation factors such as fibrinogen to protein C, hence generating an anticoagulation effect (ROUSSEL et al., 2008). Although not reported, likely the porcine islets do not express TBM (COWAN, 2022). Additionally, the porcine TBM-human thrombin complex cannot efficiently activate human protein C (ROUSSEL et al., 2008). Therefore, the expression of hTBM-tg in porcine islets could be useful in inhibiting the coagulation pathway. Other genes of interest to modulate the human coagulation pathway are the endothelial protein C receptor (EPCR), tissue factor pathway inhibitor (TFPI), and the thromboregulatory enzyme CD39 (COWAN, 2022). The incubation of islets from hCD39-tg mice with human blood significantly delayed the coagulation time compared to WT mouse islets (DWYER et al., 2006). In contrast, when incubated with human blood, no difference in coagulation time was observed between *GGTA1*-KO/hCD46-tg/hCD39-tg NPIs and *GGTA1*-KO/hCD46-tg NPIs (NAGARAJU et al., 2015). By transplanting gm APIs (*GGTA1*-KO/hCD46-tg/hTFPI-tg/CTLA4-Ig or *GGTA1*-KO/hCD46-tg/hCD39- tg/hTFPI-tg/CTLA4-Ig) into immunosuppressed diabetic cynomolgus monkeys, it has been shown that, at 2 h post-transplantation, IBMIR was significantly lower against gm APIs compared to WT or hCD46- tg APIs (BOTTINO et al., 2014). However, the long-term survival of APIs was highly variable (BOTTINO et al., 2014), suggesting the need for further studies and preclinical trials to find a suitable set of genetic modifications.

4.4. Anti-inflammatory strategies

The expression of transgenes to reduce inflammatory responses has also been suggested. For instance, the ubiquitin-editing enzyme A20 is a natural suppressor of islet inflammation, and hA20-tg NPIs reduced islets' inflammatory response by inhibiting the activation of NF-κB by TNF-α, *in vitro* (ZAMMIT et al., 2021). When transplanted in the immunodeficient mice, hA20-tg NPIs had improved function and elongated survival (ZAMMIT et al., 2021). Soluble TNF-α receptor (sTNFR) and heme oxygenase-1 (HO-1) are also antiinflammatory molecules, and APIs from both sTNFR-tg or HO-1-tg pigs reduced the infiltration of host immune cells and increased survival time post-transplantation in mice (LEE et al., 2015; YAN et al., 2016).

4.5. Modulating the innate cellular immune response

4.5.1. Macrophages

The innate cellular immune reaction against the xenograft is driven mainly by macrophages, natural killer (NK) cells, and neutrophils **(Figure 3)**. Macrophages were reported to be among the first immune cells to infiltrate the porcine islet graft transplanted in a rodent model (HU et al., 2022) and are involved not only in CXR but also in NAb-mediated HAR and DXR (CADILI & KNETEMAN, 2008). The infiltration of macrophages into the xenograft is triggered by C3a and C5a chemoattractants (YAN et al., 2022), MCP1 (also known as C-C motif chemokine ligand 2 (CCL2)) (EHRNFELT et al., 2004; MOK et al., 2019), CCL3 (MIP-1α), CCL4 (MIP-1β), and CCL5 (RANTES) (MOK et al., 2019). After xenogeneic islet cell transplantation, macrophages can be activated by: (i) the interaction between antigen-antibody immune complexes with Fc receptors (FcRs) on macrophages (FOX et al., 2001; MAEDA et al., 2022); (ii) the interaction between galectin-3, an abundant molecule on macrophages, and α-Gal on porcine cells (MAEDA et al., 2022), (iii) the interaction with other immune cells infiltrating into the xenograft, such as neutrophils, NK cells, and Th1 cells (JIN et al., 2006; GREENWALD et al., 2009); and (iv) the interaction between DAMPs released by the damaged islets and Toll-like receptors (TLRs) (XU et al., 2002). Macrophages destroy the xenograft either through their direct cytotoxic effect or by facilitating the recruitment of T cells (FOX et al., 2001; CADILI & KNETEMAN, 2008). The direct cytotoxic effect of macrophages is exerted by the secretion of proinflammatory cytokines such as IL1, IL6, and TNF-α, and reactive oxygen species (ROS) (EL-OUAGHLIDI et al., 1999). Upon contact with the xenoislets, macrophages function as antigen-presenting cells (APCs) to generate Th1 and Th17 cells, facilitating the recruitment of $CD4^+$ and $CD8^+$ T cells into the xenograft (FOX et al., 2001; YI et al., 2003). Macrophages differentiate between self and non-self cells through an inhibitory signaling pathway (IDE et al., 2007). The first protein in this signaling pathway is the cluster of differentiation 47 (CD47), also known as integrin-associated protein (IAP), which is a “marker of self” (OLDENBORG et al., 2000). The second protein, which acts as a CD47 receptor, is the signal regulatory protein alpha (SIRPα) expressed on macrophages and neutrophils (GITIK et al., 2011). Binding of CD47 to SIRPα generates the “do not eat me” signal and the cells expressing CD47 are identified as “self” and protected (IDE et al., 2007). However, porcine CD47 is not compatible with human or baboon SIRPα, hence the porcine cells are not protected when exposed to human macrophages *in vivo* (TENA et al., 2014; TENA et al., 2017) or *in vitro* (NOMURA et al., 2020). Transgenic expression of hCD47 in pigs has been proven to be protective against macrophages, and hCD47-tg porcine hematopoietic cells

or skin xenografts performed better than control xenografts in baboon models (TENA et al., 2014; TENA et al., 2017). Similarly, following intraportal transplantation in mice, rat islets expressing mouse CD47 were protected against IBMIR-mediated disruption and exhibited improved engraftment and function compared to the control islets (SHRESTHA et al., 2020). The impact of hCD47 expression in porcine islets on pig-to-NHP islet xenotransplantation and post-transplantation islets' survival and function is yet to be explored.

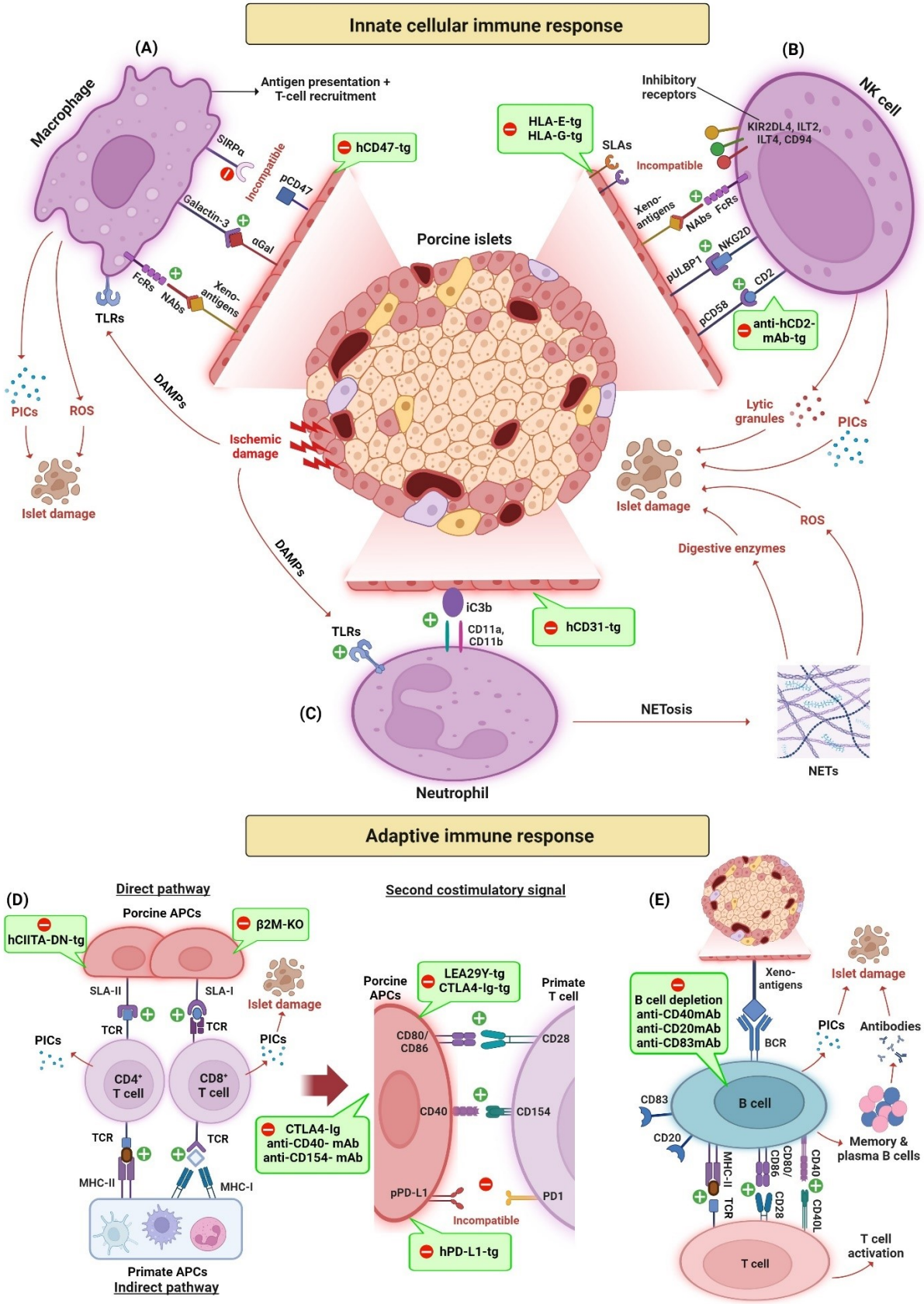

Figure 3: Innate cellular and adaptive immune response in islet xenotransplantation.

(A) Macrophages can be activated by the interaction between antigen-antibody immune complexes on porcine cells and FcRs on macrophages, the interaction between galectin-3 on macrophages and α-Gal on porcine cells, the interaction with other immune cells infiltrating into the xenograft, and the interaction between DAMPs released

by the damaged islets and TLRs. Moreover, macrophages can also act as APCs and activate T cells. Transgenic expression of hCD47 in porcine islets can inhibit macrophage-mediated xenogeneic islet rejection through the hCD47-SIRPα signaling pathway. (B) NK cells can be activated by an interaction between their FcRs and immune complexes in the porcine cells. Moreover, an interaction between NK cell activating receptors, NKG2D and CD2, and their ligands on porcine cells activates NK cells. NK cell inhibitory receptors are not compatible with SLAs, and transgenic expression of HLAs or anti-hCD2-mAb in porcine islets can inhibit NK cell-mediated rejection. (C) Neutrophils can be activated by the PICs released by macrophages, by DMAPs released by damaged islets, and through the interaction between their CD11a and CD11b receptors with iC3b complexes on xenogeneic cells. Neutrophilmediated cytotoxicity can be inhibited by transgenic expression of hCD31 in porcine cells. (D) T cells can be activated by direct and indirect pathways. In the direct pathway, TCRs on $CD4^+$ and $CD8^+$ primates' T cells interact with SLA-II- and SLA-I peptide complexes on porcine APCs, respectively. Transgenic expression of hCIITA-DN and β2M KO in pigs can abrogate SLAII and SLA-I expression on porcine cells, respectively, and reduce the direct immune response of T cells. In the indirect pathway, TCRs on primates' $CD4^+$ and $CD8^+$ T cells interact with MHC-II and MHC-I peptide complexes on primate APCs, respectively. Moreover, CD80/CD86-CD28 and CD40-CD154 are important co-stimulatory axes in T-cell activation, whereas as PD-1/PD-L1 axis is an inhibitory pathway but porcine PD-L1 is incompatible with human PD-1. Costimulatory signals can be inhibited by administrating drugs, such as CTLA4-Ig, aCD154mAb, and aCD40mAb. Moreover, transgenic expression of hCTLA4-Ig, LEA29Y, and hPD-L1 in pigs can also inhibit T-cell mediated cytotoxicity. (E) B cells interact with the xenogeneic antigens on porcine cells through BCRs and later present the xenogeneic peptide to T cells through MHC-II-peptide complexes. Furthermore, the interaction between CD40 or CD80/86 receptors on B cells to their ligands on T cells triggers the differentiation of B cells into antibody-producing plasma B cells. B cell depletion using anti-CD40 mAb, anti-CD83 mAb, and anti-CD20 mAb can alleviate B cell-mediated xenograft rejection. Abbreviations: NAbs: natural antibodies; FcRs: Fc receptors; TLRs: Toll-like receptors; PICs: proinflammatory cytokines; ROS: reactive oxygen species; SLAs: swine leukocyte antigens; NK cell: natural killer cell; DAMPs: damage-associated molecular patterns. Created with BioRender.com.

4.5.2. Natural killer cells

NK cells play a pivotal role in islet destruction and are activated by the abundant proinflammatory cytokines released in response to IBMIR and by the macrophages (ISHIYAMA et al., 2011; SAEKI et al., 2017). NK cells can cause xenograft destruction either by their direct interaction with the xenogeneic cells or by antibody-dependent cellular cytotoxicity (ADCC) (MAEDA et al., 2022). In the direct pathway, NK cells can interact with their target cells by activating or inhibitory receptors. The activating NK cell receptors, NKG2D and CD2, interact with pULBP1 and a CD58 ortholog on the porcine cells, respectively, leading to NK cell activation. The activated NK cells secrete lytic particles and cytokines (TNF-α and IFN-γ), leading to the target cell's lysis (FORTE et al., 2005; LILIENFELD et al., 2006). The inhibitory NK cell receptors (KIR2DL4, ILT2, ILT4, and CD94/NKG2A) on human NK cells bind major histocompatibility complex (MHC) class I molecules such as human leukocyte antigen G (HLA-G) and HLA-E and generate an inhibitory signal. However, they cannot

effectively interact with the swine leukocyte antigens (SLAs) and an inhibitory signal is not generated by the porcine cells, subsequently resulting in cell lysis (LOPEZ et al., 2022). In ADCC, Fc receptors (FcRs) on NK cells interact with the antibodies deposited on the xenogeneic cells, leading to the release of lytic granules and target cell apoptosis (LOPEZ et al., 2022). A possible strategy to alleviate the action of human NK cells on porcine cells is the transgenic expression of NK cell inhibitory ligands, such as HLA-E and HLA-G in the donor pigs. The inhibitory ILT receptors on NK cells, monocytes, and T and B lymphocytes bind HLA-G1 on the target cells and generate an inhibitory signal (RAO et al., 2021). Through a similar mechanism, HLA-E inhibits the action of human NK cells via the CD94/NKG2A inhibitory receptor (WEISS et al., 2009). Porcine endothelial cells expressing HLA-E are protected against human NK cells *in vitro* (WEISS et al., 2009). Rao et al. (2021) generated *GGTA1*-KO/HLA-G1-tg pigs and demonstrated that *GGTA1*-KO/HLA-G1-tg porcine fibroblasts were protected against the action of T cells, macrophages, and NK cells compared to WT porcine fibroblasts. Moreover, G*GTA1*-KO/HLA-G1-tg APIs transplanted under the kidney capsule of diabetic nude mice restored normoglycemia and had a longer survival time compared to WT APIs (RAO et al., 2021). However, this study was terminated at day 32, and the long-term survival of APIs and the *in vivo* host immune response were not assessed or reported.

4.5.3. Neutrophils

Neutrophils are recruited into the xenograft in response to the IBMIR, proinflammatory cytokines released by macrophages, and DAMPs, or can also independently interact with the xenogeneic cells (LU et al., 2022). Neutrophils can also be activated by an interaction of their CD11a and CD11b receptors to iC3b protein (a part of the complement system) deposited in porcine cells (LU et al., 2022). In response to different stimuli, the activated neutrophils undergo “NETosis”, a type of programmed cell death (VOROBJEVA & CHERNYAK, 2020). NETosis results in the formation of neutrophil extracellular traps (NETs) that contain serine proteases and antibacterial peptides. NETs can generate reactive oxygen species (ROS) and digestive enzymes which damage the xenograft cells (SCHOFIELD et al., 2013; VOROBJEVA & CHERNYAK, 2020). The cluster of differentiation 31 (CD31), also known as the platelet EC adhesion molecule 1 (PECAM1), is expressed on hemopoietic and endothelial cells and functions as an inhibitor of mitochondrial apoptosis (VOCKOVA et al., 2021). Interestingly, the porcine cells expressing CD31 suppress NETosis and the resultant cytotoxicity (WANG et al., 2018). Therefore, the hCD31 expression in pigs can be used to inhibit neutrophil-mediated xenograft rejection.

4.6. Alleviating the adaptive immune response

4.6.1. T cells

The islets that escape the IBMIR and hyper-acute rejection can be subjected to acute cellular rejection by the T cells (HU et al., 2022). T cells are the key players in the islet xenograft rejection and both $CD4^+$ and $CD8^+$ cells can infiltrate the xenograft (SCALEA et al., 2012). There are two pathways of T cell activation: the direct pathway and the indirect pathway **(Figure 3)** (HU et al., 2022). In the direct pathway, the intact SLA-I and SLAII on porcine APCs (such as endothelial cells and resident dendritic cells) interact directly with the host's T cell receptors (TCRs) on $CD8^+$ and $CD4^+$ T cells, respectively (GRIESEMER et al., 2014). In the indirect pathway, peptides derived from the porcine tissue are presented by the host's APCs to the host's $CD8^+$ and $CD4^+$ T cells (GRIESEMER et al., 2014). TCR-induced T cell activation is amplified by the costimulatory signals generated mainly by the interaction between CD154 or CD28 on the host's T cells and CD40 or CD80/CD86 on the 16 xenogeneic APCs, respectively (LU et al., 2020). The costimulatory signals are critical for full T cell activation, proliferation, and differentiation (SUNDQVIST, 2018). In contrast, the interaction between programmed cell death protein 1 (PD-1) on $CD4^+$ and $CD8^+$ T cells and human programmed death ligand-1 (hPD-L1) on the target cells generates a coinhibitory signal and blocks T cell proliferation and activation (LI et al., 2009). However, hPD-1 or hPD-L1 are not compatible with their porcine counterparts (PLEGE et al., 2010). T cells not only exert their cytotoxic effect by producing inflammatory cytokines but also amplify the cellular xenograft rejection by recruiting and activating macrophages and directing B cell response (HU et al., 2022). Based on the above-described mechanisms, the T cell-mediated cytotoxicity against the xenograft can be alleviated by: (i) removing SLAs; (ii) suppressing co-stimulatory signals; and (iii) transgenic expression of inhibitory signaling molecules. Removal of SLAs can suppress T cell responses against the porcine xenografts; however, SLAs also have protective immune functions in pigs and their complete removal can be harmful to the animals (SAKE et al., 2019). Therefore, rather than a complete knockout, a reduced expression of SLAs can help alleviate T cell-mediated cytotoxicity as well as avoid the potential side effects of complete inhibition of SLAs (HEIN et al., 2020). Transgenic pigs expressing a human dominant-negative mutant class II transactivator transgene (hCIITA-DN-tg) have a significantly reduced expression of SLAII on APCs (HARA et al., 2013), whereas knockout of porcine beta 2-microglobulin (β2M) abrogates SLA-I expression on porcine cells (SAKE et al., 2019). Costimulatory pathways can be blocked by specific monoclonal antibodies or by generating gm pigs secreting immunomodulatory molecules. For instance, the CD40–CD154 costimulatory signal can be blocked by either

anti-CD154 or anti-CD40 monoclonal antibodies (LEI et al., 2022). Whereas the CD28-CD80/CD86 costimulatory signal can be inhibited either by soluble human cytotoxic T-lymphocyte antigen 4-immunoglobulin (CTLA4-Ig) or by generating gm pigs expressing CTLA4-Ig (VABRES et al., 2014). LEA29Y is a high-affinity variant of CTLA4-Ig, and gm pigs with islet-specific LEA29Y expression have been generated (KLYMIUK et al., 2012; BUERCK et al., 2017). When transplanted into diabetic mice with a humanized immune system, LEA29Y-tg NPIs not only reversed hyperglycemia in 70% of the recipients but also survived for more than 6 months compared to WT NPIs that were rejected even before reaching maturity (BUERCK et al., 2017). CD2 is an activating receptor on T cells required for their interaction with APCs (LI et al., 2022a). Nottle et al. (2017) generated *GGTA1*-KO/anti-hCD2-mAb-tg pigs, whose islets might be tolerated the human/NHP immune system. Lastly, the xenografts from gm pigs expressing hPD-L1 might evade the human T-cell-mediated immune rejection (YI et al., 2021). For instance, human islet-like organoids expressing PD-L1 survived for more than 50 days in immunocompetent diabetic mice (YOSHIHARA et al., 2020). The cells isolated from hPD-L1-tg pigs reduced both the proliferation and cytotoxic effect of human $CD4^+$ T cells (BUERMANN et al., 2018). In a recent study, Lei et al. (2023) transplanted NPIs from WT or hPD-L1-tg pigs into humanized diabetic mice. At 16 weeks after transplantation, recipients transplanted with hPD-L1-tg NPIs achieved a superior normoglycemic rate (50% versus 0%), significantly higher plasma C-peptide levels, and reduced intragraft infiltration of immune cells compared to the WT group (LEI et al., 2023). Another protein that can suppress the T cell-mediated immune rejection is the tumor necrosis factor-related apoptosis-inducing ligand (TRAIL). However, only the dendritic cells from huTRAIL transgenic pigs exerted an antiproliferative effect on T cells (KEMTER et al., 2012), which questions the application of this genetic modification in porcine islet xenotransplantation.

4.6.2. B cells

A direct interaction between B cell receptor (BCR) and xenoantigens on porcine cells activates the B cells which later become potent APCs **(Figure 3)** (WENNHOLD et al., 2019). As APCs, B cells present MHC-II peptide complexes that interact with TCR on T cells. Moreover, an interaction between CD40 and CD80/86 on B cells with CD40L and CD28 on T cells, respectively, triggers the differentiation of B cells into antibody-producing plasma cells or memory B cells and T cells into effector T cells (KARAHAN et al., 2017). B cells can lead to graft rejection by producing xeno-specific antibodies, priming effector T cells, antigen presentation, and cytokine production (SHEN & FILLATREAU, 2015; AZZI & ALEGRE, 2019; LEE et al., 2020). Immune-competent diabetic C57BL/6 (B6) mice transplanted with

encapsulated NPIs showed a slight decrease in blood glucose level at 1 week post-transplantation and the hyperglycemia returned to the pre-transplantation level at 2 weeks post-transplantation, indicating the rejection of encapsulated NPIs. Moreover, an overgrowth of $CD4^+$ T cells, macrophages, and B cells was found on the surface of encapsulated islets, and there was a significant correlation between cellular overgrowth and islet cell death (KOBAYASHI et al., 2006). Whereas, in *Rag1*-knockout diabetic B6 mice that do not contain mature B and T lymphocytes, encapsulated NPIs maintained normoglycemia for up to 100 days post-transplantation without any immune cell growth (KOBAYASHI et al., 2006). Therefore, B cell depletion or alleviation of B cell function by anti-CD40, anti-CD20, or anti-CD83 antibodies prolongs xenograft survival (MOHIUDDIN et al., 2014; LEI et al., 2022). In rat-to-mouse islet xenotransplantation, the combined depletion of B and T cells led to the inhibition of donor-specific antibody production and indefinite xenograft survival (WANG et al., 2013). However, using a similar approach in pig-to-mouse islet xenotransplantation, long-term survival of islets was not achieved and the islets were lost by a combined response of B and T cells (KANG et al., 2017; LEE et al., 2020).

Table 2: Gene editing strategies for immunoprotection of porcine islets.

Target	Genetic modification		Gm pigs	Islet XTx in rodents	Islet XTx in NHPs
Carbohydrate antigens					
Deletion of carbohydrate antigens against which humans have pre-formed antibodies	*GGTA1*-KO	α-1,3-galactosyltransferase knockout	(PHELPS et al., 2003)	-	(THOMPSON et al., 2011a)
	CMAH-KO	cytidine monophosphate-N-acetylneuraminic acid hydroxylase knockout	(KWON et al., 2013; LUTZ et al., 2013)	(SALAMA et al., 2017)	-
	B4GALNT2-KO	β-1,4-N-acetyl-galactosaminyl transferase 2 knockout	(ESTRADA et al., 2015)	-	-
Complementary system					
Expression of human complement-regulatory genes	hCD46-tg	human membrane cofactor protein transgene	(DIAMOND et al., 2001)	(MCKENZIE et al., 2003)	(VAN DER WINDT et al., 2009)
	hCD55-tg	human decay-accelerating factor transgene	(COZZI & WHITE, 1995)	-	(MANDEL et al., 1997; HAWTHORNE et al., 2014)
	hCD59-tg	human membrane inhibitor of reactive lysis transgene	(FODOR et al., 1994)	-	(HAWTHORNE et al., 2014)
	hC1-INH-tg	human complement-regulatory protein C1 inhibitor transgene	(KWON et al., 2017)	-	-
Coagulation system					
Expression of human coagulation-regulatory genes	hTM-tg	human thrombomodulin transgene	(WUENSCH et al., 2014)	-	-
	hEPCR-tg	human endothelial protein C receptor transgene	(IWASE et al., 2014)	-	-
	hTFPI-tg	human tissue factor pathway inhibitor transgene	(LIN et al., 2010)	-	(BOTTINO et al., 2014)
	hCD39-tg	human ectonucleoside triphosphate diphosphohydrolase-1 transgene	(WHEELER et al., 2012)	(HUANG et al., 2017)	(BOTTINO et al., 2014)
	hCD73-tg	human ecto-5′-nucleotidase transgene	(LEE et al., 2017)	-	-

T cells					
Inhibition of T cell activation	LEA29Y-tg	the transgenic human variant of CTLA4-Ig	(KLYMIUK et al., 2012)	(KLYMIUK et al., 2012; BUERCK et al., 2017)	-
	hCTLA4-Ig-tg	human cytotoxic T-lymphocyte associated protein 4 transgene	(MARTIN et al., 2005)	-	-
	pCTLA4-Ig-tg	porcine CTLA4-Ig transgene	(PHELPS et al., 2009)	-	(BOTTINO et al., 2014)
	hTRAIL-tg	human TNF-related apoptosis-inducing ligand transgene	(KLOSE et al., 2005; KEMTER et al., 2012)	-	-
	PD-L1-tg	human programmed cell death 1 ligand 1 transgene	(BUERMANN et al., 2018)	(LEI et al., 2023)	-
	SLA KO	swine leukocyte antigen knockout	(REYES et al., 2014)	-	-
	CIITA-DN-tg	human dominant-negative mutant class II transactivator transgene	(HARA et al., 2013)	-	-
NK cells and macrophages					
Inhibition of NK cells and macrophages activation	HLA-E/β2M-tg	HLA-E/human β2-microglobulin transgene	(WEISS et al., 2009)	-	-
	hCD47-tg	human signal regulatory protein alpha transgene	(TENA et al., 2014)	-	-
Inflammation					
Expression of anti-inflammatory proteins	A20-tg	human tumor necrosis factor α–induced protein 3 (TNFAIP3) transgene	(OROPEZA et al., 2009)	(ZAMMIT et al., 2021)	-
	hHO-1-tg	human heme oxygenase 1 transgene	(PETERSEN et al., 2011; PARK et al., 2014)	(LEE et al., 2015; YAN et al., 2016)	-
	shTNFRI-Fc-tg	soluble human TNFRI-Fc transgene	(PARK et al., 2014)	(LEE et al., 2015; YAN et al., 2016)	-

5. Monitoring islet graft function and fate: the purpose of reporter transgenes

The success in islet transplantation depends hugely on the graft quality being transplanted, on the engraftment and revascularization of the islets that the graft is getting in function *in vivo*, and on the longitudinal graft fate. The optimization of the transplant product and the transplant procedure to improve islet engraftment, graft function and long-term survival would benefit from the possibility of non-invasive monitoring of the islet transplants. One modality for non-invasive *in vivo* graft monitoring is the usage of tissue expressing reporter proteins such as fluorophores **(Figure 4)**. Knowledge about critical parameters such as islet engraftment, changes in graft mass, long-term survival, and signs of graft failure could help to optimize transplantation strategies (KEMTER et al., 2022).

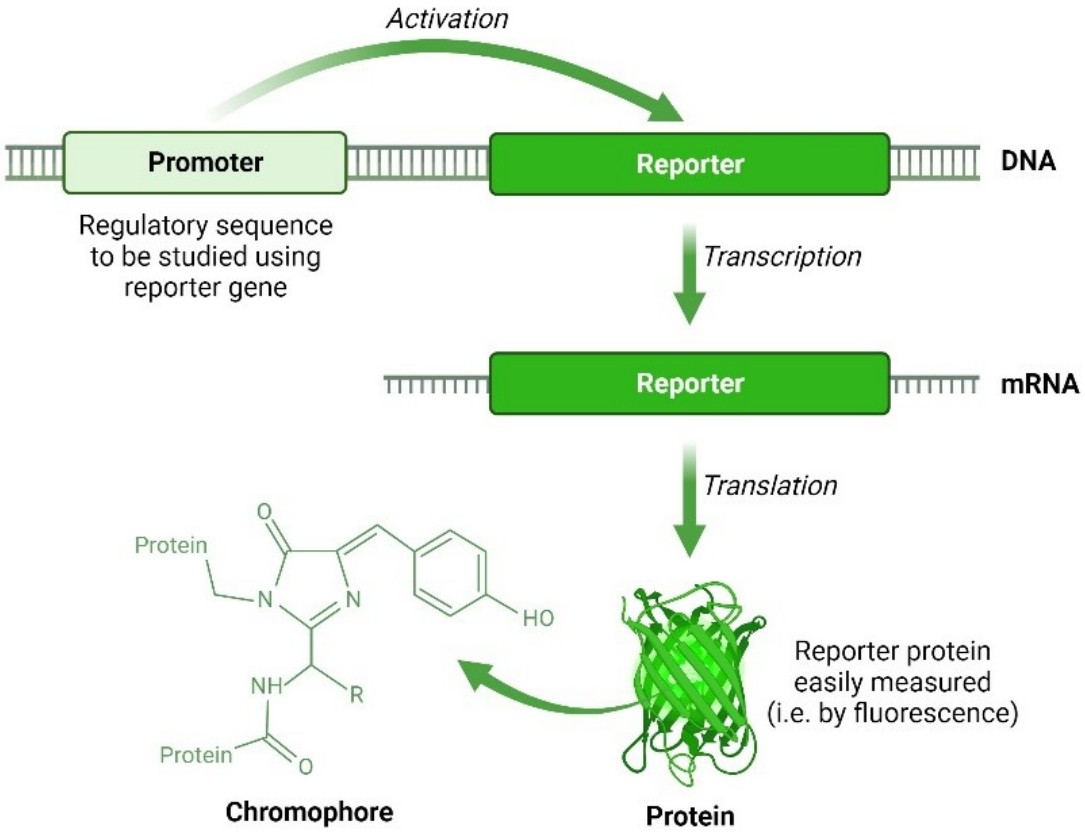

Figure 4: Principle of the reporter gene expression system.

Key features of a fluorescence reporter system are the selection of the promoter and of the fluorophore protein. The promoter sequence is responsible for the transgene expression pattern and intensity. Upon activation of the promoter by binding of the active DNA polymerase complex, transcription occurs, during which the DNA sequence of the reporter gene is transcribed into RNA, followed by translation, whereby the RNA is converted into a reporter protein. The fluorescent spectra with its excitation and emission profile of the fluorescent reporter transgene and its brightness and stability predicts its usability for *in vitro* and *in vivo* monitoring studies. Adapted from “Reporter Gene Expression System”, by BioRender.com (2024).

To explore porcine β-cell maturation both *in vitro* and *in vivo*, Kemter et al. (2017) engineered transgenic pigs expressing the enhanced green fluorescent protein (eGFP) under the control of the porcine *INS* gene promoter. The expression of eGFP in β-cells did not adversely affect insulin secretion, as evidenced by static glucose-stimulated insulin secretion (GSIS) assays conducted on NPIs. The functional performance of *INS*-eGFP transgenic NPIs was evaluated by *in vivo* studies involving transplantation at different sites. Initially, NPIs were transplanted into the left lower hind limb muscle of streptozotocin-treated NOD-scid Il2rγnull (NSG) mice. Before transplantation, NPIs were cultured for 4-6 days, and the NSG mice received either transgenic or wild-type NPIs. The time to achieve normoglycemia was comparable between mice transplanted with transgenic (median 64 days; mean 71 ± 10 days) or WT (median 72 days; mean 90 ± 14 days) NPIs. Immunohistological examinations of graft-bearing muscles at 12 and 16 weeks post-transplantation showed a strong staining for insulin and of eGFP in transgenic NPIs. Furthermore, *INS*-eGFP transgenic NPIs, after 7 days of *in vitro* culture, were transplanted into the anterior chamber of the eye (ACE) of NOD-scid mice. Grafts were monitored longitudinally *in vivo* in the ACE of these mice using confocal and two-photon microscopy at 0.5, 2, 8, and 16 weeks post-transplantation. Backscattered laser light and eGFP signals were used to assess β-cell granularity and eGFP-positive cell volumes, representing readout about β-cell maturity and β-cell mass, respectively. Vessel networks were visualized by injecting Qtracker 655, and surface rendering techniques were used to calculate the fractional volumes of islet vessels and eGFP-positive cells. Longitudinal *in vivo* imaging over 16 weeks demonstrated an increase in granularity, eGFP-positive fraction, and islet vessel fraction, suggesting that NPI grafts were well engrafted and revascularized, and that NPIs underwent a distinct proliferation, differentiation and maturation process in the post-transplant period. The mature graft exhibited cell granularity pattern in β-cells similar to that of adult porcine islets (KEMTER et al., 2017).

Additionally, eGFP-expressing β-cells can be harvested through fluorescence-activated cell sorting, enabling omics analyses like single-cell RNA sequencing. Studying β-cells throughout various pre- and postnatal stages could offer novel molecular understandings of porcine β-cell development, potentially uncovering novel markers and approaches to enhance the maturation of NPIs and evaluate the quality of islet products for xenotransplantation, as discussed by Kemter et al. (2018) and Kemter & Wolf (2018).

Matsunari H. et al. (2014) generated transgenic pigs expressing the GFP variant Venus under the control of the murine *Pdx1* (pancreatic and duodenal homeobox 1) promoter. The *Pdx1*-Venus transgenic pigs developed similarly to their wild-type littermate controls. Their

blood glucose and insulin levels were within normal ranges. While the *Pdx1*-Venus transgene was observed in acinar cells in the fetal pancreas, it was restricted to β cells in postnatal samples. Thus, this model could serve as a valuable model for pancreatic development and regeneration studies, akin to *INS*-eGFP transgenic pigs (KEMTER et al., 2017).

Tissue expressing reporter transgene having a spectral absorbance and emission wavelength in the visible color range can be used for *in vitro* studies or in islet transplant studies in the ACE system. However, these reporter expressing tissues are not suitable for fluorescence imaging in vascularized tissues due to autofluorescence of endogenous proteins such as hemoglobin from erythrocytes, exhibiting similar emission and excitation spectra. Therefore, no clear differentiation of reporter signal from that of endogenous fluorophores such as hemoglobin in the tissue in fluorescence *in vivo* imaging is possible. However, there is an optical window in tissue in the near-infrared wavelength range where light penetration into tissue is superior and autofluorescence interference is minimal (ALGORRI et al., 2021). Therefore, the use of near-infrared fluorescent protein (iRFP) is advantageous for fluorescence imaging (FI) and multispectral optoacoustic tomography (MSOT). Kemter et al. (2022) generated reporter pigs ubiquitously expressing iRFP, enabling the visualization of NPIs transplanted into streptozotocin-diabetic immunodeficient NSG mice.-Of note, grafts from *CAG*-iRFP transgenic NPIs demonstrated functional equivalence with grafts from wild-type NPIs. *In vivo* FI conducted four weeks after transplantation of either 1000 NPIs or 4000 NPIs under the kidney capsule of NSG mice revealed a twofold higher FI signal in mice receiving the 4000-NPI compared to 1000-NPI grafts. Ten weeks post-transplantation, the fluorescence intensity of the 4000-NPI graft inversely correlated with glycemic status of these mice. *In vivo* imaging using MSOT technology, that combines laser light for tissue stimulation with ultrasound for detecting the resulting acoustic signals, also exhibited dose-dependent signals for grafts of 750, 1500, and 3000 NPIs after intramuscular transplantation into diabetic NSG mice. Moreover, MSOT demonstrates versatility by enabling graft imaging in subcutaneous sites in large animal models. Dose-dependent MSOT signals were observed in a pig model, with stronger signals after subcutaneous (depth ∼6 mm) compared to submuscular (depth ∼15 mm) NPI placement (KEMTER et al., 2022)

III. OBJECTIVES

In recent years, there has been continuous progress in preclinical research on islet xenotransplantation, advancing toward clinical translation. Genetically modified islet donor pigs intended for clinical application must meet several prerequisites: (I) genetic modifications (gm) should include a set of multiple alterations including gene depletion and transgene expression of human immune regulatory proteins, (II) gm tissue donor pigs should easily and efficiently be obtained by breeding, (III) the gm donor pigs have to exhibit a robust and predictable transgene expression pattern, and (IV) the gm should not negatively affect graft function and graft properties.

Therefore, the main objective of this doctoral thesis was the generation, characterization, and optimization of genetically multi-modified islet donor pigs with a robust and predictable transgene expression pattern and minimal segregation of the gm during breeding. The multi-modified islet donor pigs should harbor the following genetic modifications: (1) the elimination of the α-Gal epitopes, to which human have performed antibodies against it; (2) the expression of LEA29Y and hPDL-1 to inhibit T cell activation; (3) the expression of hCD47 to protect it from macrophage activation, and (4) the deletion of *CCL2* to mitigate pro-inflammatory signals **(Figure 5 A)**.

Additionally, a second objective was the generation and characterization of a new calcium sensor reporter pig model. Monitoring intracellular calcium flows enables to study the functionality and maturity of β-cells as calcium flows are involved in regulated insulin secretion **(Figure 5 B)**. For this purpose, GCaMP6-expressing NPIs may be useful for preclinical islet xenotransplantation studies, both *in vitro* and *in vivo*.

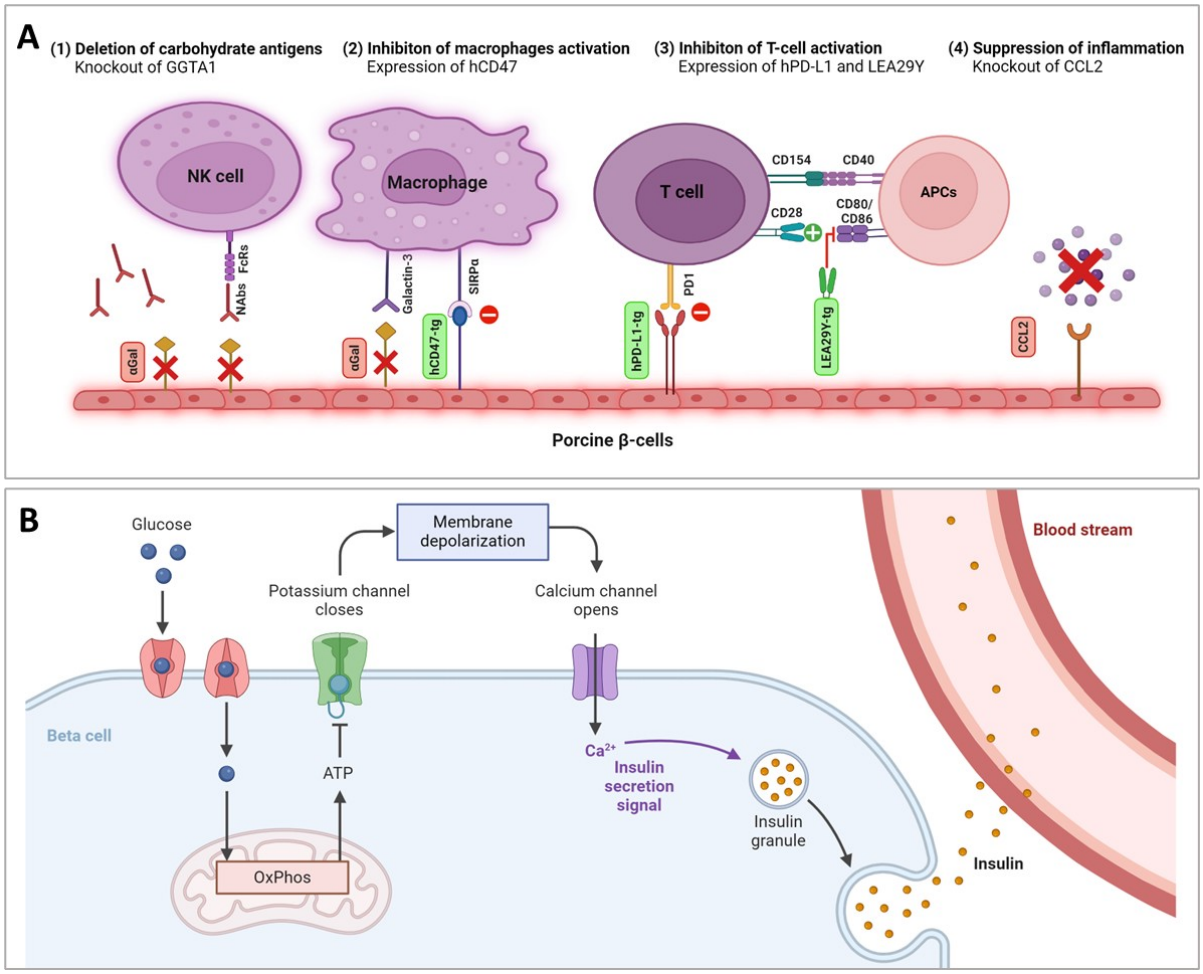

Figure 5: Study design: Optimization and characterization of multiple genetically modified pigs.

(A) To overcome the immunological barriers of islet xenotransplantation multiple genetic modifications were used: (1) Deletion of carbohydrate antigens: the α-Gal epitope is an immunogenic glycan epitope. Although absent in humans, preformed antibodies against the α-Gal epitope are present due to their natural production as an immunological response to intestinal bacteria bearing the α-Gal structures on their lipopolysaccharide chains. (2) Inhibition of macrophages activation: human CD47 expressed on cellular surfaces, functions as a 'do not eat me' signal. (3) Inhibition of T cell activation: LEA29Y functions as a T cell co-stimulation blocking molecule, that acts by binding on CD80/CD86 in APC cells and thereby blocks the CD28-CD80/CD86 T cell costimulation axis. Transgene expression of human PD-L1 inhibits T cell activation by binding on the inhibitory receptor PD1 on T cells. (4) Suppression of inflammation: since *CCL2* plays a decisive role in the infiltration of monocytes and macrophages into the xenograft, knocking out the gene could lead to an attenuated or delayed inflammatory reaction. Created with BioRender.com. **(B)** Calcium is an important driver for insulin secretion: glucose is transported into the cell via the GLUT2 transporter and enters glycolysis where the resulting reducing equivalents are used in oxidative phosphorylation to produce ATP. Consequently, ATP-regulated potassium channels are closing, resulting in cell membrane depolarization. The depolarization initiates the opening of voltage-gated calcium channels, allowing calcium influx into the β-cells. The increase in intracellular calcium levels prompts the exocytosis of stored insulin, indicating a functioning and mature β-cell. Adapted from “Insulin Production Pathway”, by BioRender.com (2024).

IV. ANIMALS, MATERIALS AND METHODS

1. Animals

1.1. Preexisting gm pig lines

In this study, preexisting genetically modified (gm) pig lines with the following modifications to their genome were used either for breeding purposes or for introducing additional genetic modifications. All pig lines, except for *GGTA1*-knockout (KO) and hCD46-transgenic (tg) pigs (Revivicor, Inc.), were generated at the Chair for Molecular Animal Breeding and Biotechnology, LMU Munich.

1.1.1. *GGTA1*-KO pig lines

The *GGTA1*-KO pig line was established in 2002 at Revivicor Inc. in Blacksburg, VA, USA, on a Large White breed background. In this pig line, the catalytic domain in exon 9 of the α1,3-galactosyl-transferase (*GGTA1*) gene was disrupted by targeted integration via homologous recombination of a neomycin resistance cassette, resulting in a loss of *GGTA1* gene function. The *GGTA1*-KO (BAC) pig line was generated by targeted integration of a floxed neomycin resistance cassette into the *GGTA1* gene (KUROME et al., 2019), replacing the start codon-containing exon 5. To achieve this, a bacterial artificial chromosome (BAC) containing the genomic sequence of the porcine *GGTA1* gene locus was used, in which the neomycin resistance cassette was inserted to disrupt the coding sequence of *GGTA1*. Following nucleofection and selection of SCCs with targeted integration of the floxed resistance cassette, cells were transfected for transient expression of Cre recombinase to excise the resistance cassette. Finally, *GGTA1*-KO δneo porcine kidney cells (PKCs) were used as donor cells for somatic cell nuclear transfer (SCNT) for the generation of a breeding herd.

1.1.2. hCD46-transgenic pig line

The hCD46-tg (Revivicor, Inc.) pig line was established by Loveland et al. (2004) using a transgene construct that included a genomic fragment of human CD46. This fragment comprised the CD46 promoter, exons 1 and 2, a cDNA fragment spanning exons 3 to 12, and a SV40 polyadenylation site. The hCD46 minigene construct was integrated through additive gene transfer into an unidentified genomic region. Double genetically modified founder animals were produced by breeding hCD46 transgenic pigs with homozygous *GGTA1*-KO pigs at Revivicor Inc., Blacksburg, VA (HARA et al., 2008). A breeding herd was generated using primary cells from a *GGTA1*-KO/hCD46-tg boar as donor cells for SCNT.

1.1.3. *CCL2*-KO pig line

For generation of the *CCL2*-KO pig line, disruption of the coding region of the *CCL2* gene was introduced by using a CRISPR/Cas9 gene editing approach. In detail, two gRNAs were used targeting exon 1 and exon 2 of the *CCL2* gene to introduce non-homologous repair mechanism, leading to a frameshift mutation in the coding region of *CCL2*.

1.1.4. *INS*-LEA29Y transgenic pig line

The *INS*-LEA29Y-tg pig line specifically expresses the CTLA4-Ig derivative LEA29Y within the β-cells of the pancreas. For generation of this pig line, an *INS*-LEA29Y expression cassette containing the cDNA sequence of a fusion protein of the CTLA4-Ig derivative LEA29Y and human IgG was generated. This was placed under the control of the 1.3 kb long porcine insulin (*INS*) promoter and combined with a neomycin antibiotic resistance expression cassette. Porcine kidney cells were nucleofected with the linearized expression cassette. The cells were cultured in neomycin-containing media for two weeks. Cells without stable integration of the expression cassette died, resulting in a bulk cell population with random integration of the cassette. This bulk cell population was then used for SCNT for generation of founder pigs. The founder pig line, which exhibited the strongest β-cell specific expression of LEA29Y, was selected for establishing a breeding herd at the CiMM (Center for Innovative Medical Models). The transgene integration site was identified in a non-coding region on chromosome 6 (SSC6) by Targeted Locus Amplification (TLA) technology (Cergentis B.V., The Netherlands) (unpublished).

1.2. Housing

All animals were housed in a designated-pathogen-free environment (DPF) at the CiMM located within the Ludwig-Maximilians-University Munich. Adequate amounts of food and water were provided freely available to the animals. All animals received an intramuscular injection of 1 ml Eisen20 (bela-pharm) for iron supplementation three days postpartum. Furthermore, the piglets were immunized against porcine circovirus type 2 (PCV2) using CircoFLEX® (Ingelvac) vaccine 21 days postpartum.

The experiments were conducted in compliance with the German Animal Welfare Act and Directive 2010/63/EU (Protection of animals used for scientific purposes). Approval for all experiments was granted by the Government of Upper Bavaria.

2. Materials

2.1. Laboratory equipment

Accu-jet® pro pipette controller	Brand GmbH, Germany
Analytik Jena US UVP GelStudio Plus	Thermo Fisher Scientific, USA
Barnstead™ Easypure™ II	Thermo Fisher Scientific, USA
Benchtop 96 tube working rack	Stratagene, USA
BIORAD PowerPac™ Basic	Bio-Rad, USA
Bunsen burner Gasprofi 1SCS	WLD TEC, Germany
Cellavista® 4	Synentec GmbH, Germany
Cellavista® automated cell culture microscope	Synentec, Germany
Centrifuge, Rotina 380R	Hettich, Germany
Chemostar Touch ECL Imager	INTAS, Germany
Combimag RCH magnetic stirrer	IKA-Works Inc., USA
Corning® CoolCell™	Sigma Aldrich, USA
Daewoo KOC-154K microwave	Daewoo, South Korea
Embedding molds premium	Medite Medical GmbH, Germany
Eppendorf Centrifuge 5417 R	Eppendorf, Germany
Eppendorf Centrifuge 5424	Eppendorf, Germany
Eppendorf Centrifuge 5804	Eppendorf, Germany
Eppendorf Centrifuge 5910 R	Eppendorf, Germany
Erlenmeyer flask 500 mL, 1 L	Schott AG, Germany
Excelsior™ AS A82310100	Epredia™, USA
Five Easy F20 pH meter	Mettler Toledo,USA
Freezer -20°C, LGex 34 10-24A-001	Liebherr, Germany
Freezer -80°C, VIP ECO MDF-DU502VH-PE	PHC Europe B.V., Netherlands
Gel chambers EasyCast™ B2	Thermo Fisher Scientific, USA
Gel imager, UVP Gelstudio Plus	Analytic Jena, Germany

Grant JB Nova 5 water bath	Grant Instruments Ltd, UK
Grant Sub 14 water bath	CLF, Germany
Heraeus Biofuge pico	Heraeus, Germany
HeraSafe workbench	Heraeus, Germany
HLC Cooling-ThermoMixer MKR 13	Ditabis, Germany
Homogenisierer, MiniBatch	Miccra®, Germany
Incubator with CO_2 and humidity regulation	Binder, Germany
Labcycler thermocycler	SensoQuest GmbH, Germany
Leica microscope type DMC4500	Leica Microsystems, Switzerland
Microm HM 325 rotary microtome	Thermo Fisher Scientific, USA
Microwave MS-196VUT	LG, South Korea
Milli-Q® water system	Millipore, USA
Mini-PROTEAN® Casting Stand Gaskets	Thermo Fisher Scientific, USA
Mini-PROTEAN® Comb, 15-well, 1.0 mm	Thermo Fisher Scientific, USA
Mini-PROTEAN® Spacer Plates with 1.0 mm	Thermo Fisher Scientific, USA
Mini-PROTEAN® Tetra Cell Casting Stand	Thermo Fisher Scientific, USA
Mini-PROTEAN® Tetra Cell	Thermo Fisher Scientific, USA
Nucleofector® 2b Device	Lonza, Switzerland
Olympus microscope BX43F	Olympusy, Japan
Owl™ EasyCast™ B2 Minigel combs	Thermo Fisher Scientific, USA
Owl™ EasyCast™ B2 Minigel Electroph. Syst.	Thermo Fisher Scientific, USA
Paraffin dispensing station, TES 99	Medite, Germany
PCR Cycler, Labcycler Basic	Sensoquest GmbH, Germany
Pipets Pipetman	Gilson Inc., USA
Rotilabo® mini centrifuge	Carl Roth, Germany
Select vortexer	Select BioProducts, USA
Shaking Incubator GFL 3031 with orbital motion	Lauda-GFL, Germany

SimpliNano™ spectrophotometer	Biochrom GmbH, Germany
Spark® Multimode Microplate Reader	Tecan Group, Switzerland
Stationary incubator	Memmert, Germany
TES 99 modular paraffin embedding system	Medite Medical GmbH, Germany
Thermoblock HTM	HTA-BioTec, Germany
Thermomixer, HTM	HTA-BioTec, Germany
Tissue cool plate COP 30	Medite Medical GmbH, Germany
Tissue float bath 1052	GFL, Germany
Trans-Blot® Turbo™ Transfer System	Thermo Fisher Scientific, USA
VHC Pro vacuum pump	Vacuubrand GmbH, Germany
Vortexer MS1 minishaker	IKA-Works Inc, USA

2.2. Consumables

Cell culture plates (10 cm, 6 well, 96-well half area, 96-well full area)	Sigma-Aldrich, USA
Cryoconservation vials 1.5 ml	Thermo Fisher Scientific, USA
Disposable scalpel #21	Henry Schein, USA
Electroporation cuvettes	Carl Roth, Germany
Embedding cassettes UniLink	Engelbrecht, Germany
Falcon® (15 ml, 50 ml)	Greiner Holding, Austria
Glass pipets	Thermo Fisher Scientific, USA
Greiner Bio-One Cellstar™ tubes (15 ml, 50 ml)	Thermo Fisher Scientific, USA
Histoplast PE Paraffin	Epredia, Netherlands
Immobilion®-P PVDF Membrane	Merck, Germany
Latex gloves	Brightway, Malaysia
Microtome blade S35	FEATHER®; Japan
Parafilm®	Bemis, USA

PCR reaction tubes (0.2 ml)	Brand GmbH, Germany
Petri dish 94x16	Greiner BioOne, Austria
Petri-dish 10 cm for bacteria	Sigma-Aldrich, USA
Pipet tips (10 µl – 1250 µl)	Eppendorf, Germany
Pipet tips with filter (10 µl – 1250 µl)	Eppendorf, Germany
Safe-Lock reaction tubes (1.5 ml, 2 ml)	Eppendorf, Germany
Serological pipettes (5 ml, 10 ml, 25 ml)	Sarstedt, Germany
STARFROST® microscope slides	Engelbrech, Germany
Western Blotting Filter Paper, extra thick	Thermo Fisher Scientific, USA

2.3. Drugs

Azaperone, 40 mg/ml	Serumwerk, Germany
Boar semen extender, M III® with Gentamicin	Minitüb, Germany
Fentanyl (Fentadon), 50 mg/ml	Dechra, UK
Ketamine (Ursotamin®), 100 mg/ml	Serumwerk, Germany
Xylazine, 20 mg/ml	Serumwerk, Germany

2.4. Chemicals and Reagents

All chemicals were purchased from Carl Roth, Sigma Aldrich, Thermo Scientific or VWR, if not otherwise indicated. Chemicals listened below are limited to those beyond standard laboratory equipment of chemicals.

10x CutSmart® Buffer	New England Biolabs, USA
10x PCR Buffer	Qiagen, Germany
5X Phusion GC Buffer	New England Biolabs, USA
5X Q5 High GC Enhancer	New England Biolabs, USA
5X Q5 Reaction Buffer	New England Biolabs, USA
Acetic acid (HoAc), 100%	Carl Roth, Germany

Acrylamide/Bis Solution, 30%	Serva, Germany
Albumin Fraction V (BSA)	Carl Roth, Germany
Ammoniumperoxodisulfat (APS)	Carl Roth, Germany
Amphotericin B	Thermo Fisher Scientific, USA
Ampicillin	Carl Roth, Germany
Bromophenol blue	Carl Roth, Germany
Caustic soda (2N) (NaOH)	Carl Roth, Germany
Cell culture grade water	Biowest, France
Chloramphenicol	Carl Roth, Germany
Chloroform, 100%	Merck, Germany
Collagen	Thermo Fisher Scientific, USA
Collagenase powder	Thermo Fisher Scientific, USA
CutSmart Buffer®	New England Biolabs, USA
Dimethylsulfoxide (DMSO)	Sigma Aldrich, USA
Disodium hydrogen phosphate (Na_2HPO_4)	Carl Roth, Germany
Dithiothreitol (DTT)	Carl Roth, Germany
DNA Ladder, 10 bp DNA, GeneRuler	Thermo Fisher Scientific, USA
dNTP mix (100 mM)	Agilent Technologies, USA
dNTPs (dATP, dCTP, dGTP, dTTP)	Thermo Fisher Scientific, USA
Eosin, 2%	Morphisto, Germany
Ethanol (EtOH), 99.8%	Carl Roth, Germany
Ethylenediaminetetraacetic acid (EDTA)	VWR, USA
Fetal Calf Serum (FCS)	Thermo Fisher Scientific, USA
GelRed® Nucleic Acid Gel Stain	Biotium, USA
Gene Ruler™ 1 kb DNA ladder	Thermo Fisher Scientific, USA
Geneticin™ Selective Antibiotic	Thermo Fisher Scientific, USA
Gibco™ Hanks' Balanced Salt Solution (HBSS)	Thermo Fisher Scientific, USA

Gibco™ DMEM GlutaMAX™	Thermo Fisher Scientific, USA
Gibco™ Hepes Buffer Solution	Thermo Fisher Scientific, USA
Gibco™ MEM NEAA	Thermo Fisher Scientific, USA
Glucose	Carl Roth, Germany
Glutaraldehyde, 25%	Serva, Germany
Glycerol	Carl Roth, Germany
Herculase II Reaction Buffer	Agilent Technologies, USA
Histokitt	Hecht, Assistant®, Austria
Hydrochloric acid (HCl), 25%	Carl Roth, Germany
Hydrogen peroxide (H_2O_2), 35%	Carl Roth, Germany
Isoamyl alcohol	Carl Roth, Germany
Isopropanol iPrOH	Carl Roth, Germany
Lysogeny broth (LB) Agar	Carl Roth, Germany
Lysogeny broth (LB) Medium	Carl Roth, Germany
Magnesium chloride ($MgCl_2$)	Qiagen, Germany
Mercaptoethanol	Sigma Aldrich, USA
Methanol, 100%	Carl Roth, Germany
Meyer's Hemalum	Sigma-Aldrich, USA
Milk, powdered	Carl Roth, Germany
Natrium chloride (NaCl)	Carl Roth, Germany
Neutral serum	Biozol, Germany
O.C.T. Compound, Tissue-Tek®	Sakura Finetek, Netherlands
PageRuler™ prestained protein ladder	Thermo Fisher Scientific, USA
PageRuler™ unstained protein ladder	Thermo Fisher Scientific, USA
Paraformaldehyde	Carl Roth, Germany
Penicillin-streptomycin (10,000 U/ml)	Thermo Fisher Scientific, USA
Phosphate-buffered saline (PBS)	Sigma Aldrich, USA

Ponceau S	Sigma Aldrich, USA
Potassium acetate (KOAc)	Carl Roth, Germany
Potassium chloride (KCl)	Merck, USA
Potassium hydrogen phosphate (KH_2PO_4)	Carl Roth, Germany
Propanol	Carl Roth, Germany
Q-Solution	Qiagen, Germany
Restriction enzyme reaction buffers	Thermo Fisher Scientific, USA
Sodium acetat (NaOAc)	Carl Roth, Germany
Sodium dodecyl sulfate (SDS)	Serva, Germany
Sodium hydroxide (NaOH)	Carl Roth, Germany
T4 DNA ligase buffer	Thermo Fisher Scientific, USA
T4 Ligation buffer	Thermo Fisher Scientific, US
TEMED	Carl Roth, Germany
Trichlormethan/Chloroform	Carl Roth, Germany
Tris-hydroxymethyl-aminomethane (Tris)	Carl Roth, Germany
Tri-sodium citrate dihydrate	Carl Roth; Germany
Triton™ X-100	Merck, Germany
TRIzol® Reagent	Thermo Fisher Scientific, USA
Trypsin	Thermo Fisher Scientific, USA
Tween® 20	Carl Roth, Germany
Universal Agarose	Bio&SELL, Germany
Xylene, 100%	Avantor™/VWR™, USA
Xylol	VWR; USA
β-Mercaptoethanol	Merck, Germany

2.5. Buffers, Media and Solutions

Aqua bidest., deionized in Barnstead™ EASYpure™ II ultrapure water system (Wilhelm Werner GmbH, Leverkusen), was used as solvent.

Cell culture

Culture medium for PKCs (15%)

DMEM

15% FCS

1% non-essential amino acid

10 mM HEPES-buffer

0.1 mM mercaptoethanol

Stop medium

10% sterile FCS

90% DMEM

Freezing medium for SCCs

90% sterile FCS

10% DMSO

Phosphate-buffered saline (PBS) without Calcium and Magnesium for cell culture

8 g	NaCl
0.2 g	KCl
0.2 g	KH_2PO_4
2.14 g	$Na_2HPO_4 \cdot 2\ H_2O$
1000 ml	Aqua bidest.

mix and adjust to pH 7.2-7.4

PBS/BSA solution (1%)

1 g	BSA
100 ml	PBS w/o Ca/Mg

ProtK digestion of SCCs

PK-Buffer (20 ml):

4 ml	1 M Tris, pH 7.5
4 ml	1 M NaCl
1.6 ml	0.5 M EDTA
fill up to 20 ml	Aqua bidest.

Agarose gel electrophoresis

50x TAE buffer (stock solution)

242 g	Tris
100 ml	0.5 M EDTA, pH 8.0
57 ml	Glacial acid, 100%
1000 ml	Aqua bidest.

Agarose gel (1%)

1 g	Agarose standard
fill up to 100 ml	1x TAE buffer

Tissue fixation

10x phosphate buffered salt solution (PBS), pH 7.4

79.5 g	NaCl
11.5 g	$Na_2HPO_4 \cdot 2\ H_2O$
2.0 g	KCl

2.0 g	KH_2PO_4
950 ml	Aqua bidest.

mix and adjust to pH 7.35-7.4

fill up to 1000 ml	Aqua bidest.

4% PBS-buffered paraformaldehyde (PFA) solution, pH 7.4

40 g	Paraformaldehyde
100 ml	10x PBS buffer, pH7.4
ad 900 ml	Aqua bidest.
ad 100 µl	NaOH, 5 M

dissolve PFA in warm water bath (50 °C)

cool down to room temperature

adjust to pH 7.35-7.4

fill up to 1000 ml	Aqua bidest.

Methacarn (modified Carnoy) solution

600 ml	Methanol
300 ml	Chloroform
100 ml	Acetic acid (100%)

Immunohistochemistry

10x TBS buffer, pH 7.6 (stock solution)

83.33 g	NaCl
60.57 g	Tris
900 ml	Aqua bidest.

adjust pH at 7.6 with 25% HCl

fill up to 1000 ml	Aqua bidest.

Tris-EDTA-buffer, pH 9.0

1.21 g	Tris
2 ml	0.5 M EDTA, pH 8.0
0.5 ml	Tween 20
900 ml	Aqua bidest.
adjust pH at 9.0	
fill up to 1000 ml	Aqua bidest.

Sodium citrate buffer, pH 6.0

2.94 g	Tri-sodium-citrate
0.5 ml	Tween 20
900 ml	Aqua bidest.
adjust pH at 7.6	
fill up to 1000 ml	Aqua bidest.

1mM EDTA pH 8,0

2 ml	0.5 M EDTA
998 ml	Aqua bidest.
adjust pH at 8.0	

Western Blot

5x Laemmli buffer

62.5 ml	1 M Tris, pH 6.8
100 ml	Glycerine
2 ml	0.5 M EDTA, pH 8.0
20 g	SDS
0.01%	Bromophenol Blue
fill up to 200 ml	Aqua bidest.

1xLaemmli/ 2-mercaptoethanol solution

8.55 µl	2-Mercaptoethanol
9.45 µl	1x Laemmli buffer

Protein extraction buffer

2 ml	1 M Tris, pH 7.5
2 ml	Triton X-100
20 ml	Laemmli Buffer (5%)
76 ml	Aqua bidest.

TBS buffer, pH 7,4 (stock solution)

30.0 g	Tris, pH 5.5
80.0 g	NaCl
1000 ml	Aqua bidest.

adjust pH at 8.0

TBS-T (0.1%) buffer

100 ml	TBS buffer, pH7,4 stock solution
1 ml	Tween 20
fill up to 1000 ml	Aqua bidest.

Blocking buffer

3% powdered Milk in TBS-T working solution

SDS-page running buffer (stock solution)

30.3 g	Tris
144 g	Glycin
10 g	SDS
1000 ml	Aqua bidest.

Elution buffer (stock solution)

58 g	Tris
29 g	Glycin
3.7 g	SDS
1000 ml	Aqua bidest.

Elution buffer (working solution)

20 ml	Stock solution elution buffer
140 ml	Aqua bidest.
40 ml	Methanol

Ponceau S-solution

0.2 g	Ponceau S
3 ml	Glacial acetic acid
fill up to 1000 ml	Aqua bidest.

Stripping buffer

25 ml	250 mM Tris HCl, pH 6.7
20 ml	10% SDS
55 ml	Aqua bidest.
700 µl	2-Mercaptoethanol

2.6. Kits

Amaxa™ Basic Nucleofector™ Kit	Lonza, Switzerland
Avidin/Biotin Blocking Kit	Vector Laboratories Inc., USA
Avidin-Biotin Complex (ABC)	Vector Laboratories Inc.; USA
BD Cytofix/Cytoperm Fixation/Permeabilization Kit	BD Biosciences, Switzerland
DAB Substrate Kit (HRP), with Nickel	Vector Laboratories Inc., USA
E.Z.N.A.® Endo-Free Plasmid DNA Midi/Maxi Kit	Omega Bio-Tek Inc, Georgia
Endofree Plasmid Maxi Kit	Quiagen, Germany
Exo-CIP™ Rapid PCR Cleanup Kit	New England Biolabs; USA
Gibson Assembly® Cloning Kit	New England Biolabs, USA
ImmPACT® DAB Substrat Kit (HRP)	Vector Laboratories Inc.; USA
Monarch® DNA Gel Extraction Kit	New England Biolabs, USA
Monarch® Genomic DNA Purification Kit	New England Biolabs, USA
Quiagen® Plasmid Mini, Midi and Maxi Kit	Quiagen, Germany
SuperSignal™ West Atto Substrate	Thermo Fisher Scientific, USA
SuperSignal™ West Atto Substrate	Thermo Fisher Scientific, USA
SuperSignal™ West Dura Substrate	Thermo Fisher Scientific, USA
SuperSignal™ West Femto Substrate	Thermo Fisher Scientific, USA

2.7. Enzymes

HotStarTaq Plus DNA Polymerase (5 U/µL)	Qiagen, Germany
Phusion® High-Fidelity DNAPolymerase	New England Biolabs, USA
Proteinase K, ready to use	Agilent Technologies, USA
Q5® High-Fidelity DNA Polymerase	New England Biolabs, USA
Restriction enzymes	Thermo Fisher Scientific, USA
RNAse A	Thermo Fisher Scientific, USA
T4 Ligase	Thermo Fisher Scientific, USA
Taq DNA Polymerase (5 U/µL)	Qiagen, Germany

2.8. Antibodies and lectins

Table 3: Western blot antibodies

Targeted gene	Primary antibody	Secondary antibody
hPD-L1	Rabbit anti-PD-L1 (Invitrogen, #28076-1-AP) 1:2000	HRP-goat anti-rabbit IgG (Cell Signaling) 1:2000
hCD47	Rabbit anti-hCD47 (abcam, #ab218810) 1:4000	HRP-goat anti-rabbit IgG (Cell Signaling) 1:2000
GFP	Rabbit anti-GFP pAb (Cell Signaling, #2555) 1:1000	HRP-goat anti-rabbit IgG (Cell Signaling) 1:2000
GAPDH	Rabbit anti-GAPDH (Cell Signaling, #2118) 1:4400	HRP-goat anti-rabbit IgG (Cell Signaling) 1:2000

Table 4: Immunohistochemistry antibodies

Targeted epitope	Heat-induced epitope retrieval	Primary antibody	Secondary antibody
alpha Gal	TARGET Retrieval Sol	Mouse anti-Gal IgM (Alexis, #Alx 801-090) 1:8	Biotinylated goat anti-mouse IgM (Vector Laboratories, #BA-2020) 1:100
hPD-L1	Tris-EDTA-buffer + 0.05% Tween pH 9.0	Rabbit anti-hPD-L1 (Cell Signaling, #13684) 1:400	Biotinylated goat anti-rabbit IgG (Vector, #BA-1000) 1:200
hCD47	Tris-EDTA-buffer + 0,05% Tween pH 9.0	Rabbit anti-huCD47 (abcam, #ab218810) 1:3000	Biotinylated goat anti-rabbit IgG (Vector, #BA-1000) 1:200
LEA29Y	-	Mouse αnti-huIgG Fc (JacksonImmuoResearch, #209-005-098) 1:900	Biotinylated goat anti-mouse IgG (JacksonImmuoResearch, #115-065-146) 1:250
Insulin	10mM citrate buffer pH 6.0 + 0.05% Tween	Mouse anti-Insulin IgG (Sigma, 2018) 1:3000	Biotinylated goat anti-mouse IgG (JacksonImmuoResearch, #115-065-146) 1:250
GFP	10mM citrate buffer pH 6.0 + 0,05% Tween	Mouse anti-GFP (Sigma Aldrich, #11814460001) 1:600	Biotinylated goat anti-mouse IgG (JacksonImmuoResearch, #115-065-146) 1:250

Table 5: FACS analysis antibodies

Targeted epitope	Antibody
α-Gal	FITC Isolectin B4 (Enzo Life Sciences Inc., #ALX-650-001-MC05)
hPD-L1	PE anti-human CD274 (eBioscience, #12-5983-42)
hCD47	Alexa Fluor® 700 anti-human CD47 (Biolegend, #323125)

Table 6: Immunofluorescence staining antibodies

Targeted epitope	Antibody
hPD-L1	Alexa Fluor ™ 488 mouse anti-human PD-L1 (Biosciences, #568926) 1:40
hCD47	Alexa Fluor™ 647 mouse anti-human CD47 (Biosciences, #561249) 1:40

2.9. Cells

2.9.1. Bacterial strains

5-alpha Competent *E. coli* (High Efficiency) New England Biolabs, USA

5 alpha Competent *E. coli* own production

TOP 10 Competent *E. coli* own production

2.9.2. Eukaryotic cell lines

Primary fibroblasts of porcine kidneys derived from the cell lines:

1-ml-DLxDL (WT)

5-ml-DLxDL (WT)

#7697 (*GGTA1*-het/hCD46/*INS*-LEA29Y)

#7700 (*GGTA1*-het/hCD46/*INS*-LEA29Y)

2.10. Oligonucleotides

2.10.1. gRNA

gRNAs were designed with the web-based tool CRISPOR and then purchased from Synthego, USA. Sequence is shown 5’ to 3’.

Table 7: gRNAs without PAM sequence

gRNA	Sequence without PAM
GGTA1-1 gRNA	5’-CCTGTAGCTGAGCCACCGAC-3’
GGTA1-2 gRNA	5’-ACGAGTTCACCTACGAGAGG-3’
CCL2-1 gRNA	5’-GCTGCATACCTGGCTGGGCA-3’
CCL2-2 gRNA	5’-GTAAGAAGATCTCGATGCAG-3’
Chr6-2 gRNA	5’-CACGGCTGAGTGGTTCTCAG-3’
GGTA1-5 gRNA	5’-TTTCCGAGCTGGTTTAACAA-3’
B2M-1 gRNA	5’-AGTAGCGATGGCTCCCCTCG-3’
R26 gRNA	5’-AATCCCGCCCATAATCGAGA-3’

2.10.2. Primer

Primers were manually designed, except for the gRNA cloning primers which were selected using the web-based tool CRISPOR and then purchased from Metabion **(Table 8)**.

Table 8: Primer

	Forward primer	Reverse primer	Annealing temp.	Elongation time	bp
Genotyping-PCRs					
INS-LEA29Y tg	INS-LEA_1_for 5'-AAGTCTGTGCGGCAACCTACAT-3'	INS-LEA_2_rev 5'-GCAAACAACAGATGGCTGGCAA-3'	64 °C	1m 20s	~ 1000 bp
hPD-L1 tg	huPDL1_1_for 5'-CCTGGC TGCACTAATTGTCTA-3'	huPDL1_2_rev 5'-ACGTCTCCTCCAAATGTGTATC-3'	62 °C	1m 20s	~ 600 bp
hCD47 tg	hCD47_7_for 5'-TAGCCTATATCCTCGCTG-3'	hCD47_15_rev 5'-ACTGCGGCCGCTTATTCATCATTCATC-3'	60 °C	1m 20s	~ 250 bp
3'long UTR middle	hCD47_34_for 5'-TTGGGCATCATTGGGCCAGTTCC-3'	hCD47_37_rev 5'-AGGACCCCAGCAGGTGATGGCAG-3'	60 °C	1m 20s	~ 800 bp
3'long UTR polyA tail	hCD47_30_for 5'-AGATGAGCAGTGAGTGACCAGGCAG-3'	hCD47_32_rev 5'AGATGCTCAAGGGGCTTCATGATG-3'	60 °C	1m 20s	~ 760 bp
CCL2 long	CCL2_8_for 5'-TGTCGTCCTGCCATGCGTCAGTGG-3'	CCL2_13_rev 5'-AGGATCTGAATAAGAACCCAGACGG-3'	64 °C	1m 20s	~1800 bp
CCL2 short 1	CCL2_20_for 5'-TCTTCTAGCTCTGAGGCACAGGCAG-3'	CCL2_13_rev 5'-AGGATCTGAATAAGAACCCAGACGG-3'	62 °C	1m 20s	~ 760 bp
CCL2 short 2	CCL2_16_for 5'-TCCTGACCCTCTGCTTCCCTCTC-3'C	CCL2_10_rev 5'-TAGGCTCCAAGTCATCTCTGC-3'	62 °C	1m 20s	~ 470 bp
GGTA1 exon 10	GGTA1_1_for 5'-ACATTGAGCATTACTTGGAGGAG-3'	GGTA1_5_rev 5'-ACAAGGCTCAAAGTTGCAAGGAAG-3'	60 °C	1m 20s	~ 900 bp
GGTA1 exon 10	GGTA1_8_for 5'-ATGCCTTTGATAGAGCTGGGTCCTC-3'	GGTA1_5_rev 5'-ACAAGGCTCAAAGTTGCAAGGAAG-3'	50 °C	1m 10s	~ 900 bp

GGTA1 exon 7	GGTA1_13_for 5'-ACAACTGGAAAGGGGCAGATCC-3'	GGTA1_15_rev 5'-AGCGTATGTAAGCTCATGACAGCC-3'	58 °C	1m 10s	~ 700 bp
B2M	B2M_1_for 5'-AGATTGGGGGACGACATACAGAGAG-3'	B2M_6_rev AGCTGAACCTGGCGGGTGCCTGG-3'	40 °C	1m 20s	~ 1000 bp
INS-LEA29Y in *SSC6*	Chr6_LEA_17_for 5'-AGCCAGCTCAGCTGCAAGTCTAG-3'	LEAchr6_13_rev 5'-TTCCAGCCCTGGCCTCTCTCG-3'	60 °C	1m 30s	~ 1000 bp
hPD-L1 in *SSC6* 5'HA	LEAchr6_3_for 5'-AGGCATTATGTCTGAATGCAGTGCTTGG-3'	Chr6_10_rev 5'-ACATGTTCACAGGCAACATTATGCAC-3'	60 °C	40s	~ 1800 bp
hPD-L1 in *SSC6* 3'HA	hPDL1_3_for 5'-AAGTGATACACATTTGGAGGAGACG-3'	Chr6_12_rev 5'-AGGGAACTTCTGCATGCTGATGGTG-3'	60 °C	40s	~ 450 bp
hPD-L1 in *GGTA1* ex 7 5'HA	GGTA1_53_for 5'-TGGACATCTGAGCATGTGTGTGG-3'	A2UCOE_5_rev 5'-AGCGGCTGAACGTCCGGAAAGAGG-3'	60 °C	1m 50s	~ 800 bp
hPD-L1 in *GGTA1* ex 7 3'HA	hPDL1_8_for 5'-AGAACTACCTCTGGCACATCCTCC-3'	GGTA1_57_rev 5'-ATGGCCCTGTTGCCTACACAGCCC-3'	60 °C	1m 50s	~ 1100 bp
hCD47 in *GGTA1* ex 10 5'HA	GGTA1_41_for 5'-AGGCCCTGGGCTTCCAAATCTTGAACC-3'	A2UCOE_5_rev AGCGGCTGAACGTCCGGAAAGAGG-3'	56 °C	1m 20s	~ 750 bp
hCD47 in *GGTA1* ex 10 3'HA	hCD47_27_for 5'-TGCTGCTACAGCAGACCACAAGCAC-3'	GGTA1_33_rev 5'-TCTGCTGTTGAAATCATCTGAGG-3'	59 °C	1m 50s	~ 1100 bp
GCaMP6	GCaMP6_2_for 5'-ACAAAGACCTGGCGACCATGGTGG-3'	GCaMP6_5_rev 5'-AATGGTTGTCAGGCAAGAGCACGG-3'	62 °C	50s	~ 300 bp
GAPDH	GAPDH_1_for 5'-CAACTCCCTCAAGATCGTCAG-3'	GAPDH_2_rev 5'-GAGCTTGACGAAGTGGTCGTT-3'	60°C	40s	~ 1100 bp
Cloning PCRs					
hCD47 Insert ex 10 PCR 5'HA	1_CD47_GGTA1_5HA_for_long 5'-ATATCGGCGCGCCAGTACTCCAAGCTTGCATGC CTGCAGGAGGCCTGTAGCTGAGCCACCGACTGGC GGTCGACCACAGAATTAGAAAGACTTAG-3'	2_CD47_GGTA1_5HA_rev_long 5'-AGTGGCACGAAATGGGATTGGAGCATTTTGGGGT GTTTAGCCCAGGGTCTCCACCCCAAAGTTGTTTTGG-3'	60 °C	60s	~ 800 bp

hCD47 Insert ex 10 PCR 3'HA (nested 1)	11_CD47_GGTA1_3HA_for_template 5'-GGCACATCCTGACGAGTTCACCTACGAGAGGC GGAAGGAGTCCGCAGCCTACATTCCGTTTGGC-3'	12_CD47_GGTA1_3HA_rev_template 5'-GAGGCCTGTAGCTGAGCCACCGACTGGGTCGACC CAGTATCTGCGCAGAAGC-3'	57 °C	60s	~ 750 bp
hCD47 Insert ex 10 PCR 3'HA (nested 2)	9_CD47_GGTA1_3HA_for_short 5'-GGGCAAATCATTTAAAACATCAGAATGAGTATT TGGTTTGGGCACATCCTGACGAGTTCAC-3'	10_CD47_GGTA1_3HA_rev_short 5'-GCGCCATTGGGATGGATCCATCGGCGCGCCTTCG AGGGGGAGGCCTGTAGCTGAGCC-3'	57 °C	60s	~ 800 bp
hPD-L1 Insert ex 7 5' HA	12_5HA_GalPDL1_lon_for 5'-AGTGGCACGAAATGGGATTGGAGCATTTTGGGG TGTTTAGAAACCAGCTCGGAAACCACCAG-3'	10_5HA_GalPDL1_lon_rev 5'-ATATCGGCGCGCCAGTACTCCAAGCTTGCATGCC TGCTTTCCGAGCTGGTTTAACAAAGGTCGACCTTCG GGTTTAGAAACCCTCAGGTTTC-3'	58 °C	60s	~ 750 bp
hPD-L1 Insert ex 7 3' HA	14_3HA_GalPDL1_lon_for 5'-TGGTTTAGAGTTTGGCAACATATGTGCCGCCA CCTGGTACAATGGGTAAGACTGGGAAACGGCCAT C-3'	16_3HA_GalPDL1_long-rev 5'-GCGCGCCATTGGGATATCGGCGCGCCTTCGAGCT CGGTACTTTCCGAGCTGGTTTAACAATGGGGTACCT TGCCTATAGCGTCTTCTTCTTCGTGG-3'	58 °C	60s	~ 600 bp
hPD-L1 Insert *SSC6* 5'HA	1_5HA_hPDL1_long_for 5'-ATATCGGCGCGCCAGTACTCCAAGCTTGCATGC CTGCAGGGGTCGACTTAGGACAGAACACGGCTGA GTGGTTCTCAGGGGTTGGCCACCCTCATAGCATGC AGAAATTCC-3'	3_5HA_hPDL1_rev 5'-AGTGGCACGAAATGGGATTGGAGCATTTTGGGGT GTTTAGCTGAGGAAAGGCGGATGGGAG-3'	58 °C	60s	~ 910 bp
hPD-L1 Insert *SSC6* 3'HA (nested 1)	3_HA_hPDL1_kurz_for 5'-AGACCAATATATTCTGAGTGTTTCATACAATAC ATGACC-3'	3_HA_hPDL1_short_rev 5'-TGAGGATGTGGAGAAATCAGGAACCC-3'	58 °C	60s	~ 840 bp
hPD-L1 Insert *SSC6* 3'HA (nested 2)	5_3HA_hPDL1_long_for 5'-TGGTTTAGAGTTTGGCAACATATGTGCCGCCAC CTGGTACTAGGAGACCAATATATTCTGAGTGTTTC ATACAATACATG-3'	7_3HA_hPDL1_long_rev 5'-GGCGCGCCATTGGGATATCGGCGCGCCTTCGAGC TCGGTACCGGTACCTAGGACAGAACACGGCTGAGT GGTTCTCAGGGGGGTGAGGATGTGGAGAAATCAGG AACCC-3'	58 °C	60s	~ 840 bp

2.11. Plasmids

p3s-Sniper-Cas9	Addgene, #113912
pX458M-53BP1-DN1S	Addgene, #131045
WT_hCD47-LU	in house, modified from Addgene #65474 (GFP_CD47_LU)
pA2UCOE-CAG-hCD47-LU	in house
INS-LEA29Y-loxPneo	in house
pA2UCOE-CAG-hPD-L1	in house
pA2UCOE-CAG-GCaMP6	in house U6-gRNA vectors in house, gRNA expression vector under control of human U6 polymerase III promoter, containing gRNA sequences for targeting *CCL2* or *Rosa26* gene loci, respectively

2.12. Software

BioRender	Science Suite Inc., Canada
DeepL	DeepL GmbH, Germany
Endnote20	Clarivate Analytics, UK
FlowJo	FlowJo LLC, USA
GraphPad Prism v.5.10	GraphPad Software, USA
Microsoft Office 2016 ProPlus	Microsoft Corporation, USA
SnapGene Viewer 6.0	Graph Pad Software, USA
TIDE	NKI, Netherland

3. Methods

3.1. Generation of expression vectors for gene targeting

3.1.1. DNA restriction enzyme digestion

To perform DNA plasmid cloning and analytical verification of plasmid length and/or composition, plasmids were subjected to restriction enzyme (RE) digestion. For analytical digestion, 0.5 – 1 µg of plasmid DNA was used in a final digest volume of either 10 or 20 µl. For preparative digestion, up to 1 µg of plasmid DNA was used in a digest approach of up to 1 µl. All digests were performed according to the manufacturer's instructions. For RE digestion using two or more different REs, the protocol advised by NEB® cloner was applied (https://nebcloner.neb.com/#!/redigest). Of note, the amount of RE used should not exceed 10% of the final digest volume due to the inhibitory impact of glycerol. The incubation time and temperature were followed as indicated, followed by heat inactivation. **Table 9** shows an exemplary analytical digest using the restriction enzyme *Sal*I.

Table 9: Analytical digest using restriction enzyme *Sal*I

DNA	0.5–1 µg
10x Buffer Cut Smart	2 µl
*Sal*I (20 U/µl)	0.5 µl
H_2O bidest.	ad to 20 µl

After adding an appropriate amount of 6x loading buffer, size differentiation of DNA fragments from the analytical plasmid DNA approach was performed using 0.8% agarose gel electrophoresis.

3.1.2. Dephosphorylation of cleaved DNA

Plasmid DNA obtained from preparative RE digestion was processed by a CiAP treatment **(**refer to **Table 10)** prior to heat inactivation. CiAP is used to remove 5' phosphate groups from the DNA ends, preparing it for the ligation process. The incubation initially was carried out at 37 °C for 30 min, followed by 65 °C for 20 min. Then, the sample was placed on ice.

Table 10: CiAP treatment

rSAP	1 µl
10xBuffer Cut Smart	1 µl
H_2O bidest.	ad to 10 µl

3.1.3. Purification of DNA fragments

To prepare DNA fragments for further use, microdialysis, column DNA purification, or agarose gel electrophoresis can be used depending on their size. Microdialysis was performed for up to 2 h on a dialysis membrane containing DNA and 10 mM Tris pH 7.5 at a 1:1 ratio. DNA fragments were separated using gel electrophoresis on a 0.8% agarose gel. After gel electrophoresis and photographic documentation of the gel under UV light (see also Chapter 3.4.3.), the required DNA fragment was excised from the gel under UV light using a scalpel blade and transferred into a 1.5 ml reaction vessel. Subsequently, the DNA was isolated from the gel using the QIAquick® Gel Extraction Kit according to the manufacturer's instructions. Following this, the concentration of the isolated DNA was measured using the NanoDrop instrument.

3.1.4. Cloning by ligation

For the ligation of DNA fragments with a vector backbone, T4 DNA ligase was employed. In a 20 µl reaction, 50 ng of vector DNA was incubated with 37.5 ng of the insert fragment, along with 1 µl of T4 DNA ligase and 2 µl of 10x ligation buffer. The required amount of insert DNA was calculated using the NEBioCalculator: https://nebiocalculator.neb.com/#!/ligation. After an incubation period of 2 h at room temperature or overnight at 16 °C, enzyme inactivation was carried out at 65 °C for 10 min.

3.1.5. Gibson assembly cloning

The Gibson Assembly Cloning relies on a combination of exonuclease, polymerase, and DNA ligase activities to assemble multiple DNA fragments into a single contiguous piece. This method is efficient and versatile, allowing for the assembly of large DNA constructs without the need for restriction enzymes or DNA ligases **(**see **Figure 6)**. In contrast, cloning by T4 ligation involves the use of the T4 DNA ligase enzyme to join DNA fragments with compatible cohesive ends generated by restriction enzymes. The limitation of T4 ligation is due to the availability of suitable restriction sites and the necessity for compatible cohesive ends, whereas Gibson Assembly offers greater flexibility in fragment design and assembly.

In Gibson assembly cloning, vector plasmids were prepared by RE digestion and purification, while insert DNA fragments were generated by PCR amplification. The primer design for PCR-generated DNA inserts was performed using the SNAPgene software. If indicated, additional RE cutting sites were introduced in the primer at appropriate sites.

Ligation of DNA fragments to vectors was performed using the Gibson assembly protocol, following the manufacturer's instructions (#E5510S, New England Biolabs). This process utilized linearized vectors and corresponding homologous arms (inserts). To ensure efficient assembly, it is recommended to use a total of 0.2-1.0 pmoles of the insert DNA. The required amount of insert DNA was calculated using the following formula:

pmols= (weight in ng) × 1,000 / (base pairs × 650 daltons).

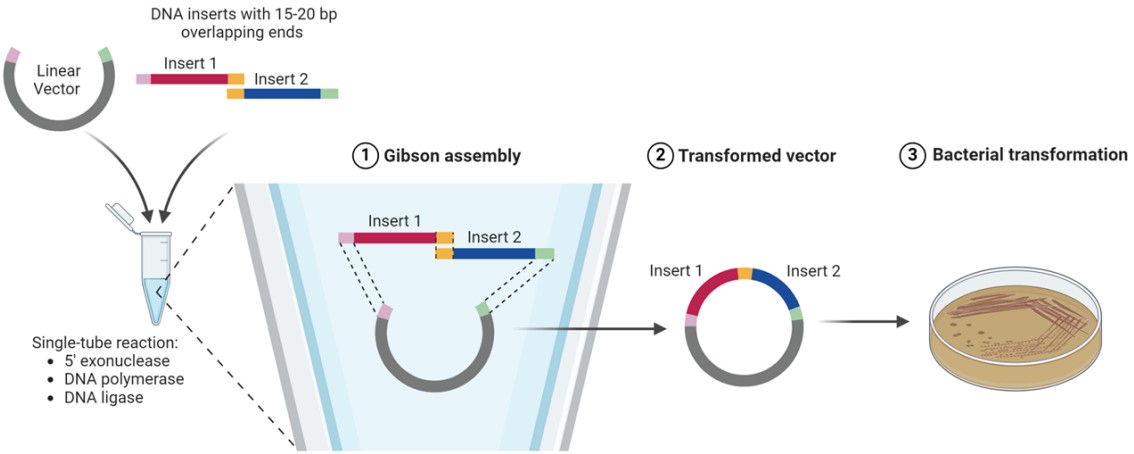

Figure 6: Principle of the Gibson Assembly Cloning.

In Gibson Assembly, three enzymatic functions work together within a single reaction: 5' exonuclease activity, the 3'-extension capacity of a DNA polymerase, and DNA ligase activity. The 5'-exonuclease activity trims the 5' end sequences, exposing complementary sequences for hybridization. Subsequently, the polymerase activity fills in the gaps within the hybridized regions. Finally, DNA ligase seals the nick and covalently joins the DNA fragments. Gibson Assembly utilizes long overlapping sequences between adjacent fragments, leading to a high percentage of correct assemblies (NEB®). Adapted from “Gibson Assembly Cloning 2”, by BioRender.com (2024).

3.1.6. Production of transformation-competent bacteria

Bacteria used for the transformation were either provided with the NEB Gibson Assembly® KIT (5-alpha Competent *E. coli* (High Efficiency) #C2987I) or prepared as follows: The bacterial strain utilized (E. coli TOP10) was initially streaked from a glycerol stock onto an LB plate and incubated overnight at 37 °C. Subsequently, a single colony was inoculated into 5 ml TYM medium (with 50 µg/ml streptomycin, Sigma) and incubated overnight at 37 °C and 170 rpm on a shaker. 1 to 2.5 ml of the pre-culture was transferred into 250 ml of TYM medium (without streptomycin) and incubated at 37 °C on a shaker. When the OD600 value reached 0.7 to 0.8 (after 2 to 4 h), the culture was transferred into six 50 ml plastic tubes (40 ml bacterial culture per tube) and rapidly cooled for 5 to 10 min in an ice-water bath. The bacteria were then centrifuged for 10 min at 800 g and 4 °C, the supernatant discarded, and the bacterial pellets resuspended in 12 ml each of ice-cold Tfb I buffer in the ice-water bath. After a ten-minute

incubation on ice, the bacteria were pelleted again by centrifugation at 600 g and 4 °C for 10 min, and the supernatant discarded. The pellet in each tube was then carefully resuspended in 1.6 ml of ice-cold Tfb II buffer. Subsequently, 100 µl of the transforming bacteria were transferred into 1.5 ml reaction tubes and stored at -80 °C.

3.1.7. Transformation of *E. coli*

The transformation process depends on the type of *E. coli* used. When employing 5-alpha competent *E. coli* (High Efficiency) from NEB®, the protocol recommended by the manufacturer was followed. For in-house prepared heat-competent *E. coli*, the transformation was conducted as follows:

3.1.7.1. Transformation of *E. coli* TOP10

A 100 µl aliquot of transformation-competent *E. coli* TOP10 cells was promptly transferred from -80 °C to wet ice and thawed slowly. 10 ng of plasmid or up to 5 µl of a ligation mixture were added to the bacterial solution, gently mixed, and incubated on ice for 30 min. Subsequently, a precise 45-second heat shock was applied at 37 °C, followed by 2-3 min on ice. Then, 800 µl of LB medium (without antibiotic) was pipetted into the transformation mixture and incubated with gentle shaking for 1 h at 37 °C in a thermoblock. The transformed *E. coli* cells were ultimately plated on LB agar plates (with 50 µg/ml ampicillin) using a sterile curved Pasteur glass pipette and incubated overnight at 37 °C. After 12 to 16 h of incubation, individual colonies became visible.

3.1.7.2. Transformation of DH5 alpha *E. coli*

For the transformation process, chemically competent DH5 alpha *E. coli* were thawed on ice. A transformation reaction was then prepared on ice, combining 50 µl of *E. coli* with 5 µl of the ligation mix. After a 30-min incubation on ice, a heat shock was administered in a water bath at 42 °C for 90 seconds, followed by a 3-min incubation on ice. 1 ml of LB medium was added, and the mixture was incubated for 30 min at 37 °C at 200 rpm. The transformed material was plated on LB-Agar plates containing 200 µg/ml ampicillin and incubated overnight at 37 °C. The next day, up to five colonies were selectively picked, inoculated into 5 ml of LB medium supplemented with 200 µl of ampicillin, and incubated overnight at 37 °C at 200 rpm. After 12 to 16 h of incubation, individual colonies became visible.

3.1.8. Isolation of plasmid DNA (Miniprep and Midiprep) from *E. coli*

Single colonies were picked from a LB agar plate using sterile pipette tips and transferred into 5 ml of LB medium (with 50 µg/ml ampicillin). After incubation for 12 to 18 h at 37 °C with constant shaking at 170 rpm, plasmid DNA was isolated from 4 ml of the bacterial culture using the QIAprep Spin Miniprep Kit™ following the manufacturer's instructions. The concentration of the isolated plasmid DNA was subsequently determined using a spectrophotometer at 260 nm/280 nm. For analysis with restriction enzymes, 500 ng of Miniprep plasmid DNA was used. In cases where larger quantities of plasmid DNA were required, such as for cell electroporation, a Midiprep was initiated. For this purpose, 50 µl of the Miniprep culture was added to 100 ml of LB medium (with 50 µg/ml ampicillin) and incubated for 12 to 18 h at 37 °C with constant shaking at 170 rpm. Subsequently, plasmid DNA was isolated using the QIAGEN™ Plasmid Midi Kit according to the manufacturer's instructions.

3.1.9. Glycerol stocks of bacteria

For long-term storage of plasmid-containing *E. coli* bacteria, a glycerol stock was generated by mixing the bacterial culture with a 50% glycerol solution in equal volumes (volume ratio 1:1). The bacteria-glycerol mixture was then transferred into cryotubes and stored at -80 °C.

3.1.10. Selection of gRNA and cloning of sgRNA into pX458M-53BP1-DN1S

The selection of gRNA sequences for the CRISPR/Cas9 targeting approach was performed using the http://crispor.tefor.net/ online tool. Oligos sgRNA-oligo-F and sgRNA-oligo-R for integration of sgRNA into vector pX458M-53BP1-DN1S were used as recommended there. **Table 7** (Chapter 2.10.1.) lists the oligos used.

The sgRNA oligos were cloned into the vectors using *Bbs*I restriction enzyme overhangs with N1-N20 as the selected Cas9 targeted sequence. Therefore, 1 µl of oligo F and 1 µl of oligo R (each 1 µg/µl) were combined in a microcentrifuge tube with 98 µl 10mM Tris pH 7.5. After incubation for 5 min at 98 °C in a heat block, the mix was allowed to cool down slowly to RT. T4 DNA ligase was used to ligate the annealed oligos with vectors. 100 ng of linearized vector DNA was incubated with 1.5 µl annealed oligos in a preparation with 1 µl of T4 DNA ligase and 1.5 µl of fresh ligase buffer and filled up to 20 µl nuclease-free water. After an incubation period of 2 h at RT or overnight at 16 °C, the enzyme was inactivated at 65 °C for 10 min. The subsequent transformation process was carried out as described previously.

3.2. Cell culture

All cell culture procedures were carried out under laminar flow cabinets to ensure a sterile working environment. Details regarding the composition of the cell culture media, buffers, and manufacturer information of the components can be found in section 2.5. To culture PKCs, plates were precoated with 0.2% collagen for 1 h. The cells were cultured in a humidified incubator at 37 °C and 5% CO_2.

3.2.1. Isolation, cultivation and cryopreservation of PKCs

Isolation of PKCs was carried out on kidneys obtained from euthanized pigs of the desired genetic background under sterile conditions. The kidneys were stored in PBS containing 2% penicillin/streptomycin and 2% amphotericin as a transport medium until further processing. A small section comprising both cortex and medulla was excised from the kidney, then washed in PBS containing 2% penicillin/streptomycin and 2% amphotericin and minced into 1-2 mm pieces in a Petri dish with 1 - 2 ml PBS. The suspension was transferred into a 50 ml Falcon tube and washed with wash medium until the supernatant became clear. 0.1% collagenase in Hanks buffered salt solution (HBSS) was added to the suspension, which was then transferred to an Erlenmeyer flask and incubated at 37 °C while stirring for approximately 1.5 h. Afterwards, the suspension was filtered through a 100 µm sieve, followed by centrifugation for 5-10 min at 54 *x g* at room temperature, and aspiration of the supernatant. The resulting pellet was washed twice before being resuspended in PKC culture medium containing 10% FCS / 1% penicillin/streptomycin, and 1% amphotericin. PKCs were cultured on 10 cm collagen-coated culture plates, maintained at 37 °C and 5% CO2 in humidified environment until reaching confluency. The medium was changed one day after isolation and thereafter every 2 – 3 days.

For splitting, freezing, and transfection, the cells were detached using EDTA/Trypsin. Alternatively, for surface antibody staining prior to flow cytometry, Accutase® cell detachment solution was used. Cryofreezing of PKCs was performed in a solution containing 50% media / 40% FCS / 10% DMSO.

3.2.2. Gene editing of PKCs

For genome editing, the PKCs in passage numbers 2 - 4 were transfected via nucleofection with the Basic Nucleofector™ Kit for Primary Mammalian Fibroblasts (Lonza), according to the manufacturer's instructions. PKCs were used at a confluency of 80 – 90%. After trypsinization of the cells, the cell number was determined using a Neubauer counting chamber during the first centrifugation step at 200 *x g* for 5 min. After discarding the supernatant, the cell pellet

was resuspended in media, and 0.5 mio cells per tube were aliquoted before a second centrifugation step was performed. After removing the supernatant, the cell pellet was resuspended in 100 µl Nucleofector Solution, immediately followed by adding 1-5 µg DNA and/or preformed ribonucleoprotein (RNP) complex to the suspension, and the transfer into an Amaxa™ certified cuvette. Program U-12 was used for nucleofection. Afterwards, cells were gently transferred into prewarmed culture medium of a well of a collagen-coated 6-well plate. After 24 h, the first media change took place.

3.2.3. Selection of gene edited cell populations as donor cells for SCNT

3.2.3.1. Cell sorting by flow cytometry

Initially, cells on the plate/flask were washed with pre-warmed PBS. Then, Accutase® was added, tailored to the specific flask size (1 ml for T25, 2 ml for T75, and 4 ml for T175), to detach the cells from the plates and left for about 5 min. To stop the detachment reaction, ice-cold PBS/BSA 1% or stop media was introduced. Following this, the cells were carefully transferred into a 50 ml Falcon tube. After two washing steps with ice-cold PBS/BSA 0.25%, wherein the cells were divided into samples designated for staining and passed through a 40 µm cell sieve. After centrifugation at 54 *x g* for 5 min with the brake engaged, the supernatant was aspirated.

A fresh solution of antibody-labelling (100 µl PBS/BSA 0.25% plus antibody, prepared in the dark) was swiftly introduced to resuspend the cell pellet, followed by immediate placement on ice in the dark. The cells were incubated on ice in the dark for approximately 30 minutes. A dual-phase washing process ensued, first with PBS/BSA 0.25% and then with PBS/BSA 1%, each followed by centrifugation at 54 *x g* for 5 min. The cells were subsequently resuspended in FACS-Buffer (PBS/BSA 2%). Sorting of cells was performed in FACS tubes, with 2 ml medium (+ penicillin/streptomycin) provided. Finally, the sorted cells were seeded onto a collagen-coated plate for further culture.

3.2.3.2. Single Cell Clones (SCCs)

For the generation of SCCs, 1-2 cells per well were seeded. SCCs were identified through routine scanning using the Cellavista cell culture microscope. The clones were split into two wells of a 96-well full area-plate when they reached approximately 75% confluence. Once reaching 90% confluence, cells from one well were harvested for storage in liquid nitrogen for potential SCNT, while cells from the other well were used for DNA analysis to screen for the desired modifications by PCR.

3.3. Somatic cell nuclear transfer (SCNT) and embryo transfer

Cells derived from gm-enriched bulk preparation or derived from SCCs were used for somatic cell nuclear transfer (SCNT) by the SCNT unit at the Chair for Molecular Animal Breeding and Biotechnology, LMU Munich (KUROME et al., 2015). The SCNT embryos were transferred to estrus-synchronized recipient sows followed by laparoscopic embryo transfer (ET) into the oviduct. The pregnancy status was routinely assessed from the 21st day post-ET onwards using a portable ultrasound system.

3.4. Genomic analysis

3.4.1. gDNA isolation using Monarch Genomic DNA Purification Kit

To identify transgenic pigs, genotyping PCRs were conducted on tissue samples collected from the piglets. Tail samples or ear punches were obtained from newborn piglets and stored at -20 °C until further processing.

To extract gDNA from tissue samples, the Monarch® Genomic DNA Purification Kit (New England Biolabs, Ipswich) was used according to the manufacturer's instructions. gDNA was stored at 4 °C for further usage.

3.4.2. gDNA isolation by high-salt precipitation

For gDNA isolation of 96-well SCCs, a master mix was prepared by combining 100 µl PK-buffer, 10 µl 10% SDS, 5 µl 1M DTT, and 2.5 µl proteinase K (20mg/ml). 117.5 µl of the master mix was added to each sample. After the incubation for 2 - 2.5 h at 60 °C, 30 µl 4.5 M NaCl was added, and tubes were placed on ice for another 10 min. After centrifuging at full speed (>10,000 rcf) for 20 min at 10 °C, the supernatant was transferred into a new tube, and 98 µl isopropanol was added. After another centrifugation at full speed (>10,000 rcf) for 20 min at room temperature, the supernatant was removed, and 200 µl 70% EtOH was added. A final centrifugation was carried out for 20 min at room temperature. After removal of the supernatant, the DNA pellet was allowed to air dry. This pellet was finally dissolved in 35-50 µl 10 mM Tris pH 7.5 and stored at 4 °C for further usage.

3.4.3. Polymerase chain reaction (PCR)

PCR was used to amplify DNA inserts for plasmid assembly, screen SCCs to confirm targeted integration of the expression cassette and/or NHEJ gene editing and genotype the gm pigs.

Details of primers and PCR conditions for SCC screening and genotyping can be found in Chapter 2.10.2., **Table 8**. PCR reactions were prepared as 20 µl mixtures in 0.2 ml PCR reaction tubes using Taq DNA polymerase (5 U/µl; Qiagen) on ice as follows:

Table 11: Single PCR reaction mixture

Aqua bidest.	8.65 µl
Q-Solution (Qiagen)	4 µl
10x Buffer (Qiagen)	2 µl
$MgCl_2$ (50 mM) (Qiagen)	1.25 µl
dNTPs (1 mM)	1 µl
forward Primer (2 µM)	1 µl
reverse Primer (2 µM)	1 µl
Taq-Polymerase (5 U/µl)	0.1 µl
DNA-sample (100 ng/µl)	1 µl

After completing the PCR, the PCR samples were cooled to 4 °C in the thermal cycler. Until further use, the samples were stored at 4 °C for a short time and at -20 °C for a longer time.
In each case, the corresponding transgene construct or DNA from a transgenic animal or transgenic cells served as a positive control for genotyping PCR, and DNA from a WT animal functioned as a negative control. In addition, distilled water was used as a non-template control to ensure that there was no contamination.

3.4.4. Agarose Gel Electrophoresis

Agarose gel electrophoresis was used to separate DNA fragments, including PCR amplicons and those derived from restriction enzyme digestion of plasmids, based on their size. An appropriate amount of agarose powder (Bio&SELL) was mixed in 1x TAE buffer and heated in a microwave until it was fully dissolved to obtain a 0.8% - 2% agarose gel. **Table 12** shows the proportions of agarose gels chosen for separating DNA fragments of different sizes.

Table 12: Gel percentage in relation to the DNA fragment size

0.8%	1000 - 20000 bp
1.0%	800 - 12000 bp
1.5%	500 – 7000 bp
2.0%	300 – 3000 bp

The gel was poured into gel electrophoresis chambers to allow it to solidify. Once the gel had set, the chamber was filled with 1x TAE buffer serve as running buffer. Each PCR sample was mixed with 2.5 µL of a 1:250 solution of GelRed® and DNA loading buffer (10x) and pipetted into single gel slots. 6 µL of GeneRuler™ 100 bp or 1 kb DNA molecular weight standard served as DNA molecular weight standard. The DNA fragments underwent separation based on their respective sizes through applying an electric current to the gel electrophoresis chamber. The DNA fragments were subsequently exposed to UV light for visualization and compared to the DNA molecular weight standard.

3.4.5. Sanger sequencing

Sanger sequencing of purified PCR products and plasmids was performed at Genewiz, Leipzig. Residual primers were removed from PCR products using the Exo-CIP™ Rapid PCR Cleanup Kit, according to the manufacturer's guidelines. For Sanger sequencing, 1 µl of the Exo-CIP™ cleaned up PCR product was mixed with 2.5 µl primer solution (10 pmol/µl) and filled up to a total volume of 10 µl with 10 mM Tris pH 7.5 in a 1.5 ml tube labelled with a pre-paid barcode. For Sanger sequencing of plasmids, 200-400 ng/µl plasmid DNA was used per reaction.

3.5. Analysis of protein expression

Analysis of protein expression, both for presence of transgene expression and absence of sugar epitopes and/or proteins, was performed on cells or tissue samples, as indicated.

3.5.1. Immunofluorescence staining of cells on slides

A 6-channel Ibidi slide coated with collagen was loaded with a 30 µl cell suspension per channel and supplied with medium after cell adhesion, typically occurring within 2-3 h. For fixation, PBS-buffered 4% paraformaldehyde (PFA) was introduced into the channels and allowed to fix for approximately 10 min. Subsequently, phosphate-buffered saline (PBS) was added, and the samples were stored at 4 °C until further processing.

To permeabilize the cells for the staining process, 0.3% Triton in PBS was applied to the channels for 10 min, followed by blocking with 0.5% bovine serum albumin (BSA) in PBS. Next, the antibodies (listed in Chapter 2.8., **Table 6**) were added and allowed to incubate in a dark chamber for 2 h. Following a PBS wash, the nuclear dye Hoechst 33342 was introduced and left to incubate for an additional 10 min in the dark chamber. Finally, the channels were washed with PBS and sealed for further analysis.

3.5.2. Expression analysis by flow cytometry

Expression analyses via flow cytometry are detailed described in Chapter 3.2.3.1. To measure tg expression on the nuclear membrane, the cells were permeabilized using the BD Cytofix/Cytoperm™ Fixation/Permeabilization Kit as indicated.

The acquired flow cytometry data were analyzed using the FloJo software program, providing a comprehensive examination of expression patterns and allowing for the quantification of the analyzed samples.

3.5.3. Protein isolation

Protein isolation was performed by transferring 20 mg of tissue samples, which had been stored at -80 °C, to 12 ml plastic tubes. 500 µl of protein extraction buffer was added to the tubes, which were then homogenized on position D (23,500 rpm) using a tissue homogenizer (ART-Miccra D8) for 1 to 2 minutes. After each sample, the homogenizer bar was cleaned with Aqua bidest. and 1x PBS. The homogenized samples were placed on ice, transferred to 1.5 ml reaction tubes and subjected to a 2-min ultrasonic bath three times. Afterwards, the samples were incubated at 55 °C for 1 h and subsequently placed on ice. After centrifugation at 15,000 *xg* and 4 °C for 5 min, the supernatants were transferred to new reaction tubes. Additionally, 10 µl of the supernatant were used for protein concentration determination. The protein samples were stored at -20 °C until further use.

3.5.4. Determination of protein concentration by BCA assay

The principle of protein determination with BCA is based on the fact that bicinchoninic acid, as a water-soluble sodium salt, reacts very sensitively, specifically, and stably with Cu^{1+} ions. Here, the Biuret reaction of the proteins is utilized, which reduces Cu^{2+} to Cu^{1+}. The resulting BCA-Cu^{1+} complex is stable, water-soluble and exhibits strong absorption at 562 nm. Therefore, this method can be used to quantify proteins in aqueous solutions at 562 nm in the spectrophotometer. Protein measurements were conducted in 96-well F plates. To prepare the samples, 10 µl of each was diluted in 40 µl of PBS in 1.5 ml reaction tubes. A stock solution of BSA was used to prepare a dilution series in PBS/extraction buffer (4:1) with six standards (50 µl each) in 1.5 ml reaction tubes. Bicinchoninic acid was mixed with 4% CuSO4 solution (50:1), and 200 µl of this solution was added to each reaction tube. After brief mixing, 100 µl of each sample and standard were pipetted twice into a 96-well plate. Following incubation at 37 °C for 30 min, the absorbance was measured at 562 nm. The protein concentration was determined using the measured calibration line.

3.5.5. Sodium dodecyl sulphate-polyacrylamide gel electrophoresis (SDS-PAGE)

The principle of sodium dodecyl sulphate polyacrylamide gel electrophoresis (SDS-PAGE), as described by Laemmli (1970), is based on the separation of proteins by the molecular sieve effect of a polymerized gel matrix of acrylamide and N,N'bisacrylamide. Regardless of the protein extraction method, the denatured protein solution prepared for gel electrophoresis contains SDS. The SDS anions bind with their hydrophobic region to approximately every second amino acid residue. Due to the mutually repulsive negative charges of the SDS molecules, the proteins become elongated, and their intrinsic charge is compensated. This results in the formation of a complex, which moves through the gel at a speed proportional to the protein's mass. By applying a voltage, the protein mixture can be separated, with smaller proteins migrating faster than larger ones towards the anode. The separation of the proteins occurs in two steps. First, the samples are passed through a coarse-pored collecting gel with low acrylamide concentration to focus them on a narrow range. Then the proteins are separated by size in a separation gel with a higher acrylamide concentration.

The SDS-PAGE investigations were carried out using the Miniprotean Tetra Cell IV system according to Laemmli's method. After pouring the separating gels into the appropriately prepared mini-gel glass plates, Isopropanol was carefully applied to coat the plates. After polymerization for 60 min, the isopropanol was removed, and the separating gel was overlaid with a 5% collecting gel. The combs were placed in the liquid collecting gel. After polymerization of the collection gel at RT for at least 60 min, the SDS-PAGE was carried out.

Table 13: Composition of the separating gel (12%, 4 gels)

Aqua bidest.	6.7 ml
1.5 M Tris-HCl (pH 8.8)	5 ml
30% Acrylamid/Bis Solution (29:1)	8.0 ml
10% SDS	200 µl
Temed	10 µl
10% APS	100 µl

Table 14: Composition of the collection gel (4 gels)

Aqua bidest.	7 ml
0.5 M Tris-HCl (pH 6.8)	1.25 ml
30% Acrylamid/Bis Solution (29:1)	1.5 ml
10% SDS	100 µl
Temed	5.5 µl
10% APS	125 µl

After assembling the Miniprotean system and filling it with 1x SDS-PAGE running buffer, the gel pockets were rinsed with running buffer after removing the combs to remove non-polymerized acrylamide residues. Prior to sample application, sample preparation was performed for 60 min at 55 °C, followed by cooling on ice and centrifugation to remove condensate from the lid. A protein molecular weight marker was applied to the gel. The gel electrophoresis was conducted using the Miniprotean Tetra Cell IV system, starting at 100 V until the separation gel was reached, and then increasing to 160 V.

3.5.6. "Semi-dry blot" method

Following gel electrophoresis, the proteins were transferred from the SDS polyacrylamide gel to a protein-binding Immobilon P-PVDF membrane using the semi-dry blot method with the Bio-Rad Trans-Blot® Turbo™ transfer system. To prepare, two thick Whatman filter papers and one PVDF membrane were cut to the appropriate size for each gel. The PVDF membrane was activated by soaking it in 100% methanol for 10 min, followed by equilibration in transfer buffer for 30 min. The blot was then assembled under semi-dry conditions, free of air bubbles, on the lower blotting unit (anode) as follows: Blot sandwich (details for one blot): • one Whatman filter paper soaked in transfer buffer • PVDF membrane, labelled with a marker pen • Gel • one Whatman filter paper soaked in transfer buffer. The upper graphite blotting unit (cathode) was then applied with slight pressure to transfer the proteins onto the membrane. The transfer occurred from the cathode towards the anode at 25 V 1.0 A/cm2 for 30 minutes. After completing the transfer, the proteins bound to the PVDF membrane were stained with Ponceau S solution for 2 to 5 min, followed by background destaining through washing with distilled water. Once the membrane was dried on an absorbent gel blotting paper, molecular weight markers were labelled on the blot using a marker pen. The membrane was stored at 4 °C until further use.

3.5.7. Western Immunoblot

Western immunoblot was used to specifically detect proteins through antigen-antibody coupling. After transferring the PVDF membrane into a 50 ml plastic tube and activating it with 7 ml of methanol (100 %) for 1 min, the membrane was washed with TBS-T (0.1%) three times for 5 min. Subsequently, the membrane was blocked with TBS-T milk (5%) for 60 min at RT in a hybridization oven. This step saturates excess protein binding sites on the membrane and prevents non-specific binding of the detection reagents. The membrane was washed three times with TBS-T (0.1%) at RT (1x 15 min and 2x 5 min followed by overnight incubation with the first antibody diluted in BSA (5%) at 4°C. Afterward, the membrane was washed three times with TBS-T (0.1%) at RT for 1x 15 min and 2x 5 min, and the second peroxidase-conjugated antibody in TBS-T milk (5%) was added for 60 min at RT. All antibodies used are listed in Chapter 2.8., **Table 3**. This was followed by three washes at RT with TBS-T (0.1%) for 1x 15 min and 2x 5 min. Signal detection was performed using an enhanced chemiluminescence (ECL) detection solution and the ChemoStar Touch 21.5.

3.5.8. Stripping of the membrane

To reuse the membrane for further Western immunoblotting, the bound antibodies were eluted from the blot. The blot membrane was transferred to a hybridization tube, rinsed briefly in TBS-T (0.1%), and then incubated in elution buffer for 30 min at 70 °C in a hybridization oven. Subsequently, the membrane was then incubated at RT twice for 10 min with distilled water and then once for 10 min with TBS-T (0.1%) in large volumes. If repeating the immunoblot, the membrane was transferred into a new 50 ml plastic tube.

3.5.9. Expression analysis by immunohistochemistry

For histological analysis to determine the protein expression pattern, tissue samples were fixed in either PBS-buffered 4% paraformaldehyde (pH 7.4) for 48 h at 4 °C or in methacarn solution for 48 h at 4 °C. The samples were then dehydrated in an ascending ethanol series and xylene before being embedded in paraffin.

Immunohistochemical analyses were conducted on various organ samples including the tail, skin, skeletal muscle, spleen, kidney, heart, liver, lung, and pancreas. WT animals and animals from preexisting lines, if available, were used as controls.

The 3 µm slides were deparaffinized in xylene (twice for 20 min) and then rehydrated through a sequential process of decreasing alcohol concentrations (2x 100%, 2x 96%, 1x 70% alcohol, 2x distilled water). **Table 15** outlines the steps, their purpose, and conditions of the immunohistochemistry protocol.

Details of the immunohistochemistry protocol for each primary antibody used are provided in Chapter 2.8., **Table 4**. Finally, the slides underwent an increasing alcohol series (distilled water, 70%, 2x 96%, 2x 99% ethanol), were cleaned with xylene, and ultimately sealed with coverslips using Histokitt.

Table 15: Immunohistochemistry protocol for PFA-fixed paraffin embedded slides

Step	Purpose	Time, Temperature
Heat-induced antigen retrieval (HIAR)*	Renaturation of antigen	Boiling, followed by subboiling temperature for 15 min (Citrat pH 6.0 HIAR) or 18 min (Tris-EDTA pH 9.0 HIAR)
Cooling	Cool down	30 min, RT
TBS buffer	Washing	10 min, RT
Hydrogen peroxide (1%)	Blocking of endogenous peroxidase	15 min, RT
TBS buffer	Washing	10 min, RT
Biotin blocking (liver & kidney**):** Avidin TBS buffer Biotin TBS buffer	Prevention of unspecific binding Blocking Washing Blocking Washing	 15 min, RT 10 min, RT 15 min, RT 10 min, RT
Goat serum 5%	Prevention of unspecific binding	60 min, RT
Primary antibody*	Primary antibody	Overnight, 4 °C
TBS buffer	Washing	10 min, RT
Secondary antibody*	Secondary antibody	60 min, RT
TBS buffer	Washing	10 min, RT
Avidin-biotin-complex, dilution 1:100	Amplification of targeted antibody signal	30 min, RT
TBS buffer	Washing	10 min, RT
DAB	Substrate, color reaction	Up to 15min, RT
Cold running tap water	Washing	5 min
Distilled water	Washing	Short dip, RT
Mayer's hemalaun solution, 1:10 dilution with distilled water	Counterstaining	Up to 5 min, RT
Cold running tap water	Hemalaun reaction and washing	5 min

*All used antibodies and HIAR are listed in **Table 4**.

3.6. NPI isolation and culture

To isolate NPIs, four distinct washing solutions are prepared, each in separate trays. Initially, the pancreas is carefully transferred to the primary washing tray, where meticulous removal of connective tissue and vessels is carried out, followed by sequential washing in trays 2 through 4. Subsequently, the tissue is minced into approximately 1 mm pieces using scissors and transferred to a 50 ml Falcon tube. To ensure cleanliness, the dish is rinsed at least twice with fresh washing solution. The Falcon tube is filled with washing solution, inverted, left to stand for 1-2 min, and excess fluid and binding tissue are aspirated with a 25 ml serological pipette until the supernatant is clear. Following centrifugation for 2 min at 54 rcf, the supernatant is aspirated. The resultant pellet is resuspended in 4-5 ml of collagen solution and transferred to a collagen vessel, securely sealed with Parafilm. The sample is digested in a water bath set to 37°C for 7 minutes with periodic swirling and inversion to ensure thorough mixing. The digestion process is then continued for an additional 7 minutes at approximately 60 rpm. The digestion process is stopped by adding ice-cold stop solution. Subsequently, digest supernatant is evenly distributed onto a sieve net using a 10 ml pipette, followed by washing with wash solution. The suspension is divided equally into two Falcon tubes using a 25 ml pipette, and the beaker is rinsed twice with wash solution. After centrifugation for 2 min at 54 rcf, the supernatant is aspirated and combined with fresh wash solution in one Falcon tube before being centrifuged once more. Finally, the supernatant is aspirated, and the suspension is resuspended in medium (25 ml for seeding on 5 trays) using a 25 ml serological pipette. It is then evenly distributed onto the trays and washed with fresh medium to ensure a total volume of 15 ml per tray. Microscopic evaluation and quality assessment are conducted. Finally, the cells are cultured in the incubator.

3.7. Xenotransplantation into diabetic mice

The transplantation of *in vitro* matured NPIs into immunocompromised nonobese diabetic-scid IL2rγnull (NSG) mice was carried out by our cooperation partner WG Prof. Jochen Seißler (Medizinische Klink und Poliklink IV, Ludwig-Maximilians-Universität, Munich) according to their specific protocols.

Briefly, neonatal porcine islets were isolated from pancreata of piglets aged up to 3 days and transplanted into diabetic NSG mice. The isolation involved collagenase digestion of piglet pancreata, followed by culturing the cell clusters in a in RPMI 1640 (PAN-Biotech, Aidenbach, Germany), 2% human serum albumin (Takeda, Konstanz, Germany), 10 mM nicotinamide, 20 ng/mL exendin-4 (Merck, Darmstadt, Germany) and 1% antibiotic-antimycotic (Thermo Fisher Scientific, Germering, Germany) for 5 to 6 days. NSG mice were made diabetic by intraperitoneal injection of 180 mg/kg streptozotocin and transplanted with either 3000 IEQ wild-type NPIs or 3000 IEQ transgene-expressing NPIs under the left kidney capsule without immunosuppression. The mice were monitored for blood glucose levels, and the observation period lasted up to 12 weeks **(Figure 7)**.

The study evaluated graft function via intraperitoneal glucose tolerance test (IPGTT) performed with 2 g glucose/kg body weight. Graft function was assessed at the end of the observation period by measuring porcine plasma insulin levels at 0 and 10 min during IPGTT (Mercordia ELISA). Immunohistochemistry was performed on graft-bearing kidney sections to evaluate insulin-positive β-cells.

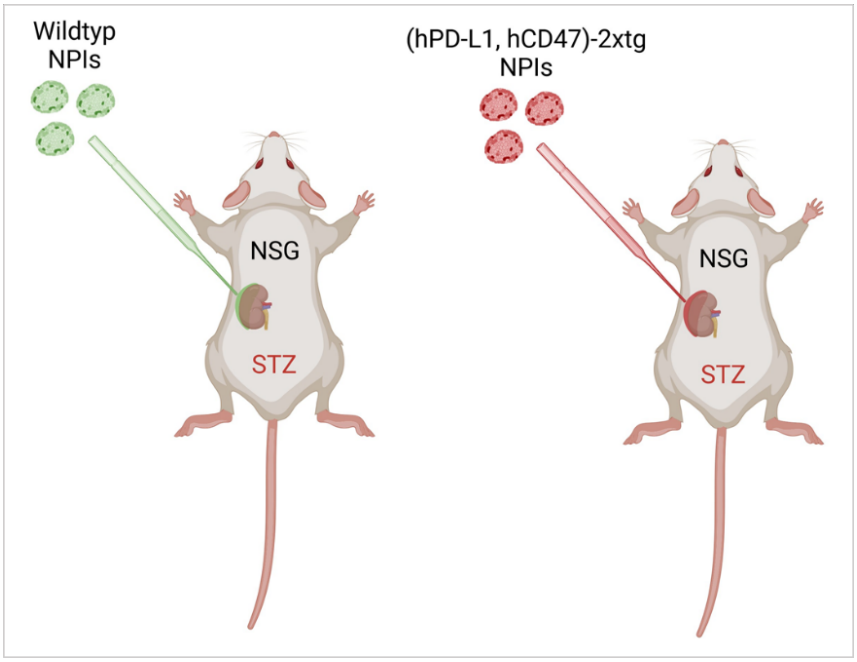

Figure 7: Illustration of islet transplantation under the left kidney capsule.
Created with BioRender.com (modified from WOLF et al., 2022).

3.8. Transplantation into the anterior chamber of the eye for *in vivo* imaging

The pancreata of the neonate offspring were used for NPI isolation. The transplantation of *in vitro* matured NPIs into NOD.CB17-Prkdcscid/J mice was carried out by our cooperation partner Dr. Christian Cohrs (Institute of Physiology, TU Dresden, Germany) according to their specific protocols.

Briefly, the isolated islets were cultivated in culture media. During transplantation at day 9 post-isolation, up to 15 isolated islets were infused into the anterior chamber of the eye (ACE) of a mouse that had previously been placed under anesthesia. For *in vivo* imaging, the mouse was anesthetized and intubated to minimize movement artifacts. *In vitro* and *in vivo* imaging of the islets was performed at different time points before and after transplantation using fluorescence live cell microscopy under a glucose-stimulated insulin secretion (GSIS) test system **(Figure 8)**.

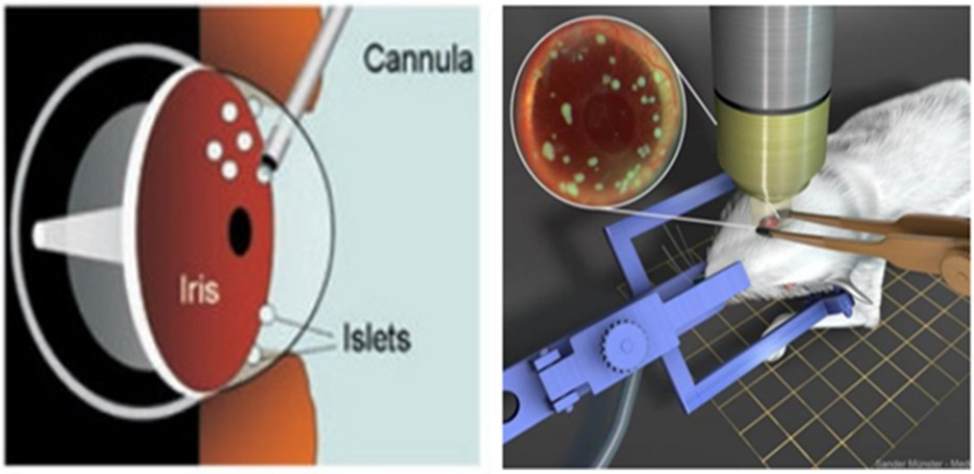

Figure 8: Illustration of islet transplantation into the anterior chamber of the eye and non-invasive *in vivo* imaging (SPEIER et al., 2008)**.**

V. RESULTS

1. Generation of optimized gm donor pigs with immunoprotective properties of islet xenograft

In the pursuit of generating optimized genetically modified donor pigs with immunoprotective properties for islet xenograft, two distinct approaches were employed. The first approach involved the generation of gm pigs derived from a bulk cell population. In the second approach, gm pigs were produced using targeted knock-in strategies, followed by the verification and selection of single-cell clones for somatic cell nuclear transfer. Subsequently, both approaches engaged in the characterization of the resulting founder animals, focusing on their transgene expression pattern and functionality as islet xenograft donors.

1.1. Generation of gm pigs derived from bulk cell population

First, an approach was applied involving the use of two linearized and excised expression cassettes. Site-directed integration into the genome was forced by CRISPR/Cas9-driven double-strand breaks in both the *GGTA1* and *CCL2* genes **(Figure 9)**. As donor cells for SCNT, a bulk population was used, which was selected by flow cytometry-based sorting of cells with cell surface expression of the immunomodulatory transgenes and absence of α-Gal sugar epitopes.

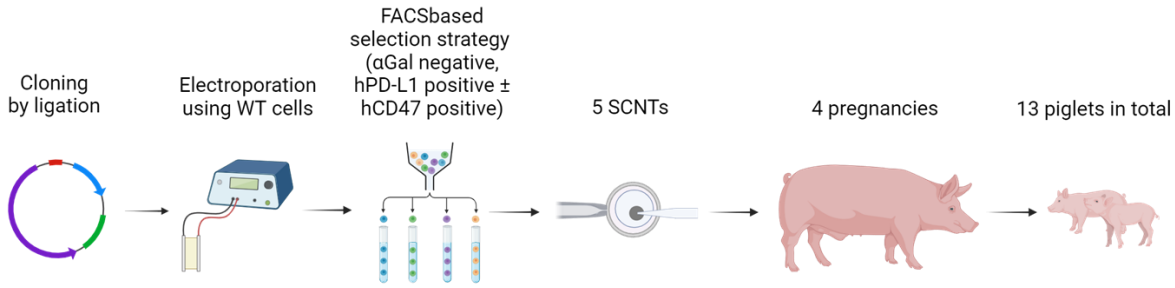

Figure 9: Key stages in the generation of transgenic pigs derived from bulk cell population.

In detail, two expression cassettes were generated. Cassette 1 carries the *INS*-LEA29Y expression cassette, which was previously used to generate the preexisting *INS*-LEA29Y pig line. In this preexisting *INS*-LEA29Y cassette, the cDNA sequence of LEA29Y was placed under the control of the 1.3 kb porcine insulin (INS) promoter and combined with a neomycin antibiotic resistance expression cassette (see also Chapter 1.1.4.). In this project objective, the *INS*-LEA29Y expression cassette was additionally combined with an expression cassette for ubiquitous expression of human PD-L1. The cDNA sequence of hPD-L1 was placed under the control of the chicken β-actin (CAG) promoter. Both expression constructs were oriented in the antisense direction. Between both 5' promoter elements, the chromatin opening element *pA2UCOE* was placed. This chromatin opening element should function bidirectionally to enhance accessibility of adjacent promoter sequences, resulting in more reliable transgene expression. Additionally, it should protect the promoter sequences from silencing. In total, the linearized purified construct of the combined (*INS*-LEA29Y, *CAG*-PD-L1)-2xtg expression cassette had a total length of 10.3 kb. Cassette 2 carried the cDNA sequence of human CD47, also under the control of the *CAG* promoter and the *pA2UCOE* element. Additionally, an appended 3' long UTR sequence was included, which is required for translational processing of hCD47. The total length of cassette 2 amounted to 9.5 kb.

For the nucleofection of primary kidney cells obtained from a wild-type boar, 1.7 µg of the linearized cassette 1 and 1.5 µg of the linearized cassette 2 were used, along with circular plasmids containing the expression cassettes for *GGTA1* gRNAs, *CCL2* gRNAs, and Cas9 protein. The target sites of the gRNAs used were exon 10 of the *GGTA1* gene for GGTA1-1 gRNA and GGTA1-2 gRNA, and exon 1 and exon 2 of the *CCL2* gene for CCL2-1 gRNA and CCL2-2 gRNA, respectively **(Figure 10 A)**. The efficiency of the gRNA/Cas9 complexes used for cutting was previously tested.

Flow cytometry was performed five days post-nucleofection to collect a bulk cell population that was negative for α-Gal epitopes (representing 61.3% of the total cell population) and strongly positive for hPD-L1 [723 cells collected (representing 0.9% of the total cell population)], or both hPD-L1 and hCD47 [851 cells collected (representing 1.0% of the total cell population] cell surface expression **(Figure 10 B)**. Both collected bulk cell populations were cultured for a few days before cryopreservation and further usage took place.

After an additional week of culture, immunofluorescence staining of the FACS-sorted cell population demonstrated dual expression of both hCD47 and hPD-L1 **(Figure 10 C)**.

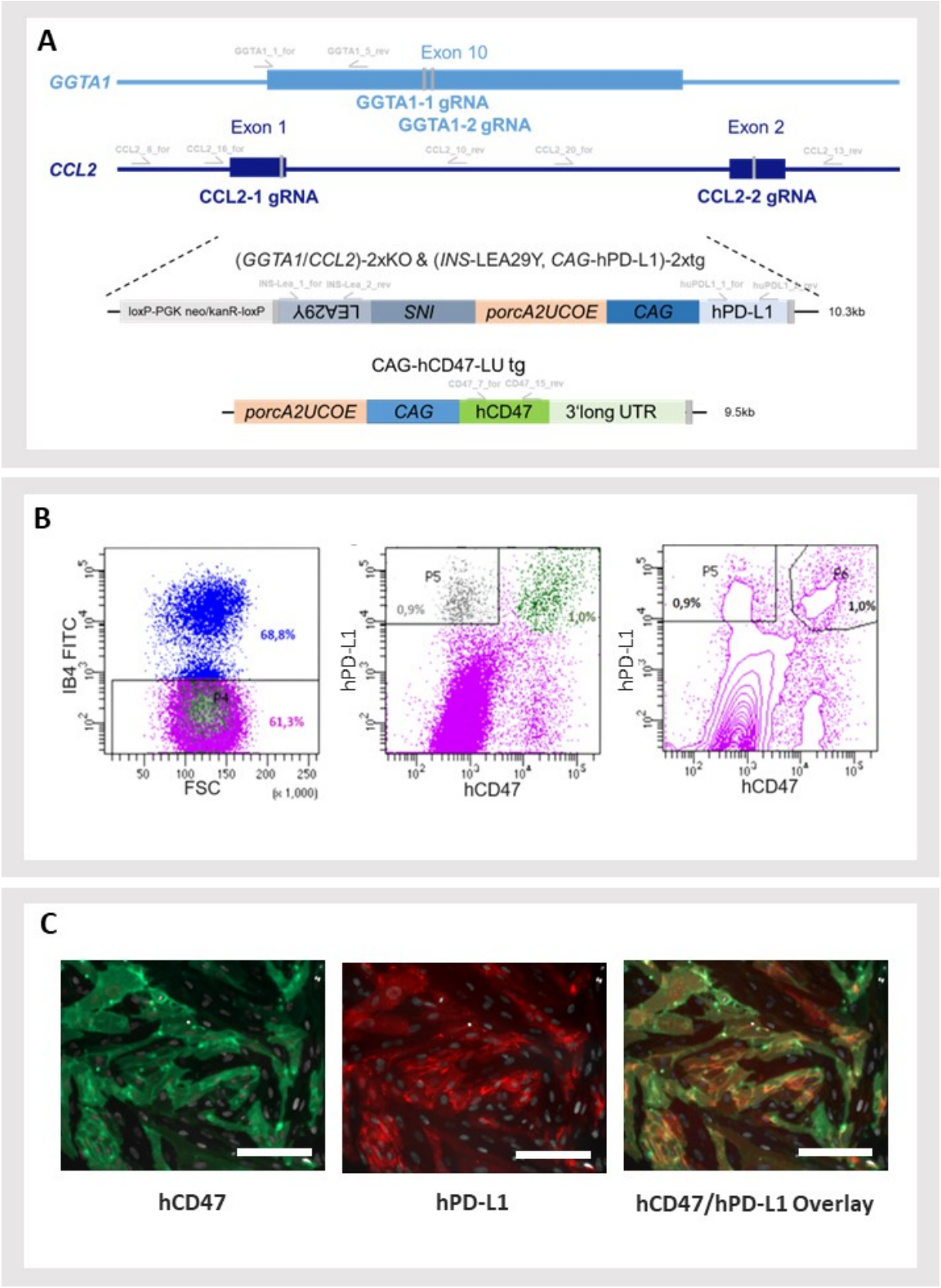

Figure 10: Targeting strategy and flow cytometry-based cell sorting for bulk cell SCNT approach.

(A) Targeting strategy for *de novo* generation of genetically multi-modified (*GGTA1*/*CCL2*)-2xKO, [(*INS*-LEA29Y, hPD-L1), hCD47]-3xtg pigs. Targeting sites of gRNAs in *GGTA1* and *CCL2* genes are shown, along with the graphical composition of both expression cassettes used. Positions of primers used for genotyping

of gm pigs are marked. (B) Dot blots of flow-cytometry-based cell sorting for collection of cells for subsequent SCNT. The cell selection criteria included the absence of α-Gal epitopes (left), as indicated by FITC-labelled IB 4 lectin staining, and the high cell surface expression of hPD-L1 and hCD47 (middle and right), both represented by gate P6. Cells of gates P5 and P6 were collected. (C) Immunofluorescence staining of the FACS-sorted cell population. Staining for hCD47 (left), staining for hPD-L1 (middle), and overlay of hPD-L1/hCD47 confirming dual positivity in the cells (right). Scale bars = 40µm. Nuclei were stained with Hoechst 33342 (blue color). Scale bars = 40 µm.

The embryo transfer from SCNT-derived embryos into five cycles-synchronized sows resulted in four pregnancies. One pregnancy was terminated on day 67 to obtain two fetuses for integration and organ expression analysis. The other three sows went to term and delivered a total of 11 piglets. Among these piglets, seven were observed to have no abnormalities in health status and habitus, while four were stillborn, as detailed in **Table 16**.

Table 16: Overview of conducted SCNTs using bulk cell populations.

SCNT No.	Bulk cell ID	FACS	Date of SCNT	No. of SCNT embryos	Pregnancy (%)	Fetuses collected	Piglets born alive	Stillborn piglets
1	**F11 6/8**	α-Gal neg hPD-L1 pos hCD47 pos	16-07-21	232	+	2	-	-
2	**F11 7**	α-Gal neg hPD-L1 pos	23-07-21	158	-	-	-	-
3	**F11 7**	α-Gal neg hPD-L1 pos	23-07-21	154	+	-	2	2
4	**F11 6/8**	α-Gal neg hPD-L1 pos hCD47 pos	06-08-21	180	+	-	3	1
5	**F11 6/8**	α-Gal neg hPD-L1 pos hCD47pos	06-08-21	175	+	-	2	1
Total				**899**	**4/5 (80%)**	**2**	**7**	**4**

All of the piglets were male, as expected from the donor cells. PCR and Sanger sequencing were used to detect the genetic modifications of the SCNT-derived piglets. The results are listed in **Table 17**.

Targeted inactivation of both *GGTA1* and *CCL2* genes was successfully achieved in all 13 SCNT-derived piglets. Furthermore, integration of the hPD-L1 transgene construct was detected in all offspring. However, three piglets lacked the presence of the LEA29Y coding sequence, indicating the absence of the full-length construct in these animals. Out of the 13 piglets, nine exhibited successful integration of the hCD47 transgene expression cassette.

Table 17: Genotypes of the founder animals derived from bulk cell populations.

#	*GGTA1*	*CCL2*	LEA29Y	hPD-L1	hCD47	Genotype
12346	KO	KO	+	+	+	(*GGTA1*/*CCL2*)-2xKO, (*INS*-LEA29Y, hPD-L1, hCD47)-3xtg
12347	KO	KO	+	+	+	(*GGTA1*/*CCL2)*-2xKO, (*INS*-LEA29Y, hPD-L1, hCD47)-3xtg
12480	KO	KO	+	+	-	(*GGTA1*/*CCL2*)-2xKO, (*INS*-LEA29Y, hPD-L1)-2xtg
12481	KO	KO	-	+	+	(*GGTA1*/*CCL2*)-2xKO, (hPD-L1, hCD47)-2xtg
12482	KO	KO	+	+	+	(*GGTA1*/*CCL2*)-2xKO, (*INS*-LEA29Y, hPD-L1, hCD47)-3xtg
12483	KO	KO	+	+	-	(*GGTA1*/*CCL2*)-2xKO, (*INS*-LEA29Y, hPD-L1)-2xtg
12556	KO	KO	+	+	-	(*GGTA1*/*CCL2*)-2xKO, (*INS*-LEA29Y, hPD-L1)-2xtg
12557	KO	KO	+	+	+	(*GGTA1*/*CCL2*)-2xKO, (*INS*-LEA29Y, hPD-L1, hCD47)-3xtg
12558	KO	KO	+	+	+	(*GGTA1*/*CCL2*)-2xKO, (*INS*-LEA29Y, hPD-L1, hCD47)-3xtg
12559	KO	KO	-	+	-	(*GGTA1*/*CCL2*)-2xKO, hPD-L1-tg
12560	KO	KO	+	+	+	(*GGTA1*/*CCL2*)-2xKO, (*INS*-LEA29Y, hPD-L1, hCD47)-3xtg
12561	KO	KO	+	+	+	(*GGTA1*/*CCL2*)-2xKO, (*INS*-LEA29Y, hPD-L1, hCD47)-3xtg
12562	KO	KO	-	+	+	(*GGTA1*/*CCL2*)-2xKO, (hPD-L1, hCD47)-2xtg
Total	**13/13 (100%)**	**13/13 (100%)**	**10/13 (76.9%)**	**13/13 (100%)**	**9/13 (69.2%)**	

1.1.1. Characterization of transgene expression patterns in gm founder pigs

The expression pattern and abundance of the transgenes were validated using tissue samples obtained from stillborn or sacrificed piglets, as well as tail samples from live-born piglets. Kidney cells were isolated from all founder piglets that were sacrificed but failed in three stillborn animals.

1.1.1.1. Depletion of α-Gal epitope by targeting *GGTA1* gene

Immunohistochemistry and FACS analysis demonstrated the successful depletion of the α-Gal epitope in all organs by targeting the *GGTA1* gene in all animals **(**see **Figure 11)**.

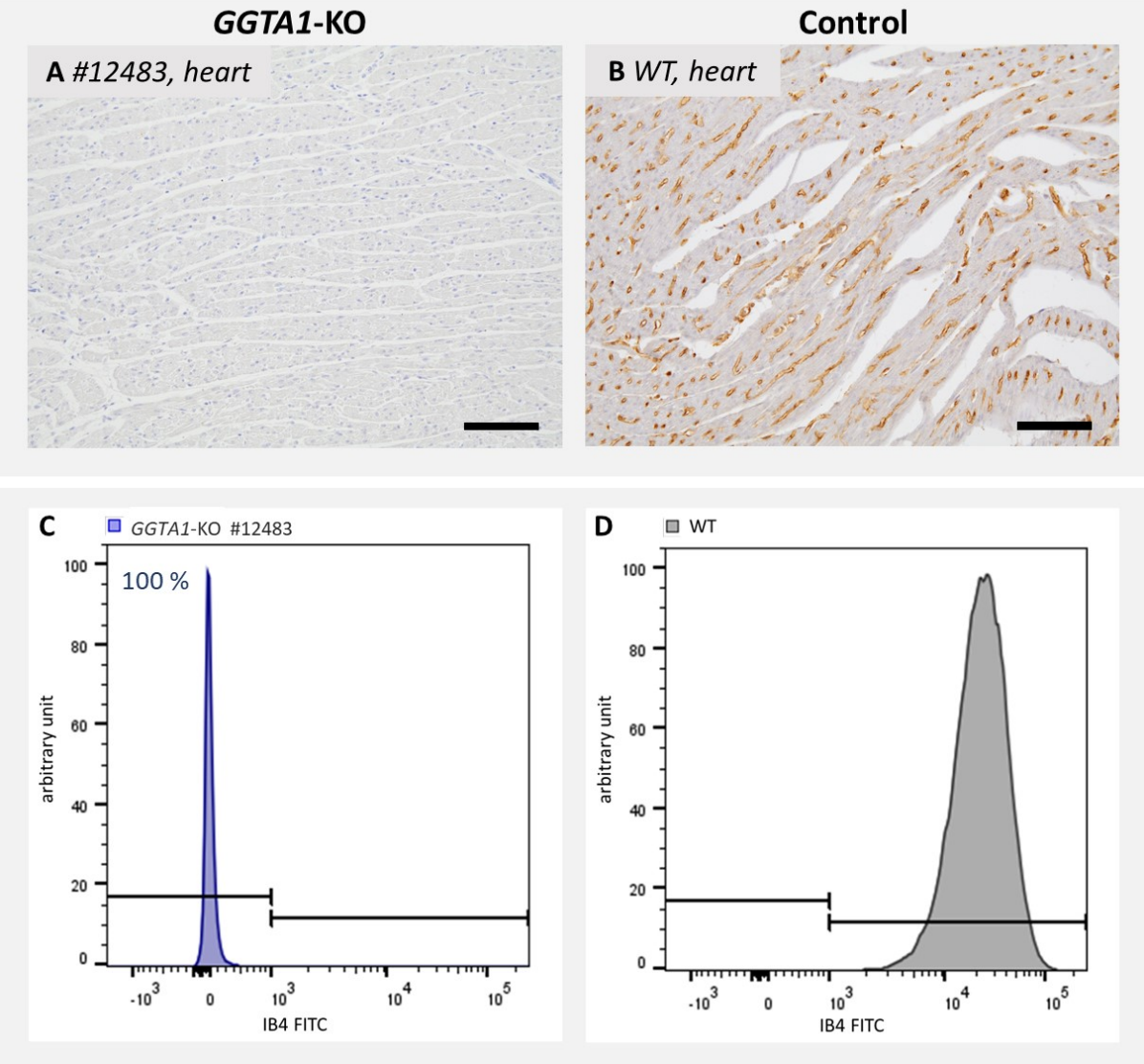

Figure 11: Absence of α-Gal epitopes in multi-gm founder piglets derived from bulk cell population.
(A, B) Representative α-Gal immunohistochemistry of heart tissue from one founder animal demonstrates the complete absence of α-Gal epitopes in the *GGTA1*-KO pig (A) in comparison to a WT control (B). DAB: brown color. Cell nuclei were stained in blue. Scale bars = 100µm. (C, D) FACS analysis confirmed the absence of α-Gal epitopes in 100% of the analyzed kidney cells of the *GGTA1*-KO pig (C) in comparison to a WT control (D).

1.1.1.2. Depletion of MCP1 by targeting *CCL2* gene

Biallelic frame-shift mutations of the *CCL2* gene were present in all SCNT offspring, as displayed in **Table 17**. Nine distinct antibodies were tested for specificity towards porcine MCP1 protein in immunohistochemistry, but all of them failed the specificity control (not shown).

1.1.1.3. *pA2UCOE-CAG* promoter driven ubiquitous expression of hCD47 and hPD-L1

Immunohistochemistry was used to analyze the transgene expression pattern in tail tissue samples obtained shortly after birth for genotyping and in organ tissue samples collected *ex vivo*. Based on the results obtained from the immunohistochemistry analysis of tail samples from piglets born alive from SCNT#4 and #5 (refer to **Table 16**), two piglets were raised to establish a breeding herd.

Due to three F0 piglets not being hCD47-transgenic (refer to **Table 17**), the IHC results were negative, as expected. Among the 10 piglets carrying the hCD47 transgene, five exhibited a diffuse homogeneous membrane staining across all examined tissues. Four piglets displayed varying degrees of a mosaic staining pattern. While founder pig #12482 and #12557 showed approximately 80% positive cells, pig #12346 and #12561 exhibited only about 50% hCD47-positive cells. **Figure 12 (A-F)** shows representative immunohistochemical stainings of pancreatic and tail tissues from one F0 founder animal with homogeneous hCD47 transgene expression, contrasting with another SCNT-derived F0 animal showing a mosaic pattern of hCD47 transgene expression. The observed expression patterns in the tail sample were highly similar to those in other organ tissue samples.

The FACS analyses conducted on PKCs revealed that the animals had either a homogeneous or a mosaic pattern of the hCD47 transgene, which is consistent with the previous findings from IHC analysis. In addition, the FACS analysis results were useful for quantifying and comparing of transgene protein abundance intensities between the different animals. Analysis of F0 pig #12346 demonstrated a ratio of negative to positive cells of 34% to 66%. #12561 displayed a lower mosaic pattern with 80% positive cells and 20% negative cells. Animal #12557 showed a very low percentage of negative cells, totaling only 1%. All other hCD47 transgenic F0 pigs examined exhibited 100% hCD47-positive cells, as representatively shown in **Figure 12 (G-I)**.

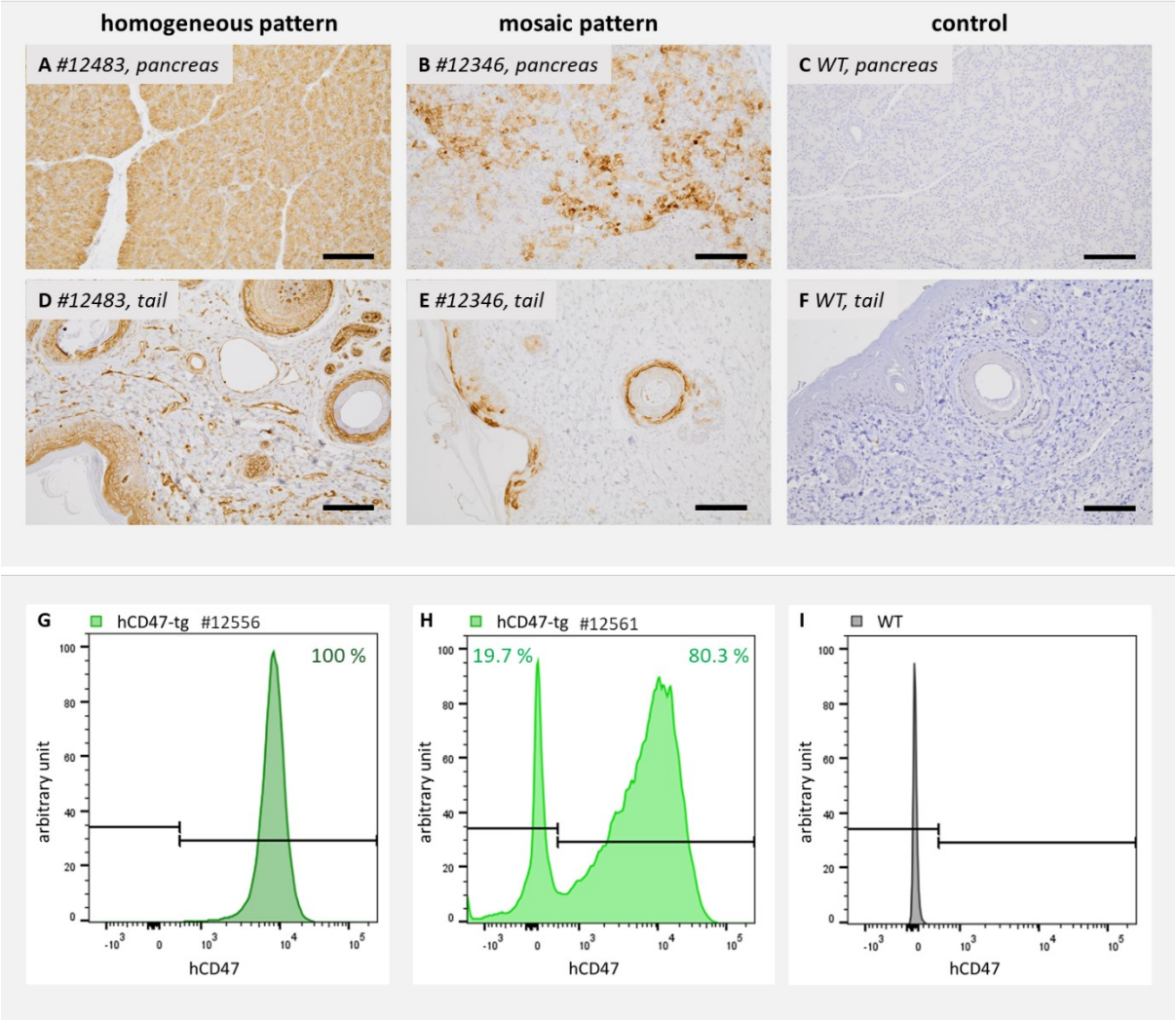

Figure 12: Notable differences in the hCD47 expression pattern in the F0 pigs derived from the bulk cell population.

(A – F) Representative immunohistochemistry stainings for hCD47 demonstrate consistency of staining pattern in different tissues of hCD47 transgenic SCNT offspring. (A & D) Homogeneous staining pattern; (B & E) mosaic-like staining pattern; (C & F) wild-type negative control. (A – C) Pancreatic tissue; (D – F) the corresponding tail tissue of the same animals as for pancreatic tissue. DAB: brown color. Cell nuclei were stained in blue. Scale bars = 100µm. (G – I) Representative FACS analysis shows 100% transgene positivity of all cells analyzed in one F0 animal (G), mosaic pattern with a negative (19.7%) and positive fraction (80.3%) of the analyzed cells in another F0 animal (H), as well as the negative result for hCD47 seen in cells of a WT control (I).

Of note, founder pig #12558 exhibited a nuclear membrane-forced staining pattern of hCD47 that differed from the cell membrane-forced staining pattern of all other hCD47-tg founder pigs in IHC analysis **(Figure 13 A)**. To confirm the IHC findings, we compared permeabilized and non-permeabilized PKCs in the FACS analysis. This revealed a pronounced rightward shift of hCD47-positive cells upon cell permeabilization (non-permeabilized: 54.3% positive cells vs. permeabilized: 98.4% positive cells), thus confirming a particularly high transgene abundance within the cell **(Figure 13 B)**. As the 3' UTR sequence of CD47 was described to be essential for post-translational processing of the CD47 protein and correct translocation to the cell membrane, we next analyzed the presence of the 3' UTR sequence of the hCD47 expression cassette integrated into the genome of the F0 founder pigs. For the PCR analyses, two distinct primer pairs were used: one for amplify the middle region of the long UTR and the other one for confirming the presence of the polyA tail sequence region. However, in the case of founder animal #12558, the PCR to detect the middle 3' UTR sequence did not yield any discernible PCR band **(Figure 13 C)**.

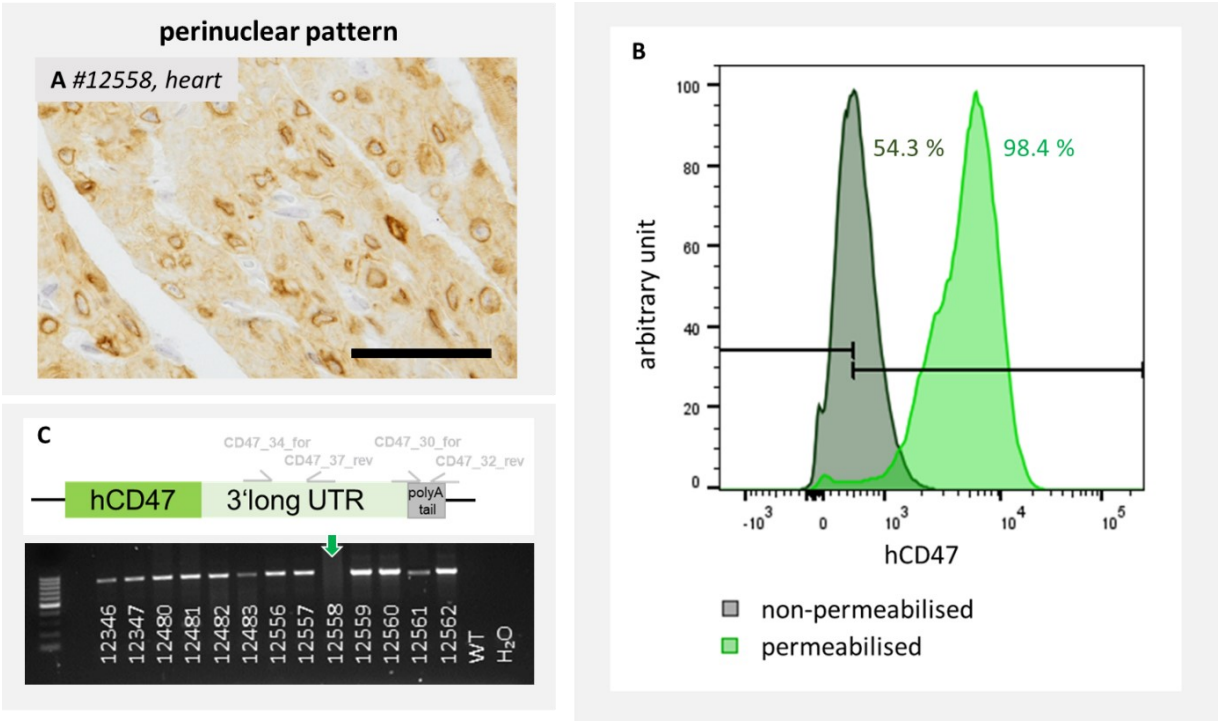

Figure 13: Defective hCD47 post-translational processing by absence of 3'LU sequence in SCNT offspring #12558.

(A) IHC staining of hCD47 revealed a nuclear-membrane staining pattern in founder pig #12558. DAB: brown color. Cell nuclei were stained in blue. Scale bars = 40µm. (B) Histogram of FACS analysis comparing permeabilized and non-permeabilized cell stains revealed a distinct right shift in positive cells of the permeabilized approach. (C) PCR results for the LU tail in the middle of the long UTR with a missing band in F0 animal #12558.

All F0 pigs carrying the hPD-L1 transgene **(Table 17)** exhibited a cell membrane-forced staining pattern of hPD-L1. While nine piglets exhibited a strong and homogeneous hPD-L1 expression in all cells of all organs studied, four F0 pigs showed a mosaic-like staining pattern of varying degrees. Founder animal #12557 showed the strongest mosaic pattern staining, with only about 30% of cells positive for expressing hPD-L1. Founder #12346 had approximately 50% hPD-L1-positive cells, while founder #12480 had around 80%. The selected breeding boar, #12560, also exhibited a slight mosaic pattern in a tail tissue sample, with roughly 90% positive cells. **Figure 14 (A-F)** provides representative illustrations of the immunohistochemical staining of pancreatic and tail tissues of the founder animals, with highly comparable findings between the tail sample and all other examined organ tissues.

Further FACS analyses were performed to determine the hPD-L1 transgene protein abundance. Founder #12346 had the highest proportion of hPD-L1 negative cells at 80%. Animal #12557 also exhibited a mosaic pattern with a 62% negative cell fraction. Founder #12480 had a negative fraction of approximately 3% in the kidney cells **(Figure 14 G-I)**.

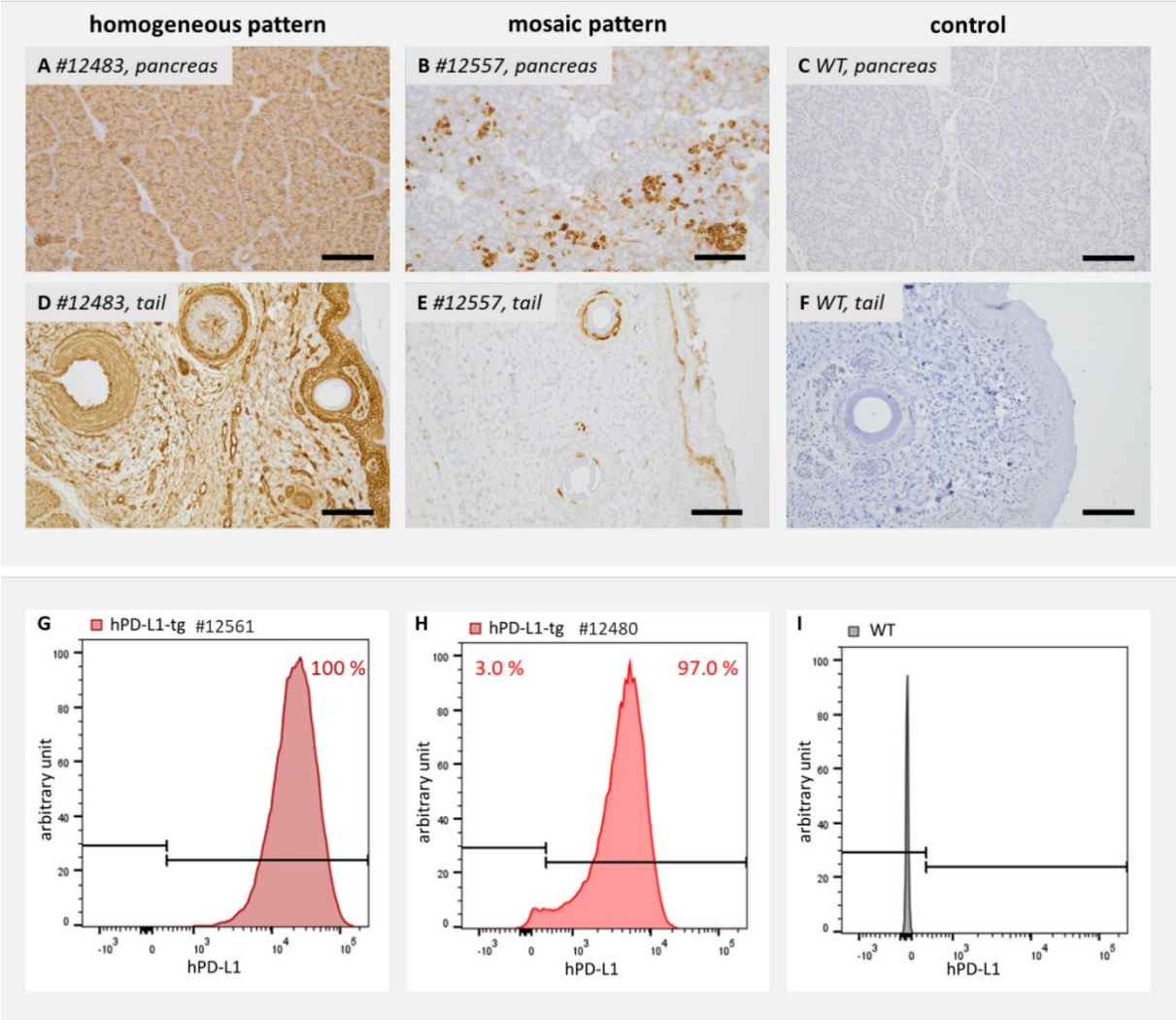

Figure 14: Notable differences in the hPD-L1 expression pattern in the F0 pigs derived from bulk cell population.

(A – F) Representative immunohistochemistry stains for hPD-L1 demonstrate consistency of staining pattern in different tissues of hPD-L1 transgenic SCNT offspring. (A & D) Homogeneous staining pattern; (B & E) mosaic-like staining pattern; (C & F) wild-type negative control. (A – C) Pancreatic tissue; (D – F) the corresponding tail tissue of the same animals as for pancreatic tissue. DAB: brown color. Cell nuclei were stained in blue. Scale bars = 100µm. (G – I) Representative FACS analysis shows 100% transgene positivity of all analyzed cells in one F0 pig (G) and a mosaic pattern with a negative (3%) and positive fraction (97%) of the analyzed cells in another F0 pig (H) in comparison to a WT control (I).

Table 18: Summary of the expression patterns of the F0 pigs derived from bulk cell population.

#	α-Gal		*CCL2*	hCD47		hPD-L1		LEA29Y
	IHC	FACS		IHC	FACS	IHC	FACS	IHC
12346	100% absence	100% negative	n.a.	mosaic (50% pos)	66% pos	mosaic (50% pos)	20% pos	100% negative
12347		100% negative		homogenous (100% pos)	100% pos	homogenous (100% pos)	100% pos	100% negative
12480		100% negative		homogenous (100% pos)	100% pos	mosaic (80% pos)	97% pos	100% negative
12481		100% negative		0% pos	0% pos	homogenous 100% pos	100% pos	100% negative
12482		n.a.		mosaic (80% pos)	n.a.	mosaic (95% pos)	n.a.	100% negative
12483		100% negative		0% pos	0% pos	homogenous (100% pos)	100% pos	100% negative
12556		100% negative		homogenous (100% pos)	100% pos	homogenous (100% pos)	100% pos	100% negative
12557		100% negative		mosaic (80% pos)	99% pos	mosaic (30% pos)	38% pos	100% negative
12558		100% negative		mosaic (80% pos) nuclear - membrane!	non-perm: 23% perm: 98% pos	homogenous (100% pos)	100% pos	100% negative
12559		n.a.		0% pos	n.a.	homogenous (100% pos)	n.a.	100% negative
12560		n.a.		homogenous (100% pos)	n.a.	mosaic (90% pos)	n.a.	100% negative
12561		100% negative		mosaic (50% pos)	80% pos	homogenous (100% pos)	100% pos	slightly positive
12562		n.a.		homogenous (100% pos)	n.a.	homogenous (100% pos)	n.a.	100% negative

1.1.1.4. *pA2UCOE-INS* promoter driven β-cell-specific expression of LEA29Y

Whereas the promoter *pA2UCOE-CAG*, as described and shown above, promises ubiquitous transgene expression, the porcine insulin (*INS*) promoter was chosen for β-cell-specific expression of the secreted transgene LEA29Y, to ensure site-specific expression of the transgene without any systemic immunosuppressive effects. PCR analysis detected the coding region of LEA29Y in 10 out of 13 F0 pigs resulting from SCNT of the bulk cell approach. However, this region was absent in three F0 pigs, although carrying the coding region of the hPD-L1 transgene. Among the 10 F0 pigs that harbored the *pA2UCOE-INS*-LEA29Y transgene as a fusion expression cassette with *CAG*-hPD-L1, LEA29Y expression was studied in pancreatic tissue in nine F0 pigs using immunohistochemistry. No LEA29Y protein was detected in any of the eight F0 animals, except for the pancreas tissue from animal #12561. Comparing the transgene protein abundance in the pancreas of #12561 with that of animals from the preexisting *INS*-LEA29Y pig line, the LEA29Y protein expression was weaker in the islets of founder #12561, and a lower proportion of cells exhibited compared to the preexisting transgenic line **(Figure 15)**.

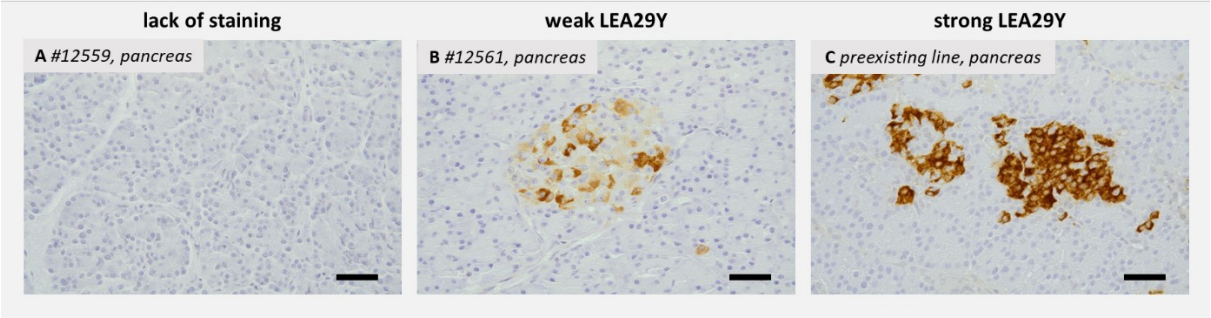

Figure 15: Distinct lower transgene protein abundance of LEA29Y in the F0 pigs derived from the bulk cell population compared to the preexisting transgenic line.

(A - C) LEA29Y IHC results of exemplary founder animals showing representative non-expression (A) and weak LEA29Y expression of founder animal #12561 (B) in comparison to the preexisting high expressing LEA29Y line (C) on pancreatic tissue. DAB: brown color. Cell nuclei were stained in blue. Scale bars = 100µm.

1.1.2. Characterization of breeding properties and gm robustness in F1 offspring

Based on the findings of immunohistochemical evaluation of expression patterns of hCD47 and hPD-L1 in tail samples, two 5x gm male F0 pigs, #12560 and #12561, were raised to establish breeding lines. Using boar #12560, numerous pregnancies were obtained resulting in the birth of genetically multi-modified offspring. In contrast, #12561 turned out to be infertile.

The F1 offspring of F0 boar #12560 were used for further transgene expression investigations, pancreatic isolations for mouse xenotransplantation experiments, and for the establishment of a gm breeding herd. Throughout this doctoral thesis, 13 matings occurred. All piglets underwent genotyping by PCR to determine their genomic status.

In the context of the (*GGTA1/CCL2*)-2xKO genotype, where the father carries recessive mutations on both alleles, it was expected that all offspring would inherit one defective allele for both *GGTA1* and *CCL2*. This expectation was confirmed by the observation that all offspring were heterozygous for both genes, except when the sire was paired with sows that were already *GGTA1*-KO or -het, or *CCL2*-KO or -het, resulting in knockout offspring **(Figure 16)**.

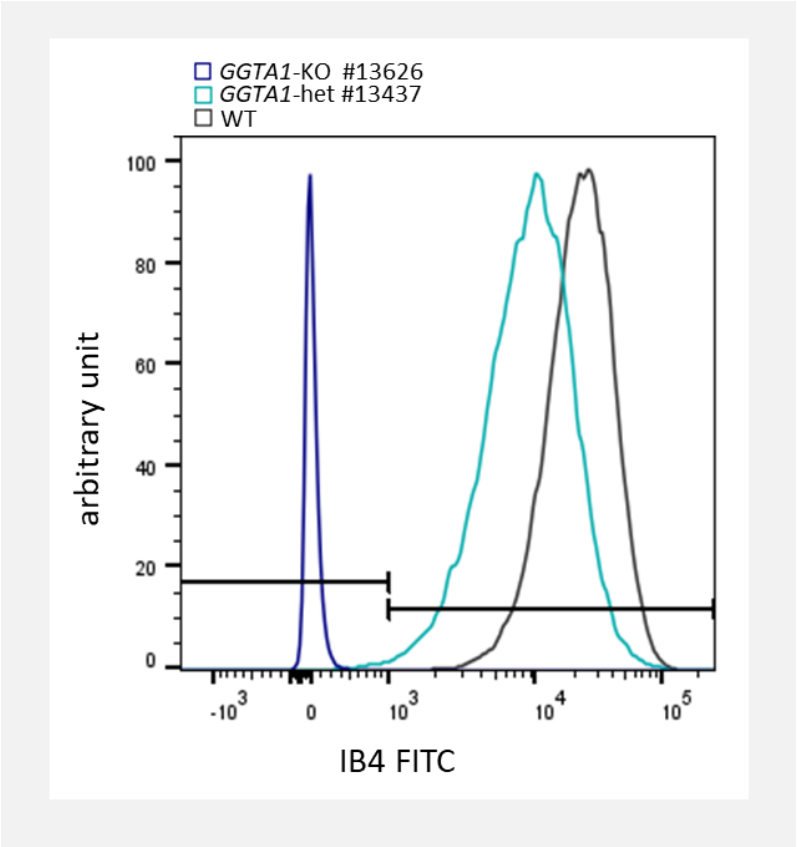

Figure 16: Complete absence or less α-Gal epitopes in the offspring of founder boar #12560.
Representative FACS analysis confirmed the complete absence of α-Gal epitopes in *GGTA1*-KO offspring (dark blue) or reduced α-Gal epitopes in *GGTA1*-het offspring (light blue) compared to a WT control (grey).

Regarding the transgene cassettes (*INS*-LEA29Y/hPD-L1)-2xtg and (hCD47)-tg, representing a heterozygous combination on one allele, are expected to be passed on to 50% of the offspring. Notably, despite the presence of two independent transgene expression cassettes, hPD-L1 and hCD47 were consistently co-inherited, whereas LEA29Y was absent in a few offspring. The transgene expression pattern of F1 offspring of F0 founder pig #12560 was studied for all three transgenes, comparing it to other F1 offspring and those of other F0 pigs derived from the bulk cell approach.

Immunohistochemical staining of various organs and FACS analysis of PKCs from a representative selection of offspring derived from the founder animal #12560 revealed the inheritance of the high transgene expression pattern as observed in the sire's tail sample.

Specifically hCD47 exhibited a remarkably strong and homogeneous expression pattern across all examined tissues, as demonstrated in **Figure 17 (A-D)**. The FACS analyses also confirmed the reliable and robust inheritance of the hCD47 transgene in the offspring, with all offspring showing 100% positive cells and similar mean fluorescence intensity (MFI) levels **(Figure 17 E-F)**.

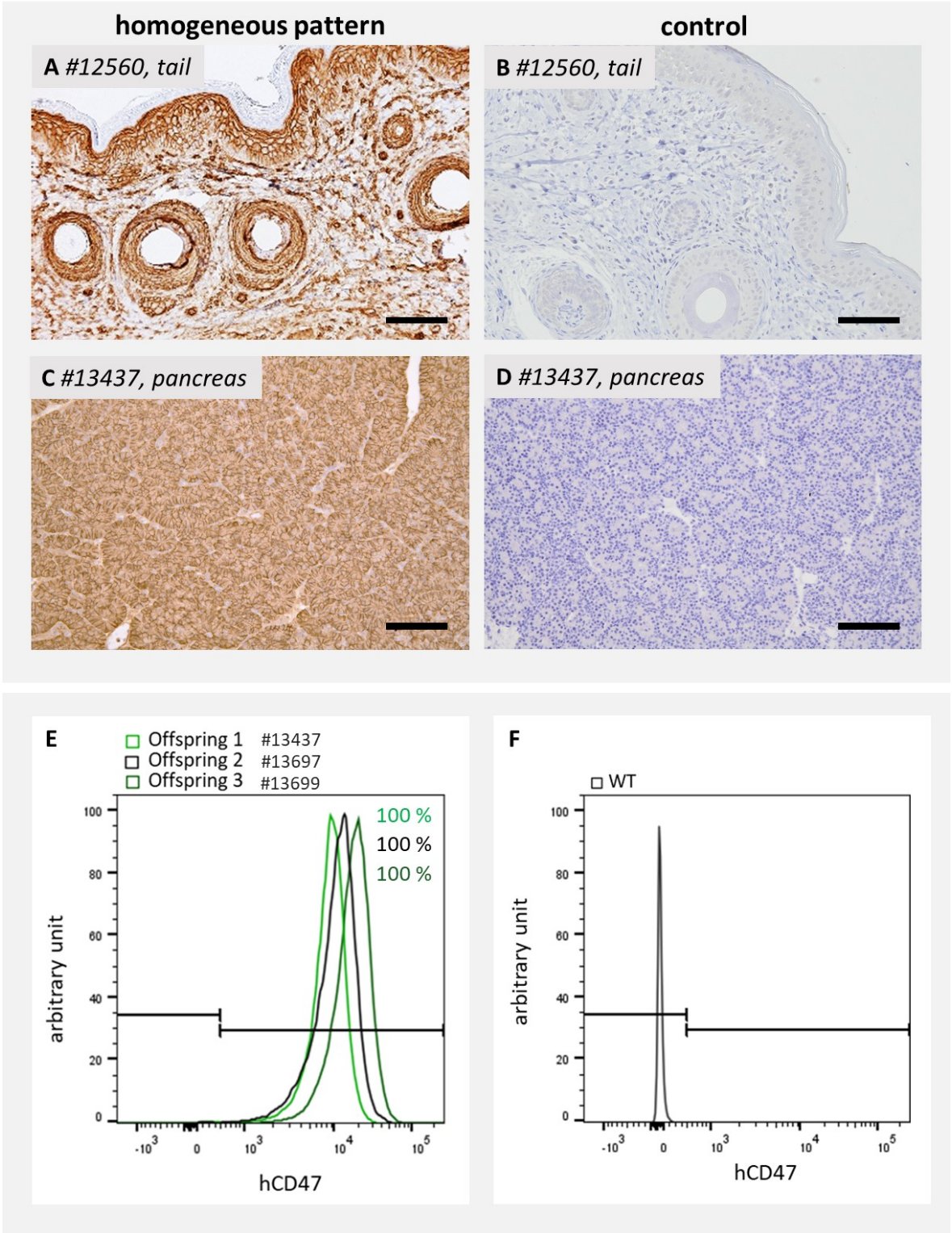

Figure 17: Robust high expression of the hCD47 transgene in the offspring of founder #12560.

(A – D) IHC staining of hCD47: (A) Homogeneous staining pattern in the tail sample of founder #12560 compared to (B) wild-type tail control. (C) Homogeneous staining pattern in the pancreatic tissue of an exemplary offspring from founder #12560 compared to (D) wild-type pancreatic control. DAB: brown color. Cell nuclei were stained in blue. Scale bars = 100µm. (E – F) FACS analyses of the offspring showed 100% positive cells with similar MFI levels (C) in comparison to a WT control (D).

Similarly, a subtle mosaic pattern was observed across all examined organs of the offspring, consistent with the hPD-L1 immunohistochemical findings of the sire's tail sample (**Figure 18 A-D)**. The FACS analyses of PKCs from randomly selected offspring further revealed variation in the number of non-hPD-L1-expressing cells among the offspring. Nevertheless, all examined offspring showed well over 90% positive cells with similar MFI rates **(Figure 18 E-F)**.

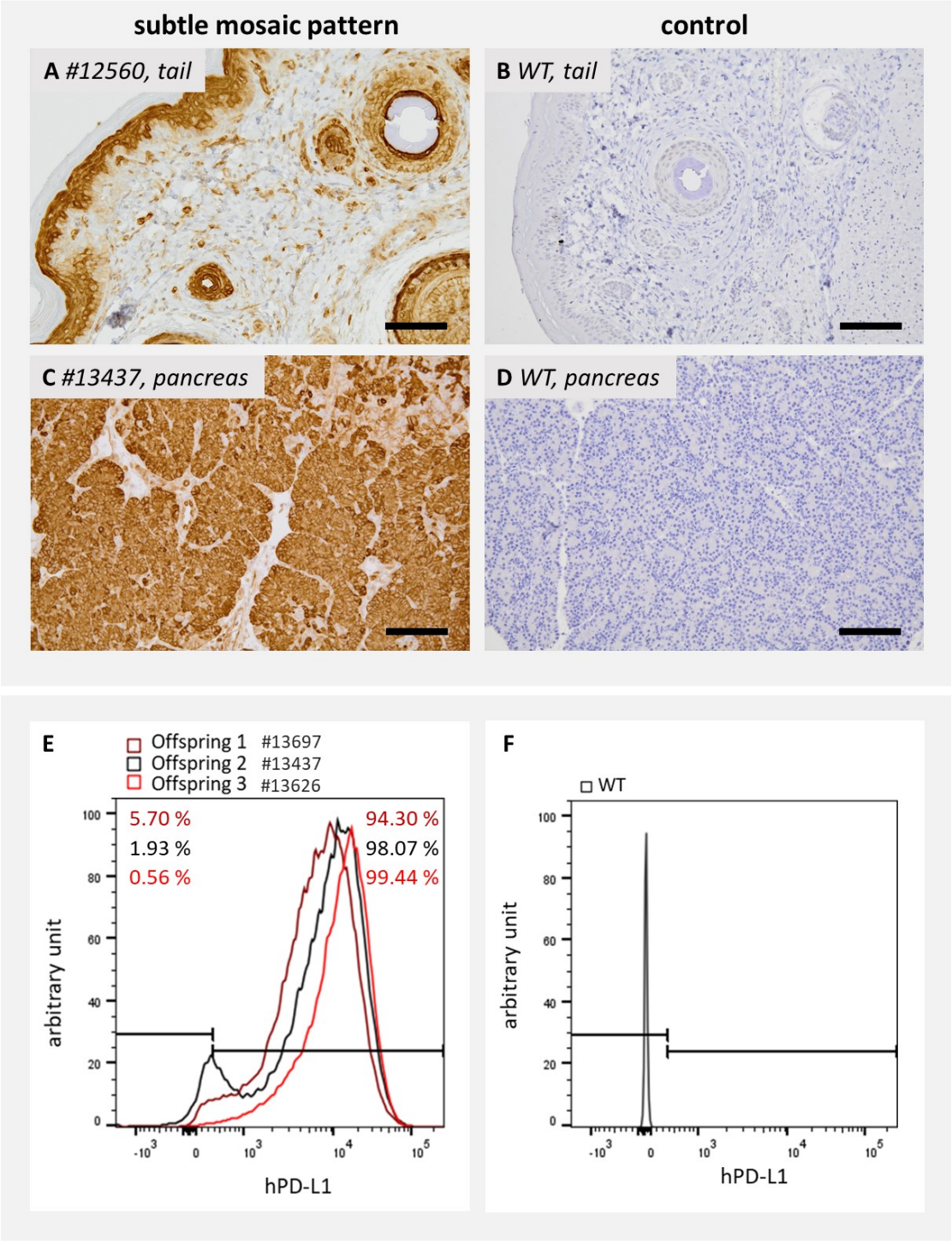

Figure 18: Despite slight mosaic pattern, the offspring of founder #12560 exhibited high expression of the hPD-L1 transgene.

(A – D) IHC staining of hPD-L1: (A) Subtle mosaic pattern in the tail sample of founder #12560 compared to (B) wild-type tail control. (C) Subtle pattern in the pancreatic tissue of an exemplary offspring from founder #12560 compared to (D) a wild-type pancreatic control. DAB: brown color. Cell nuclei were stained in blue. Scale bars = 100µm (E, F) FACS analyses of the offspring showed variation in the number of negative cells but were consistently below 10%. The positive cells reached similar MFI levels (E). WT control for comparison (F).

Interestingly, one examined descendant, #13445, exhibited weak LEA29Y expression. However, even in this case, the expression was considerably weaker than in the already existing line. Additionally, matings was carried out involving the founder boar #12560 and transgenic sows from the preexisting *INS*-LEA29Y line **(Figure 19)**, resulting in offspring that inherited robust expression of hPD-L1 and hCD47 from the sire, as well as high LEA29Y expression from the dam.

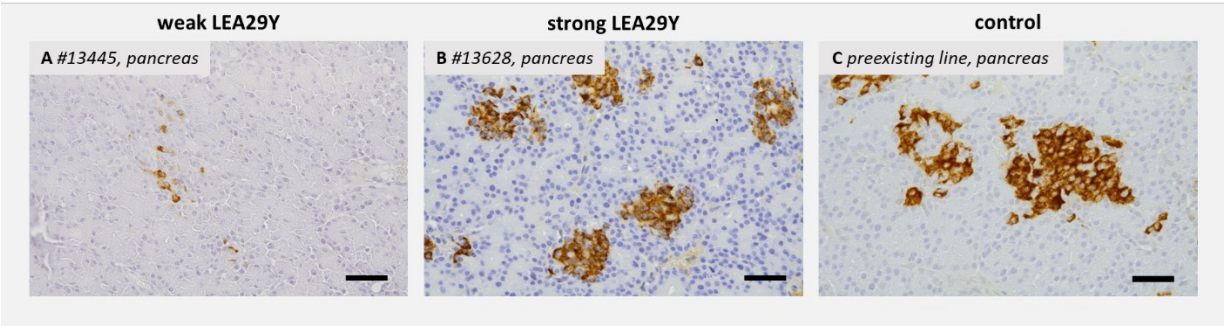

Figure 19: LEA29Y expression found in offspring from founder #12560.
(A-C) LEA29Y IHC results of exemplary offspring from founder #12560 showing weak LEA29Y expression in animal #12445 (A) compared to offspring resulting from mating (B) with a LEA29Y-transgenic sow from the preexisting high-expressing LEA29Y line (C). DAB: brown color. Cell nuclei were stained in blue. Scale bars = 100µm.

1.1.3. Limitations of bulk cell approach in the generation of multi-gm islet donor pigs

Reflecting on the results obtained from the bulk cell approach in the *de novo* generation of multi-gm islet donor pigs, several new bottlenecks were identified that must be addressed to achieve the objective goal of a multi-gm optimized islet donor pig line with reliable and robust transgene expression and combined heritability. The most prominent limitations identified are:

(I) The porcine *INS* promoter was found to be unreliable in enabling β-cell-specific robust transgene expression, despite the presence of a chromatin opening element.

(II) A low degree of mosaic pattern expression of the transgenes was observed, despite the presence of a chromatin opening element and the *CAG* promoter.

(III) Error-prone integration of transgene expression cassettes occurred, resulting in unpredictable alterations and fragmentations of these cassettes.

1.2. Generation of gm pigs with targeted knock-in validation strategy

Based on the findings of the bulk cell approach and the identification of the bottleneck to achieve the objectives, a second approach was developed. This approach involved a targeted knock-in strategy, which integrated single expression cassettes into three defined gene loci: exon 7 and exon 10 of the *GGTA1* gene, and 1 kb distal of the *INS*-LEA29Y transgene integration site on *SSC6* of the preexisting *INS*-LEA29Y transgenic line. The aim of this approach was to achieve gm pigs with the following genetic modifications:

(1) *B2M*-KO/*GGTA1*-KO_*pA2UCOE-CAG*-hPD-L1-tg (in exon 7 of *GGTA1*),

(2) *GGTA1*-KO_*pA2UCOE-CAG*-hCD47-LU-tg (in exon 10 of *GGTA1*),

(3) *GGTA1*-KO/ (*INS*-LEA29Y, *pA2UCOE-CAG*-hPD-L1)-2xtg (in *SSC6*).

Therefore, WT cells were used to obtain *de novo* gm pigs for settings (1) and (2), whereas *GGTA1*-het/*INS*-LEA29Y-tg (*SSC6*) cells were used for nucleofection to obtain gm pigs for setting (3).

Each expression cassette was flanked by homologous arms ranging from 600 to 860 bp in length, corresponding to the gene integration sites. A gRNA target sequence specific to the corresponding targeted genomic region was placed between each flanking region of homologous arms and the plasmid backbone. Circular plasmids containing the large expression cassettes were used for nucleofection without prior linearization. Similar to the bulk cell approach, a strategy of CRISPR-Cas9-driven double-strand break of the genomic region of interest was applied, which should favor targeted integration of the transgene expression cassette. Nucleofection was performed using circular expression cassette plasmids containing the gRNA target regions.

Similar to the design of the first approach, flow cytometry was used to select cells that were negative for α-Gal epitopes and positive for a ubiquitously expressed cell membrane-anchored transgenes. However, in contrast to the first approach, flow cytometry-based cell sorting was performed on day 3 post-nucleofection instead of day 5. The selected cells were then directly seeded on 96-well plates at a low density of one or two cells per well on average to propagate SCCs. PCR analyses were then used to screen the SCCs and confirm the correct integration of the transgene in the specific gene locus. **Figure 20** provides an overview of the individual steps of this new approach.

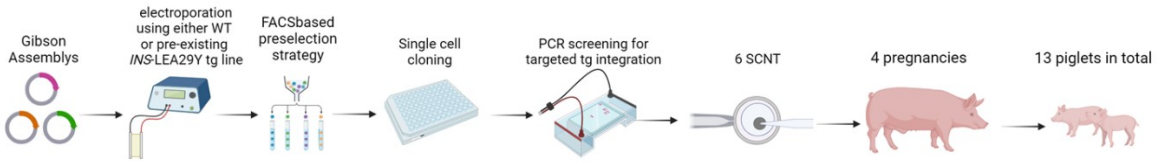

Figure 20: Key stages of the targeted knock-in validation strategy to generate multi-gm pigs.

1.2.1. Locus-specific integration of the *pA2UCOE-CAG*-hPD-L1 transgene nearby the *INS*-LEA29Y *SSC6* site of preexisting gm pig line

In this approach, kidney cells from two gm pigs from the preexisting pig line were used, taking advantage of the robust LEA29Y expression. Specifically, cells isolated from two *GGTA1*-het/hCD46-tg/*INS*-LEA29Y-tg male animals, #7697 and #7700, were used. To prevent segregation of the transgenes during breeding, the *pA2UCOE-CAG*-hPD-L1 expression cassette was positioned nearby the *INS*-LEA29Y expression site on *SSC6* **(Figure 21 A)**.

Using the CRISPOR tool, three gRNAs targeting *SSC6* gDNA 1 kb distal to the *INS*-LEA29Y transgene integration site were selected for cloning into the pX458M-53BP1-DN1S plasmid. The efficiency of the plasmid-based gRNA/Cas9 induction of a double-strand break after nucleofection of porcine kidney cells was tested using the TIDE analysis tool. The TIDE analysis showed that the best cutting efficiency of the gRNAs was achieved with 48.6% by gRNA Chr6-2 **(Figure 21 B)**.

Three days after nucleofection with circular plasmids containing the *pA2UCOE-CAG*-hPD-L1 *SSC6*-HA expression cassette, and transient expression of gRNA and Sniper-Cas9 in cells from animals #7697 and #7700, a total of 8,977 cells (1.2% of total cells) from cell line #7697 and 9,975 cells (1.6% of total cells) from cell line #7700 were collected via flow cytometry. These cells exhibited the absence of the α-Gal epitope and the highest hPD-L1 protein surface expression **(Figure 21 C)**.

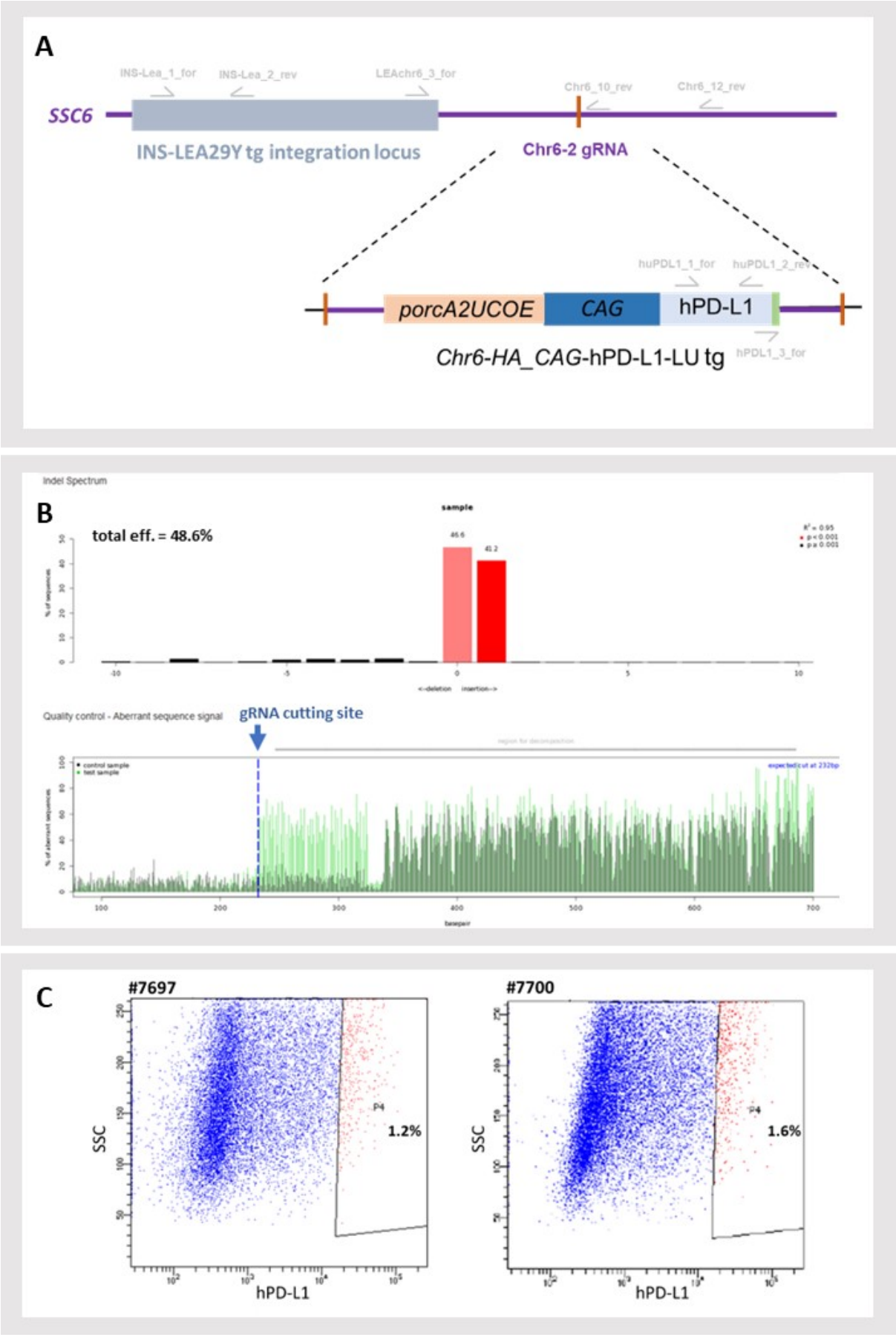

Figure 21: Construct design and pre-selection of cells with targeted hPD-L1 integration into the *SSC6* locus.

(A) Construct design. The *CAG*-hPD-L1 expression cassette should be integrated nearby the *INS*-LEA29Y transgene integration site on *SSC6*. Therefore, the *pA2UCOE-CAG*-hPD-L1 construct was flanked with *SSC6* homologous arms. The position of primers that were used for genotyping of gm pigs is marked. (B) Highest cutting efficiency of gRNA was achieved with 48.6% by Chr6-2 gRNA, as shown by TIDE analysis. Shown is the proportion of frameshift events and the gRNA cutting site, which were expected to lead to frameshift mutations through NHEJ, along with the overall efficiency of gene editing (top). Genome editing in the *SSC6* locus was analyzed using the TIDE online tool, showing the editing position by the blue arrow (bottom). (C) Dot blots of flow-cytometry-based cell sorting for the collection of hPD-L1 positive cells (gate P4) for subsequent SCC propagation.

Subsequently, six 96-well plates were seeded with a cell density of one cell per well from each cell line immediately after cell sorting. The remaining cells were plated as a bulk population. In total, 61 SCCs were harvested and screened for the correct integration of the transgene expression cassette. Among them, 47 cell clones had integrated the hPD-L1 transgene, with 27 cells also integrating the transgene at the intended gene location **(**refer to **Table 19**).

1.2.2. Generation of *de novo B2M*-KO/*GGTA1*-KO_*pA2UCOE-CAG*-hPD-L1-tg (in exon 7 of *GGTA1*) multi-gm pigs

In this targeted knock-in approach, the *pA2UCOE-CAG*-hPD-L1 expression cassette was inserted into exon 7 of the *GGTA1* gene. To achieve this, a circular plasmid was designed, carrying the *pA2UCOE-CAG*-hPD-L1 construct flanked by homologous arms from exon 7 of the *GGTA1* gene **(Figure 22 A)**. Two different RNP complexes were utilized: one for editing the *GGTA1* gene in exon 7 and the other for editing the *B2M* gene (not shown).

The CRISPOR tool was used to select two gRNAs targeting *GGTA1* gDNA in exon 7. The best cutting efficiencies of gDNA were achieved with 67% by GGTA1-5 gRNA in combination with Cas9 v2 protein, as demonstrated by TIDE analysis **(Figure 22 B)**. For targeting the *B2M* gene, gRNA B2M-1 was selected, achieving a cutting efficiency of 50.2% in combination with HiFi Cas9 protein **(Figure 22 C)**.

Porcine kidney cells from a German Landrace WT boar, which were free of Perv C integrants and carrying blood group 0, were used for nucleofection. Three days after nucleofection, a total of 60,941 cells (3.4% of the total cells) were selected via flow cytometry, exhibiting the highest hPD-L1 surface expression and the absence of α-Gal epitopes **(Figure 22 D)**.

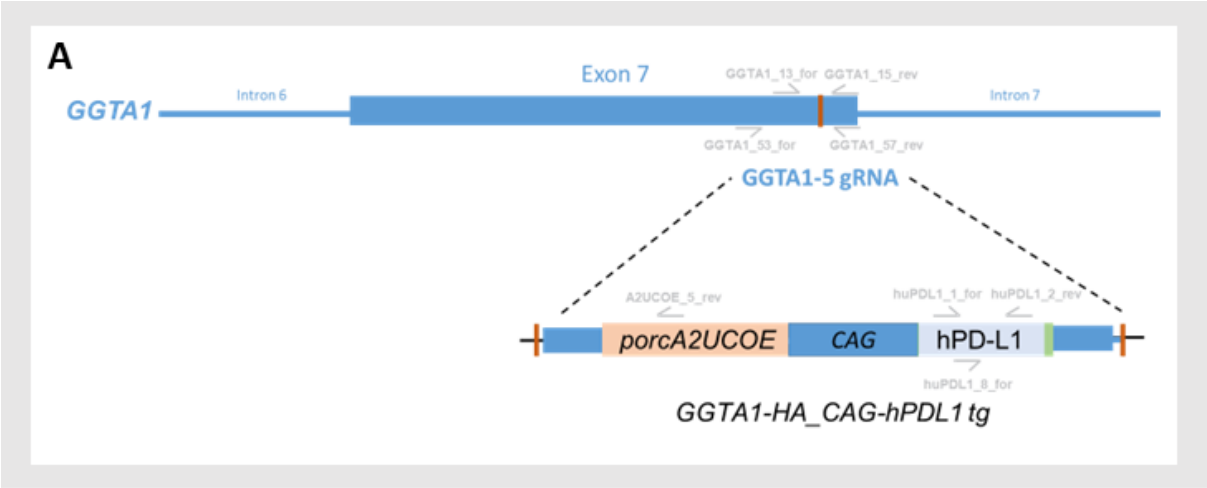
A
GGTA1
Intron 6
Exon 7
Intron 7
GGTA1_13_for
GGTA1_15_rev
GGTA1_53_for
GGTA1_57_rev
GGTA1-5 gRNA
A2UCOE_5_rev
huPDL1_1_for
huPDL1_2_rev
porcA2UCOE
CAG
hPD-L1
huPDL1_8_for
GGTA1-HA_CAG-hPDL1 tg

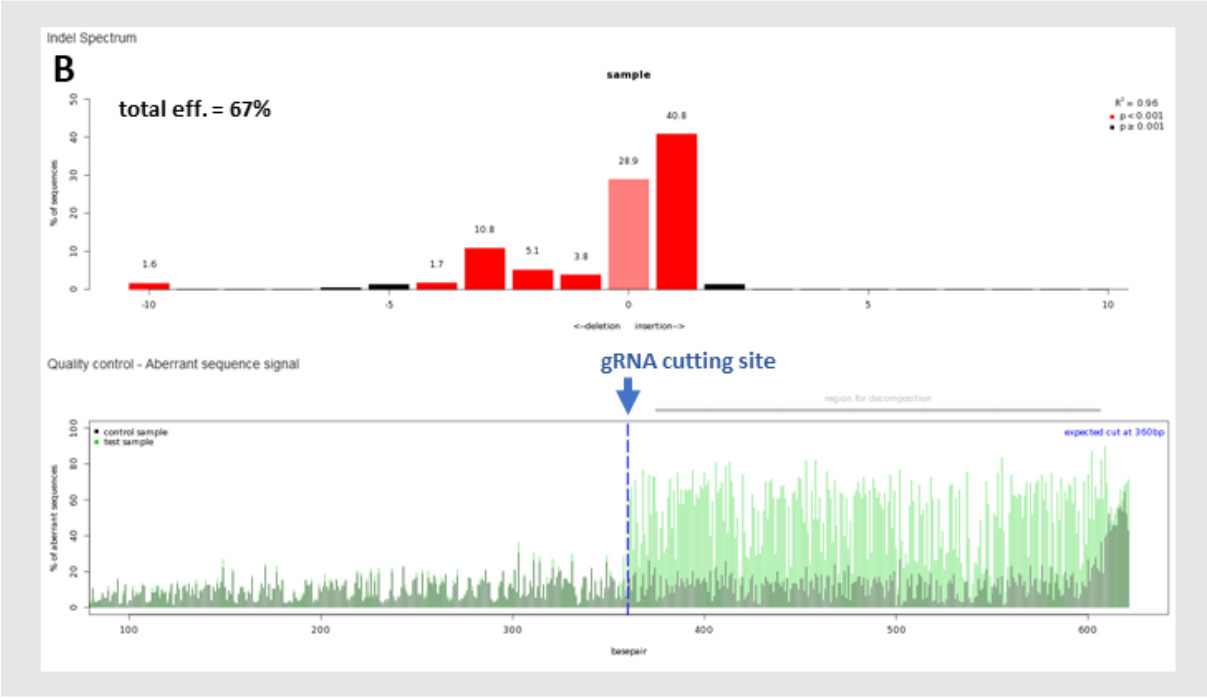
Indel Spectrum
B
sample
total eff. = 67%
40.8
28.9
10.8
5.1
3.8
1.7
1.6
% of sequences
<-deletion insertion->
Quality control - Aberrant sequence signal
gRNA cutting site
control sample
test sample
expected cut at 360bp
% of aberrant sequences
basepair

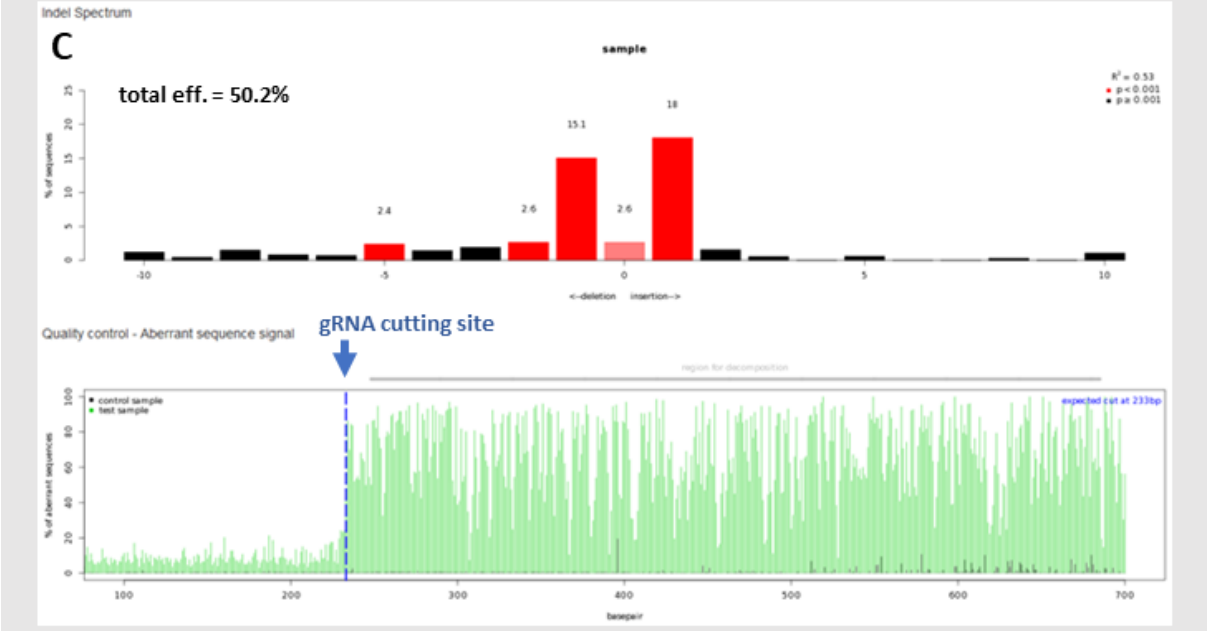
Indel Spectrum
C
sample
total eff. = 50.2%
18
15.1
2.6
2.6
2.4
% of sequences
<-deletion insertion->
Quality control - Aberrant sequence signal
gRNA cutting site
control sample
test sample
expected cut at 233bp
% of aberrant sequences
basepair

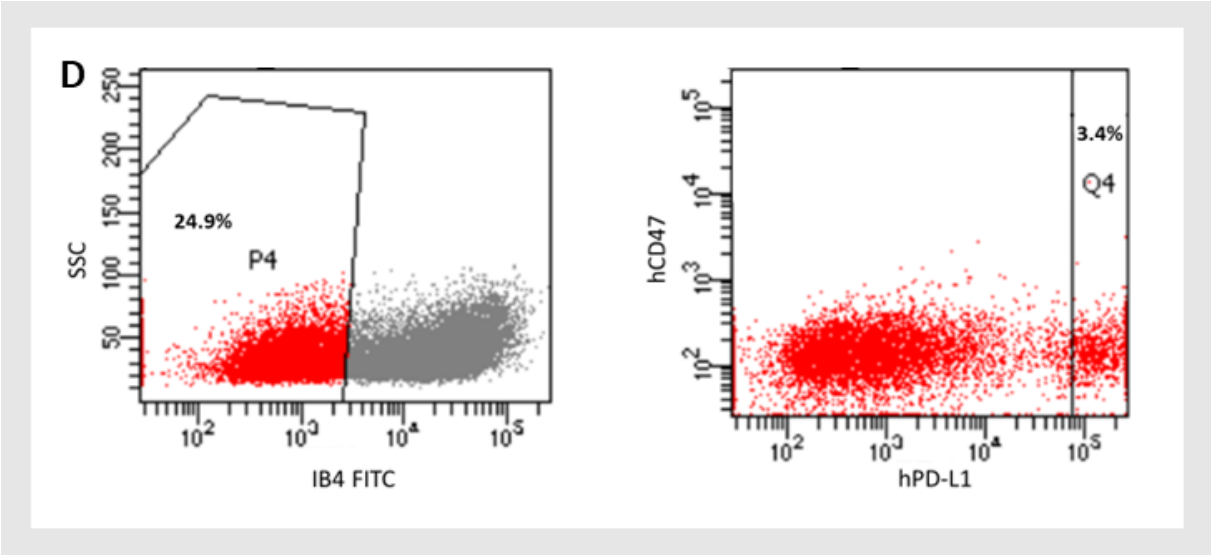

Figure 22: Construct design and pre-selection of cells with targeted hPD-L1 integration into exon 7 of *GGTA1* gene.

(A) Construct design. A circular plasmid was designed, carrying the *pA2UCOE-CAG*-hPD-L1 construct flanked by homologous arms from exon 7 of the *GGTA1* gene. The position of primers used for genotyping of gm pigs is marked. (B) TIDE analysis. Best cutting efficiencies of gRNA were achieved with 67% by GGTA1-5 gRNA, as demonstrated by TIDE analysis. Shown is the proportion of frameshift events and the gRNA cutting site, which were expected to lead to frameshift mutations through NHEJ, along with the overall efficiency of gene editing (top). Genome editing in the *GGTA1* locus was analyzed using the TIDE online tool, showing the editing position by the blue arrow (bottom). (C) For targeting the *B2M* gene, gRNA B2M-1 was selected, which achieved a cutting efficiency of 50.2%. (D) Dot blots of flow-cytometry-based cell sorting for collection of cells without α-Gal epitopes (gate P4) and positive for hPD-L1 (gate Q4).

Subsequently, ten 96-well plates were seeded with a cell density of two cells per well immediately after cell sorting, while the remaining cells were plated as a bulk population. A total of 206 SCCs were collected, of which 31 underwent screening for the correct transgene integration. Of these, 30 cell clones had integrated the hPD-L1 transgene, with seven integrating the transgene at the intended location in exon 7 of the *GGTA1* gene **(**refer to **Table 19**).

1.2.3. Targeted integration of *pA2UCOE-CAG*-hCD47-LU expression cassette in exon 10 of *GGTA1* gene

In order to achieve co-expression of hPD-L1 and hCD47 in subsequent breeding while avoiding segregation, the *CAG*-hCD47 expression cassette was inserted into exon 10 of the *GGTA1* gene. For this purpose, the *pA2UCOE-CAG*-hCD47-LU construct was flanked with homologous arms specific for the transgene integration site **(Figure 23 A)**. Porcine kidney cells from a German Landrace wild-type (WT) boar, as utilized in Chapter 1.2.2., were subjected to electroporation using the previously established GGTA1-1 gRNA. Three days after nucleofection, a total of 90,609 cells (3.6% of the total cells) were selected via flow cytometry, exhibiting the highest hCD47 surface expression and the absence of α-Gal epitopes **(Figure 23 B)**.

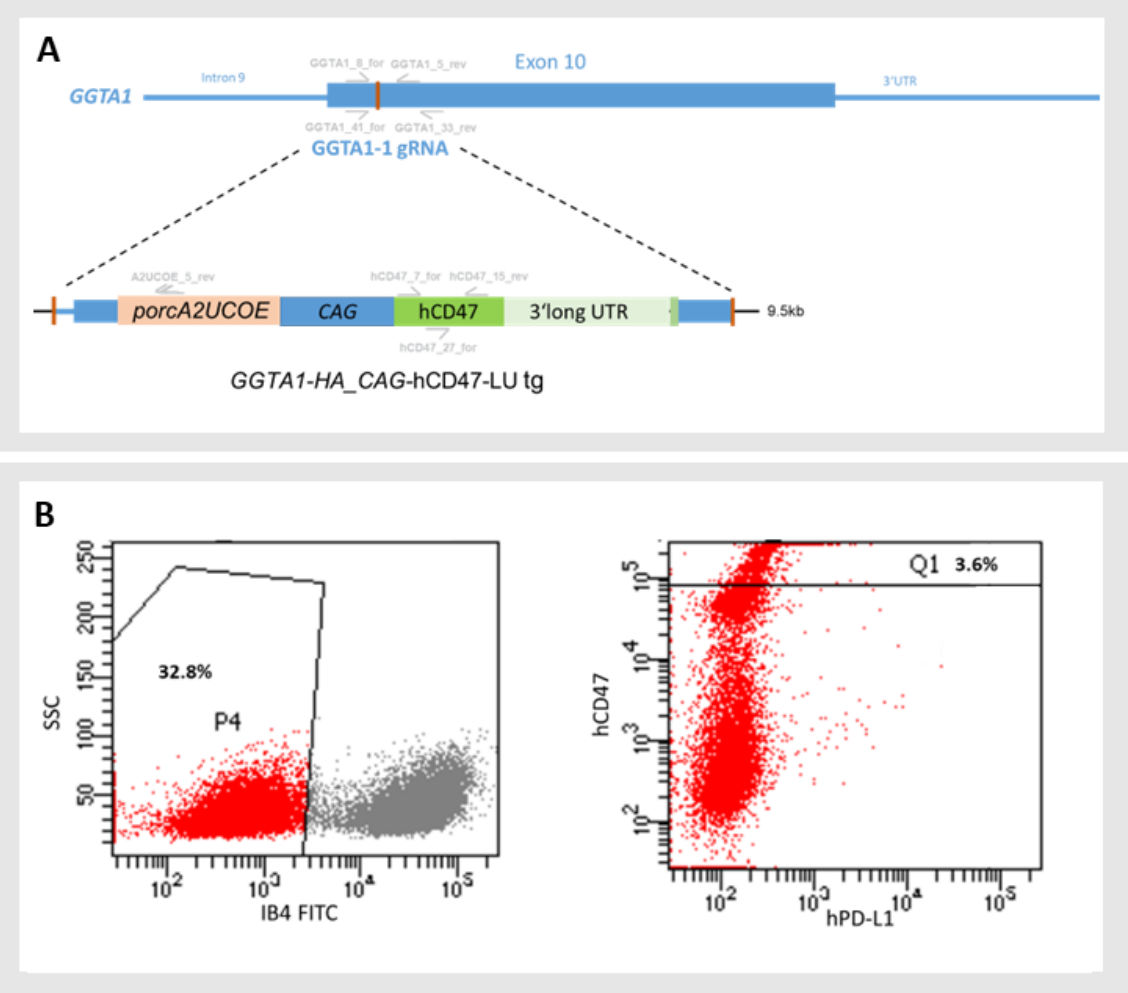

Figure 23: Construct design and pre-selection of cells with targeted hCD47 integration into exon 10 of *GGTA1* gene.

(A) Construct design. The *pA2UCOE-CAG*-hCD47-LU construct was flanked by homologous arms from exon 10 of the *GGTA1* gene. Positions of primers used for genotyping of gm pigs are marked. The previously established gRNA for integration into exon 10 of the *GGTA1* gene was employed. (B) Dot blots of flow cytometry-based cell sorting for collection of cells lacking α-Gal epitopes (gate P4) and positive for hCD47 (gate Q4).

Subsequently, ten 96-well plates were seeded immediately after cell sorting, with each well containing a cell density of two cells, while the remaining cells were plated as a bulk population. In total, 221 SCCs were collected. Of these, 93 SCCs underwent screening for the correct transgene integration. Among them, 54 cell clones had integrated the hPD-L1 transgene, with 45 of them integrating the transgene at the intended site in exon 10 of the *GGTA1* gene (refer to **Table 19**).

Table 19: Overview of validation results from SCC screening for targeted transgene integration.

Transfection		No. cells transfected (in mio)	FACS	No. of cells plated per well	No. of SCCs harvested	No of SCCs analyzed	Transgene integrated (% of analyzed)	Transgene in correct position (% of analyzed)
F36	#7679	0.7	hPD-L1pos	1 cell/well 6 plates	61	61 (100%)	47 (77%)	27 (44%)
	#7700	0.7	hPD-L1pos	1 cell/well 6 plates				
F38		0.5	α-Gal neg hCD47pos	2 cells/well 10 plates	221	93 (42%)	54 (58%)	45 (48%)
F39		0.5	α-Gal neg hPD-L1pos	2 cells/well 10 plates	206	31 (15%)	30 (97%)	7 (23%)
Total					**488**	**185 (38%)**	**131 (71%)**	**79 (43%)**

1.2.4. Generation of F0 gm pigs with targeted knock-in validation strategy by SCNT

A total of 10 SCCs were selected for mixed somatic cell nuclear transfers (SCNTs). Clones containing the genetic modifications *pA2UCOE-CAG*-hPD-L1 in *SSC6*, *pA2UCOE-CAG*-hPD-L1 in exon 7 of *GGTA1*, and *pA2UCOE-CAG*-hCD47-LU in exon 10 of *GGTA1*, as described previously, were used. Six SCNTs were performed, resulting in four pregnancies and the birth of 13 piglets. Among them, nine piglets were born alive without any discernible abnormalities in health status and morphology, while four were stillbirths, as detailed in **Table 20**.

Table 20: Overview of conducted SCNTs using SCCs.

SCNT no.	ID of SCCs used	Date of SCNT	No. of SCNT embryos transferred	Pregnancy (%)	Liveborn piglets	Stillborn piglets
1	F36 13/29/40 F38 25/27/28 F39 11/31	31-03-23	159	+	2	-
2		31-03-23	164	-	-	-
3		31-03-23	153	-	-	-
4	F36 11 F38 22/40/45 F39 12/16/31	26-05-23	143	+	-	2
5		26-05-23	142	+	4	1
6		26-05-23	142	+	3	1
Total			**903**	**4/6 (66.7%)**	**9**	**4**

The genomic status of the founder animals was initially assessed through genotyping PCRs and Sanger sequencing. The acquired genotypes are shown in **Table 21**.

Table 21: Genotypes of the founder animals derived from SCCs.

Founder #	*GGTA1*	*B2M*	hCD46	LEA29Y	hPD-L1	hCD47	Genotype	Descent from SCC ID*
14060	KO	WT	-	-	-	+	*GGTA1*-KO_hCD47 (Ex10)	F38 40 or 45
14061	KO	KO	-	-	+	-	*GGTA1*-KO_hPD-L1 (Ex7) / *B2M*-KO	F39 31
14272	KO	WT	+	+	+	-	*GGTA1*-KO (Ex10) / hCD46-tg / *INS*-LEA_hPD-L1-tg (chr6)	F36 11
14273	KO	WT	+	+	+	-	*GGTA1*-KO (Ex10) / hCD46-tg / *INS*-LEA_hPD-L1-tg (chr6)	F36 11
14274	KO	KO	-	-	+	-	*GGTA1*-KO_hPD-L1-het (Ex7) / *B2M*-KO	F39 12 or 16
14275	KO	KO	-	-	+	-	*GGTA1*-KO_hPD-L1 (Ex7) / *B2M*-KO	F39 31
14276	KO	KO	-	-	+	-	*GGTA1*-KO_hPD-L1 (Ex7) / *B2M*-KO	F39 31
14277	KO	WT	-	-	-	+	*GGTA1*-KO_hCD47 (Ex10)	F38 40 or 45
14278	KO	WT	-	-	-	+	*GGTA1*-KO_hCD47 (Ex10)	F38 40 or 45
14279	KO	KO	-	-	+	-	*GGTA1*-KO_hPD-L1-het (Ex7) / *B2M*-KO	F39 12 or 16
14280	KO	KO	-	-	+	-	*GGTA1*-KO_hPD-L1-het (Ex7) / *B2M*-KO	F39 12 or 16
14281	KO	WT	-	-	-	+	*GGTA1*-KO_hCD47 (Ex10)	F38 40 or 45
14282	KO	KO	-	-	+	-	*GGTA1*-KO_hPD-L1-het (Ex7) / *B2M*-KO	F39 12 or 16
Total	**13/13 (100%)**	**7/13 (53.9%)**	**2/13 (15.4%)**	**2/13 (15.4%)**	**9/13 (69.2%)**	**4/13 (30.8%)**		

*colour coding ≙ descent from identical SCC

1.2.5. Characterization of transgene expression pattern of SCNT offspring

Tissue samples were collected for expression analysis from both stillborn piglets and offspring born alive who were either sacrificed or died in the postnatal period, in addition to the tail samples obtained for genotyping. Furthermore, kidney cells were isolated from piglets derived from all used SCCs.

1.2.5.1. *GGTA1*-KO_*pA2UCOE-CAG*-hCD47-LU-tg (in exon 10 of *GGTA1*)

Figure 24 (A-B) displays the immunohistochemical staining of pancreatic tissue from the founder animals. All piglets, which carry the hCD47 transgene targeted and integrated into exon 10 of the *GGTA1* gene, showed a strong and homogeneous cell membrane-forced staining in all examined organs. No mosaic-like expression patterns were observed. FACS analyses confirmed these findings, with 100% of hCD47-positive cells in all hCD47-transgenic F0 pigs **(Figure 24 C-D)**. In addition, the complete absence of α-Gal epitopes was confirmed, indicating a knockout of the *GGTA1* gene (not shown).

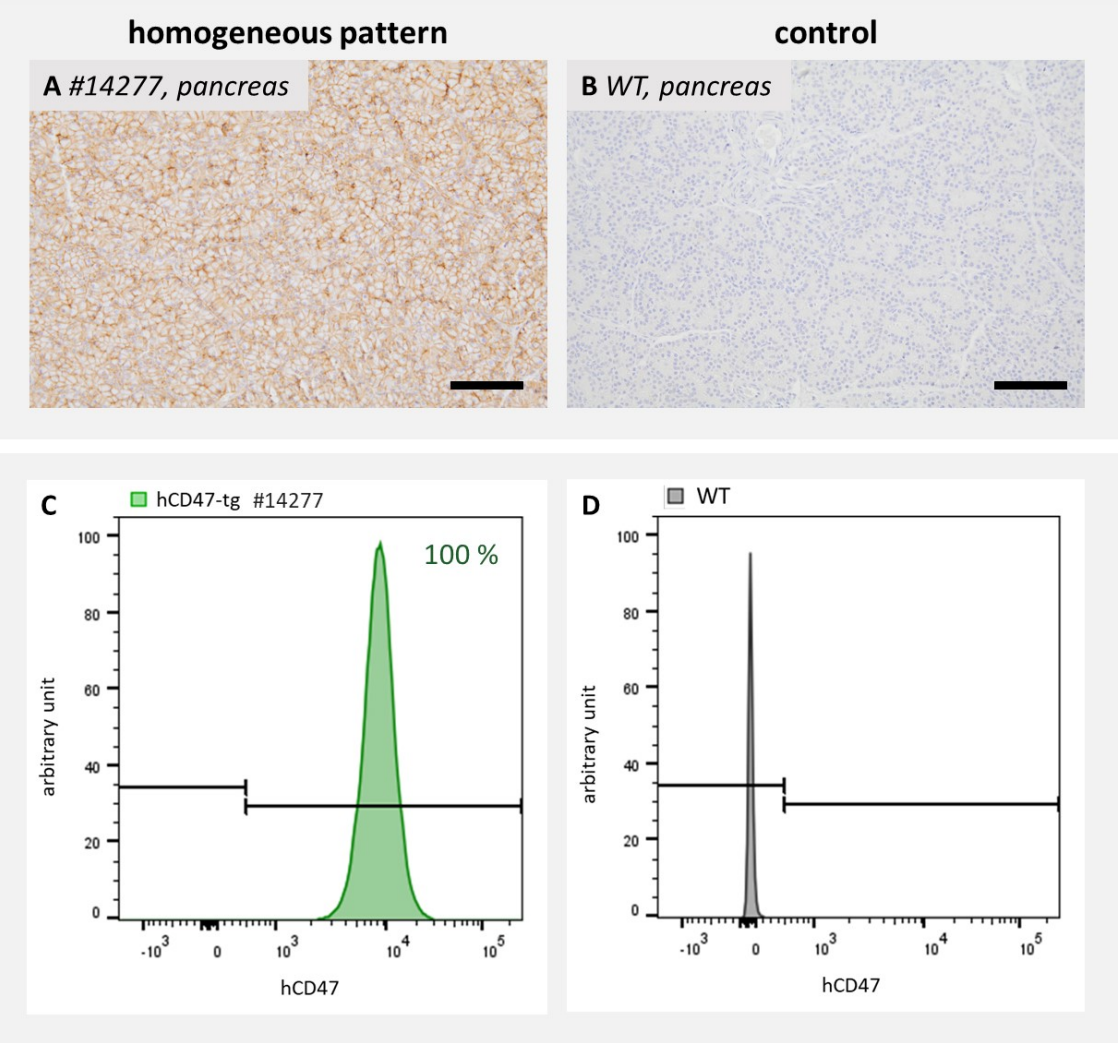

Figure 24: High homogeneous cell membrane-localized transgene expression of hCD47 integrated in exon 10 of the *GGTA1* gene.

(A, B) hCD47 IHC results of an exemplary founder animal showing strong homogeneous staining (A) in comparison to a wild-type control (B) of pancreatic tissue. DAB: brown color. Cell nuclei were stained in blue. Scale bars = 100µm. (C, D) Representative FACS analysis histogram shows 100% transgene positivity of all analyzed PKCs of a transgenic F0 founder animal (C) in comparison to a WT control (D).

1.2.5.2. *B2M*-KO/*GGTA1*-KO_*pA2UCOE-CAG*-hPD-L1-tg (in exon 7 of *GGTA1*)

The hPD-L1 transgene, targeted-integrated into exon 7 of the *GGTA1* gene, consistently exhibited robust and homogeneous expression across all examined organs as confirmed by immunohistochemistry staining. This was observed in animals with both monoallelic and biallelic expression cassette integration, as shown in **Figure 25 (A-D)**. Moreover, precise quantification through FACS analyses demonstrated that cells with biallelic integration of the hPD-L1 transgene had a slight rightward shift in expression intensity, as measured by mean fluorescence intensity (MFI) **(Figure 25 E-F)**. Additionally, the complete absence of α-Gal epitopes was confirmed, indicating a knockout of the *GGTA1* gene (not shown).

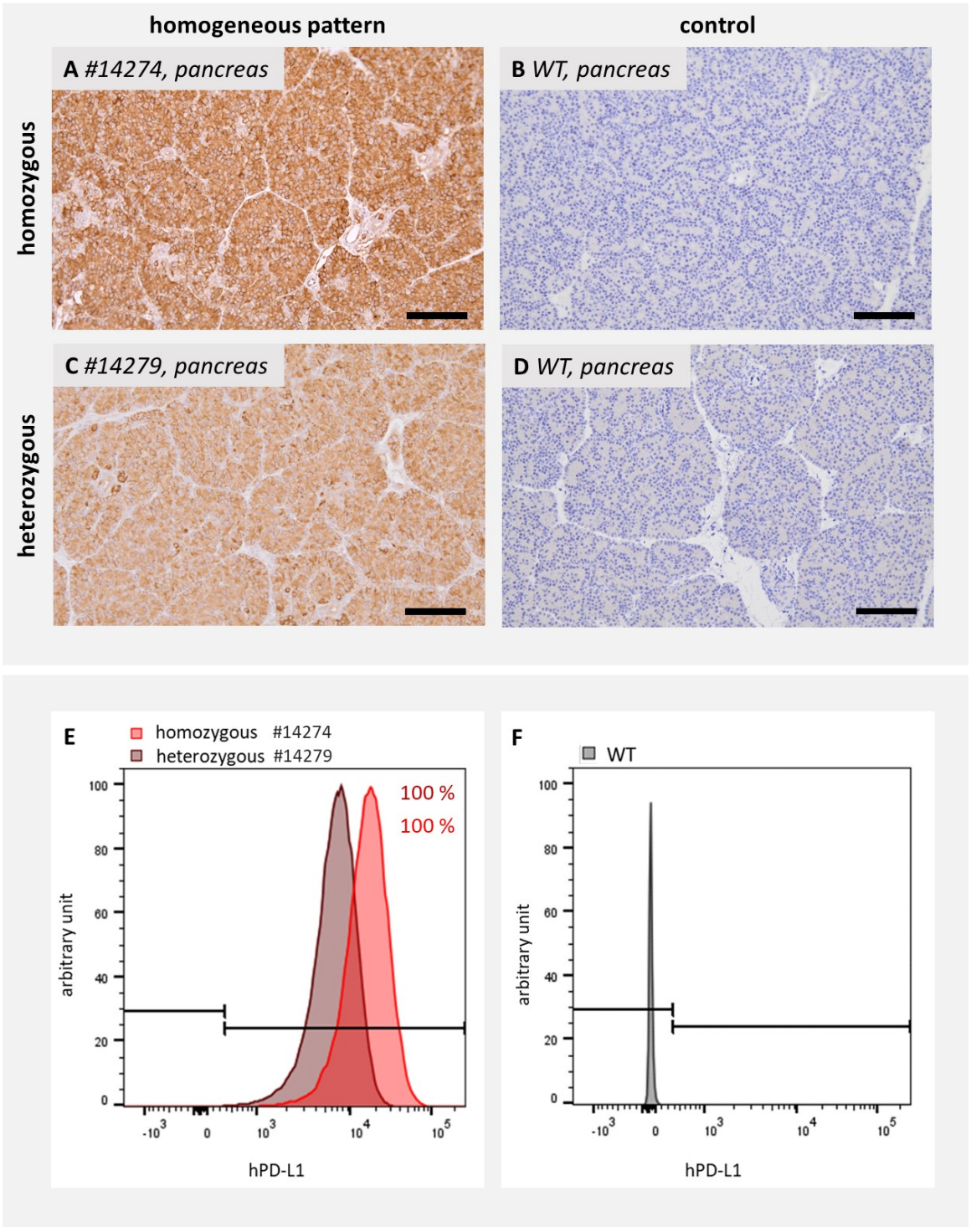

Figure 25: High homogeneous membrane-localized transgene expression of hPD-L1 integrated in exon 7 of the *GGTA1* gene.

(A – D) hPD-L1 IHC results of exemplary founder animals showing a strong homogeneous expression pattern of bi- (A) and monoallelic (B) hPD-L1 integration in comparison to wild-type controls (C, D) of pancreatic tissue. DAB: brown color. Cell nuclei were stained in blue. Scale bars = 100 µm. (E) Representative FACS analysis histograms showing a rightward shift in expression intensity (measured by MFI) of homozygous hPD-L1 integration compared to monoallelic transgene integration in the *GGTA1* gene. (F) FACS histogram of a wild-type control for comparison.

1.2.5.3. *GGTA1*-KO_(*INS*-LEA29Y, *pA2UCOE-CAG*-hPD-L1)-2xtg (in *SSC6*)

The integrated hPD-L1 expression cassette, positioned approximately 1 kb downstream from the *INS*-LEA29Y integration site on *SSC6*, resulted in a similar robust and homogeneous hPD-L1 expression pattern as detected in gm animals with targeted integration of the hPD-L1 expression cassette in exon 7 of the *GGTA1* gene **(Fig. 26 A-B)**. Furthermore, the integration of a large cassette nearby the preexisting transgene integration site of the *INS*-LEA29Y transgene did not show any negative effect on the expression of LEA29Y, as demonstrated by immunohistochemistry **(Figure 26 C-D)**.

PKCs derived from animals that have integrated the hPD-L1 transgene into the *SSC6* locus reached an expression level that ranks between those of PKCs from animals with mono- and biallelic hPD-L1 integration in exon 7 of the *GGTA1* gene, as demonstrated by FACS analysis histograms **(Figure 26 E-F)**. Furthermore, the absence of α-Gal epitopes confirms a knockout of the *GGTA1* gene (not shown).

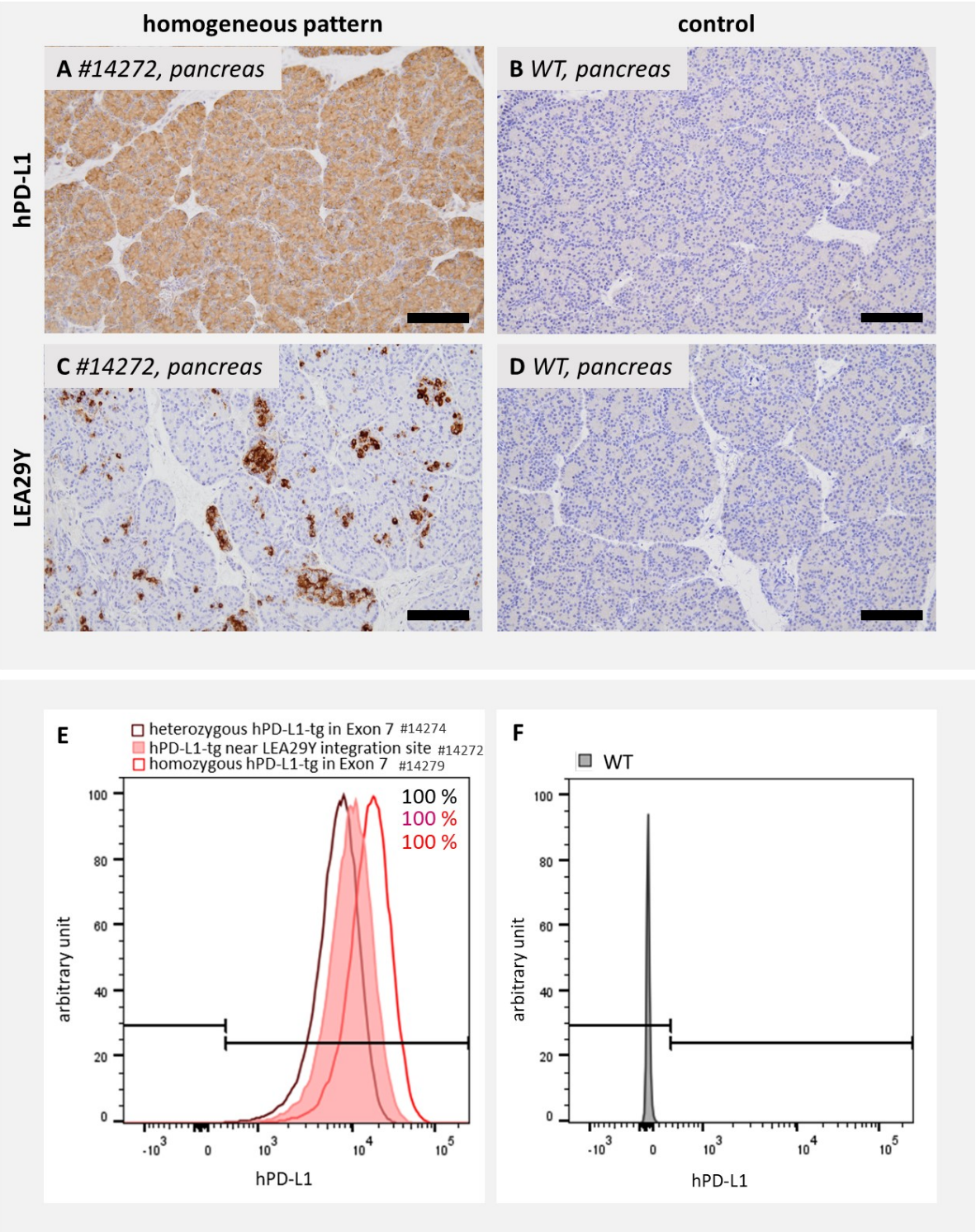

Figure 26 High homogeneous cell membrane-localized transgene expression of hPD-L1 integrated 1 kb downstream form the *INS*-LEA29 integration site on *SSC6*.

(A – D) Strong homogeneous hPD-L1 (A) and β-cell-specific LEA29Y (C) expression pattern of the co-expressing founder animals in comparison to a wild-type control (B, D) of pancreatic tissue. DAB: brown color. Cell nuclei were stained in blue. Scale bars = 100 µm. (E, F) Representative FACS analysis histograms demonstrate an intermediate expression intensity (measured by MFI) of cells with hPD-L1 integration near the LEA29Y integration site, which ranks between that of PKCs from animals with mono- and biallelic hPD-L1 integration in exon 7 of the *GGTA1* gene (E) in comparison to a WT control (F).

1.3. Comparison of transgene expression level in regard of genomic integration site

To evaluate the transgene protein abundance across different gm F0 founder pigs, Western immunoblot analyses were conducted using pancreatic tissue samples. Considerable variations in transgene expression intensity were observed among the different F0 pigs derived from the bulk cell population approach. In Western blot assays, the hCD47 protein was identified with an approximate molecular weight of 50 kDa in all hCD47-transgenic F0 pigs. In animals #12481, #12483, and #12559, no hCD47 protein could be detected, which is in line with the absence of hCD47 transgene integration in these F0 pigs. Founder animals #12346, #12347, #12480, and #12482 exhibited less than 25% transgene protein abundance compared to founder #12557, which displayed the highest protein abundance. F0 pigs #12556, #12562, and #12558 demonstrated intermediate levels, ranging around ±50%. F0 pig #12558 presented a noticeably lower band. In that animal, hCD47 protein with a size of 30 kDa was detected **(Figure 27)**.

There were also notable differences in hPD-L1 expression levels among the analyzed F0 pigs. In all F0 pigs, a protein band corresponding to hPD-L1 with a size of 50 kDa was detected in the analyzed pancreatic tissue lysates. Founder animals #12346, #12347, #12480, #12559, and #12557 showed transgene protein abundances of less than 25% compared to founder #12558, which exhibited the highest protein abundance. F0 pigs #12481, #12482, #12483, #12556, and #12562 demonstrated intermediary levels, with abundances ranging approximately ±50% **(Figure 27)**.

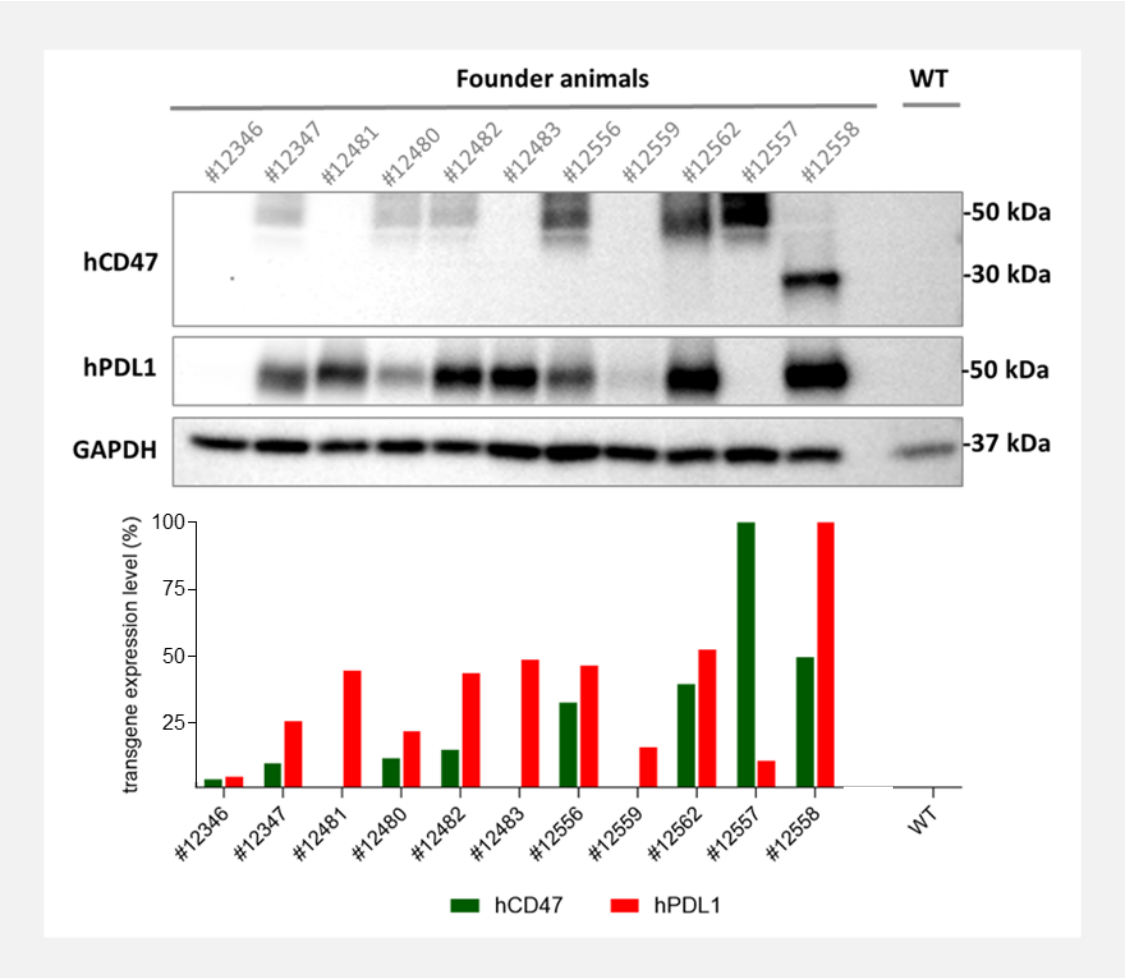

Figure 27: Western blot analyses showing distinct variations in the expression level of hCD47 and hPD-L1. in the F0 pigs derived from bulk cell population.

Western blot analyses of pancreatic tissue showing protein abundance of hCD47 and hPD-L1 in percent of F0 pigs derived from the bulk cell population, in comparison to a WT control.

The Western blot analyses findings were confirmed by FACS analyses. **Figure 28** shows the measured MFI levels in percentage (excluding negative cells) of the F0 pigs derived from the bulk cell population approach and the offspring of founder #12560.

The F0 pigs derived from the bulk cell population approach showed significant differences in expression levels. Particularly noteworthy is the finding of high expression levels of hCD47 found in founder animal #12557, which were even surpassed by the offspring of founder #12560, consistently showing an MFI of over 80%. F0 pigs #12346, #12347, and #12480 achieved levels below 25% MFI. The remaining analyzed founders attained intermediate levels. Similarly, substantial variations were observed in hPD-L1 expression levels, with founder #12561 recording the highest measured MFI. Founders #12346, #12347, #12480, and #12557 achieved levels below 25%. The remaining founder animals fell in between. The offspring resulting from breeding founder #12560 consistently exhibited levels over 75%.

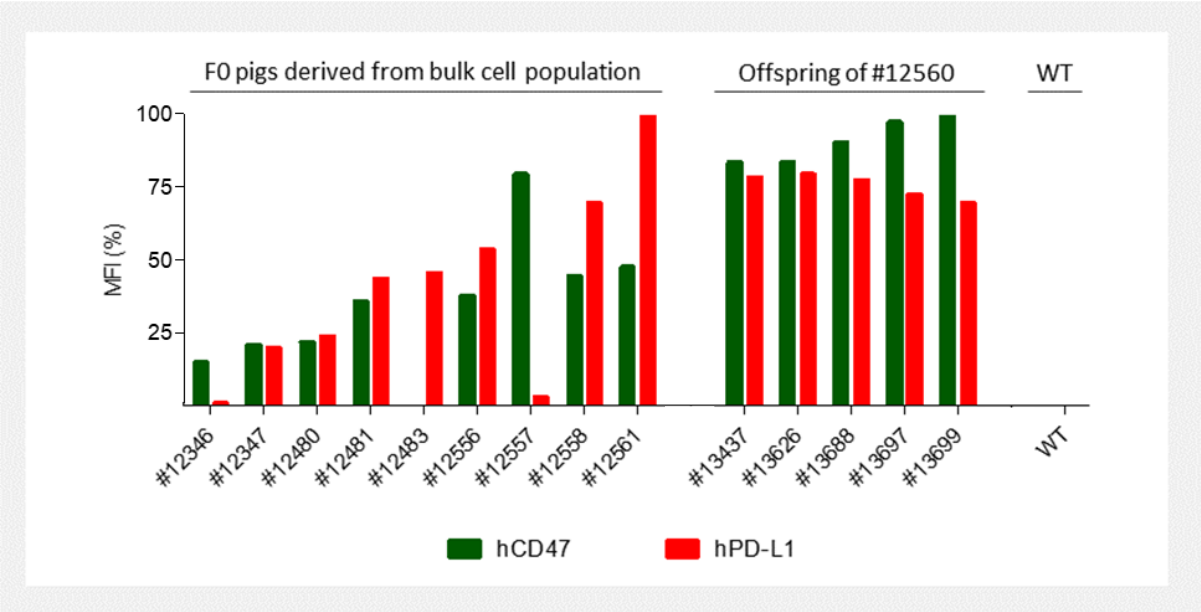

Figure 28: MFI level of F0 pigs derived from the bulk cell population showing grand variations, while offspring exhibited consistent MFI levels.

FACS analyses showing MFI in percent of F0 pigs derived from the bulk cell population in comparison to offspring of founder pig #12560 and WT control.

To compare the protein abundance between the F0 pigs derived from the bulk cell population approach and those derived from targeted transgene integration, additional Western blot and FACS analyses were conducted. Within the Western blot assays, the hCD47 protein was detected in all hCD47-transgenic F0 pigs, exhibiting an approximate molecular weight of 50 kDa. As demonstrated previously, high variations in transgene expression intensity were observed among the F0 founder pigs derived from the bulk cell population. In contrast, F0 pigs #14277, #14281, and #14278, harboring the integrated hCD47 transgene targeted in exon 10 of the *GGTA1* gene, displayed only minimal differences in the protein abundance. Collectively, they maintained a consistent level, exceeding 80%, albeit slightly less than founder animal #12557. Variations in molecular weights, as observed in F0 pig #12558, were not detected among the newer founder animals **(Figure 29)**.

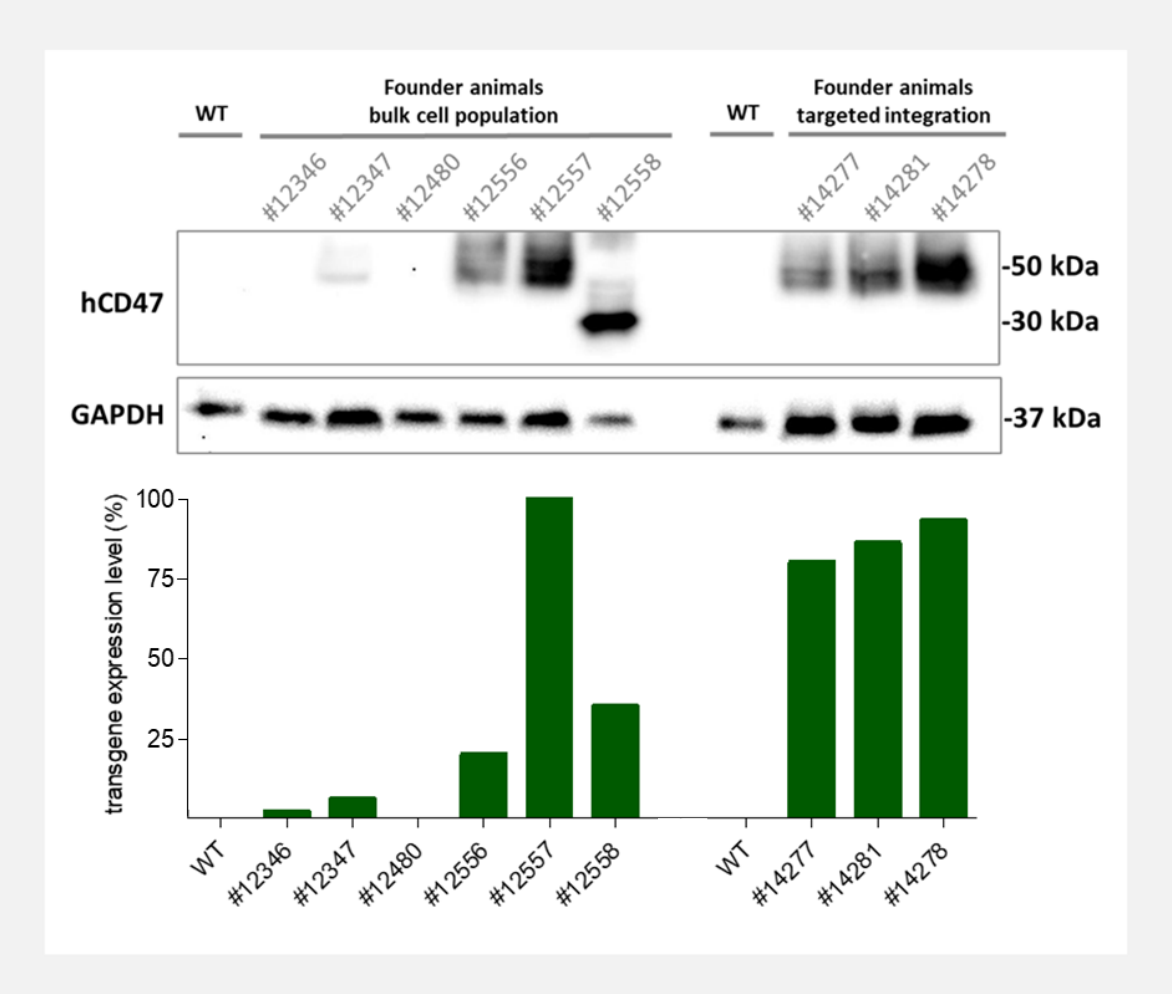

Figure 29: Western blot analyses revealed a consistently high level of hCD47 protein abundance inF0 pigs derived from targeted transgene integration.

Western blot analyses of pancreatic tissue showing protein abundance in percent of F0 pigs derived from the bulk cell population, in comparison to F0 pigs derived from targeted hCD47-tg integration in exon 10 of the *GGTA1* gene, and a WT control.

In line with the observations on the hCD47 transgene, all F0 pigs with targeted integration of the hPD-L1 showed only slight differences in protein abundance The presence of the 50 kDa hPD-L1 protein band was detected of pancreatic tissue in all F0 pigs. Distinct variations in protein abundance were observed for hPD-L1 among the different F0 pigs analyzed. These variations were previously detailed and were not found in the F0 pigs derived from targeted transgene integration. Additionally, the pigs derived from targeted transgene integration displayed even higher levels of protein abundance (80-100%) compared to those derived from the bulk cell approach. Notable differences between founder animals with targeted hPD-L1 integration in exon 7 of the *GGTA1* gene (#14282, #14279, #14274, and #14061) and those with targeted hPD-L1 integration in the *SSC6* locus (#14273 and #14272) were not observed **(Figure 30)**.

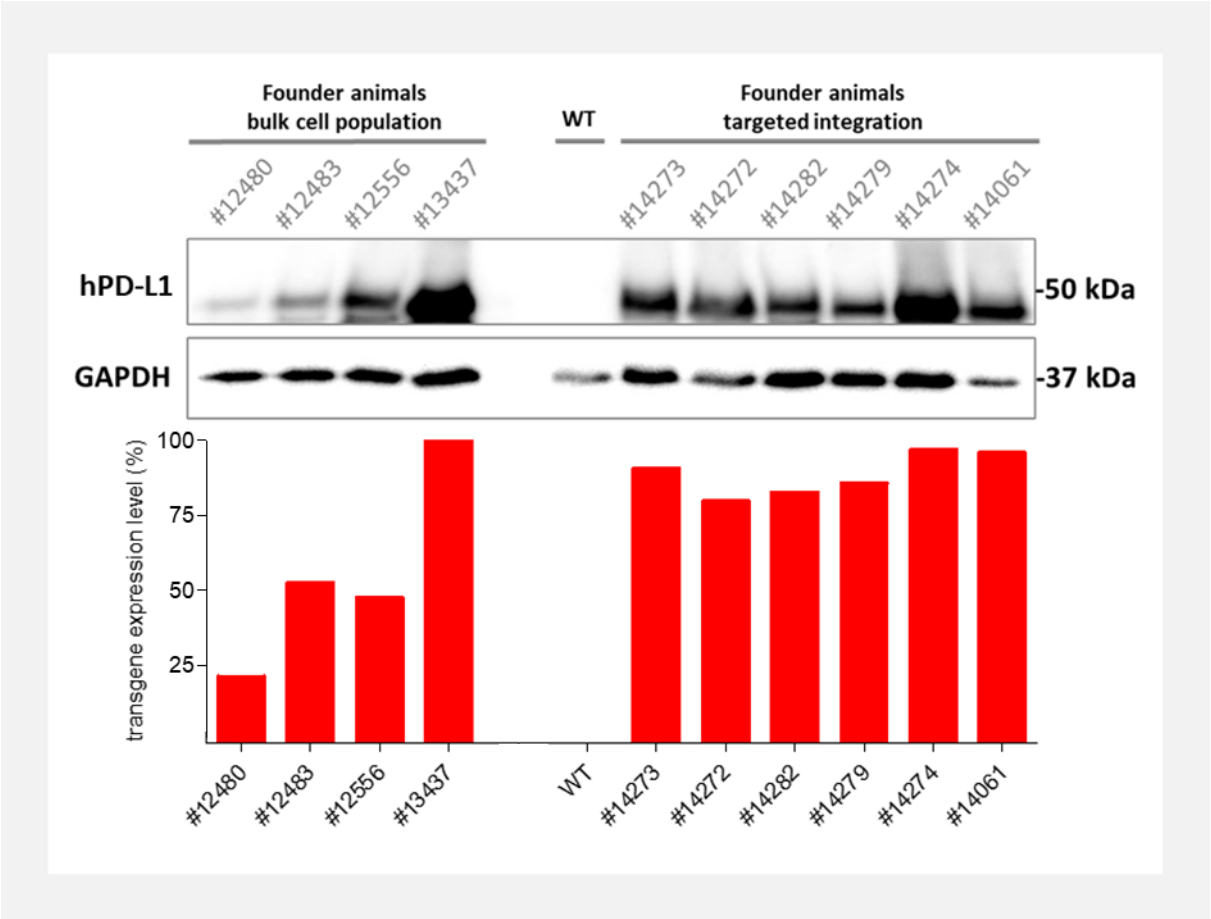

Figure 30: Western blot analyses revealed a consistently high level of hPD-L1 protein abundance in F0 pigs derived from targeted transgene integration.

Western blot analyses of pancreatic tissue showing protein abundance in percent of F0 pigs derived from the bulk cell population in comparison to F0 pigs derived from targeted hPD-L1-tg integration in exon 7 of the *GGTA1* gene and WT control.

The results regarding the differences in transgene expression intensities between the different F0 founder pigs obtained in the Western blot analyses were confirmed by FACS analyses. **Figure 31** shows a comparison of the measured MFI levels in flow cytometry analyses, expressed as a percentage (excluding negative cells), between the F0 pigs derived from the bulk cell population approach and those derived from targeted transgene integration. Although founder animals derived from the bulk cell population showed significant variations in MFI levels, as described in the Western Blot analyses findings, the MFI levels of F0 pigs from targeted transgene integration showed only minor differences. In terms of hCD47 expression levels, the F0 founder animals resulting from the targeted transgene integration approach consistently exhibited MFI levels exceeding 90%. These levels were even slightly higher than those of the best-performing offspring #13699 from the bulk cell population.

Similarly, the MFI levels of the hPD-L1 expression on PKCs of F0 pigs derived from the targeted transgene integration approach were within a similar range of ± 80%. However, they were lower compared to the best-performing founder #12561 from the bulk cell population. No significant differences in MFI levels were detected between the two hPD-L1 transgene integration sites, *GGTA1* and *SSC6*.

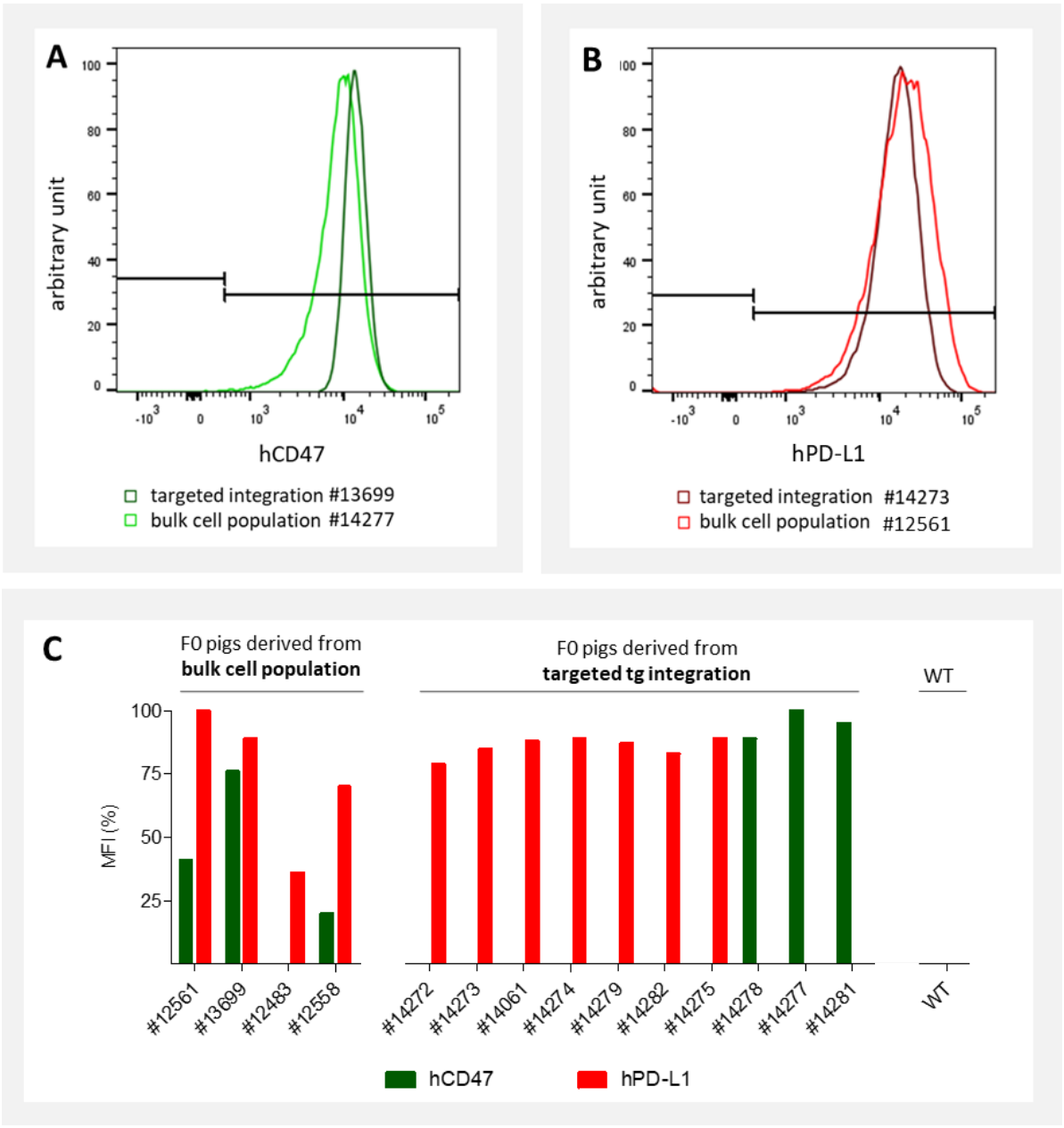

Figure 31: FACS analyses revealed a consistently high MFI level of hCD47 and hPD-L1 in F0 pigs derived from targeted transgene integration.

FACS analysis histograms comparing transgene expression levels of both, hCD47 (A) and hPD-L1 (B) of pigs derived from the bulk cell approach vs. pigs derived from targeted tg integration. (C) MFI levels of F0 pigs derived from targeted tg integration in comparison to F0 pigs derived from bulk cell population and WT control.

1.4. Validation of functionality of gm NPIs *in vivo*

The functionality of the NPIs from the gm pig line was tested in a preclinical transplantation model. In this model, NPIs were transplanted under the kidney capsule in immunodeficient streptozotocin-induced diabetic NSG mice. One group of mice received NPIs derived from pancreata of WT piglets (NPI_{wt} Tx group), whereas the other group of mice received NPIs derived from pancreata of gm F1 offspring (NPI_{gm} Tx group), which were obtained from matings with the F0 founder boar #12560. Of note, strong expression of both hCD47 and hPD-L1was confirmed on isolated NPIs prior to transplantation (not shown), as well as on the graft after explantation by immunohistochemistry **(Figure 32 A-C)**. Mice of both NPI transplant groups were similar in their capability to attain normoglycemia (NPI_{wt} vs. NPI_{gm} Tx group $p>0.05$) **(Figure 32 D)**. To assess whether the grafts functioned similarly between the two NPI recipient groups, an intraperitoneal glucose tolerance test was conducted on graft-bearing mice after achieving a normoglycemic status. The blood glucose response and insulin secretion in response to the glucose challenge were similar in both NPI graft recipient groups (NPI_{wt} vs. NPI_{gm} Tx group $p>0.05$ for all parameters) **(Figure 32 E-F)**. These results show that the genetic modifications and transgene expression on the NPIs did not have a negative impact on engraftment and graft function.

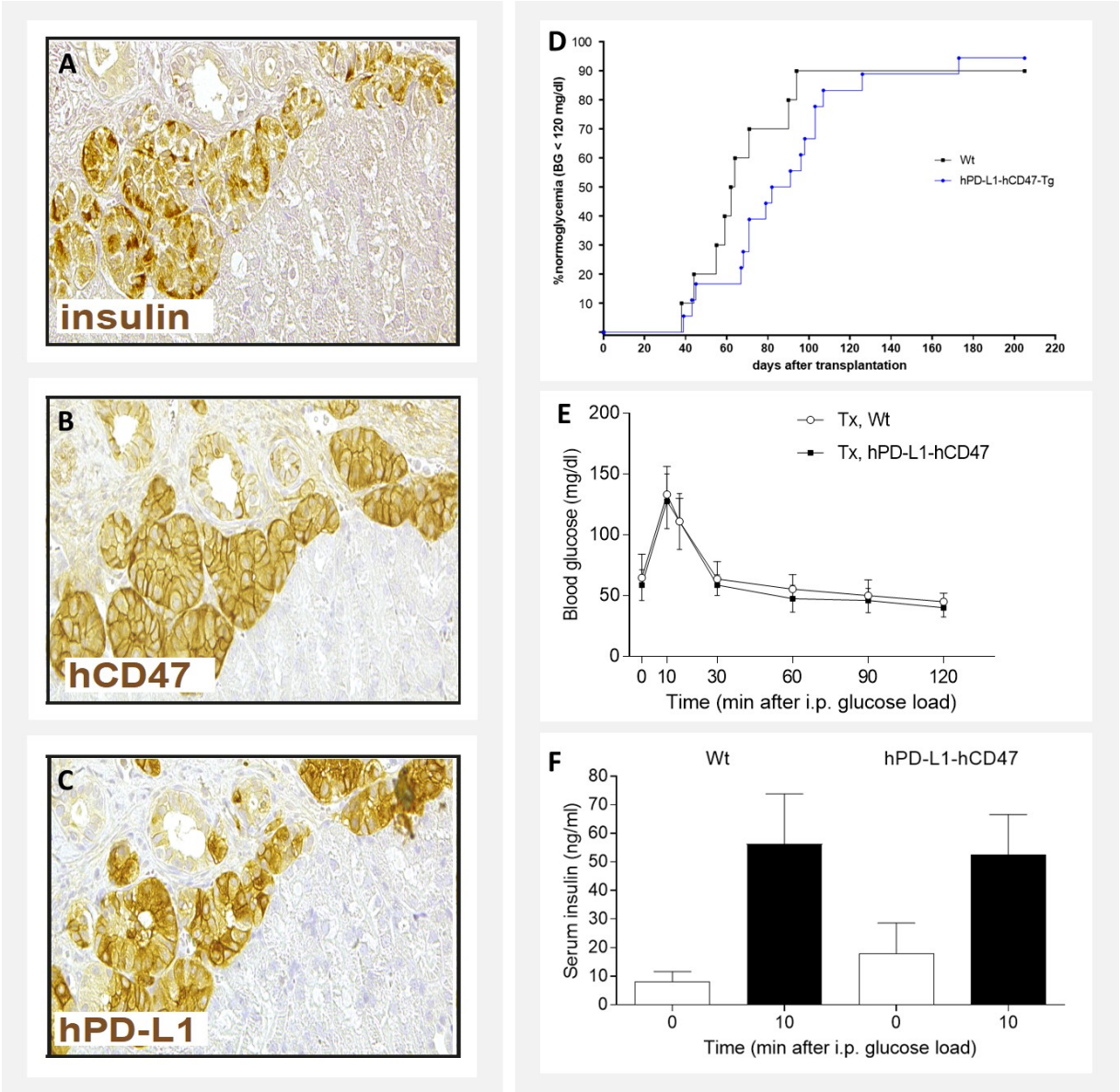

Figure 32: Transgenic expression hCD47 and hPD-L1 did not adversely affect NPI graft function.
(A-C) Representative images of the (hPD-L1, hCD47)-2xtg NPI graft after transplantation stained for insulin (A), hCD47 (B), and hPD-L1 (C). DAB: brown color. Cell nuclei were stained in blue. (D) Development of normoglycemia after transplantation in a monitoring period of 220 days. (E-F) Normoglycemic mice harboring a (hPD-L1, hCD47)-2xtg NPI graft had a similar response upon intraperitoneal glucose tolerance test as the NIP transplant group that received WT NPIs. Glucose clearance (E) and glucose-stimulated insulin secretion at 0 and 10 minutes (F) during intraperitoneal (i.p.) glucose tolerance test were comparable in mice transplanted with (hPD-L1, hCD47)-2xtg (squares, black bars) to mice transplanted with WT (cycles, open bars) NPIs. Data provided by Prof. Dr. Jochen Seißler, (Medizinische Klink und Poliklink IV, Ludwig-Maximilians-Universität, Munich).

2. Calcium sensor reporter pigs

2.1. Generation of calcium sensor reporter pigs

For the establishment of reporter pigs with a green fluorescent calcium sensor protein expressed ubiquitously, a linearized *CAG*-GCaMP6 expression cassette was used for nucleofection of male PKCs derived from a male German Landrace pig. Site-directed integration into the genome was intended to be facilitated through CRISPR/Cas9-driven double-strand breaks in the *Rosa26* gene. For SCNT, a bulk population of donor cells was selected using flow cytometry of green fluorescent signal-positive cells based on spontaneous intracellular calcium flows in GCaMP6 protein-containing cells.

In detail, the GCaMP6 expression sequence, which is codon-optimized for improved expression in mammalian cells, was placed under the control of a ubiquitous *CAG* promoter. Preceding the promoter sequence, the chromatin opening element *pA2UCOE* was positioned, resulting in a linearized purified construct with a total length of 5.2kb. By nucleofection of PKCs obtained from a wild-type boar, 2.5 µg of the linearized *pA2UCOE*-*CAG*-GCaMP6 expression cassette along with circular plasmids for R26 gRNA and Sniper-Cas9 protein were introduced into the cells. The previously established gRNA R26 was designed to induce a double-strand break in the non-coding safe harbor *Rosa26* gene, as illustrated in **Figure 33 (A)**.

Five days after electroporation, a total of 593 green fluorescent cells (1.2% of the total cells) were selected by flow cytometry **(Figure 33 B-C)**.

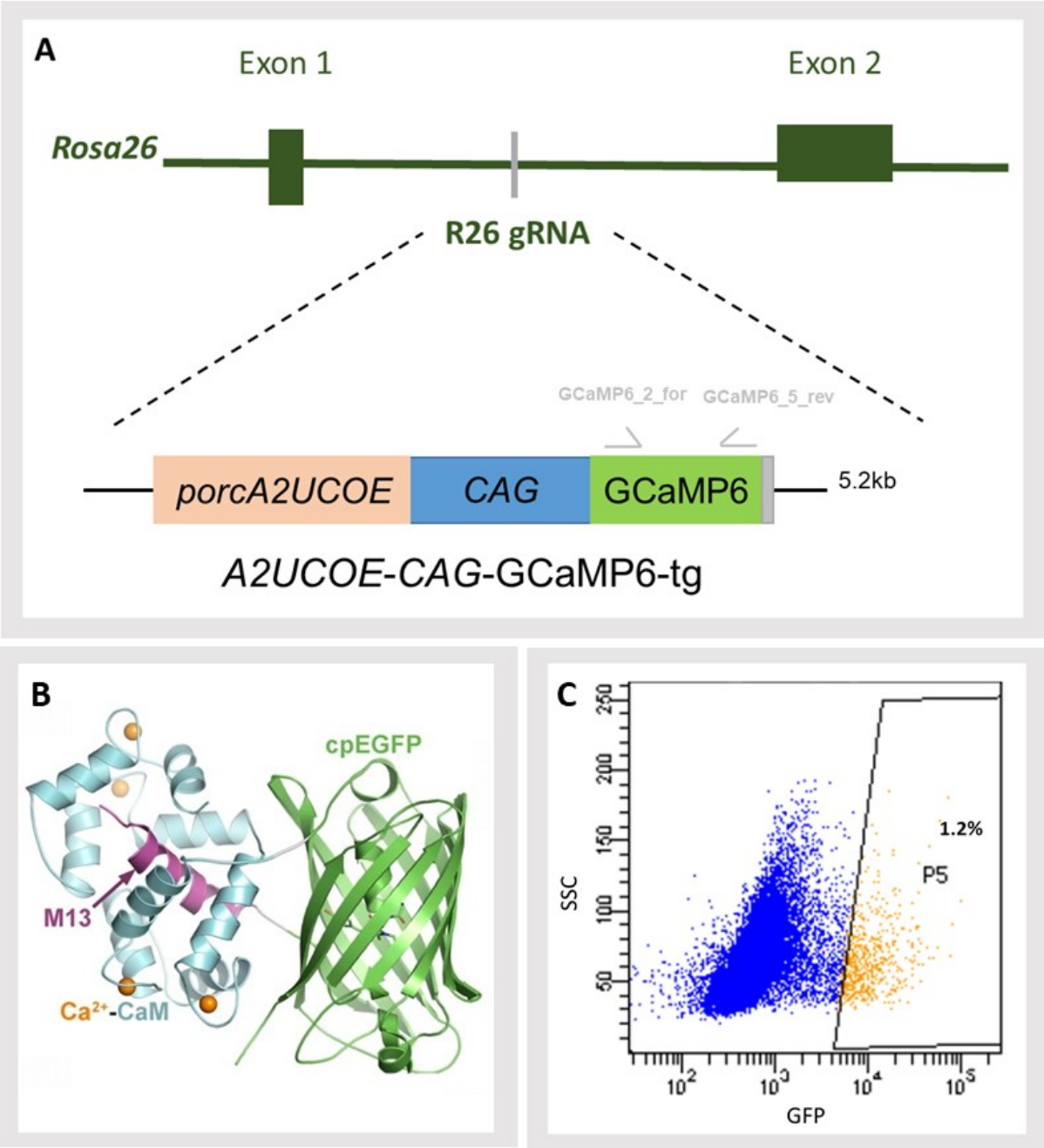

Figure 33: Targeting strategy and flow cytometry-based cell sorting of GCaMP6 expressing cells.

(A) Targeting strategy for *de novo* generation of GCaMP6 transgenic pigs. Targeting site of the gRNA that is used to induce a double-strand break in the *Rosa26* gene is shown. Graphical composition of the GCaMP6-carrying expression cassette is shown. Positions of the primers used for genotyping of gm pigs are indicated. (B) GCaMP6, a synthetic fusion of green fluorescent protein (GFP), calmodulin (CaM), and M13, a peptide sequence from myosin light-chain kinase, bound to Ca^{2+}(AKERBOOM et al., 2009). (C) Dot blots of flow-cytometry based cell sorting for collection of cells for subsequent SCNT. The cell selection criteria included green fluorescent signals, based on spontaneous intracellular calcium flows in GCaMP6 protein-containing cells.

The subsequent SCNTs resulted in one pregnancy and the birth of two male piglets (#12068 and #12069), of which one was stillborn **(Table 22)**. To confirm the integration of the GCaMP6 transgene, a genotyping PCR was performed, confirming the presence of transgene integration in the genome of both piglets. Nanopore sequencing was used to verify the integration of GCaMP6 into the *Rosa26* locus from founder #12068 (not shown).

Table 22: Overview of conducted SCNTs of flow cytometry preselected bulk cell population of *pA2UCOE-CAG*-GCaMP6 transfected cells.

SCNT No.	Epo ID	FACS	Date of SCNT	No. of SCNT embryos	Pregnancy (%)	Piglets born alive	Stillborn piglets
1	F1	green fluorescence positive	19-03-21	164	+	1	1
2			19-03-21	110	-	-	-
Total				**274**	**1 (50%)**	**1**	**1**

2.2. Characterization of the *pA2UCOE-CAG*-GCaMP6 F0 pigs

Expression analysis of the GCaMP6 protein was performed on a tail sample from the F0 piglet, #12068, which was born alive, as well as on tissue samples from the stillborn piglet #12069. Immunohistochemistry was conducted using a GFP antibody with epitope binding in the conserved eGFP protein region. The tail sample of the founder pig #12068 born alive showed a strong cytoplasmic expression of the GCaMP6 transgene that was homogeneously detected in all cells. In contrast, a mosaic-like transgene expression pattern of the transgene was observed in the tissues of the stillborn piglet #12069, with approximately 50% of the cells exhibiting positive staining.

Considering the promising transgene expression pattern observed in the tail sample, F0 pig #12068 was raised to establish a GCaMP6-tg breeding herd.

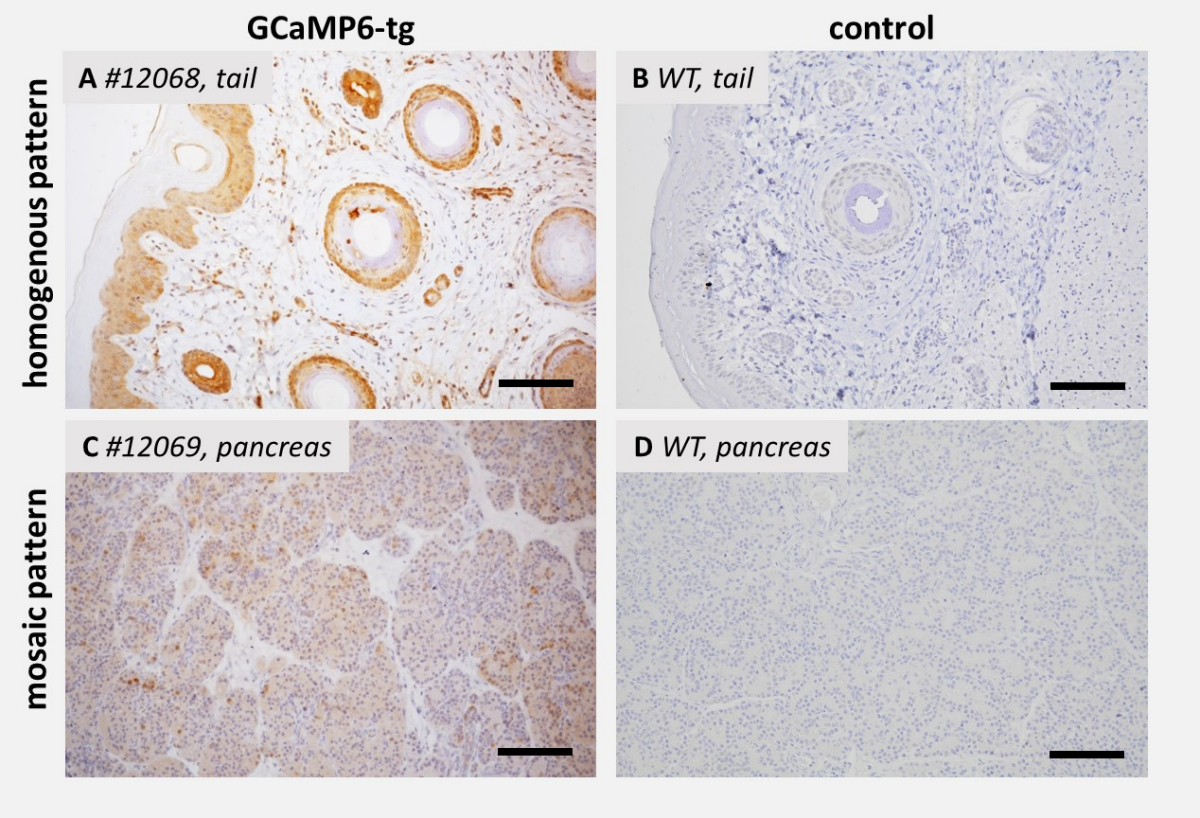

Figure 34: IHC analysis of GFP expression in GCaMP6 transgenic founder animals.

GFP IHC showing a homogeneous staining in the tail sample of founder animal #12068 (A) and a mosaic-like staining pattern in pancreatic tissue of founder animal #12069 (C), both in comparison to a wild-type control (B, D). DAB: brown color. Cell nuclei were stained in blue. Scale bars = 100 µm.

2.3. Characterization of breeding properties and gm robustness in F1 offspring

Founder #12068 successfully mated several sows. The offspring were used for additional studies on transgene expression, isolating pancreas for *in vitro* and *in vivo* mouse transplantation experiments, and for establishing a transgenic breeding population. Throughout this doctoral thesis, five matings took place, resulting in a total of 61 piglets. As the GCaMP6 transgene is heterozygous in one allele of the sire, it is expected that 50% of the transgene will be passed on to the offspring. Indeed, 33 out of the 61 piglets born were transgenic (54%).

The performed GFP immunohistochemistry performed showed a robust, homogeneous, and ubiquitous staining of all examined tissue samples, including the pancreas of the offspring **(**see **Figure 35)**.

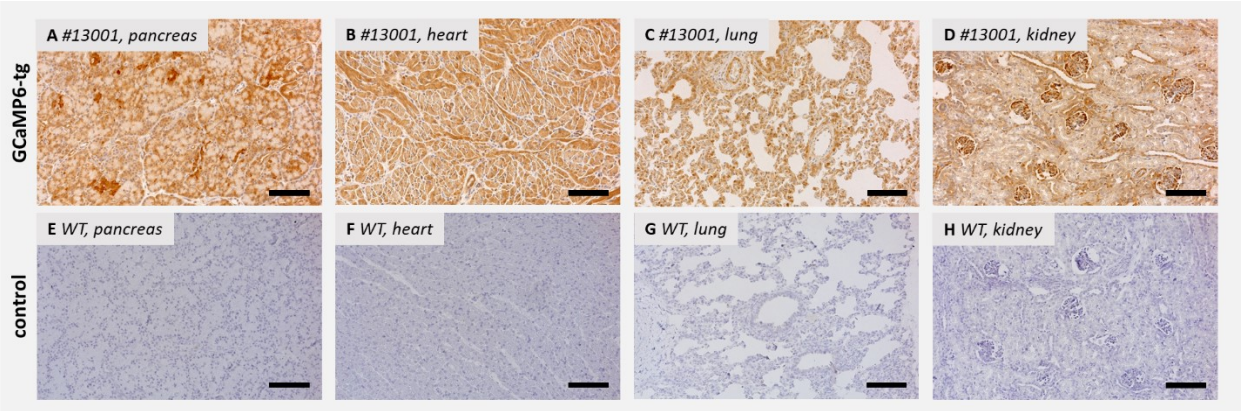

Figure 35: High, homogeneous cytoplasmic transgene expression across all tested organs in GCaMP6-tg F1 offspring.

Representative tissues of GFP immunohistochemistry from a GCaMP6-tg F1 offspring from founder #12068 (A-D) and from an age-matched wild-type control animal (E-H) are shown. DAB: brown color. Cell nuclei were stained in blue. Scale bars = 100 µm.

Furthermore, Western blot analyses demonstrated consistent protein abundance of the transgene in tissue lysates of GCaMP6 transgenic F1 offspring, indicating robust transgene expression **(Figure 36)**. GFP was identified in Western blot assays with an approximate molecular weight of 40 kDa. Of note, relative expression levels varied depending on the organ being investigated. Notably, pancreatic tissue demonstrated exceptionally high transgene abundance in relation to the equal protein amount used from tissue lysates of various organs Heart, lung, liver, and muscle tissues showed moderate expression levels, while the kidney exhibited relatively weaker transgene expression levels.

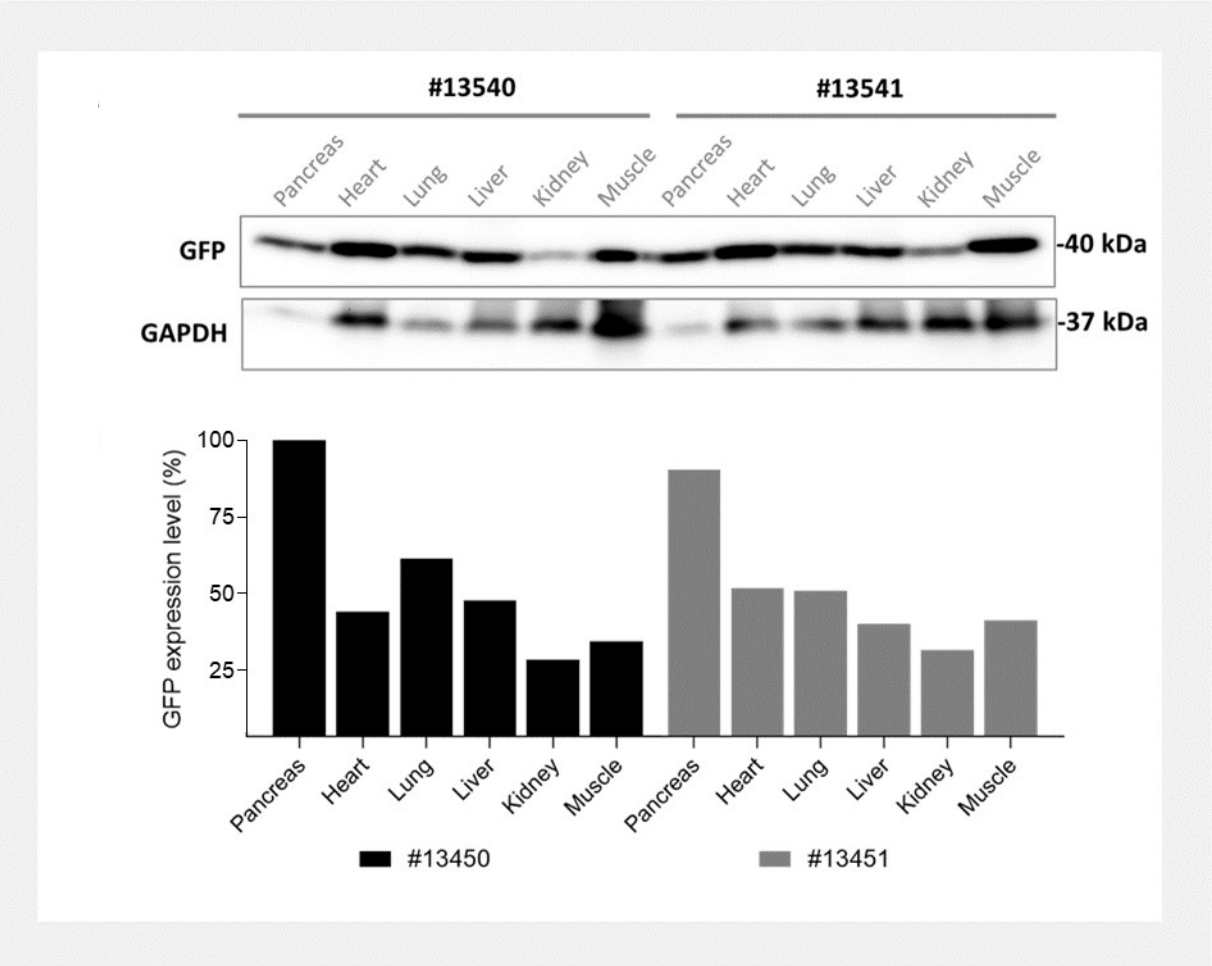

Figure 36: Western blot analyses confirm high protein abundance in pancreatic tissue compared to other organs.

Western blot analyses showing protein abundance in different organ tissues of two representative offspring of founder boar #12068.

2.4. *In vitro* imaging of Ca^{2+} flows in NPIs

After isolation of NPIs from neonate offspring, a strong, ubiquitous GCaMP6 expression of the NPIs was detected. *In vitro* GSIS showed a glucose-induced Ca^{2+}-induced response, represented by a wave of increased measured fluorescence intensity in a few cells of *in vitro* matured NPIs in culture. Upon potassium chloride challenge, most cells of NPIs showed the highest fluorescence response **(Figure 37)**.

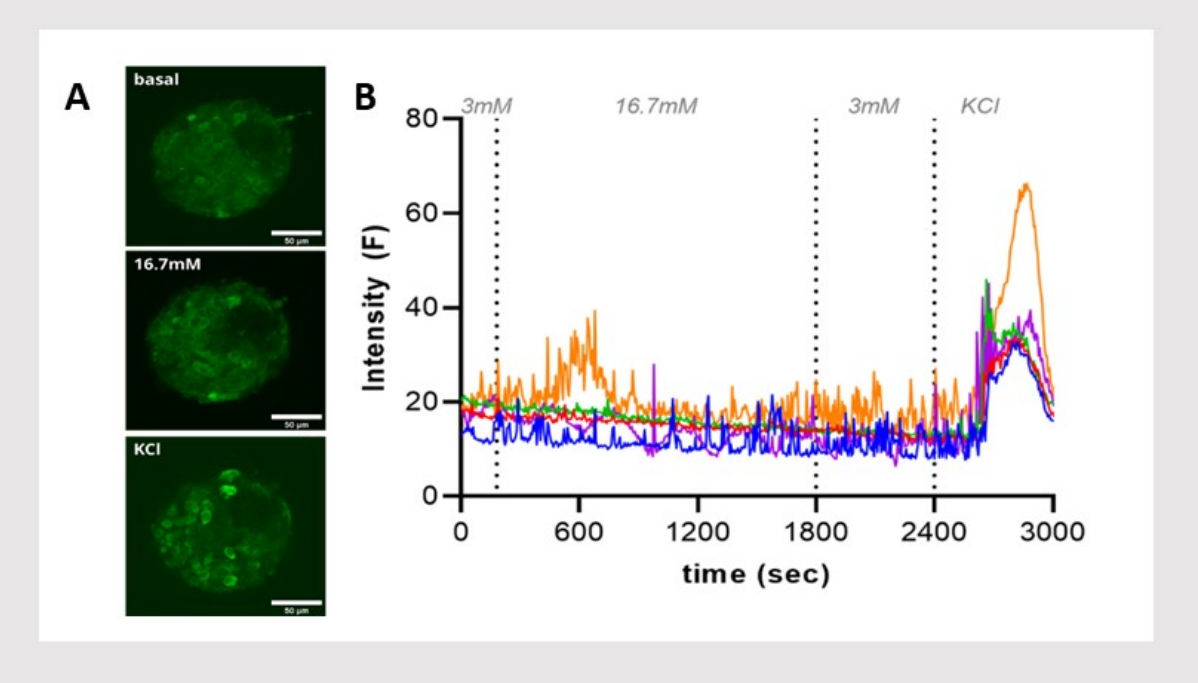

Figure 37*: In vitro* imaging of Ca^{2+} flows in NPIs.

(A) Ubiquitous GCaMP6 expression upon different stimuli. (B) *In vitro* GSIS showed a glucose induced Ca^{2+} response in a few cells (orange trace). Data provided by Dr. Christian Cohrs, Institute of Physiology, TU Dresden, Germany.

2.5. *In vivo* imaging of NPI grafts in the ACE transplant model

NPIs engrafted in the mouse ACE for 8 weeks did not show a Ca^{2+} reporter response upon glucose challenge due to the inhibitory effect of isoflurane anesthetic on glucose-induced ATP and Ca^{2+} increase. In contrast, a β-cell characteristic oscillatory Ca^{2+} reporter response in numerous cells was measured upon glucose stimulus on NPI grafts of ACE *ex vivo*, with the highest response observed upon the final potassium chloride stimulus. Immunohistochemical staining of the NPI grafts of ACE confirmed a high proportion of β-cells in the grafts **(Figure 38)**.

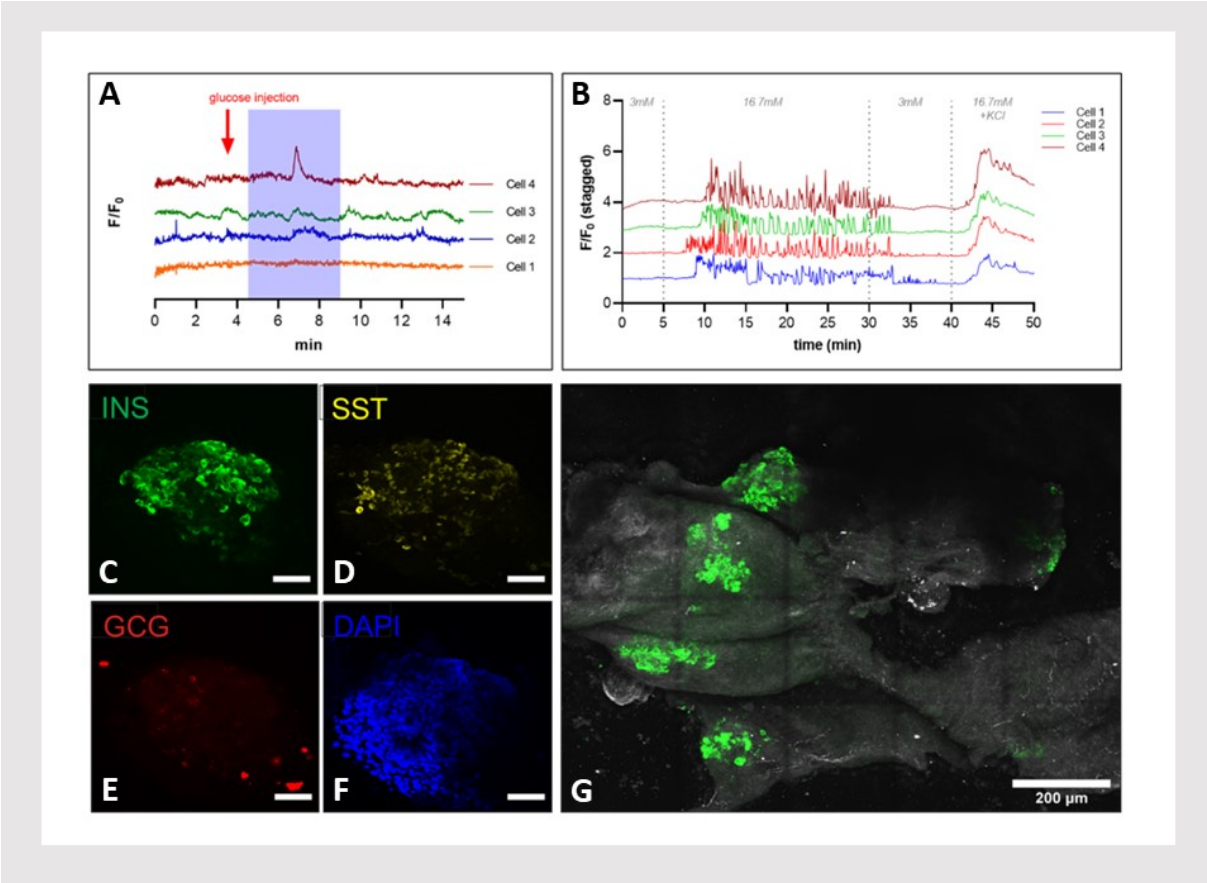

Figure 38: *In vivo* and *ex vivo* imaging of NPI grafts in the ACE transplant model.

(A) Delayed response upon iv glucose injection. (B) Multiple oscillations but no synchronous response of β-cells *ex vivo*. (C) Maximum intensity projections of an explanted iris stained for insulin (green); Zoomed view on one islet on the iris stained for insulin (green), somatostatin (yellow), glucagon (red), and DAPI (blue); Scale bars = 50 µm. Data provided by Dr. Christian Cohrs, Institute of Physiology, TU Dresden, Germany.

VI. DISCUSSION

To successfully translate islet xenotransplantation into clinical practice as a cure for diabetic patients and to address the shortage of organs and tissues in human allotransplantation, it is crucial to ensure the stability and robustness of genetic modifications and their expression patterns in the transplant. Therefore, a very detailed characterization of the organ and tissue donor source pig line is essential. Furthermore, a practical need essentially for breeding of the xenodonor pigs, is gene recombineering. This is because not only one but various genetic modifications in the donor pig might be required for local graft-derived immune protection, and the segregation of multiple transgene expression cassettes during breeding must be prevented. In this study, several approaches were employed to validate and fulfil the prerequisites necessary for the transition of xenotransplantation to clinical application.

1. Generation of optimized gm pigs with robust transgene expression

Over the past 20 years, gene editing technologies have undergone significant development, particularly in modifying the pig genome to generate gm pigs. Key milestones include the birth of piglets through somatic cell nuclear transfer (SCNT) in 2002, and the discovery of the CRISPR/Cas system, along with its application in pig gene modifications in 2014 (DMOCHEWITZ & WOLF, 2015). Since then, the generation of gm pigs with nearly every kind of genetic modification has become feasible in principle. Today, a plethora of CRISPR/Cas9 technology variants has emerged, ranging from basic non-homologous end joining (NHEJ)-mediated disruption of target genes to the precise introduction of modifications via homology-directed repair (HDR), utilizing various methods such as single-stranded overhangs, conventional targeting vectors, or bacterial artificial chromosomes (BACs) as recombination templates (MANI et al., 2021). While NHEJ is used specifically to inactivate genes, HDR can be employed to insert defined mutations or entire DNA segments into the genome. With this toolbox, gm pigs with edits to 13 genes and 42 alleles were generated *de novo* as organ donors for xenotransplantation in 2019 (YUE et al., 2021b).

Although generating gm pig models may appear straightforward nowadays, achieving robust and reliable transgene expression still relies on numerous factors that need to be identified, and strategies to be developed. There are several tools available to enhance transgene expression robustness.

Role of promoter, chromatin opening elements and transgene integration site for robust transgene expression in gm pigs

Promoters are specific genetic sequences that control the expression of transgenes, acting as regulatory elements that determine when and where the transgene is expressed in the host organism. By strategically selecting promoters, the desired expression levels of the transgene can be achieved. To date, numerous transgenic pig lines have been produced using viral, chicken, mouse, human, and porcine promoter sequences with ubiquitous or cell type-specific activity (AIGNER et al., 2010).

Although useful for expression of transgenes in cells *in vitro*, the usage of viral promoters such as the cytomegalovirus (*CMV*) promoter is not recommended for transgene expression in animals due to high susceptibility to promoter silencing (MEHTA et al., 2009). The *CAG* promoter used in our study is a chimeric promoter consisting of a CMV enhancer element and the β-actin promoter sequence from chicken. The *CAG* promoter is widely used for constitutively high and ubiquitous expression of the target genes in both *in vitro* culture systems and in gm animals, including gm pig models (FISCHER et al., 2016; BUERMANN et al., 2018; YUE et al., 2021a). To achieve high and ubiquitous expression levels, the cDNA sequences of the transgenes such as hPD-L1, hCD47, and GCaMP6 were placed under the control of the *CAG* promoter. Although most of the F0 pigs harboring such a transgene expression cassette under the control of this promoter, the different F0 pig lines exhibited variations in their expression pattern and expression levels of the transgenes, ranging from ubiquitous expression across all examined organs to high levels of promoter silencing resulting in a strong mosaic pattern. This was especially evident in pig lines derived from the bulk cell population approach. This variation might be attributed to differences in the number of integrations, transgene silencing, or positional effects from the host genome (BESTOR, 2000; BRUNETTI et al., 2008). The chromatin environment surrounding the integration site may affect both the transgenic and the host gene expression patterns, potentially causing ectopic, weak, or even undetectable gene expression (GIRALDO & MONTOLIU, 2001; HE et al., 2005). Although we used CRISPR/Cas9-based gene scissors for promoting integration of the transgene expression cassette at predefined genomic sites, it is important to note that this approach only increases the likelihood of transgene integration at these sites. It does not prevent the possibility of multiple transgenes integrating in a random orientation at these sites or at other locations within the host genome. If the expression cassette is integrated into a transcriptionally inactive region of DNA, such as constitutive heterochromatin, the transgene can become inactivated. It has been observed that a transgene may initially be expressed for a short period of time before

decreasing to undetectable levels (BESTOR, 2000). DNA methylation and chromatin modifications are key epigenetic changes that lead to transgene silencing (HE et al., 2005; HSU et al., 2010; ZHOU et al., 2014). High copy numbers of the transgene can induce transgenic silencing by modifying the promoter 's methylation pattern (GARRICK et al., 1998). In other cases, the transcriptional silencing of the transgene occurs due to the formation of repressive heterochromatin on the plasmid DNA backbone, with no involvement of promoter methylation (CHEN et al., 2008). This is in line with the findings of this study, which demonstrate that transgene expression occurred more predictably and robustly when one single copy of the transgene expression cassette was targeted for integration by HDR at predefined sites in the genome, such as the *GGTA1* gene locus or the safe harbor locus *Rosa26*.

Although the integration sites of the combined *INS*-LEA29Y_*CAG*-hPD-L1 expression cassette in most of our F0 pigs obtained from the bulk cell approach enabled hPD-L1 transgene expression under the control of the *CAG* promoter, LEA29Y transgene expression was not detectable. As this *INS*-LEA29Y expression cassette had already been used for the generation of the preexisting *INS*-LEA29Y pig line, the functionality of the porcine *INS* promoter sequence used to drive β-cell specific expression of the transgene was proven. The porcine *INS* promoter has been used for the generation of various gm pig lines in the past, such as the diabetic INS^{C94Y} pig line or the *INS*-eGFP pig line, both models generated by additive gene transfer approach with random integration (RENNER et al., 2013; KEMTER et al., 2017). Common findings in these studies were that the SCNT-derived F0 offspring varied in their β-cell specific expression of the transgene from high expression to no detectable expression. In a study by Nottle et al. (2017), a targeted integration approach into the *GGTA1* gene was employed for a porcine *INS* promoter containing expression cassette aimed at CD2 transgene expression. However, nearly no transgene expression was achieved in the gm pigs. These findings suggest that the functionality of promoters heavily relies on the integration site. Therefore, the use of a targeted knock-in strategies is preferable to random integration strategies. In addition, the prerequisites for robust transgene expression at the integration site could differ for different promoters. In consequence, the suitability of the genomic integration site for each promoter to sustain stable transgene expression should be validated for each promoter.

Chromatin opening elements such as *A2UCOE* have been reported to increase the accessibility of adjunct promoter sequences to the transcription machinery (SIZER & WHITE, 2023). Incorporating enhancer elements can boost the activity of promoters, leading to more robust and sustained transgene expression. Studies have demonstrated that *A2UCOE* functions as a dominant chromatin remodeling domain, effectively preventing transcriptional silencing or

variegated expression, even if the transgene becomes integrated within centromeric heterochromatin (ZHANG et al., 2017). To exclude species incompatibility for the functionality of the *A2UCOE* element, we used the *porcine A2UCOE* sequence. However, even with the introduction of this chromatin opening element preceding the *INS* promoter, it was insufficient to achieve robust high β-cell-specific expression. This new finding highlights the importance of the site of transgene integration into the genome of pigs and highly likely of all (higher) mammals in determining the accessibility of the promoter sequence used to drive the transcription of the transgene in a cell-type regulated manner. Identification of genomic regions that enable porcine *INS* promoter-driven robust high β-cell-specific transgene expression could be achieved by identifying the transgene integration sites of all preexisting gm pig lines in which the *INS* promoter was demonstrated to induce cell type-specific transgene expression. Tools such as so-called third-generation sequencing, like LRT sequencing and nanopore sequencing, are now available, enabling the identification of the transgene integration sites into the genome without the requirement for PCR amplification or chemical labelling of the sample (NIEDRINGHAUS et al., 2011; AMARASINGHE et al., 2020).

To address these site-specific challenges, transgene integration could be performed at designated safe harbor loci. Safe harbor loci are specific genomic regions known to tolerate the insertion of exogenous DNA without disrupting endogenous gene function or causing detrimental effects to the host organism, promising predictable transgene expression (KLATT et al., 2020). The utilization of safe harbor loci offers several advantages in the generation of transgenic animal models. By targeting these specific genomic regions, the risk of unintended genomic disruptions can be minimized, ensuring stable transgene expression over multiple generations. Furthermore, the well-defined regulatory elements and chromatin structure surrounding safe harbor loci contribute to consistent and predictable transgene expression patterns (MA et al., 2022). The *Rosa26* gene, in particular, has been extensively studied and characterized as a safe harbor locus in various organisms, including mice and pigs (LI et al., 2014).

To date, only a few safe harbor loci have been identified in pigs. In addition to the *Rosa26* gene, other examples of safe harbor loci include the *pH11* (Hipp11) locus, the *CEP112* (centrosomal protein 112) locus, the *AAVS1* (adeno-associated virus integration site 1) locus, the *COL1A1* (collagen type I alpha 1 chain) locus, and the housekeeping genes *ACTB* (beta-actin) and *GAPDH* (glyceraldehyde-3-phosphate dehydrogenase). These loci have been identified for stable and permissive exogenous DNA integration in pigs (XIANG et al., 2023).

The methodology employed in our study involved forcing site-directed integration into the *Rosa26* gene using CRISPR/Cas9-driven double-strand breaks. The transgene cassette of *CAG*-GCaMP6 founder animal #12068 was integrated into the *Rosa26* locus, as confirmed by nanopore sequencing. Transgene expression of the green fluorescent calcium sensor protein was homogeneous and robust both in the F0 and F1 animals, demonstrating the reliability and consistency of transgene expression across generations. Moreover, pigs originating from the preexisting, well-expressing line, in which the *INS*-LEA29Y construct was randomly integrated into the *SCC6* locus, continued to exhibit high levels of expression in the β-cells, even with the additional integration of the hPD-L1 transgene, which also achieved substantial expression. No adverse effects were detected on the gm animals or on the islet graft function of the preexisting *INS*-LEA29Y islet donor pig line (KLYMIUK et al., 2012). These results suggest that the *SCC6* locus may be a promising candidate for transgene integration, especially if *INS* promoter-driven β-cell-specific transgene expression will be required, resembling a safe harbor locus, and merits further investigation.

Role of regulatory elements of the expression vector for robust transgene expression and correct transgene protein processing

The findings of altered transgene protein processing in F0 pig #12558, which exhibited predominantly nuclear membrane localization of the hCD47 transgene instead of the expected cell membrane localization, raises important questions regarding post-transcriptional processing and modifications. Flow cytometry analysis comparing non-permeabilized and permeabilized cells stained for hCD47 revealed that all PKCs of animal #12558 exhibited hCD47 transgene expression, but only half of them were localized at the cell membrane where functional activity is expected. Additionally, alterations in the molecular weight of the hCD47 protein were observed, indicating potential post-transcriptional processing differences compared to correctly processed transgene proteins in all other hCD47 transgenic pig lines.

In the past, other research groups have also generated gm pig lines expressing the hCD47 transgene. Previous studies by Dr. Hawley's group in 2014 (TENA et al., 2014) generated gm pig lines, where the hCD47 expression cassette, consisting of the human *EF1a* promoter and coding sequences for splice form 1 of the hCD47 gene, was integrated using a knock-in targeting vector into the *GGTA1*gene. While FACS and RT-PCR analysis confirmed a widespread uniform cell surface expression of hCD47 in the first pig (TENA et al., 2014), a recloned second transgenic pig showed only low cell surface hCD47 expression (TENA et al., 2017). The underlying mechanism for this phenomenon remained unclear, but it may potentially result from gene silencing, as discussed previously.

The second group, led by Dr. Burlak (HOSNY et al., 2021), utilized hCD47 constructs with and without modified 3′UTR, which were inserted into the *GGTA1* locus in porcine fetal fibroblasts using CRISPR (HOSNY et al., 2021). The sequence of the 3′UTR was designed as a modified version of the proposed uridine-rich binding site sequence used by Berkovits et al. In this study by Berkovits et al., the transcribed but not translated 3'UTR sequence was identified as essential for proper and efficient trafficking of the CD47 protein to the cell membrane (BERKOVITS & MAYR, 2015). Since in that study the extracellular domain of CD47 was replaced by GFP, it was speculated whether disturbed cell membrane trafficking would also occur with WT CD47, as the extracellular domain itself should favor correct membrane trafficking. Hosny et al. used a synthetic 3'UTR in their hCD47 expression cassette, designed by aligning both hCD47 and sus scrofa CD47 3′UTR and selecting the uridine-rich element that acts as a scaffold for binding proteins to promote CD47 surface membrane processing (HOSNY et al., 2021). In addition, the proximal polyadenylation site in the 3′UTR was mutated from AAUAAA to ACUCAA in their expression cassette. Their *in vitro* study demonstrated that cells transfected with the construct lacking the 3′UTR (hCD47(3′UTR−)) predominantly exhibited intracellular expression of hCD47. These cells showed evidence of ER stress, dysregulated mitochondrial biogenesis, oxidative stress, and autophagy. Conversely, the inclusion of the 3′UTR (hCD47(3′UTR+)) reduced intracellular expression of hCD47 by 36% and increased cell surface expression by 53%. This was correlated with a significant decrease in cellular stress markers and a heightened level of protection against phagocytosis by human macrophages.

In this study, we employed the hCD47 3'UTR sequence previously investigated by Berkovits et al. Based on our findings of F0 pig #12558, we examined the presence of the 3' UTR sequence of the hCD47 expression cassette integrated into the genome of the F0 founder pigs. However, PCR analysis targeting the middle 3' UTR sequence in the case of founder animal #12558 did not yield any discernible PCR band, despite detecting the polyA tail sequence region, indicating a faulty integration of the expression cassette in that genome. This underscores the potential advantages of utilizing hCD47 constructs containing the 3′UTR sequence.

Gene stacking and combineering technology for generation of multi-gm donor pigs for xenotransplantation

The final optimal combination of gene modifications in donor pigs for xenotransplantation is yet to be determined (KEMTER et al., 2020). This combination will likely involve gene deletions and transgene expression, with some transgenes needing to be expressed in a

cell-type-specific manner. If two transgenes are integrated into different genomic regions and both are monoallelic in the breeding animal, the probability of both transgenes being inherited by the offspring is 25%. With the addition of each transgene integrated into a separate independent genomic region, the likelihood of obtaining offspring with the desired multi-gm constellation drastically decreases. Therefore, integrating numerous transgenes at one transgene integration site and combining transgene integration sites with gene deletions can circumvent the segregation of genetic modifications through breeding. Another option to avoid the segregation of multiple transgenes is gene stacking using polycistronic vectors. These constructs contain cDNA from two to three different transgenes, coupled by a 2A linker sequence, enabling the expression of all transgenes simultaneously in a single mRNA transcript (LIU et al., 2017).

Yue et al. (YUE et al., 2021b) generated 12-fold multi-gm pigs by assembling three polycistronic expression cassettes into a single transgene integration cassette placed within the *GGTA1* gene locus. In addition to *GGTA1*, the *B4GALNT2* and *CMAH* genes were depleted using gRNA-guided CRISPR/Cas9. Genetic analysis revealed the integration of the multi-transgene vector into one allele of the *GGTA1* locus, with Mendelian segregation of the 9-transgene array *en bloc* observed upon breeding. Expression comparisons between 3xKO/9xtg pig umbilical vein endothelial cells and human cells showed similar levels for most proteins, except for hTHBD. Several factors are known to affect the reliability and intensity of transgene expression, including which transgene is expressed, the position of the transgene's cDNA, and the choice of promoter. Therefore, combining smaller components e.g. cDNAs, such as 2A peptide or IRES-based polycistronic systems, could carry a risk of poor or variable expression (FISCHER et al., 2016). Factors such as distance from regulatory elements, neighboring transgenes, and chromatin context can contribute to differential expression patterns for each transgene (JEONG et al., 2013; WANG & GUO, 2020). Consequently, the impact of the transgene position within a polycistronic vector may vary for each transgene. While polycistronic systems are therefore useful for some purposes, they might not be suitable for the expression of a whole set of transgenes in a pig organ where abundant and/or tissue-specific expression is essential for immune protection and function (FISCHER et al., 2018).

Alternative means is the use of separate expression constructs to ensure independent expression (FISCHER et al., 2016). In our project, we combined two separate expression cassettes: the *INS*-LEA29Y expression cassette and an additional cassette for ubiquitous expression of hPD-L1, where the cDNA sequence of hPD-L1 was placed under the control of the *CAG* promoter. Both expression constructs were oriented in the antisense direction and separated by

the *pA2UCOE*, which should act bidirectionally as a chromatin opening element. The linearized purified construct of the combined *(INS*-LEA29Y, *CAG*-PD-L1)-2xtg expression cassette had a total length of 10.3 kb. Site-directed integration into the genome was intended to be induced by CRISPR/Cas9-mediated double-strand breaks in both the *GGTA1* and *CCL2* genes. However, we observed that the *INS* promoter lacked functionality, as discussed previously.

Based on these findings, we opted for targeted integration techniques into predefined loci, such as integrating nearby a preexisting transgene integration site or inserting expression cassettes into a gene that needs to be depleted. For this, we integrated the hPD-L1 cassette 1 kb distal to the *INS*-LEA29Y transgene integration site on *SSC6* of the preexisting *INS*-LEA29Y transgenic line, to combine both transgenes within the same locus. Furthermore, we targeted integrated single expression cassettes for both hCD47 in exon 7 and hPD-L1 in exon 10 of the *GGTA1* locus. This not only resulted in a knockout of the *GGTA1* locus but also facilitated the combination of both transgenes through mating.

Targeted integration thus helped make the breeding process more effective and predictable. However, there is a potential risk of inducing genome instability in that genomic region. There is a possibility that both the original and newly integrated transgenes could be negatively affected (CABRERA et al., 2022). Therefore, special care must be taken in validating transgene expression. In our study, we observed no negative impact in this setting.

2. Optimizing the workflow for *de novo* multi-modified gm donor cells for SCNT

Due to limited success with random integration of transgenes, as our founder animals exhibited mosaic patterns or even lacked transgene expression in some cases, we opted for site-specific integration in the genome in the next step. However, this required more complex expression cassette design and the usage of recently developed plasmid technologies in the wet lab. For almost half a century, more than 37 methods have been researched in the development of plasmid constructs (LI et al., 2022b). These can be categorized into three main groups of methods: 1) single-strand overhang cloning, 2) recombining homology arms, and 3) replacing amplified inserts as mega-primers.

We opted for single-strand overhang cloning, which includes the Gibson Assembly method. As reviewed by Li et al. (2022b), this method utilizes T5 DNA exonuclease to generate 3′ -ss overhangs, Phusion DNA polymerase for gap filling, and Taq DNA ligase for ligation, facilitating the assembly of overlapping DNAs with sizes ranging from 300 to 583 kb (GIBSON et al., 2009). With an error rate lower than 1/50 DNA molecules, this technique enables genome synthesis (GIBSON et al., 2008). In Hot Fusion, vector purification becomes unnecessary due

to the absence of Taq DNA ligase ligation (FU et al., 2015). The accuracy rates for cloning junctions, multiple inserts, and RNAi stand at 90–95%, respectively. TEDA (T5 exonuclease DNA assembly) employs solely a T5 DNA exonuclease reaction (XIA et al., 2019). Gibson assembly evolves from three enzyme reactions using DNAs with 17–30 bp overlaps to a single enzyme reaction using DNAs with 9–20 bp overlaps. Nonetheless, efficiency decreases when cloning three or more inserts, and sporadic frame shift mutations arise in the coding region (ACEVEDO-ROCHA et al., 2018). As also described by Hsieh & Vaisvila (2013), this method enables the simultaneous modification of multiple nucleotides, saving both time and reagents compared to conventional mutagenesis methods. Using the technology of Gibson cloning, we successfully generated three different transgene constructs with site-specific homologous arms within a few days, which were confirmed as correct through Sanger sequencing.

A further challenge in optimizing the workflow for *de novo* generation of multi-modified donor cells for SCNT is to increase the efficiency of targeted integration into predefined genome loci and to enhance the efficiency of preselecting cells. However, it is acknowledged that achieving knock-in efficiency in primary mammalian cells is constrained. This limitation arises because the donor DNA needs to be introduced at precise timing, and homology-directed repair (HDR) is confined to particular cell cycle phases, particularly the late S/G2 phase. Additionally, HDR encounters competition from another pathway for repairing double-strand breaks, known as non-homologous end joining (NHEJ), which is often linked with unwanted insertions or deletions (BANAN, 2020). Of note, as the gm primary cells have to be used for subsequent SCNT, quality criteria of the SCNT donor cells must be maintained, such as low passage number or chromosomal stability. PKCs are recognized as ideal donor cells for SCNT because of their elevated proliferation rate and resilience to stress during transfection (RICHTER et al., 2012; BANAN, 2020).

By using gene editing tools such as the CRISPR/Cas9 system, double-strand breaks can be induced in the genome at preselected sites, increasing the probability of targeted integration of a transgene expression site. However, a significant challenge in mammalian genome editing is the occurrence of off-target events (FU et al., 2013; PATTANAYAK et al., 2013). Double-strand breaks outside the target site can happen if there are more than three mismatched nucleotides between the gRNA and the genomic DNA. This can lead to indels, inversions, or large chromosomal translocations, causing unwanted gene knockouts, genomic instability, or activation of oncogenes (CHO et al., 2014; LI et al., 2020; NAEEM et al., 2020). Strategies to prevent off-target events and enhancing the efficiency of gene integration include selecting gRNAs and Cas9 variants with a low number of potential off-targets and high cutting efficiency,

which can be predicted by design tools such as CRISPOR and TIDE (Target Identification by Deletion, a tool for efficiency improvements). Using these tools, we have successfully selected site-specific gRNA/Cas combinations to achieve cutting efficiency within the range of 48-67%. Thereby, Cas9 variants such as sniper-Cas9, which are less prone to off-target-site cutting efficiency (AU - LEE et al., 2019), were used. Continuous improvements in cutting specificity of newer generation Cas9 variants and *in silico* prediction tools are ongoing (LI et al., 2024).

With the introduction of a foreign DNA into the cell, there is the possibility of genome integration, regardless of whether it is a precisely excised expression cassette intended for integration or if it is vector backbones or plasmids used for transient expression of CRISPR/Cas9 complex products. Another strategy, aside from plasmid-based CRISPR/Cas9 delivery system, is the usage of RNPs. The use of RNPs not only shortens the timeframe for edits compared to Cas9 delivery via plasmids (NAEEM et al., 2020), but also mitigates the potential for arbitrary vector integration (KIM & KIM, 2014; NORRIS et al., 2020). Another foreign DNA that is viewed critically in gm organ donor pigs for xenotransplantation, are expression cassettes for antibiotic resistance, such as the neomycin selection cassette, required for cell preselection *in vitro* (VALERA et al., 1994). By flanking such antibiotic resistance cassettes with loxP sites for Cre recombinase-based excision, these undesired genetic elements could be removed, and this approach has been applied in several gm pig lines (RIEBLINGER et al., 2018; HUANG et al., 2020). Additional approaches have emerged to identify cells that have stably integrated the transgene expression cassette into their genome without the usage of antibiotic preselection steps, streamlining the process. Fluorescence-Activated Cell Sorting (FACS) allows for the selection of cells depending on the expression of a reporter gene within the cell or linked to antibodies binding to cell surface proteins. Such methods have been demonstrated in various models (COLOSIMO et al., 2000), and were also very successfully applied in our study. Immunofluorescence staining of FACS-sorted cells showed dual expression of hCD47 and hPD-L1, demonstrating the effectiveness of flow cytometry-based cell selection without the need for antibiotic selection. However, it is still essential to screen for correct transgene integration at the intended site for reliable expression. Our results indicate a high success rate, with 71% of analyzed cells exhibiting transgene integration and 43% positioned correctly.

Validation tools for detailed characterization of gm donor pigs for xenotransplantation

Homogeneous, robust, and reliable expression of transgenes and their correct processing in the xenograft are crucial for the success of xenotransplantation in clinical applications. Genetically modified donor pigs must undergo meticulous characterization to ensure the reliability and consistency of transgene expression.

In some studies where gm pigs for xenotransplantation were generated, transgene expression was analyzed using tissue lysates or blood analysis. However, results of such bulk sample analyses have to be interpreted with care. For instance, the transgene expression of MHCIP-diliximab pigs, in which the CD2 mAb was intended to be expressed ubiquitously under the control of a murine MHC class I promoter for use in islet transplantation, was initially examined in serum, revealing high abundance, suggesting robust ubiquitous transgene expression (SALVARIS et al., 2023). At the transcript level, the highest transcript abundance of the transgene was measured in the pancreas, followed by spleen and heart, and low levels in kidney and liver. However, in immunohistochemistry, the transgene expression pattern differed from the results at the transcript level, showing strong expression in spleen and lung, moderate expression in heart and kidney, low expression in the liver, and a strong but patchy expression in the pancreas. The islets themselves exhibited only very weak staining intensity against CD2 mAb. Mosaic-like expression patterns are common findings in gm animals, with variations not only evident among different transgenic lines but also within tissues of the same line (DEPPENMEIER et al., 2006). The findings in our study, where we identified gm pig lines with the occurrence of mosaic patterns or incorrect transgene processing, strongly recommend analyzing the transgene expression pattern also at a cellular level, especially in organs designated for transplantation purposes.

Additionally, genomic characterization is essential to ensure error-free integration of the transgene and to exclude off-target site errors. An example of incorrect transgene integration was provided by our F0 pig #12558, whose 3'UTR sequence was improperly integrated into its genome. In another study, next-generation sequencing technologies revealed the integration of transgenes occurring in multiple copies, fragments, and/or within intron regions of genes in gm pig lines used in preclinical xenotransplantation trials (HINRICHS et al., 2021). Given the potential for off-target effects by gene scissors (FU et al., 2013; PATTANAYAK et al., 2013), it is imperative to ensure that no undesired DNA fragments have been inserted. With previous tools such as PCR and Sanger sequencing, detailed knowledge of genomic modifications and allele variants is essential before applying these methods. However, since undesired incorrect modifications in the genome are, in most cases, not targeted, a comprehensive untargeted

approach has to be employed to identify these errors. Nowadays, emerging technologies such as nanopore sequencing offer the advantage of long reads, enabling the capture of changes in the transgene integration site (KEMTER et al., 2021).

A further important aspect of characterizing gm donor pigs is to confirm their transgene expression pattern in the living animal, which must be easily accessible and enable reliable information about the transgene in the target organ. This enables the animal to be kept alive for later use as a breeding or donor animal. In our study, we selected tail samples as easily accessible tissues with heterogeneous cell composition, and we demonstrated that homogenous *CAG*-promoter driven transgene expression in this tissue sample reflected very well the transgene expression patterns of internal organs and tissues. Therefore, expression analyses of such samples could serve as valuable indicators for understanding expression patterns without sacrificing the founder animal. These learnings are relevant, because re-cloning animals sacrificed for expression analysis delays the rearing of breeding animals. However, sometimes transgenes need to be expressed in a site-specific manner. In order to examine F0 pigs for the *INS*-LEA29Y transgene, some animals needed to be sacrificed, as it was expected that the expression of the transgene would be restricted to pancreatic β-cells, which would not be achievable from living pigs.

Validation of maintained cell and organ function of gm donor pigs

Expression of an exogenous gene, particularly if it is expressed in high abundance or if the transgene can activate or inhibit intracellular pathways, has the potential to negatively influence the cell or organ function of a gm animal, and – in the setting of xenotransplantation – the graft function. Recently, it was reported by Ghimire et. al (2023) that CD47 transgene expression in β-cells could have a negative effect on β-cell function. Both mouse and human islets with added or depleted CD47 expression were examined. Superior efficacy of CD47-/- islets in normalizing blood glucose levels was demonstrated in a preclinical islet transplant model. These results were replicated by blocking CD47 signaling in islets prior to transplantation or through systemic blockade in recipients post-transplantation. Furthermore, their experiments revealed that an increased CD47 expression in diabetes-prone NOD mice progressed to overt diabetes. CD47 blockade effectively delayed the onset of overt diabetes in NOD mice without impacting insulitis, suggesting that improved insulin secretion, rather than modification of inflammation, was the primary driver of glucose homeostatic benefits. These findings indicate that CD47 receptor antagonism may optimize islet transplant function by enhancing insulin secretion (GHIMIRE et al., 2023).

In our study, we demonstrated that NPI grafts exhibited similar engraftment and maturation behavior irrespective of whether they were derived from hCD47-hPD-L1-2xtg or wild-type donor pancreas. Mice from both NPI transplant groups exhibited similar abilities to achieve normoglycemia.

3. Monitoring calcium flows on porcine islet grafts to assess β-cell function

Ca^{2+} influx into β-cells is an important driver of insulin secretion (FRIDLYAND et al., 2013), and monitoring of pulses provides therefore an important readout for the maturation of NPIs. Conventional small compound Ca^{2+}-sensor dyes are difficult to use for monitoring Ca^{2+} flows in compact cell clusters both *in vitro* and *in vivo* since they are fragile, and their three-dimensional structure prevents uniform loading of all cells. Moreover, *in situ* monitoring of islet grafts depends on the steady abundance of the sensor dye.

The utilization of reporter pigs expressing GCaMP6 provides a valuable tool for studying various biological processes, owing to the strong and ubiquitous expression driven by the *CAG* promoter. This ubiquitous expression allows for the visualization of calcium dynamics not only in pancreatic islet cells but also in other cell types, including cardiomyocytes. The ability to monitor calcium signaling in different cell types opens up new avenues for research, enabling a deeper understanding of physiological and pathological processes.

The *in vitro* experiments conducted with isolated NPIs from the GCaMP6 reporter pigs demonstrated a glucose-induced calcium response, as evidenced by an increase in fluorescence intensity in cultured NPIs upon glucose stimulation. Additionally, the response to potassium chloride challenge further validated the functionality of the GCaMP6 reporter in detecting changes in intracellular calcium levels. However, many β-cells in the *in vitro* cultured NPIs exhibited spontaneous Ca^{2+} flow, indicating that these cells were still not fully functionally matured. Furthermore, technical considerations for imaging Ca^{2+} dynamics in β-cells need to be addressed. For instance, the lack of calcium reporter response observed in NPIs engrafted in the ACE upon glucose challenge *in vivo* could be attributed to the use of isoflurane anesthesia. It is described that isoflurane has an inhibitory effect on intracellular ATP increase, which is essential for inducing Ca^{2+} influx into β-cells upon high glucose challenge in the insulin secretion signaling loop (TANAKA et al., 2009). In consequence, alternatives such as intravenous anesthetics must be used for imaging Ca^{2+} dynamics in β-cells.

Ex vivo experiments conducted with NPI grafts in the ACE of the mouse demonstrated multiple pulsatile calcium reporter responses in numerous cells upon glucose stimulus, indicating that β-cells in the NPI graft were functionally mature. These results highlight the potential of this new reporter pig model for studying dynamic calcium signaling processes under controlled experimental conditions. Additionally, this reporter pig line with ubiquitous expression of GCaMP6 offers a versatile tool for studying calcium signaling dynamics in various cell types, including pancreatic β-cells and cardiomyocytes.

4. Final conclusion and outlook

The field of genetic modifications in porcine genomes has undergone significant growth since the introduction of somatic cell nuclear transfer. The use of genome editing techniques has revolutionized the process, allowing for the creation of novel pig lines with multiple knockouts in a single step. Additionally, there are now various methods available to construct arrays of xenoprotective transgenes with efficiency and reliable expression. Although progress has been made, the ideal genotype for xenopigs is still undefined. It is possible that the most appropriate combination may differ depending on the targeted organ. The promising outcomes so far inspire confidence in the future of xeno-organ transplantation. With each advancement, the possibility of successful xenotransplantation becomes increasingly likely.

VII. SUMMARY

The efficient production of genetically modified (gm) donor pig lines for application in xenotransplantation necessitates a detailed design of transgenic approaches and comprehensive evaluations. State-of-the-art tools for designing, generating, and characterizing multi-gm animals can be used to develop optimal donor pigs tailored for xenotransplantation, fulfilling the prerequisites for advancing towards clinical application.

This study employed different strategies in two consecutive approaches for the *de novo* generation of multi-gm xenoislet donor pig lines. The genetic modifications entailed integrating transgene cassettes containing three immunomodulatory molecules. The *INS* promoter was used to selectively express LEA29Y on β-cells, while the remaining transgenes were placed under the control of the strong ubiquitous *CAG* promoter. Simultaneously, gene expression of *GGTA1* and either *CCL2* or *B2M* needed to be depleted. Additionally, a novel Ca^{2+} sensor reporter pig was developed, facilitating monitoring of β-cell function in islet xenografts. The study also assessed the impact of expression cassette components, such as chromatin opening elements, which hold promise for enhancing accessibility for transcription of the integrated cassette into the genome, or 3' long UTR sequences for intracellular protein processing. Furthermore, gene combineering, gene stacking, and gene editing strategies were applied. Subsequently, a comprehensive characterization was focused on molecular, cellular, histological, and physiological levels.

The initial strategy entailed employing a 'bulk cell approach' to generate 5-fold gm (*GGTA1*/*CCL2)*-2xKO, [(*INS*-LEA29Y, hPD-L1), hCD47]-3xtg pigs *de novo*. This involved using two linearized transgene expression cassettes: one for LEA29Y and hPD-L1 expression, and another for hCD47 expression. Both cassettes were equipped with the chromatin opening element *A2UCOE* upstream of the promoters, while the cDNA of hCD47 was followed by a 3' long UTR. CRISPR/Cas9 gene scissors were applied to target both *GGTA1* and *CCL2* genes for gene depletion and to facilitate site-specific transgene integration into the genome. Subsequently, an antibiotic-free cell selection process was adopted, based on flow cytometry-based sorting of cells expressing the immunomodulatory transgenes hPD-L1 and hCD47 on their cell surface, while lacking α-Gal sugar epitopes. These cells were used for somatic cell nuclear transfer (SCNT) and the resulting embryos were transferred into five foster sows, yielding four pregnancies and 13 F0 pigs. Upon detailed characterization of these 13 pig lines, it was observed that all were (*GGTA1*, *CCL2)*-2xKO, however, they differed in the genome integration pattern of the expression cassettes and the transgene expression pattern. In

three pig lines, both hPD-L1 and hCD47 were expressed homogeneously and ubiquitously on the cell surface. However, although expressed in the majority of their cells, the other piglets displayed varying degrees of mosaic pattern expression, indicating that the *A2UCOE* element was not sufficient to prevent gene silencing. Another important finding was that the genome integration site may play a crucial role in porcine *INS* promoter-driven β-cell-specific expression, as the LEA29Y transgene was not expressed across most lines, while the *CAG* promoter worked well at the same sites, resulting in intense hPD-L1 transgene expression. This study further evaluated the correctness of full integration of expression cassettes, correct intracellular transgene processing, and evidence of maintained graft functionality despite the multi-genetic modifications. Based on the pitfalls identified in the first approach, we developed a second strategy. This entailed employing gene stacking and targeted knock-in methods to integrate separate expression cassettes into specific gene loci. These loci were either nearby the *INS*-LEA29Y transgene integration site on *SSC6* of a preexisting *INS*-LEA29Y transgenic line or in exon 7 and exon 10 of the *GGTA1* gene. Additional modifications included employing circular plasmids instead of linearized ones, flanking of expression cassettes with homologous arms containing gRNA recognition sites, using ribonucleoprotein complexes instead of a plasmid-based CRISPR/Cas9 system, and validating correct targeted integration through processing, screening, and selection of suitable single-cell clones, subsequently used for SCNT. In contrast to the initial approach, all 13 SCNT offspring from the second strategy exhibited a homogeneous and ubiquitous transgene expression pattern. Gene stacking near the preexisting *INS*-LEA29Y transgene integration site did not induce genomic instability and led to robust co-expression of LEA29Y and hPD-L1.

Another key objective of this study was the generation and characterization of a novel Ca^{2+} sensor reporter pig. Robust and ubiquitous transgene expression of GCaMP6 was attained by integrating the *CAG*-GCaMP6 expression cassette into the safe harbor gene locus *Rosa26*. *In vitro* experiments with isolated NPIs from reporter pigs and *ex vivo* experiments with NPI transplants in mice showed a glucose-induced calcium response, indicating functional maturity of β-cells. These findings highlight the potential of this reporter pig model for invastigating dynamic calcium signaling processes under controlled conditions. Moreover, this tool offers versatility for studying calcium signaling dynamics across diverse cell types, such as pancreatic β-cells and cardiomyocytes.

In summary, we have successfully developed novel genetically modified pigs, which hold promise in advancing the efficacy and safety in the application of porcine islet xenotransplantation as a viable therapeutic option for individuals with type 1 diabetes.

VIII. ZUSAMMENFASSUNG

Die effiziente Generierung von genetisch modifizierten (gm) Spenderschweinelinien zur Verwendung in der Xenotransplantation erfordert eine detaillierte Planung und umfassende Evaluierung der gentechnischen Methoden. Durch den Einsatz modernster Techniken für das Design, die Erzeugung und die Charakterisierung von mehrfach gm Tieren können optimale Spenderschweine für die Xenotransplantation erzeugt werden, die den Anforderungen für die klinische Anwendung entsprechen.

In dieser Studie wurden unterschiedliche Strategien zur *de novo* Generierung von mehrfach gm Spenderschweinelinien für die Inselzelltransplantation verwendet. Die genetischen Modifikationen umfassten die Integration von Transgenkassetten mit drei immunmodulatorischen Molekülen. Dabei sollte LEA29Y über den *INS*-Promotor selektiv auf Betazellen exprimiert werden, während die anderen Transgene unter der Kontrolle des starken ubiquitären *CAG*-Promotors stehen. Parallel dazu sollte die Genexpression von zwei Genen, *GGTA1* und entweder *CCL2* oder *B2M*, gehemmt werden. Darüber hinaus wurde ein neues Calciumsensor-Reporterschwein generiert, das das Monitoring der Betazellfunktion in transplantierten Pankreasinseln erleichtert. Infolgedessen wurde die Auswirkungen von Expressionskassettenelementen, wie chromatinöffnenden Elementen, die die Zugänglichkeit für die Transkription der integrierten Kassette in das Genom verbessern können, oder 3'long UTR-Sequenzen, für optimierte intrazelluläre Proteinverarbeitung, untersucht. Außerdem wurden verschiedene Genkombinationen, Gen-Stacking und Gen-Editing Strategien angewendet. Anschließend erfolgte eine umfassende Charakterisierung auf molekularer, zellulärer, histologischer und physiologischer Ebene.

Die erste Strategie umfasste den Einsatz eines "Bulk-Zellansatz" für die *de novo* Generierung von fünffach genetisch modifizierten (*GGTA1/CCL2)*-2xKO, [(*INS*-LEA29Y, hPD-L1), hCD47]-3xtg Schweinen. Hierfür wurden zwei linearisierte Transgenexpressionskassetten eingesetzt: eine Kombinationskassette für die LEA29Y- und hPD-L1-Expression sowie eine weitere für die hCD47-Expression. In beiden Kassetten wurde stromaufwärts des Promotors das chromatinöffnende Element *A2UCOE* eingefügt. Auf die cDNA von hCD47 folgte eine 3'long UTR. Zusätzlich wurde eine CRISPR/Cas9-Genschere verwendet, um gezielt die Gene *GGTA1* und *CCL2* auszuschalten und die ortsspezifische Integration des Transgens in das Genom zu fördern. Anschließend wurde ein antibiotikafreies Zellselektionsverfahren angewendet, das auf einer durchflusszytometrischen Sortierung von Zellen mit einer

Zelloberflächenexpression der immunmodulatorischen Transgene hPD-L1 und hCD47 bei gleichzeitigem Fehlen von α-Gal-Epitopen, basierte. Diese Zellen wurden für den somatischen Zellkerntransfer und den Transfer der Embryonen in fünf Empfängersauen verwendet, was zu vier Trächtigkeiten und 13 F0-Schweinen führte. Die detaillierte Charakterisierung dieser 13 Schweinelinien ergab, dass alle Schweine (*GGTA1, CCL2)*-2xKO waren, sich aber im Genomintegration der Expressionskassetten und im Expressionsmuster der Transgene unterschieden. Bei drei Schweinelinien wurde eine homogene, ubiquitäre Expression von hPD-L1 und hCD47 auf der Zellmembran festgestellt. Die übrigen Ferkel wiesen, obwohl die Transgene auf der Mehrzahl der Zellen exprimiert wurden, einen unterschiedlichen Grad an Mosaikmustern auf. Dies deutet darauf hin, dass das *A2UCOE*-Element nicht ausreicht, um Gen-Silencing zu vermeiden. Eine weitere wichtige Erkenntnis ist, dass die Genomintegrationsstelle des *INS*-Promoters für die betazellspezifische Expression von großer Bedeutung sein könnte, da das LEA29Y-Transgen in fast keiner Linie exprimiert wurde, obwohl der *CAG*-Promotor an denselben Stellen gut funktionierte und zu einer starken hPD-L1-Transgenexpression führte. Zusätzlich wurden weitere wichtige Aspekte untersucht, wie die korrekte Integration der vollständigen Expressionskassetten, die korrekte intrazelluläre Verarbeitung des Transgens und der Nachweis, dass die Transplantatfunktionalität trotz mehrfacher genetischer Modifikationen erhalten bleibt.

Um die Schwierigkeiten des ersten Ansatzes zu umgehen, haben wir eine zweite Strategie entwickelt. Hierbei haben wir das Verfahren des "Gen-Stacking" verwendet und gezielte Knock-in-Methoden angewendet. Dabei wurden separate Expressionskassetten an spezifischen Genorten integriert. Zum einen in der Nähe der Integrationsstelle des *INS*-LEA29Y-Transgens im *SSC6*-Lokus einer bereits vorhandenen *INS*-LEA29Y-Linie, zum anderen in Exon 7 und Exon 10 des *GGTA1*-Gens. Weitere Anpassungen waren die Verwendung von zirkulären anstelle von linearisierten Plasmiden und die Flankierung der Expressionskassetten mit homologen Armen mit gRNA-Erkennungsstellen. Außerdem wurde anstelle des plasmidbasierten CRISPR/Cas9-Systems die Verwendung von Ribonukleoproteinkomplexen gewählt und die korrekte Transgenintegration durch Screeningverfahren validiert. Geeignete Einzelzellklone wurden ausgewählt und für den somatischen Zellkerntransfer verwendet. Im Gegensatz zum ersten Ansatz wiesen alle 13 Nachkommen des zweiten Ansatzes ein homogenes und ubiquitäres Transgenexpressionsmuster auf. Das Gene-Stacking in der Nähe der bereits vorhandenen *INS*-LEA29Y-Transgenintegrationsstelle führte nicht zu genomischer Instabilität und ergab eine robuste Koexpression von LEA29Y und hPD-L1.

Ein weiteres Ziel dieser Arbeit war die Generierung und Charakterisierung eines neuen Calciumsensor-Reporterschweins. Eine robuste ubiquitäre Transgenexpression von GCaMP6 wurde erreicht, indem die *CAG*-GCaMP6-Expressionskassette in den Safe-Harbor-Genlokus *Rosa26* integriert wurde. *In-vitro* Experimente mit isolierten NPIs von Reporterschweinen, sowie *ex vivo* Experimente mit NPI-Transplantaten in Mäusen zeigten eine glukoseinduzierte Calciumreaktion, was auf eine funktionelle Reife der β-Zellen hinweist. Diese Ergebnisse zeigen das Potenzial dieses Reporter-Schwein-Modells für die Untersuchung dynamischer Calciumsignalprozesse unter kontrollierten Bedingungen. Außerdem bietet die ubiquitäre Expression ein vielseitiges Instrument zur Untersuchung der Calciumsignaldynamik in verschiedenen Zelltypen, einschließlich der β-Zellen des Pankreas und Kardiomyozyten.

Zusammenfassend ist festzuhalten, dass wir erfolgreich neue genetisch veränderte Schweine generiert haben, die hoffentlich dazu beitragen werden, den Weg für eine verbesserte Wirksamkeit und Sicherheit bei der Anwendung der Xenotransplantation von Pankreasinseln als praktikable Therapieoption für Menschen mit Typ-1-Diabetes zu ebnen.

IX. INDEX OF FIGURES

X. INDEX OF TABLES

XI. REFERENCES

Acevedo-Rocha CG, Gamble CG, Lonsdale R, Li A, Nett N, Hoebenreich S, Lingnau JB, Wirtz C, Fares C, Hinrichs H, Deege A, Mulholland AJ, Nov Y, Leys D, McLean KJ, Munro AW, Reetz MT. P450-Catalyzed Regio- and Diastereoselective Steroid Hydroxylation: Efficient Directed Evolution Enabled by Mutability Landscaping. ACS Catalysis 2018; 8: 3395-410.

Aigner B, Klymiuk N, Wolf E. Transgenic pigs for xenotransplantation: selection of promoter sequences for reliable transgene expression. Curr Opin Organ Transplant 2010; 15: 201-6.

Akerboom J, Rivera JD, Guilbe MM, Malave EC, Hernandez HH, Tian L, Hires SA, Marvin JS, Looger LL, Schreiter ER. Crystal structures of the GCaMP calcium sensor reveal the mechanism of fluorescence signal change and aid rational design. J Biol Chem 2009; 284: 6455-64.

Algorri JF, Ochoa M, Roldan-Varona P, Rodriguez-Cobo L, Lopez-Higuera JM. Light Technology for Efficient and Effective Photodynamic Therapy: A Critical Review. Cancers (Basel) 2021; 13

Amarasinghe SL, Su S, Dong X, Zappia L, Ritchie ME, Gouil Q. Opportunities and challenges in long-read sequencing data analysis. Genome Biology 2020; 21: 30.

Au - Lee J, Au - Jung M-h, Au - Jeong E, Au - Lee JK. Using Sniper-Cas9 to Minimize Off-target Effects of CRISPR-Cas9 Without the Loss of On-target Activity Via Directed Evolution. JoVE 2019: e59202.

Azzi J, Alegre ML. Outstanding questions in transplantation: An introduction to this minireview series. Am J Transplant 2019; 19: 2149-50.

Banan M. Recent advances in CRISPR/Cas9-mediated knock-ins in mammalian cells. Journal of Biotechnology 2020; 308: 1-9.

Bartolomé A. Stem Cell-Derived beta Cells: A Versatile Research Platform to Interrogate the Genetic Basis of beta Cell Dysfunction. Int J Mol Sci 2022; 23

Berkovits BD, Mayr C. Alternative 3' UTRs act as scaffolds to regulate membrane protein localization. Nature 2015; 522: 363-7.

Bestor TH. Gene silencing as a threat to the success of gene therapy. J Clin Invest 2000; 105: 409-11.

Blixt O, Kumagai-Braesch M, Tibell A, Groth CG, Holgersson J. Anticarbohydrate Antibody Repertoires in Patients Transplanted with Fetal Pig Islets Revealed by Glycan Arrays. American Journal of Transplantation 2009; 9: 83-90.

Bornstein SR, Ludwig B, Steenblock C. Progress in islet transplantation is more important than ever. Nat Rev Endocrinol 2022; 18: 389-90.

Bottino R, Wijkstrom M, van der Windt DJ, Hara H, Ezzelarab M, Murase N, Bertera S, He J, Phelps C, Ayares D, Cooper DKC, Trucco M. Pig-to-Monkey Islet Xenotransplantation Using Multi-Transgenic Pigs. American Journal of Transplantation 2014; 14: 2275-87.

Bottino R, Trucco M. Use of genetically-engineered pig donors in islet transplantation. World J Transplant 2015; 5: 243-50.

Brunetti D, Perota A, Lagutina I, Colleoni S, Duchi R, Calabrese F, Seveso M, Cozzi E, Lazzari G, Lucchini F, Galli C. Transgene expression of green fluorescent protein and germ line transmission in cloned pigs derived from in vitro transfected adult fibroblasts. Cloning Stem Cells 2008; 10: 409-19.

Buerck LW, Schuster M, Oduncu FS, Baehr A, Mayr T, Guethoff S, Abicht J, Reichart B, Klymiuk N, Wolf E, Seissler J. LEA29Y expression in transgenic neonatal porcine islet-like cluster promotes long-lasting xenograft survival in humanized mice without immunosuppressive therapy. Sci Rep 2017; 7: 3572.

Buermann A, Petkov S, Petersen B, Hein R, Lucas-Hahn A, Baars W, Brinkmann A, Niemann H, Schwinzer R. Pigs expressing the human inhibitory ligand PD-L1 (CD 274) provide a new source of xenogeneic cells and tissues with low immunogenic properties. Xenotransplantation 2018; 25: e12387.

Byrne G, Ahmad-Villiers S, Du Z, McGregor C. B4GALNT2 and xenotransplantation: A newly appreciated xenogeneic antigen. Xenotransplantation 2018; 25: e12394.

Byrne GW, McGregor CGA, Breimer ME. Recent investigations into pig antigen and anti-pig antibody expression. Int J Surg 2015; 23: 223-8.

Cabrera A, Edelstein HI, Glykofrydis F, Love KS, Palacios S, Tycko J, Zhang M, Lensch S, Shields CE, Livingston M, Weiss R, Zhao H, Haynes KA, Morsut L, Chen YY, Khalil AS, Wong WW, Collins JJ, Rosser SJ, Polizzi K, Elowitz MB, Fussenegger M, Hilton IB, Leonard JN, Bintu L, Galloway KE, Deans TL. The sound of silence: Transgene silencing in mammalian cell engineering. Cell Syst 2022; 13: 950-73.

Cadili A, Kneteman N. The role of macrophages in xenograft rejection. Transplant Proc 2008; 40: 3289-93.

Cardona K, Korbutt GS, Milas Z, Lyon J, Cano J, Jiang W, Bello-Laborn H, Hacquoil B, Strobert E, Gangappa S, Weber CJ, Pearson TC, Rajotte RV, Larsen CP. Long-term survival of neonatal porcine islets in nonhuman primates by targeting costimulation pathways. Nat Med 2006; 12: 304-6.

Cayabyab F, Nih LR, Yoshihara E. Advances in Pancreatic Islet Transplantation Sites for the Treatment of Diabetes. Front Endocrinol (Lausanne) 2021; 12: 732431.

Chen ZY, Riu E, He CY, Xu H, Kay MA. Silencing of episomal transgene expression in liver by plasmid bacterial backbone DNA is independent of CpG methylation. Mol Ther 2008; 16: 548-56.

Cho SW, Kim S, Kim Y, Kweon J, Kim HS, Bae S, Kim JS. Analysis of off-target effects of

CRISPR/Cas-derived RNA-guided endonucleases and nickases. Genome Res 2014; 24: 132-41.

Cocha G, Tedesco V, D'Attellis C, Amorena C. An algorithm mimicking pancreas pulsatile behavior improves artificial pancreas performance. Int J Artif Organs 2021; 44: 756-64.

Colosimo A, Goncz KK, Holmes AR, Kunzelmann K, Novelli G, Malone RW, Bennett MJ, Gruenert DC. Transfer and expression of foreign genes in mammalian cells. Biotechniques 2000; 29: 314-8, 20-2, 24 passim.

Contreras JL, Eckstein C, Smyth CA, Bilbao G, Vilatoba M, Ringland SE, Young C, Thompson JA, Fernandez JA, Griffin JH, Eckhoff DE. Activated Protein C Preserves Functional Islet Mass After Intraportal Transplantation: A Novel Link Between Endothelial Cell Activation, Thrombosis, Inflammation, and Islet Cell Death. Diabetes 2004; 53: 2804-14.

Cowan PJ. Chapter 9 - Transgenic pigs for islet xenotransplantation. In: Pancreas and Beta Cell Replacement. Hawthorne WJ, ed.: Academic Press 2022: 153-66.

Cozzi E, White DJG. The generation of transgenic pigs as potential organ donors for humans. Nature medicine 1995; 1: 964-6.

Deppenmeier S, Bock O, Mengel M, Niemann H, Kues W, Lemme E, Wirth D, Wonigeit K, Kreipe H. Health status of transgenic pigs expressing the human complement regulatory protein CD59. Xenotransplantation 2006; 13: 345-56.

Dermawan D, Kenichi Purbayanto MA. An overview of advancements in closed-loop artificial pancreas system. Heliyon 2022; 8: e11648.

Diamond LE, Quinn CM, Martin MJ, Lawson J, Platt JL, Logan JS. A human CD46 transgenic pig model system for the study of discordant xenotransplantation. Transplantation 2001; 71: 132-42.

Dmochewitz M, Wolf E. Genetic engineering of pigs for the creation of translational models of

human pathologies. Animal Frontiers 2015; 5: 50-6.

Dovi KS, Bajinka O, Conteh I. Evidence and possible mechanisms of probiotics in the management of type 1 diabetes mellitus. J Diabetes Metab Disord 2022; 21: 1081-94.

Dwyer KM, Mysore TB, Crikis S, Robson SC, Nandurkar H, Cowan PJ, D'Apice AJ. The transgenic expression of human CD39 on murine islets inhibits clotting of human blood. Transplantation 2006; 82: 428-32.

Ehrnfelt C, Kumagai-Braesch M, Uzunel M, Holgersson J. Adult porcine islets produce MCP-1 and recruit human monocytes in vitro. Xenotransplantation 2004; 11: 184-94.

Eisenbarth SC. Dendritic cell subsets in T cell programming: location dictates function. Nat Rev Immunol 2019; 19: 89-103.

Eisenson DL, Hisadome Y, Santillan MR, Yamada K. Progress in islet xenotransplantation: Immunologic barriers, advances in gene editing, and tolerance induction strategies for xenogeneic islets in pig-to-primate transplantation. Front Transplant 2022; 1

El-Ouaghlidi A, Jahr H, Pfeiffer G, Hering BJ, Brandhorst D, Brandhorst H, Federlin K, Bretzel RG. Cytokine mRNA expression in peripheral blood cells of immunosuppressed human islet transplant recipients. Journal of Molecular Medicine 1999; 77: 115-7.

Estrada JL, Martens G, Li P, Adams A, Newell KA, Ford ML, Butler JR, Sidner R, Tector M, Tector J. Evaluation of human and non-human primate antibody binding to pig cells lacking GGTA1/CMAH/beta4GalNT2 genes. Xenotransplantation 2015; 22: 194-202.

Feng H, Li T, Du J, Xia Q, Wang L, Chen S, Zhu L, Pan D, Wang Y, Chen G. Both Natural and Induced Anti-Sda Antibodies Play Important Roles in GTKO Pig-to-Rhesus Monkey Xenotransplantation. Front Immunol 2022; 13: 849711.

Fischer K, Kraner-Scheiber S, Petersen B, Rieblinger B, Buermann A, Flisikowska T, Flisikowski K, Christan S, Edlinger M, Baars W, Kurome M, Zakhartchenko V, Kessler B,

Plotzki E, Szczerbal I, Switonski M, Denner J, Wolf E, Schwinzer R, Niemann H, Kind A, Schnieke A. Efficient production of multi-modified pigs for xenotransplantation by 'combineering', gene stacking and gene editing. Sci Rep 2016; 6: 29081.

Fischer K, Kind A, Schnieke A. Assembling multiple xenoprotective transgenes in pigs. Xenotransplantation 2018; 25: e12431.

Fodor WL, Williams BL, Matis LA, Madri JA, Rollins SA, Knight JW, Velander W, Squinto SP. Expression of a functional human complement inhibitor in a transgenic pig as a model for the prevention of xenogeneic hyperacute organ rejection. Proceedings of the National Academy of Sciences 1994; 91: 11153-7.

Forte P, Lilienfeld BG, Baumann BC, Seebach JD. Human NK cytotoxicity against porcine cells is triggered by NKp44 and NKG2D. J Immunol 2005; 175: 5463-70.

Fox A, Mountford J, Braakhuis A, Harrison LC. Innate and adaptive immune responses to nonvascular xenografts: evidence that macrophages are direct effectors of xenograft rejection. J Immunol 2001; 166: 2133-40.

Fridlyand LE, Jacobson DA, Philipson LH. Ion channels and regulation of insulin secretion in human beta-cells: a computational systems analysis. Islets 2013; 5: 1-15.

Fu C, Donovan WP, Shikapwashya-Hasser O, Ye X, Cole RH. Hot Fusion: An Efficient Method to Clone Multiple DNA Fragments as Well as Inverted Repeats without Ligase. PLoS One 2015; 9: e115318.

Fu Y, Foden JA, Khayter C, Maeder ML, Reyon D, Joung JK, Sander JD. High-frequency off-target mutagenesis induced by CRISPR-Cas nucleases in human cells. Nature Biotechnology 2013; 31: 822-6.

Fuchs J, Hovorka R. Benefits and Challenges of Current Closed-Loop Technologies in Children and Young People With Type 1 Diabetes. Front Pediatr 2021; 9: 679484.

Galili U. Anti-Gal: an abundant human natural antibody of multiple pathogeneses and clinical benefits. Immunology 2013; 140: 1-11.

Garrick D, Fiering S, Martin DI, Whitelaw E. Repeat-induced gene silencing in mammals. Nat Genet 1998; 18: 56-9.

Geller A, Yan J. The Role of Membrane Bound Complement Regulatory Proteins in Tumor Development and Cancer Immunotherapy. Front Immunol 2019; 10: 1074.

Ghimire K, Kale A, Li J, Julovi SM, O'Connell P, Grey ST, Hawthorne WJ, Gunton JE, Rogers NM. A metabolic role for CD47 in pancreatic β cell insulin secretion and islet transplant outcomes. Sci Transl Med 2023; 15: eadd2387.

Gibson DG, Benders GA, Andrews-Pfannkoch C, Denisova EA, Baden-Tillson H, Zaveri J, Stockwell TB, Brownley A, Thomas DW, Algire MA, Merryman C, Young L, Noskov VN, Glass JI, Venter JC, Hutchison CA, Smith HO. Complete Chemical Synthesis, Assembly, and Cloning of a Mycoplasma genitalium Genome. Science 2008; 319: 1215-20.

Gibson DG, Young L, Chuang R-Y, Venter JC, Hutchison CA, Smith HO. Enzymatic assembly of DNA molecules up to several hundred kilobases. Nature Methods 2009; 6: 343-5.

Giraldo P, Montoliu L. Size matters: use of YACs, BACs and PACs in transgenic animals. Transgenic Res 2001; 10: 83-103.

Gitik M, Liraz-Zaltsman S, Oldenborg PA, Reichert F, Rotshenker S. Myelin down-regulates myelin phagocytosis by microglia and macrophages through interactions between CD47 on myelin and SIRPalpha (signal regulatory protein-alpha) on phagocytes. J Neuroinflammation 2011; 8: 24.

Goto M, Johansson H, Maeda A, Elgue G, Korsgren O, Nilsson B. Low molecular weight dextran sulfate prevents the instant blood-mediated inflammatory reaction induced by adult porcine islets. Transplantation 2004; 77: 741-7.

Greenwald AG, Jin R, Waddell TK. Galectin-3-mediated xenoactivation of human monocytes. Transplantation 2009; 87: 44-51.

Gregory GA, Robinson TIG, Linklater SE, Wang F, Colagiuri S, de Beaufort C, Donaghue KC, Harding JL, Wander PL, Zhang X, Li X, Karuranga S, Chen H, Sun H, Xie Y, Oram R, Magliano DJ, Zhou Z, Jenkins AJ, Ma RCW, Magliano DJ, Maniam J, Orchard TJ, Rai P, Ogle GD. Global incidence, prevalence, and mortality of type 1 diabetes in 2021 with projection to 2040: a modelling study. The Lancet Diabetes & Endocrinology 2022; 10: 741-60.

Griesemer A, Yamada K, Sykes M. Xenotransplantation: immunological hurdles and progress toward tolerance. Immunol Rev 2014; 258: 241-58.

Groth CG, Korsgren O, Tibell A, Tollemar J, Möller E, Bolinder J, Östman J, Reinholt FP, Hellerström C, Andersson A. Transplantation of porcine fetal pancreas to diabetic patients. The Lancet 1994; 344: 1402-4.

Hara H, Long C, Lin YJ, Tai HC, Ezzelarab M, Ayares D, Cooper DK. In vitro investigation of pig cells for resistance to human antibody-mediated rejection. Transpl Int 2008; 21: 1163-74.

Hara H, Witt W, Crossley T, Long C, Isse K, Fan L, Phelps CJ, Ayares D, Cooper DK, Dai Y, Starzl TE. Human dominant-negative class II transactivator transgenic pigs - effect on the human anti-pig T-cell immune response and immune status. Immunology 2013; 140: 39-46.

Hawthorne WJ, Salvaris EJ, Phillips P, Hawkes J, Liuwantara D, Burns H, Barlow H, Stewart AB, Peirce SB, Hu M, Lew AM, Robson SC, Nottle MB, D'Apice AJ, O'Connell PJ, Cowan PJ. Control of IBMIR in neonatal porcine islet xenotransplantation in baboons. Am J Transplant 2014; 14: 1300-9.

He J, Yang Q, Chang LJ. Dynamic DNA methylation and histone modifications contribute to lentiviral transgene silencing in murine embryonic carcinoma cells. J Virol 2005; 79: 13497-508.

Hein R, Sake HJ, Pokoyski C, Hundrieser J, Brinkmann A, Baars W, Nowak-Imialek M, Lucas-

Hahn A, Figueiredo C, Schuberth HJ, Niemann H, Petersen B, Schwinzer R. Triple (GGTA1, CMAH, B2M) modified pigs expressing an SLA class I(low) phenotype-Effects on immune status and susceptibility to human immune responses. Am J Transplant 2020; 20: 988-98.

Hering BJ, Wijkstrom M, Graham ML, Hardstedt M, Aasheim TC, Jie T, Ansite JD, Nakano M, Cheng J, Li W, Moran K, Christians U, Finnegan C, Mills CD, Sutherland DE, Bansal-Pakala P, Murtaugh MP, Kirchhof N, Schuurman HJ. Prolonged diabetes reversal after intraportal xenotransplantation of wild-type porcine islets in immunosuppressed nonhuman primates. Nat Med 2006; 12: 301-3.

Hinrichs A, Riedel EO, Klymiuk N, Blutke A, Kemter E, Langin M, Dahlhoff M, Kessler B, Kurome M, Zakhartchenko V, Jemiller EM, Ayares D, Bidlingmaier M, Flenkenthaler F, Hrabe de Angelis M, Arnold GJ, Reichart B, Frohlich T, Wolf E. Growth hormone receptor knockout to reduce the size of donor pigs for preclinical xenotransplantation studies. Xenotransplantation 2021; 28: e12664.

Hogrebe NJ, Ishahak M, Millman JR. Developments in stem cell-derived islet replacement therapy for treating type 1 diabetes. Cell Stem Cell 2023; 30: 530-48.

Hosny N, Matson AW, Kumbha R, Steinhoff M, Sushil Rao J, El-Abaseri TB, Sabek NA, Mahmoud MA, Hering BJ, Burlak C. 3'UTR enhances hCD47 cell surface expression, self-signal function, and reduces ER stress in porcine fibroblasts. Xenotransplantation 2021; 28: e12641.

Hsieh PC, Vaisvila R. Protein engineering: single or multiple site-directed mutagenesis. Methods Mol Biol 2013; 978: 173-86.

Hsu CC, Li HP, Hung YH, Leu YW, Wu WH, Wang FS, Lee KD, Chang PJ, Wu CS, Lu YJ, Huang TH, Chang YS, Hsiao SH. Targeted methylation of CMV and E1A viral promoters. Biochem Biophys Res Commun 2010; 402: 228-34.

Hu M, Hawthorne WJ, Yi S, O'Connell PJ. Cellular Immune Responses in Islet Xenograft Rejection. Front Immunol 2022; 13: 893985.

Huai G, Qi P, Yang H, Wang Y. Characteristics of alpha-Gal epitope, anti-Gal antibody, alpha1,3 galactosyltransferase and its clinical exploitation (Review). Int J Mol Med 2016; 37: 11-20.

Huang D, Wang Y, Hawthorne WJ, Hu M, Hawkes J, Burns H, Davies S, Gao F, Chew YV, Yi S, O'Connell PJ. Ex vivo-expanded baboon CD39 + regulatory T cells prevent rejection of porcine islet xenografts in NOD-SCID IL-2rgamma(-/-) mice reconstituted with baboon peripheral blood mononuclear cells. Xenotransplantation 2017; 24

Huang J, Wang A, Huang C, Sun Y, Song B, Zhou R, Li L. Generation of Marker-Free pbd-2 Knock-in Pigs Using the CRISPR/Cas9 and Cre/loxP Systems. Genes (Basel) 2020; 11

Ide K, Wang H, Tahara H, Liu J, Wang X, Asahara T, Sykes M, Yang Y, Ohdan H. Role for CD47-SIRPα signaling in xenograft rejection by macrophages. Proceedings of the National Academy of Sciences 2007; 104: 5062-6.

Ishiyama K, Rawson J, Omori K, Mullen Y. Liver natural killer cells play a role in the destruction of islets after intraportal transplantation. Transplantation 2011; 91: 952-60.

Iwase H, Ekser B, Hara H, Phelps C, Ayares D, Cooper DK, Ezzelarab MB. Regulation of human platelet aggregation by genetically modified pig endothelial cells and thrombin inhibition. Xenotransplantation 2014; 21: 72-83.

Jeong Y-H, Park C-H, Jang G-H, Jeong Y-I, Hwang I-S, Jeong Y-w, Kim Y-K, Shin T, Kim N-H, Hyun S-H, Jeung E-B, Hwang W-S. Production of Multiple Transgenic Yucatan Miniature Pigs Expressing Human Complement Regulatory Factors, Human CD55, CD59, and H-Transferase Genes. PLoS One 2013; 8: e63241.

Jin R, Greenwald A, Peterson MD, Waddell TK. Human monocytes recognize porcine endothelium via the interaction of galectin 3 and alpha-GAL. J Immunol 2006; 177: 1289-95.

Johansson H, Lukinius A, Moberg L, Lundgren T, Berne C, Foss A, Felldin M, Källen R, Salmela K, Tibell A, Tufveson G, Ekdahl KN, Elgue G, Korsgren O, Nilsson B. Tissue Factor

Produced by the Endocrine Cells of the Islets of Langerhans Is Associated With a Negative Outcome of Clinical Islet Transplantation. Diabetes 2005; 54(6): 1755-62.

Kale A, Rogers NM. No Time to Die-How Islets Meet Their Demise in Transplantation. Cells 2023; 12

Kanak M, Saravanan P, Levy M. Inflammatory response and its impact on outcome of islet transplantation. CellR4 2019: e2739.

Kanak MA, Takita M, Kunnathodi F, Lawrence MC, Levy MF, Naziruddin B. Inflammatory response in islet transplantation. Int J Endocrinol 2014; 2014: 451035.

Kang HK, Wang S, Dangi A, Zhang X, Singh A, Zhang L, Rosati JM, Suarez-Pinzon W, Deng X, Chen X, Thorp EB, Hering BJ, Miller SD, Luo X. Differential Role of B Cells and IL-17 Versus IFN-gamma During Early and Late Rejection of Pig Islet Xenografts in Mice. Transplantation 2017; 101: 1801-10.

Karahan GE, Claas FH, Heidt S. B Cell Immunity in Solid Organ Transplantation. Front Immunol 2017; 7: 686.

Kemter E, Lieke T, Kessler B, Kurome M, Wuensch A, Summerfield A, Ayares D, Nagashima H, Baars W, Schwinzer R, Wolf E. Human TNF-related apoptosis-inducing ligand-expressing dendritic cells from transgenic pigs attenuate human xenogeneic T cell responses. Xenotransplantation 2012; 19: 40-51.

Kemter E, Cohrs CM, Schafer M, Schuster M, Steinmeyer K, Wolf-van Buerck L, Wolf A, Wuensch A, Kurome M, Kessler B, Zakhartchenko V, Loehn M, Ivashchenko Y, Seissler J, Schulte AM, Speier S, Wolf E. INS-eGFP transgenic pigs: a novel reporter system for studying maturation, growth and vascularisation of neonatal islet-like cell clusters. Diabetologia 2017; 60: 1152-6.

Kemter E, Denner J, Wolf E. Will Genetic Engineering Carry Xenotransplantation of Pig Islets to the Clinic? Curr Diab Rep 2018; 18: 103.

Kemter E, Wolf E. Recent progress in porcine islet isolation, culture and engraftment strategies for xenotransplantation. Curr Opin Organ Transplant 2018; 23: 633-41.

Kemter E, Schnieke A, Fischer K, Cowan PJ, Wolf E. Xeno-organ donor pigs with multiple genetic modifications - the more the better? Curr Opin Genet Dev 2020; 64: 60-5.

Kemter E, Muller A, Neukam M, Ivanova A, Klymiuk N, Renner S, Yang K, Broichhagen J, Kurome M, Zakhartchenko V, Kessler B, Knoch KP, Bickle M, Ludwig B, Johnsson K, Lickert H, Kurth T, Wolf E, Solimena M. Sequential in vivo labeling of insulin secretory granule pools in INS-SNAP transgenic pigs. Proc Natl Acad Sci U S A 2021; 118

Kemter E, Citro A, Wolf-van Buerck L, Qiu Y, Bottcher A, Policardi M, Pellegrini S, Valla L, Alunni-Fabbroni M, Kobolak J, Kessler B, Kurome M, Zakhartchenko V, Dinnyes A, Cyran CC, Lickert H, Piemonti L, Seissler J, Wolf E. Transgenic pigs expressing near infrared fluorescent protein-A novel tool for noninvasive imaging of islet xenotransplants. Xenotransplantation 2022; 29: e12719.

Kim H, Kim J-S. A guide to genome engineering with programmable nucleases. Nature Reviews Genetics 2014; 15: 321-34.

Klatt D, Cheng E, Hoffmann D, Santilli G, Thrasher AJ, Brendel C, Schambach A. Differential Transgene Silencing of Myeloid-Specific Promoters in the AAVS1 Safe Harbor Locus of Induced Pluripotent Stem Cell-Derived Myeloid Cells. Hum Gene Ther 2020; 31: 199-210.

Klose R, Kemter E, Bedke T, Bittmann I, Kelsser B, Endres R, Pfeffer K, Schwinzer R, Wolf E. Expression of biologically active human TRAIL in transgenic pigs. Transplantation 2005; 80: 222-30.

Klymiuk N, van Buerck L, Bahr A, Offers M, Kessler B, Wuensch A, Kurome M, Thormann M, Lochner K, Nagashima H, Herbach N, Wanke R, Seissler J, Wolf E. Xenografted islet cell clusters from INSLEA29Y transgenic pigs rescue diabetes and prevent immune rejection in humanized mice. Diabetes 2012; 61: 1527-32.

Kobayashi T, Harb G, Rajotte RV, Korbutt GS, Mallett AG, Arefanian H, Mok D, Rayat GR. Immune mechanisms associated with the rejection of encapsulated neonatal porcine islet xenografts. Xenotransplantation 2006; 13: 547-59.

Kochar IS, Jain R. Pancreas transplant in type 1 diabetes mellitus: the emerging role of islet cell transplant. Ann Pediatr Endocrinol Metab 2021; 26: 86-91.

Krentz NAJ, Shea LD, Huising MO, Shaw JAM. Restoring normal islet mass and function in type 1 diabetes through regenerative medicine and tissue engineering. Lancet Diabetes Endocrinol 2021; 9: 708-24.

Kurome M, Kessler B, Wuensch A, Nagashima H, Wolf E. Nuclear transfer and transgenesis in the pig. Methods Mol Biol 2015; 1222: 37-59.

Kurome M, Baehr A, Simmet K, Jemiller EM, Egerer S, Dahlhoff M, Zakhartchenko V, Nagashima H, Klymiuk N, Kessler B, Wolf E. Targeting alphaGal epitopes for multi-species embryo immunosurgery. Reprod Fertil Dev 2019; 31: 820-6.

Kwon DJ, Kim DH, Hwang IS, Kim DE, Kim HJ, Kim JS, Lee K, Im GS, Lee JW, Hwang S. Generation of alpha-1,3-galactosyltransferase knocked-out transgenic cloned pigs with knocked-in five human genes. Transgenic Res 2017; 26: 153-63.

Kwon DN, Lee K, Kang MJ, Choi YJ, Park C, Whyte JJ, Brown AN, Kim JH, Samuel M, Mao J, Park KW, Murphy CN, Prather RS, Kim JH. Production of biallelic CMP-Neu5Ac hydroxylase knock-out pigs. Sci Rep 2013; 3: 1981.

Ladowski J, Martens G, Estrada J, Tector M, Tector J. The desirable donor pig to eliminate all xenoreactive antigens. Xenotransplantation 2019; 26: e12504.

Laemmli UK. Cleavage of structural proteins during the assembly of the head of bacteriophage T4. Nature 1970; 227: 680-5.

Lee FT, Dangi A, Shah S, Burnette M, Yang YG, Kirk AD, Hering BJ, Miller SD, Luo X.

Rejection of xenogeneic porcine islets in humanized mice is characterized by graft-infiltrating Th17 cells and activated B cells. Am J Transplant 2020; 20: 1538-50.

Lee HS, Lee JG, Yeom HJ, Chung YS, Kang B, Hurh S, Cho B, Park H, Hwang JI, Park JB, Ahn C, Kim SJ, Yang J. The Introduction of Human Heme Oxygenase-1 and Soluble Tumor Necrosis Factor-α Receptor Type I With Human IgG1 Fc in Porcine Islets Prolongs Islet Xenograft Survival in Humanized Mice. American Journal of Transplantation 2015; 16: 44-57.

Lee SC, Lee H, Oh KB, Hwang IS, Yang H, Park MR, Ock SA, Woo JS, Im GS, Hwang S. Production and Breeding of Transgenic Cloned Pigs Expressing Human CD73. Dev Reprod 2017; 21: 157-65.

Lee W, Hara H, Ezzelarab MB, Iwase H, Bottino R, Long C, Ramsoondar J, Ayares D, Cooper DK. Initial in vitro studies on tissues and cells from GTKO/CD46/NeuGcKO pigs. Xenotransplantation 2016; 23: 137-50.

Lei T, Chen L, Wang K, Du S, Gonelle-Gispert C, Wang Y, Buhler LH. Genetic engineering of pigs for xenotransplantation to overcome immune rejection and physiological incompatibilities: The first clinical steps. Front Immunol 2022; 13: 1031185.

Lei Y, Buerck LW, Honarpisheh M, Zhang Y, Schwinzer R, Petersen B, Seissler J. Neonatal islets from hPD-L1 transgenic pigs reduce immune cell activation and cellular rejection in humanized NSG mice. Am J Transplant 2023;

Li B, Zhong M, Qian J, Li R, Davidson D, Tang Z, Zhu K, Argenty J, Gonzalez de Peredo A, Malissen B, Roncagalli R, Veillette A. Cis interactions between CD2 and its ligands on T cells are required for T cell activation. Science immunology 2022a; 7: eabn6373.

Li H, Yang Y, Hong W, Huang M, Wu M, Zhao X. Applications of genome editing technology in the targeted therapy of human diseases: mechanisms, advances and prospects. Signal Transduction and Targeted Therapy 2020; 5: 1.

Li J, Wu P, Cao Z, Huang G, Lu Z, Yan J, Zhang H, Zhou Y, Liu R, Chen H, Ma L, Luo M.

Machine learning-based prediction models to guide the selection of Cas9 variants for efficient gene editing. Cell Reports 2024; 43: 113765.

Li X, Yang Y, Bu L, Guo X, Tang C, Song J, Fan N, Zhao B, Ouyang Z, Liu Z, Zhao Y, Yi X, Quan L, Liu S, Yang Z, Ouyang H, Chen YE, Wang Z, Lai L. Rosa26-targeted swine models for stable gene over-expression and Cre-mediated lineage tracing. Cell Research 2014; 24: 501-4.

Li X, Jin J, Guo Z, Liu L. Evolution of plasmid-construction. Int J Biol Macromol 2022b; 209: 1319-26.

Li XC, Rothstein DM, Sayegh MH. Costimulatory pathways in transplantation: challenges and new developments. Immunological reviews 2009; 229: 271-93.

Lilienfeld BG, Garcia-Borges C, Crew MD, Seebach JD. Porcine UL16-binding protein 1 expressed on the surface of endothelial cells triggers human NK cytotoxicity through NKG2D. J Immunol 2006; 177: 2146-52.

Lin CC, Ezzelarab M, Hara H, Long C, Lin CW, Dorling A, Cooper DK. Atorvastatin or transgenic expression of TFPI inhibits coagulation initiated by anti-nonGal IgG binding to porcine aortic endothelial cells. J Thromb Haemost 2010; 8: 2001-10.

Lin YK, Fisher SJ, Pop-Busui R. Hypoglycemia unawareness and autonomic dysfunction in diabetes: Lessons learned and roles of diabetes technologies. J Diabetes Investig 2020; 11: 1388-402.

Liu Z, Chen O, Wall JBJ, Zheng M, Zhou Y, Wang L, Ruth Vaseghi H, Qian L, Liu J. Systematic comparison of 2A peptides for cloning multi-genes in a polycistronic vector. Scientific Reports 2017; 7: 2193.

Lopez KJ, Cross-Najafi AA, Farag K, Obando B, Thadasina D, Isidan A, Park Y, Zhang W, Ekser B, Li P. Strategies to induce natural killer cell tolerance in xenotransplantation. Front Immunol 2022; 13: 941880.

Loveland BE, Milland J, Kyriakou P, Thorley BR, Christiansen D, Lanteri MB, Regensburg M, Duffield M, French AJ, Williams L, Baker L, Brandon MR, Xing PX, Kahn D, McKenzie IF. Characterization of a CD46 transgenic pig and protection of transgenic kidneys against hyperacute rejection in non-immunosuppressed baboons. Xenotransplantation 2004; 11: 171-83.

Lu T, Yang B, Wang R, Qin C. Xenotransplantation: Current Status in Preclinical Research. Frontiers in immunology 2020; 10: 3060.

Lu TY, Xu XL, Du XG, Wei JH, Yu JN, Deng SL, Qin C. Advances in Innate Immunity to Overcome Immune Rejection during Xenotransplantation. Cells 2022; 11

Lutz AJ, Li P, Estrada JL, Sidner RA, Chihara RK, Downey SM, Burlak C, Wang ZY, Reyes LM, Ivary B, Yin F, Blankenship RL, Paris LL, Tector AJ. Double knockout pigs deficient in N-glycolylneuraminic acid and galactose alpha-1,3-galactose reduce the humoral barrier to xenotransplantation. Xenotransplantation 2013; 20: 27-35.

Ma X, Zeng W, Wang L, Cheng R, Zhao Z, Huang C, Sun Z, Tao P, Wang T, Zhang J, Liu L, Duan X, Niu D. Validation of reliable safe harbor locus for efficient porcine transgenesis. Funct Integr Genomics 2022; 22: 553-63.

Maeda A, Kogata S, Toyama C, Lo PC, Okamatsu C, Yamamoto R, Masahata K, Kamiyama M, Eguchi H, Watanabe M, Nagashima H, Okuyama H, Miyagawa S. The Innate Cellular Immune Response in Xenotransplantation. Front Immunol 2022; 13: 858604.

Mandel TE, Koulmanda M, Cozzi E, Waterworth P, Tolan M, Langford G, White DJG. Transplantation of Normal and DAF-Transgenic Fetal Pig Pancreas Into Cynomolgus Monkeys. Transplantation proceedings 1997; 29: 940-.

Mani I, Arazoe T, Singh V. Chapter Two - CRISPR-Cas systems for genome editing of mammalian cells. In: Progress in Molecular Biology and Translational Science. Singh V, ed.: Academic Press 2021: 15-30.

Martens GR, Reyes LM, Li P, Butler JR, Ladowski JM, Estrada JL, Sidner RA, Eckhoff DE, Tector M, Tector AJ. Humoral Reactivity of Renal Transplant-Waitlisted Patients to Cells From GGTA1/CMAH/B4GalNT2, and SLA Class I Knockout Pigs. Transplantation 2017; 101: e86-e92.

Martin BM, Samy KP, Lowe MC, Thompson PW, Cano J, Farris AB, Song M, Dove CR, Leopardi FV, Strobert EA, Jenkins JB, Collins BH, Larsen CP, Kirk AD. Dual islet transplantation modeling of the instant blood-mediated inflammatory reaction. Am J Transplant 2015; 15: 1241-52.

Martin C, Plat M, Nerriere-Daguin V, Coulon F, Uzbekova S, Venturi E, Conde F, Hermel JM, Hantraye P, Tesson L, Anegon I, Melchior B, Peschanski M, Le Mauff B, Boeffard F, Sergent-Tanguy S, Neveu I, Naveilhan P, Soulillou JP, Terqui M, Brachet P, Vanhove B. Transgenic expression of CTLA4-Ig by fetal pig neurons for xenotransplantation. Transgenic Res 2005; 14: 373-84.

Matsunari H, Kobayashi T, Watanabe M, Umeyama K, Nakano K, Kanai T, Matsuda T, Nagaya M, Hara M, Nakauchi H, H N. Transgenic pigs with pancreas-specific expression of green fluorescent protein. J Reprod Dev 2014; 60: 230-7.

McCall M, Pawlick R, Kin T, Shapiro AM. Anakinra potentiates the protective effects of etanercept in transplantation of marginal mass human islets in immunodeficient mice. Am J Transplant 2012; 12: 322-9.

McKenzie IFC, Li YQ, Xing PX, Dinatale I, Koulmanda M, Loveland BE, Sandrin MS. CD46 protects pig islets from antibody but not cell-mediated destruction in the mouse. Xenotransplantation 2003; 10: 615-21.

Mehta AK, Majumdar SS, Alam P, Gulati N, Brahmachari V. Epigenetic regulation of cytomegalovirus major immediate-early promoter activity in transgenic mice. Gene 2009; 428: 20-4.

Miyagawa S, Maeda A, Toyama C, Kogata S, Okamatsu C, Yamamoto R, Masahata K,

Kamiyama M, Eguchi H, Watanabe M, Nagashima H, Ikawa M, Matsunami K, Okuyama H. Aspects of the Complement System in New Era of Xenotransplantation. Front Immunol 2022; 13: 860165.

Moberg L, Johansson H, Lukinius A, Berne C, Foss A, Kallen R, Ostraat O, Salmela K, Tibell A, Tufveson G, Elgue G, Nilsson Ekdahl K, Korsgren O, Nilsson B. Production of tissue factor by pancreatic islet cells as a trigger of detrimental thrombotic reactions in clinical islet transplantation. Lancet 2002; 360: 2039-45.

Moberg L, Olsson A, Berne C, Felldin M, Foss A, Kallen R, Salmela K, Tibell A, Tufveson G, Nilsson B, Korsgren O. Nicotinamide inhibits tissue factor expression in isolated human pancreatic islets: implications for clinical islet transplantation. Transplantation 2003; 76: 1285-8.

Mohiuddin MM, Singh AK, Corcoran PC, Hoyt RF, Thomas ML, 3rd, Lewis BG, Eckhaus M, Dabkowski NL, Belli AJ, Reimann KA, Ayares D, Horvath KA. Role of anti-CD40 antibody-mediated costimulation blockade on non-Gal antibody production and heterotopic cardiac xenograft survival in a GTKO.hCD46Tg pig-to-baboon model. Xenotransplantation 2014; 21: 35-45.

Mok D, Black M, Gupta N, Arefanian H, Tredget E, Rayat GR. Early immune mechanisms of neonatal porcine islet xenograft rejection. Xenotransplantation 2019; 26: e12546.

Mou L, Shi G, Cooper DKC, Lu Y, Chen J, Zhu S, Deng J, Huang Y, Ni Y, Zhan Y, Cai Z, Pu Z. Current Topics of Relevance to the Xenotransplantation of Free Pig Islets. Front Immunol 2022; 13: 854883.

Naeem M, Majeed S, Hoque MZ, Ahmad I. Latest Developed Strategies to Minimize the Off-Target Effects in CRISPR-Cas-Mediated Genome Editing. Cells 2020; 9

Nagaraju S, Bertera S, Tanaka T, Hara H, Rayat GR, Wijkstrom M, Ayares D, Trucco M, Cooper DK, Bottino R. In vitro exposure of pig neonatal isletlike cell clusters to human blood. Xenotransplantation 2015; 22: 317-24.

Naziruddin B, Kanak MA, Chang CA, Takita M, Lawrence MC, Dennison AR, Onaca N, Levy MF. Improved outcomes of islet autotransplant after total pancreatectomy by combined blockade of IL-1beta and TNFalpha. Am J Transplant 2018; 18: 2322-9.

NEB®. Gibson Assembly®. https://www.neb.com/en/applications/cloning-and-synthetic-biology/dna-assembly-and-cloning/gibson-assembly. 25.01.2024.

Nelson J, Alvey N, Bowman L, Schulte J, Segovia MC, McDermott J, Te HS, Kapila N, Levine DJ, Gottlieb RL, Oberholzer J, Campara M. Consensus recommendations for use of maintenance immunosuppression in solid organ transplantation: Endorsed by the American College of Clinical Pharmacy, American Society of Transplantation, and the International Society for Heart and Lung Transplantation. Pharmacotherapy 2022; 42: 599-633.

Niedringhaus TP, Milanova D, Kerby MB, Snyder MP, Barron AE. Landscape of next-generation sequencing technologies. Anal Chem 2011; 83: 4327-41.

Nomura S, Ariyoshi Y, Watanabe H, Pomposelli T, Takeuchi K, Garcia G, Tasaki M, Ayares D, Sykes M, Sachs D, Johnson R, Yamada K. Transgenic expression of human CD47 reduces phagocytosis of porcine endothelial cells and podocytes by baboon and human macrophages. Xenotransplantation 2020; 27: e12549.

Norris AL, Lee SS, Greenlees KJ, Tadesse DA, Miller MF, Lombardi HA. Template plasmid integration in germline genome-edited cattle. Nature Biotechnology 2020; 38: 163-4.

Nottle MB, Salvaris EJ, Fisicaro N, McIlfatrick S, Vassiliev I, Hawthorne WJ, O'Connell PJ, Brady JL, Lew AM, Cowan PJ. Targeted insertion of an anti-CD2 monoclonal antibody transgene into the GGTA1 locus in pigs using FokI-dCas9. Sci Rep 2017; 7: 8383.

Oldenborg PA, Zheleznyak A, Fang YF, Lagenaur CF, Gresham HD, Lindberg FP. Role of CD47 as a marker of self on red blood cells. Science 2000; 288: 2051-4.

Oropeza M, Petersen B, Carnwath JW, Lucas-Hahn A, Lemme E, Hassel P, Herrmann D, Barg-Kues B, Holler S, Queisser AL, Schwinzer R, Hinkel R, Kupatt C, Niemann H. Transgenic

expression of the human A20 gene in cloned pigs provides protection against apoptotic and inflammatory stimuli. Xenotransplantation 2009; 16: 522-34.

Park SJ, Cho B, Koo OJ, Kim H, Kang JT, Hurh S, Kim SJ, Yeom HJ, Moon J, Lee EM, Choi JY, Hong JH, Jang G, Hwang J-I, Yang J, Lee BC, Ahn C. Production and characterization of soluble human TNFRI-Fc and human HO-1(HMOX1) transgenic pigs by using the F2A peptide. Transgenic Research 2014; 23: 407-19.

Pattanayak V, Lin S, Guilinger JP, Ma E, Doudna JA, Liu DR. High-throughput profiling of off-target DNA cleavage reveals RNA-programmed Cas9 nuclease specificity. Nature Biotechnology 2013; 31: 839-43.

Petersen B, Ramackers W, Lucas-Hahn A, Lemme E, Hassel P, Queisser AL, Herrmann D, Barg-Kues B, Carnwath JW, Klose J, Tiede A, Friedrich L, Baars W, Schwinzer R, Winkler M, Niemann H. Transgenic expression of human heme oxygenase-1 in pigs confers resistance against xenograft rejection during ex vivo perfusion of porcine kidneys. Xenotransplantation 2011; 18: 355-68.

Phelps CJ, Koike C, Vaught TD, Boone J, Wells KD, Chen SH, Ball S, Specht SM, Polejaeva IA, Monahan JA, Jobst PM, Sharma SB, Lamborn AE, Garst AS, Moore M, Demetris AJ, Rudert WA, Bottino R, Bertera S, Trucco M, Starzl TE, Dai Y, Ayares DL. Production of alpha 1,3-galactosyltransferase-deficient pigs. Science 2003; 299: 411-4.

Phelps CJ, Ball SF, Vaught TD, Vance AM, Mendicino M, Monahan JA, Walters AH, Wells KD, Dandro AS, Ramsoondar JJ, Cooper DK, Ayares DL. Production and characterization of transgenic pigs expressing porcine CTLA4-Ig. Xenotransplantation 2009; 16: 477-85.

Plege A, Borns K, Beer L, Baars W, Klempnauer J, Schwinzer R. Downregulation of cytolytic activity of human effector cells by transgenic expression of human PD-ligand-1 on porcine target cells. Transpl Int 2010; 23: 1293-300.

Rajeswar C, Abid H, Gopalakrishnan L, Siddharth N, Gene DP, Appakalai NB. Porcine Islet Cell Xenotransplantation. In: Xenotransplantation. Shuji M, ed. Rijeka: IntechOpen 2020: Ch.

3.

Rao JS, Hosny N, Kumbha R, Naqvi RA, Singh A, Swanson Z, Levy H, Matson AW, Steinhoff M, Forneris N, Walters E, Hering BJ, Burlak C. HLA-G1(+) Expression in GGTA1KO Pigs Suppresses Human and Monkey Anti-Pig T, B and NK Cell Responses. Front Immunol 2021; 12: 730545.

Rayat GR, Rajotte RV, Hering BJ, Binette TM, Korbutt GS. In vitro and in vivo expression of Galalpha-(1, 3) Gal on porcine islet cells is age dependent. Journal of Endocrinology 2003; 177: 127-35.

Renner S, Braun-Reichhart C, Blutke A, Herbach N, Emrich D, Streckel E, Wünsch A, Kessler B, Kurome M, Bähr A, Klymiuk N, Krebs S, Puk O, Nagashima H, Graw J, Blum H, Wanke R, Wolf E. Permanent neonatal diabetes in INS(C94Y) transgenic pigs. Diabetes 2013; 62: 1505-11.

Reyes LM, Estrada JL, Wang ZY, Blosser RJ, Smith RF, Sidner RA, Paris LL, Blankenship RL, Ray CN, Miner AC, Tector M, Tector AJ. Creating class I MHC-null pigs using guide RNA and the Cas9 endonuclease. J Immunol 2014; 193: 5751-7.

Richter A, Kurome M, Kessler B, Zakhartchenko V, Klymiuk N, Nagashima H, Wolf E, Wuensch A. Potential of primary kidney cells for somatic cell nuclear transfer mediated transgenesis in pig. BMC Biotechnology 2012; 12: 84.

Rieblinger B, Fischer K, Kind A, Saller BS, Baars W, Schuster M, Wolf-van Buerck L, Schaffler A, Flisikowska T, Kurome M, Zakhartchenko V, Kessler B, Flisikowski K, Wolf E, Seissler J, Schwinzer R, Schnieke A. Strong xenoprotective function by single-copy transgenes placed sequentially at a permissive locus. Xenotransplantation 2018; 25: e12382.

Roussel JC, Moran CJ, Salvaris EJ, Nandurkar HH, d'Apice AJ, Cowan PJ. Pig thrombomodulin binds human thrombin but is a poor cofactor for activation of human protein C and TAFI. Am J Transplant 2008; 8: 1101-12.

Russell M, Cardona K, Shaffer V, Korbutt G, Cano J, Jiang W, Strobert E, Rajotte R, Pearson T, Larsen C (2007) Engraftment of neonatal porcine islets in diabetic non-human primates by blockade of the CD28/CD40 costimulatory pathways. 423-

Saeki Y, Ishiyama K, Ishida N, Tanaka Y, Ohdan H. Role of Natural Killer Cells in the Innate Immune System After Intraportal Islet Transplantation in Mice. Transplant Proc 2017; 49: 139-44.

Sake HJ, Frenzel A, Lucas-Hahn A, Nowak-Imialek M, Hassel P, Hadeler KG, Hermann D, Becker R, Eylers H, Hein R, Baars W, Brinkmann A, Schwinzer R, Niemann H, Petersen B. Possible detrimental effects of beta-2-microglobulin knockout in pigs. Xenotransplantation 2019; 26: e12525.

Sakran N, Graham Y, Pintar T, Yang W, Kassir R, Willigendael EM, Singhal R, Kooreman ZE, Ramnarain D, Mahawar K, Parmar C, Madhok B, Pouwels S. The many faces of diabetes. Is there a need for re-classification? A narrative review. BMC Endocr Disord 2022; 22: 9.

Salama A, Mosser M, Leveque X, Perota A, Judor JP, Danna C, Pogu S, Moure A, Jegou D, Gaide N, Abadie J, Gauthier O, Concordet JP, Le Bas-Bernardet S, Riochet D, Le Berre L, Hervouet J, Minault D, Weiss P, Guicheux J, Brouard S, Bosch S, Lagutina I, Duchi R, Lazzari G, Cozzi E, Blancho G, Conchon S, Galli C, Soulillou JP, Bach JM. Neu5Gc and alpha1-3 GAL Xenoantigen Knockout Does Not Affect Glycemia Homeostasis and Insulin Secretion in Pigs. Diabetes 2017; 66: 987-93.

Salvaris EJ, Fisicaro N, McIlfatrick S, Thomas A, Fuller E, Lew AM, Nottle MB, Hawthorne WJ, Cowan PJ. Characterisation of transgenic pigs expressing a human T cell-depleting anti-CD2 monoclonal antibody. Xenotransplantation 2023; 31: e12836.

Samsu N. Diabetic Nephropathy: Challenges in Pathogenesis, Diagnosis, and Treatment. Biomed Res Int 2021; 2021: 1497449.

Samy KP, Davis RP, Gao Q, Martin BM, Song M, Cano J, Farris AB, McDonald A, Gall EK, Dove CR, Leopardi FV, How T, Williams KD, Devi GR, Collins BH, Kirk AD. Early barriers

to neonatal porcine islet engraftment in a dual transplant model. American Journal of Transplantation 2018; 18: 998-1006.

Samy KP, Gao Q, Davis RP, Song M, Fitch ZW, Mulvihill MS, MacDonald AL, Leopardi FV, How T, Williams KD, Devi GR, Collins BH, Luo X, Kirk AD. The role of human CD46 in early xenoislet engraftment in a dual transplant model. Xenotransplantation 2019; 26: e12540.

Scalea J, Hanecamp I, Robson SC, Yamada K. T-cell-mediated immunological barriers to xenotransplantation. Xenotransplantation 2012; 19: 23-30.

Schofield ZV, Woodruff TM, Halai R, Wu MC, Cooper MA. Neutrophils--a key component of ischemia-reperfusion injury. Shock 2013; 40: 463-70.

Shah VN, Grimsmann JM, Foster NC, Dost A, Miller KM, Pavel M, Weinstock RS, Karges W, Maahs DM, Holl RW. Undertreatment of cardiovascular risk factors in the type 1 diabetes exchange clinic network (United States) and the prospective diabetes follow-up (Germany/Austria) registries. Diabetes Obes Metab 2020; 22: 1577-85.

Shahjalal HM, Abdal Dayem A, Lim KM, Jeon TI, Cho SG. Generation of pancreatic beta cells for treatment of diabetes: advances and challenges. Stem Cell Res Ther 2018; 9: 355.

Shen P, Fillatreau S. Antibody-independent functions of B cells: a focus on cytokines. Nat Rev Immunol 2015; 15: 441-51.

Shilleh AH, Russ HA. Cell Replacement Therapy for Type 1 Diabetes Patients: Potential Mechanisms Leading to Stem-Cell-Derived Pancreatic beta-Cell Loss upon Transplant. Cells 2023; 12

Shin JS, Kim JM, Kim JS, Min BH, Kim YH, Kim HJ, Jang JY, Yoon IH, Kang HJ, Kim J, Hwang ES, Lim DG, Lee WW, Ha J, Jung KC, Park SH, Kim SJ, Park CG. Long-term control of diabetes in immunosuppressed nonhuman primates (NHP) by the transplantation of adult porcine islets. Am J Transplant 2015; 15: 2837-50.

Shrestha P, Batra L, Tariq Malik M, Tan M, Yolcu ES, Shirwan H. Immune checkpoint CD47 molecule engineered islets mitigate instant blood-mediated inflammatory reaction and show improved engraftment following intraportal transplantation. Am J Transplant 2020; 20: 2703-14.

Sizer RE, White RJ. Use of ubiquitous chromatin opening elements (UCOE) as tools to maintain transgene expression in biotechnology. Comput Struct Biotechnol J 2023; 21: 275-83.

Song M, Fitch ZW, Samy KP, Martin BM, Gao Q, Patrick Davis R, Leopardi FV, Huffman N, Schmitz R, Devi GR, Collins BH, Kirk AD. Coagulation, inflammation, and CD46 transgene expression in neonatal porcine islet xenotransplantation. Xenotransplantation 2021; 28: e12680.

SoRelle JA, Itoh T, Peng H, Kanak MA, Sugimoto K, Matsumoto S, Levy MF, Lawrence MC, Naziruddin B. Withaferin A inhibits pro-inflammatory cytokine-induced damage to islets in culture and following transplantation. Diabetologia 2013; 56: 814-24.

Speier S, Nyqvist D, Cabrera O, Yu J, Molano RD, Pileggi A, Moede T, Kohler M, Wilbertz J, Leibiger B, Ricordi C, Leibiger IB, Caicedo A, Berggren PO. Noninvasive in vivo imaging of pancreatic islet cell biology. Nat Med 2008; 14: 574-8.

Springer SA, Diaz SL, Gagneux P. Parallel evolution of a self-signal: humans and new world monkeys independently lost the cell surface sugar Neu5Gc. Immunogenetics 2014; 66: 671-4.

Sundqvist KG. T Cell Co-Stimulation: Inhibition of Immunosuppression? Front Immunol 2018; 9: 974.

Sykes M, Sachs DH. Progress in xenotransplantation: overcoming immune barriers. Nat Rev Nephrol 2022; 18: 745-61.

Takaki T, Shimoda M. Pancreatic islet transplantation: toward definitive treatment for diabetes mellitus. Glob Health Med 2020; 2: 200-11.

Tan X, Lee LK, Huynh S, Pawaskar M, Rajpathak S. Sociodemographic disparities in the

management of type 2 diabetes in the United States. Current Medical Research and Opinion 2020; 36: 967-76.

Tanaka K, Kawano T, Tomino T, Kawano H, Okada T, Oshita S, Takahashi A, Nakaya Y. Mechanisms of Impaired Glucose Tolerance and Insulin Secretion during Isoflurane Anesthesia. Anesthesiology 2009; 111: 1044-51.

Tector AJ, Mosser M, Tector M, Bach JM. The Possible Role of Anti-Neu5Gc as an Obstacle in Xenotransplantation. Front Immunol 2020; 11: 622.

Templer S. Closed-Loop Insulin Delivery Systems: Past, Present, and Future Directions. Front Endocrinol (Lausanne) 2022; 13: 919942.

Tena A, Kurtz J, Leonard DA, Dobrinsky JR, Terlouw SL, Mtango N, Verstegen J, Germana S, Mallard C, Arn JS, Sachs DH, Hawley RJ. Transgenic expression of human CD47 markedly increases engraftment in a murine model of pig-to-human hematopoietic cell transplantation. Am J Transplant 2014; 14: 2713-22.

Tena AA, Sachs DH, Mallard C, Yang YG, Tasaki M, Farkash E, Rosales IA, Colvin RB, Leonard DA, Hawley RJ. Prolonged Survival of Pig Skin on Baboons After Administration of Pig Cells Expressing Human CD47. Transplantation 2017; 101: 316-21.

Thompson P, Badell IR, Lowe M, Cano J, Song M, Leopardi F, Avila J, Ruhil R, Strobert E, Korbutt G, Rayat G, Rajotte R, Iwakoshi N, Larsen CP, Kirk AD. Islet xenotransplantation using gal-deficient neonatal donors improves engraftment and function. Am J Transplant 2011a; 11: 2593-602.

Thompson P, Cardona K, Russell M, Badell IR, Shaffer V, Korbutt G, Rayat GR, Cano J, Song M, Jiang W, Strobert E, Rajotte R, Pearson T, Kirk AD, Larsen CP. CD40-specific costimulation blockade enhances neonatal porcine islet survival in nonhuman primates. Am J Transplant 2011b; 11: 947-57.

Thompson P, Badell IR, Lowe M, Turner A, Cano J, Avila J, Azimzadeh A, Cheng X, Pierson

RN, 3rd, Johnson B, Robertson J, Song M, Leopardi F, Strobert E, Korbutt G, Rayat G, Rajotte R, Larsen CP, Kirk AD. Alternative immunomodulatory strategies for xenotransplantation: CD40/154 pathway-sparing regimens promote xenograft survival. Am J Transplant 2012; 12: 1765-75.

Tjernberg J, Ekdahl KN, Lambris JD, Korsgren O, Nilsson B. Acute antibody-mediated complement activation mediates lysis of pancreatic islets cells and may cause tissue loss in clinical islet transplantation. Transplantation 2008; 85: 1193-9.

Vabres B, Le Bas-Bernardet S, Riochet D, Cherel Y, Minault D, Hervouet J, Ducournau Y, Moreau A, Daguin V, Coulon F, Pallier A, Brouard S, Robson SC, Nottle MB, Cowan PJ, Venturi E, Mermillod P, Brachet P, Galli C, Lagutina I, Duchi R, Bach JM, Blancho G, Soulillou JP, Vanhove B. hCTLA4-Ig transgene expression in keratocytes modulates rejection of corneal xenografts in a pig to non-human primate anterior lamellar keratoplasty model. Xenotransplantation 2014; 21: 431-43.

Valera A, Perales JC, Hatzoglou M, Bosch F. Expression of the neomycin-resistance (neo) gene induces alterations in gene expression and metabolism. Hum Gene Ther 1994; 5: 449-56.

van der Windt DJ, Bottino R, Casu A, Campanile N, Smetanka C, He J, Murase N, Hara H, Ball S, Loveland BE, Ayares D, Lakkis FG, Cooper DK, Trucco M. Long-term controlled normoglycemia in diabetic non-human primates after transplantation with hCD46 transgenic porcine islets. Am J Transplant 2009; 9: 2716-26.

Velazco-Cruz L, Goedegebuure MM, Millman JR. Advances Toward Engineering Functionally Mature Human Pluripotent Stem Cell-Derived beta Cells. Front Bioeng Biotechnol 2020; 8: 786.

Vockova P, Molinsky J, Klanova M, Karban J, Spacek M, Havranek O, Kupcova K, Kazantsev D, Trneny M, Klener P. CD31/PECAM-1 impacts engraftment, growth and spread of mantle cell lymphoma cells and positively correlates with extramedullary involvement. Leuk Lymphoma 2021; 62: 861-7.

von Zur-Muhlen B, Lundgren T, Bayman L, Berne C, Bridges N, Eggerman T, Foss A, Goldstein J, Jenssen T, Jorns C, Morrison Y, Ryden M, Schwieger T, Tufveson G, Nilsson B, Korsgren O. Open Randomized Multicenter Study to Evaluate Safety and Efficacy of Low Molecular Weight Sulfated Dextran in Islet Transplantation. Transplantation 2019; 103: 630-7.

Vorobjeva NV, Chernyak BV. NETosis: Molecular Mechanisms, Role in Physiology and Pathology. Biochemistry (Mosc) 2020; 85: 1178-90.

Walker JT, Saunders DC, Brissova M, Powers AC. The Human Islet: Mini-Organ With Mega-Impact. Endocr Rev 2021; 42: 605-57.

Wang HT, Maeda A, Sakai R, Lo PC, Takakura C, Jiaravuthisan P, Mod Shabri A, Matsuura R, Kodama T, Hiwatashi S, Eguchi H, Okuyama H, Miyagawa S. Human CD31 on porcine cells suppress xenogeneic neutrophil-mediated cytotoxicity via the inhibition of NETosis. Xenotransplantation 2018; 25: e12396.

Wang J, Sun Z, Gou W, Adams DB, Cui W, Morgan KA, Strange C, Wang H. alpha-1 Antitrypsin Enhances Islet Engraftment by Suppression of Instant Blood-Mediated Inflammatory Reaction. Diabetes 2017; 66: 970-80.

Wang S, Tasch J, Kheradmand T, Ulaszek J, Ely S, Zhang X, Hering BJ, Miller SD, Luo X. Transient B-cell depletion combined with apoptotic donor splenocytes induces xeno-specific T-and B-cell tolerance to islet xenografts. Diabetes 2013; 62: 3143-50.

Wang TY, Guo X. Expression vector cassette engineering for recombinant therapeutic production in mammalian cell systems. Appl Microbiol Biotechnol 2020; 104: 5673-88.

Wang X, Brown NK, Wang B, Shariati K, Wang K, Fuchs S, Melero-Martin JM, Ma M. Local Immunomodulatory Strategies to Prevent Allo-Rejection in Transplantation of Insulin-Producing Cells. Adv Sci (Weinh) 2021; 8: e2003708.

Weiss EH, Lilienfeld BG, Muller S, Muller E, Herbach N, Kessler B, Wanke R, Schwinzer R,

Seebach JD, Wolf E, Brem G. HLA-E/human beta2-microglobulin transgenic pigs: protection against xenogeneic human anti-pig natural killer cell cytotoxicity. Transplantation 2009; 87: 35-43.

Wennhold K, Shimabukuro-Vornhagen A, von Bergwelt-Baildon M. B Cell-Based Cancer Immunotherapy. Transfus Med Hemother 2019; 46: 36-46.

Wheeler DG, Joseph ME, Mahamud SD, Aurand WL, Mohler PJ, Pompili VJ, Dwyer KM, Nottle MB, Harrison SJ, d'Apice AJ, Robson SC, Cowan PJ, Gumina RJ. Transgenic swine: expression of human CD39 protects against myocardial injury. J Mol Cell Cardiol 2012; 52: 958-61.

Wolf E, Kemter E, Bürck LW-v, Seissler J. Xenotransplantation von Pankreasinseln – aktueller Stand. Die Diabetologie 2022; 18: 803-10.

Wuensch A, Baehr A, Bongoni AK, Kemter E, Blutke A, Baars W, Haertle S, Zakhartchenko V, Kurome M, Kessler B, Faber C, Abicht JM, Reichart B, Wanke R, Schwinzer R, Nagashima H, Rieben R, Ayares D, Wolf E, Klymiuk N. Regulatory sequences of the porcine THBD gene facilitate endothelial-specific expression of bioactive human thrombomodulin in single- and multitransgenic pigs. Transplantation 2014; 97: 138-47.

Xia Y, Li K, Li J, Wang T, Gu L, Xun L. T5 exonuclease-dependent assembly offers a low-cost method for efficient cloning and site-directed mutagenesis. Nucleic Acids Research 2019; 47: e15-e.

Xiang G-m, Zhang X-l, Xu C-j, Fan Z-y, Xu K, Wang N, Wang Y, Che J-j, Xu S-s, Mu Y-l, Li K, Liu Z-g. The collagen type I alpha 1 chain gene is an alternative safe harbor locus in the porcine genome. Journal of Integrative Agriculture 2023; 22: 202-13.

Xu XC, Goodman J, Sasaki H, Lowell J, Mohanakumar T. Activation of natural killer cells and macrophages by porcine endothelial cells augments specific T-cell xenoresponse. Am J Transplant 2002; 2: 314-22.

Yan JJ, Yeom HJ, Jeong JC, Lee JG, Lee EW, Cho B, Lee HS, Kim SJ, Hwang JI, Kim SJ, Lee BC, Ahn C, Yang J. Beneficial effects of the transgenic expression of human sTNF-alphaR-Fc and HO-1 on pig-to-mouse islet xenograft survival. Transpl Immunol 2016; 34: 25-32.

Yan LL, Ye LP, Chen YH, He SQ, Zhang CY, Mao XL, Li SW. The Influence of Microenvironment on Survival of Intraportal Transplanted Islets. Front Immunol 2022; 13: 849580.

Yao M, Domogatskaya A, Agren N, Watanabe M, Tokodai K, Brines M, Cerami A, Ericzon BG, Kumagai-Braesch M, Lundgren T. Cibinetide Protects Isolated Human Islets in a Stressful Environment and Improves Engraftment in the Perspective of Intra Portal Islet Transplantation. Cell Transplant 2021; 30: 9636897211039739.

Yi M, Niu M, Xu L, Luo S, Wu K. Regulation of PD-L1 expression in the tumor microenvironment. J Hematol Oncol 2021; 14: 10.

Yi S, Hawthorne WJ, Lehnert AM, Ha H, Wong JK, van Rooijen N, Davey K, Patel AT, Walters SN, Chandra A, O'Connell PJ. T cell-activated macrophages are capable of both recognition and rejection of pancreatic islet xenografts. J Immunol 2003; 170: 2750-8.

Yoshihara E, O'Connor C, Gasser E, Wei Z, Oh TG, Tseng TW, Wang D, Cayabyab F, Dai Y, Yu RT, Liddle C, Atkins AR, Downes M, Evans RM. Immune-evasive human islet-like organoids ameliorate diabetes. Nature 2020; 586: 606-11.

Yoshimatsu G, Kunnathodi F, Saravanan PB, Shahbazov R, Chang C, Darden CM, Zurawski S, Boyuk G, Kanak MA, Levy MF, Naziruddin B, Lawrence MC. Pancreatic beta-Cell-Derived IP-10/CXCL10 Isletokine Mediates Early Loss of Graft Function in Islet Cell Transplantation. Diabetes 2017; 66: 2857-67.

Yue Y, Xu W, Kan Y, Zhao HY, Zhou Y, Song X, Wu J, Xiong J, Goswami D, Yang M, Lamriben L, Xu M, Zhang Q, Luo Y, Guo J, Mao S, Jiao D, Nguyen TD, Li Z, Layer JV, Li M, Paragas V, Youd ME, Sun Z, Ding Y, Wang W, Dou H, Song L, Wang X, Le L, Fang X, George H, Anand R, Wang SY, Westlin WF, Guell M, Markmann J, Qin W, Gao Y, Wei HJ,

Church GM, Yang L. Extensive germline genome engineering in pigs. Nat Biomed Eng 2021a; 5: 134-43.

Yue Y, Xu W, Kan Y, Zhao H-Y, Zhou Y, Song X, Wu J, Xiong J, Goswami D, Yang M, Lamriben L, Xu M, Zhang Q, Luo Y, Guo J, Mao S, Jiao D, Nguyen TD, Li Z, Layer JV, Li M, Paragas V, Youd ME, Sun Z, Ding Y, Wang W, Dou H, Song L, Wang X, Le L, Fang X, George H, Anand R, Wang SY, Westlin WF, Güell M, Markmann J, Qin W, Gao Y, Wei H-J, Church GM, Yang L. Extensive germline genome engineering in pigs. Nature Biomedical Engineering 2021b; 5: 134-43.

Zammit NW, Seeberger KL, Zamerli J, Walters SN, Lisowski L, Korbutt GS, Grey ST. Selection of a novel AAV2/TNFAIP3 vector for local suppression of islet xenograft inflammation. Xenotransplantation 2021; 28: e12669.

Zeyland J, Lipinski D, Slomski R. The current state of xenotransplantation. J Appl Genet 2015; 56: 211-8.

Zhang F, Santilli G, Thrasher AJ. Characterization of a core region in the A2UCOE that confers effective anti-silencing activity. Sci Rep 2017; 7: 10213.

Zhou H, Hara H, Cooper DKC. The complex functioning of the complement system in xenotransplantation. Xenotransplantation 2019; 26: e12517.

Zhou Q, Li T, Wang K, Zhang Q, Geng Z, Deng S, Cheng C, Wang Y. Current status of xenotransplantation research and the strategies for preventing xenograft rejection. Front Immunol 2022; 13: 928173.

Zhou Y, Zhang T, Zhang QK, Jiang Y, Xu DG, Zhang M, Shen W, Pan QJ. Unstable expression of transgene is associated with the methylation of CAG promoter in the offspring from the same litter of homozygous transgenic mice. Mol Biol Rep 2014; 41: 5177-86.

XII. ACKNOWLEDGEMENTS

First and foremost, I would like to thank my supervisor, Prof. Dr. Elisabeth Kemter, for her guidance and support.

I am deeply thankful to Prof. Eckhard Wolf for providing me with the opportunity to pursue my doctoral thesis at the Chair for Molecular Animal Breeding and Biotechnology. I am particularly grateful for the chance to present my research findings at the IPITA-IXA-CTMR Joint Congress 2023 in San Diego, which was truly an unforgettable experience.

My profound gratitude goes to our cooperation partners Prof. Dr. Jochen Seißler and Dr. Christian Cohrs for the successful cooperation, and for generously sharing their data with me. I also extend my gratitude to the cloning team, Prof. Dr. Valerie Zakhartchenko, Dr. Mayuko Kurome, and Dr. Barbara Keßler, without whom, the generation of our transgenic pigs would not have been possible.

A warm thank you to everyone working at the Moorversuchsgut. Special recognition goes to Tatiana Schroeter, whose patience and dedication have been instrumental in passing on her wealth of technical laboratory knowledge and experience to me. I also express my sincere appreciation to Florentine Stotz, Christina Blechinger and Anja Palme for their exceptional technical support. Furthermore, I am grateful to all animal caretakers for their outstanding care of our animals.

A heartfelt thanks goes to Christian, my family and my friends for their unwavering support, genuine interest, and belief in me. Special shout out to my colleagues-turned-friends, Johanna Pilz, Yasmin Eckstein, Nicol Gloddek, Richard Lindner, and Findus, who made going to work each day a joy.

Last but certainly not least, I would like to direct my focus and gratitude to the true protagonists of this doctoral thesis: my experimental pigs, without whom our research in xenotransplantation would not be possible.